Phase separations and self-assembly of hydrophilic polymers and double hydrophilic block copolymers

Alexander Plucinski

Submitted in fulfilment of the requirements for the Degree of
Doctor of Philosophy

School of Chemistry

College of Science and Engineering

University of Glasgow

Glasgow, August 2022

Abstract

Aqueous multi-phase systems have attracted a broad interest in recent years, which is mainly due to their applicability in biology for purification and isolation of biomolecules and also for separation of particles as well as an environment for enzymatic reactions. Furthermore, the self-assembly of block copolymers constitutes a timely research area in polymer science with implications for applications like sensing or drug-delivery. Here, the phase separation and formation of water-in-water emulsions of different ultra-high molar mass poly(acrylamides) and pullulan was investigated. The ultra-high molar mass poly(acrylamides) were synthesised via photo iniferter reversible addition–fragmentation chain-transfer (PI RAFT) polymerisation (M_n > 700,000 g·mol^{-1}). The polymers were combined to form aqueous multi-phase systems with low total polymer concentration as low as 1.1 to 2.1 wt %. Furthermore, the aqueous multi-phase system could be transformed into water-in-water (w/w) emulsions, stabilised by different stabilisers. Confocal laser scanning microscopy (CLSM) imaging showed that at first polymer-containing droplets in water were formed directly after dispersion and water droplets in polymer matrix after phase separation. Furthermore, a pH sensitive w/w emulsion was observed using pullulan ultra-high molar mass poly(acrylamides). Additionally, the self-assembly of double hydrophilic block copolymers (DHBC), based on poly(acrylamides) in organic and aqueous environment was investigated. The hydrophilic block copolymer induced phase separation at high concentration in aqueous solution leading to giant droplets. However, the mesoscale phase separation at high concentration (>20 wt%) was reversible upon dilution. In order to stabilise the giant droplets during dilution crosslinking via oxime formation was applied. However, the successful crosslinked block copolymer droplets were not stable upon dilution. Additionally, the block copolymer displayed aggregates at lower concentration in aqueous and organic solution. Furthermore, the unprecedented aggregation behaviour of high molar mass block copolymer poly(*N*,*N*-diethylacrylamide)-*b*-poly(4-acryloylmorpholine) (PDEA-*b*-PAM) (M_n > 400 kg mol^{-1}) in organic solvent tetrahydrofuran (THF) was investigated. The aggregate formation was assigned to the unprecedented upper critical solution temperature behaviour of PAM in THF at elevated concentrations (> 6 wt.%) and high molar masses. With adequate stability and required concentration, aggregates formed via DHBC or w/w emulsion open pathways for potential biomedical applications in the future.

Table of contents

Chapter 1

1 Introduction

In our modern society polymer-based materials are our daily companion. During the day it is nearly impossible to avoid the contact with polymeric materials. During our morning routine with our toothbrush or in the evening during a movie night, polymers are always present. Influence of polymer-based materials in all sectors of the economy was growing exponentially in the twenty-first century. In particular, water-based polymer systems constitute an important area e.g., medicine[1] or biology.[1, 2] The widespread and continuing use of polymeric materials is due to their unique properties, economic benefits, and numerous applications; their performance is superior to those of other conventional materials such as metals or natural fibres.[3-5]

Furthermore, molecular self-assembly is omnipresent in nature and in our daily life e.g. phospholipids self-assembly to form the membrane of living cells or surfactants in soap.[6] The majority of the omnipresent self- assembly rely on the smaller molecules, consisting of a hydrophilic head group and one or more hydrophobic tails. Nevertheless, the design of small molecules is constrained by the molecule size. Macromolecules, on the other hand, provide an almost limitless number of opportunities for tailored design. Here polymers have a strength with the sheer unlimited variation of architecture and possible modifications e.g., introducing functional groups or crosslinking for higher stability. As a consequence, the approach of macromolecular self-assembly has been in the focus of polymer science e.g., block copolymer self-assembly.[6, 7] Frequently used are aggregates like micelles[8] or vesicles[9] that are formed from amphiphilic block copolymers. A significant drawback for the application of aggregates formed by amphiphilic block copolymers e.g. polymersome in biomedical applications, is their poor biocompatibility and the insufficient permeability of the hydrophobic part of the polymersome membrane.[10]

One of the most important methods to synthesise polymers in modern polymer chemistry is radical polymerisation. However, the classic free radical polymerisation has limitations and is difficult to control.[11] To refine radical polymerisation, reversible deactivation radical polymerisation (RDRP) techniques have been developed e.g. nitroxide-mediated radical polymerisation (NMP),[12] atom transfer radical polymerisation (ATRP),[13] and reversible

addition–fragmentation chain transfer (RAFT)[14, 15] polymerisation. Utilising RDRP, polymers with improved control over molar mass and end groups can be formed. Consequently, radical polymerisation is a good avenue for the synthesis of hydrophilic polymers and block copolymers.

Self-assembly in aqueous solution is a focus of research, with applications such as drug-delivery[16, 17] carriers or dispersing material.[18] As a consequence, hydrophilic polymers and water-based polymer systems have generated considerable attention in past decades due to their applications in a wide range of interdisciplinary fields including drug-delivery,[19] tissue-engineering,[20] catalysis,[21] membrane technology,[22] aggregate formation.[23, 24] However, the field still faces a lot of challenges for example the required polymer concentration, which come along with high viscosity for phase separation or self-assembly.[25]

The present thesis is focussing on the phase behaviour of hydrophilic homopolymer phase separation, as well as the crosslinked and non-crosslinked self-assembly of DHBCs in aqueous and organic solvent. In particular, crosslinking and solvent change are investigated to decrease the required polymer concentration for self-assembly and phase separation.

Chapter 2

2 Background and Fundamental Principles

2.1 Polymerisation techniques

Over 100 years ago, Hermann Staudinger introduced the concept of macromolecular chemistry and generated the foundation stone for a new class of materials, which are influencing our daily life more and more until today.[26] During the early-stage of radical process, polymerisation was based on a free radical mechanism. The advantage of radical polymerisation is due to a significant number of monomers that can be polymerised and convenient reaction conditions (usually between room temperature and 100 °C). [11, 27] Free radical polymerisation is still one of the most common methods in the area of polymer chemistry. The polymerisation can be explained in three steps (Scheme 2.1): initiation, chain growth, and termination.

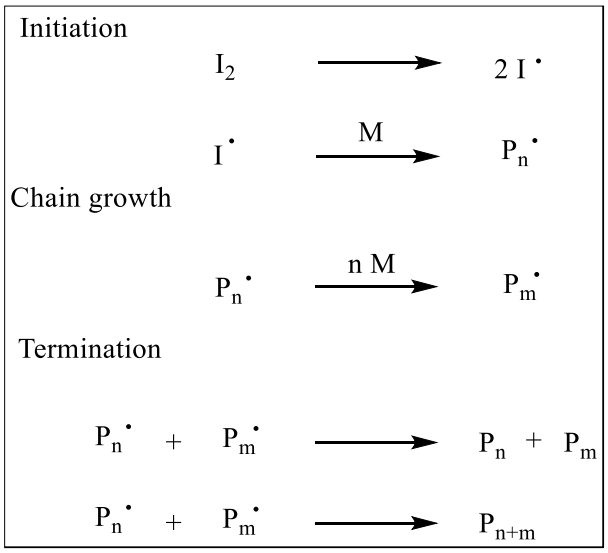

Scheme 2.1. Steps of free radical polymerisation.[28]

In the first step, the initiation, an initiator molecule will build free radicals under elevated temperature or light irradiation. The radical reacts with the monomer and the chain grows. The chain-growth reaction continues until the radical chain ends with a termination reaction. For

the termination, two chains with a radical undergo a recombination or a disproportionation. During recombination, the degree of polymerisation increases. During disproportionation, the degree of polymerisation remains the same.[28] However, the chain growth process during free radical polymerisation is uncontrolled, which leads to a restricted control over molar mass, molecular weight distribution and end groups. Additionally, synthesis of more defined polymer architectures e.g., block copolymers is challenging by using free radical polymerisation. In the 1950s Szwarc firstly introduced the concept of living polymerisation by means of anionic polymerisation. In contrast to free radical polymerisation, the initiation process, propagation, and termination are separated from each other. Szwarc and co-workers[29, 30] described the polymerisation of styrene initiated by sodium naphthalene complex to generate a carbanion at the styrene monomer (Scheme 2.2).

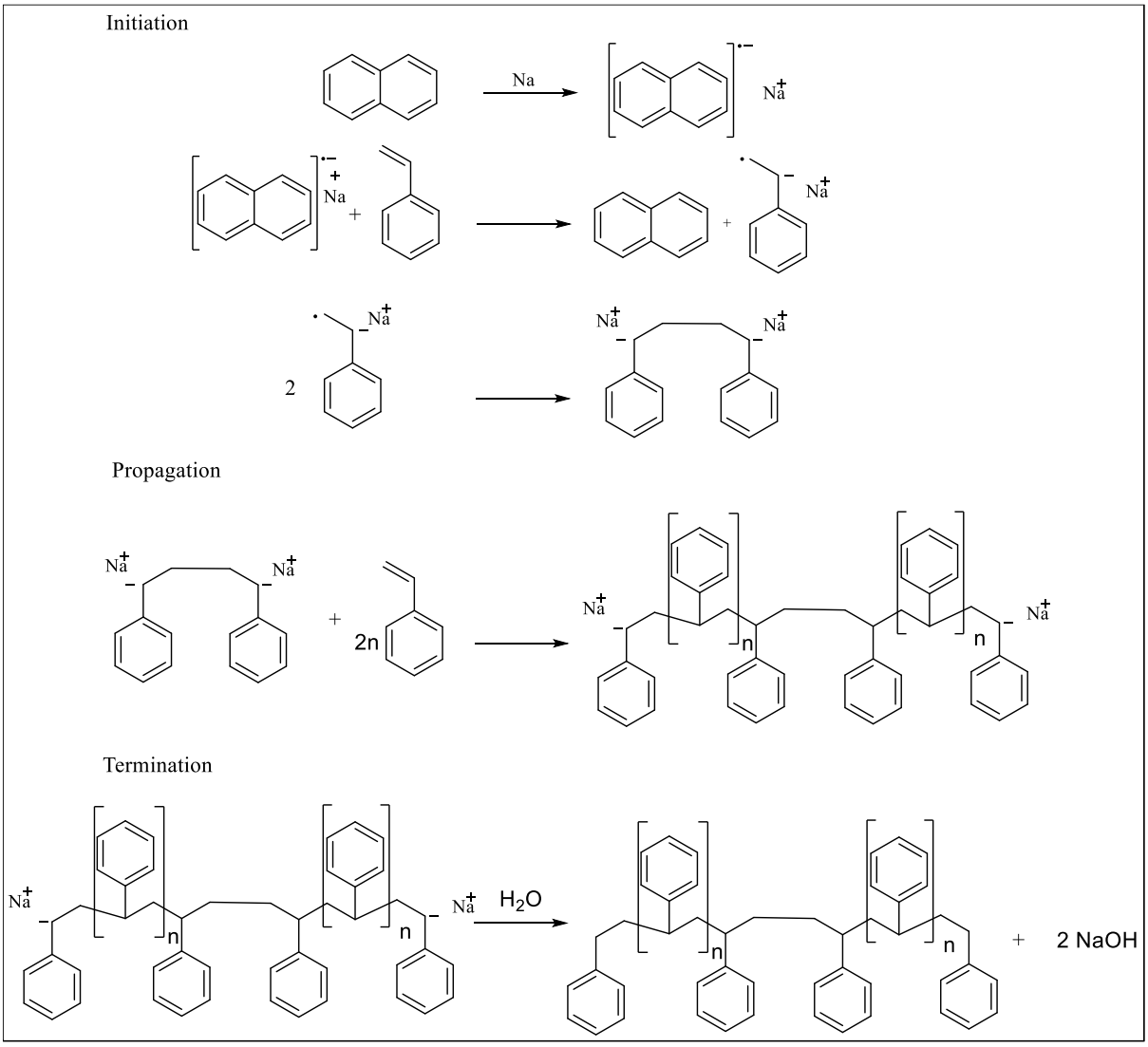

Scheme 2.2. Steps of the anionic polymerisation of styrene using sodium naphthalene complex reported by Szwarc. [29]

The separation of initiation, propagation and termination leads to improved control over molar mass of the polymer by an adjustment of the ratio of initiator and monomer. Furthermore, a narrow molecular weight distribution can be obtained. The living character of anionic polymerisation is due to the absence of termination in an ideal anionic polymerisation. Additionally, end groups can be easily modified for example to introduce a new monomer for new reactions to synthesise an AB block copolymer. Due to all these advantages anionic polymerisation opened the pathway for the synthesis of various polymer architectures. However, anionic polymerisation has a few drawbacks e.g. the monomer is required to be stable under strong basic conditions and the intolerance for impurities like water or oxygen that lead to termination reactions. As a consequence of the monomer requirements not all monomers are suitable for anionic polymerisation e.g. acrylic acid cannot be polymerised via anionic polymerisation. Similar to anionic polymerisation, cationic polymerisation was introduced.[31, 32] Here the vinyl monomers were polymerised via transfer of β-protons to the active chain in acidic environment leading to an undesired reinitiation. Therefore, cationic polymerisation with simple protic acids leads to a large number of dead chains ends because causing a relatively broad molecular mass distribution. Overall, several important polymers can be just synthesised via living polymerisation with high effort and low-cost efficiency. Free radical polymerisation can be used only partly for these polymers, which results in a broad molecular weight distribution. Moad and co-workers[33] introduced a solution for the drawbacks of the radical polymerisation by applying an alkoxyamine derived compound which undergoes a homolytical cleavage of the weak C─O bond to afford a stable nitroxide radical and a polymeric radical which can undergo chain propagation. The nitroxide radical can recombine reversibly with the active polymer radical to generate unreactive dormant species (Scheme 2.3).

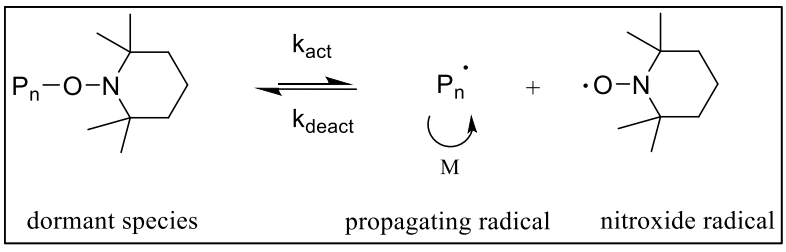

Scheme 2.3. Reversible activation and deactivation of a radical in Nitroxide-mediated radical polymerisation (NMP) using (2,2,6,6-tetramethylpiperidin-1-yl)oxyl (TEMPO).[33]

However, the nitroxide radical is unable to create the radical species. The reversible generation and recombination of radicals is defined by a temperature depending equilibrium. The temperature depending over active and dormant species allows more control over the polymerisation.[34] Nitroxide-mediated radical polymerisation (NMRP) set the starting point for reversible deactivation radical polymerisation (RDRP) techniques.[35] In order to refine radical polymerisation, more RDRP techniques have been developed. Now, polymers with enhanced control over molar mass and end groups can be formed using RDRP.

In the mid-1990, Matyjaszewski and co-workers[13] and Sawamoto and co-workers[36] independently developed a polymerisation technique based on transition metals with a similar concept of dormant and active species. In the new developed atom transfer radical polymerisation (ATRP) the radical is generated by abstraction of a halide from an initiator to a transition metal complex. Here, the transition metal halide e.g., Cu(I)Cl and subtle ligand e.g., 2,2'-bipyridine form a catalyst. The new formed catalyst is able to undergo a reversible single electron oxidation *via* abstraction of a chlorine radical from an initiator molecule e.g., ethyl-2-chloro-2-methylpropanoate and an active initiation radical is formed. Henceforward the polymer chain can grow until it undergoes a recombination with a chlorine from the oxidised Cu(II) complex to form the inactive species and the reduced Cu(I) complex.[37] Due to the predominately shift of the radical equilibrium to the dormant species a small amount of active propagation chains is present, supressing chain termination and leading to good control over the polymerisation. Depending on ligand and initiator a wide range of polymers can be synthesised. Additionally, the synthesis of block copolymers is accessible due to the termination of the polymer with an alkyl halide. The synthesised polymer can now be used as a macro initiator for a block copolymer formation. Furthermore, the halide can be substituted with other functional groups to prepare for further synthesis or more complex macromolecule architectures.[38] One drawback of the ATRP is the contamination with the toxic metal copper[39] in the final product, which is challenging to remove. Furthermore, ATRP cannot polymerise vinyl esters and vinyl ether.

Another RDRP technique and the main polymerisation technique used in this thesis is reversible addition-fragmentation chain transfer (RAFT) polymerisation. RAFT polymerisation was developed in the group of Rizzardo in the end of the 1990s.[15]

2.1.1 Reversible addition–fragmentation chain transfer (RAFT) polymerisation

An easy avenue to form polymers like polyacrylamides is reversible addition-fragmentation chain transfer (RAFT) polymerisation. A benefit of RAFT polymerisation is the possibility of using different kinds of solvents *e.g.*, aqueous environment and the tolerance of functional groups. Especially the tolerance of functional groups, opens the pathway for different polymer architectures e.g., polymer brushes. One advantage of the RAFT process is the two substituents at the chain transfer agent (CTA) for modification, the R and the Z group, which allows a variety of past polymerisation modifications.[14, 40] The RAFT process can be separated into five distinct reaction sequences: Initiation, pre-equilibrium, reinitiation, equilibrium and termination. The mechanism of the RAFT process is shown in Scheme 2.4.[15]

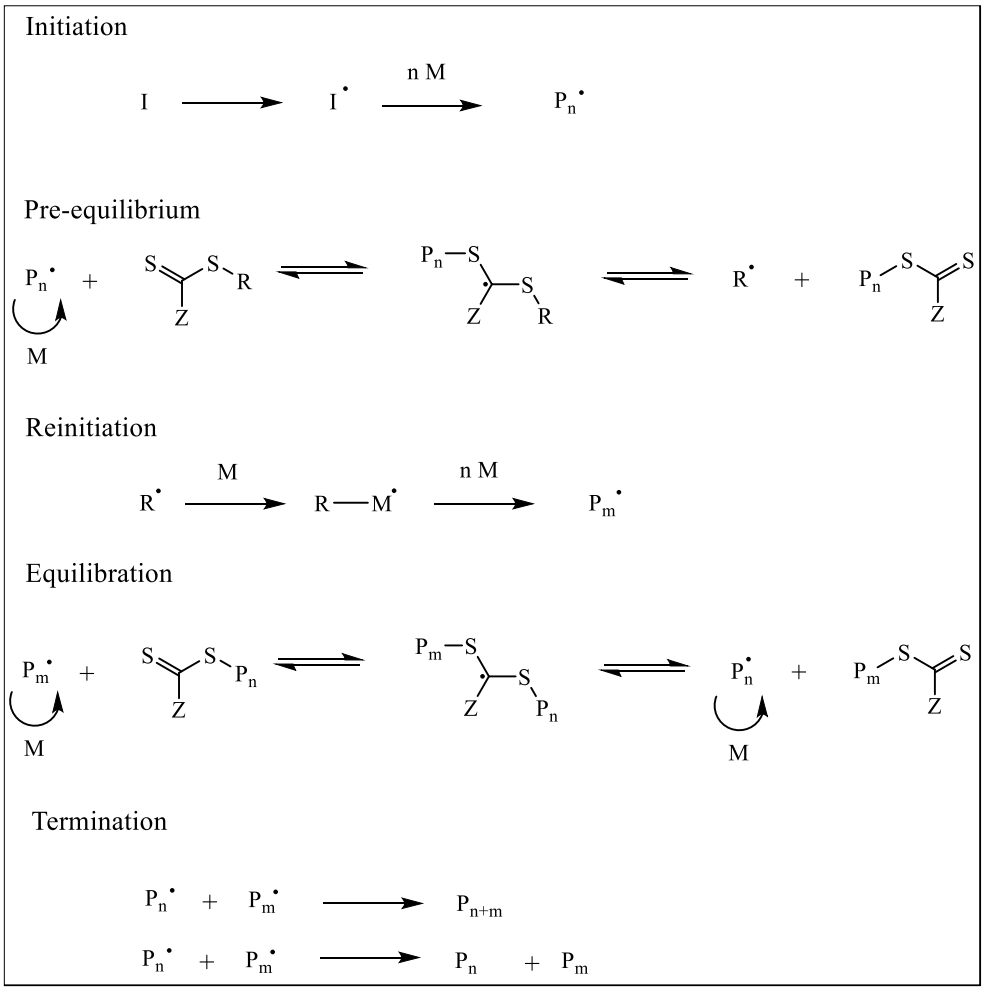

Scheme 2.4. Mechanism of RAFT polymerisation.[15]

The initiation of RAFT polymerisation is the same as for the free radical polymerisation. An initiator I forms radicals I• under, for example, thermal treatment. The chain growth starts when the initiator radical reacts with the monomer to form oligomers P_n•. The chain grows until the formed oligomers add to the CTA molecule, which leads to an intermediary radical in an equilibrium reaction. Subsequently, the intermediate radical fragments to a terminated oligomer and a new radical R•. The radical R• reacts with monomer to a new growing chain P_m•. Due to the fast reaction between growing chains and polymeric CTA, all chains grow with the same probability, which results in the polymer with a narrow molecular weight distribution.[15, 40, 41] In RAFT polymerisation, the CTA controls the radical concentration via chain transfer to a dormant and fragmentation to an active species. The radical species reacts with the CTA to a dormant species. This reaction is reversible, which means that the radical can revert back to an active species and continue the chain growth. The termination functions similarly to the free radical polymerisation: Two chains with a radical undergo a recombination or a disproportionation. The higher the free radical concentration, the higher is the probability for chain termination. However, the transfer reaction between active and dormant species is faster in comparison to termination reactions. The controlling factor of the RAFT polymerisation is the small number of propagating radicals in contrast to the majority of the dormant species.[14, 15, 40] However, if the amount of termination reactions were too high, a significant number of polymers with dead ends will be present and a final polymer with smaller chain length will be formed. The number of termination processes equals the number of initiations. To obtain longer chains, like ultra-high molecular weight (UHMW) polymers, the concentration of CTA is a key factor.

Furthermore, with RAFT polymerisation, polymers can be functionalised in form of different substituents at the CTA. Additionally, with these end groups the functionalised macromolecule can be reinitiated for chain extension *e.g.,* for the formation of block copolymers. In comparison to free radical polymerisation in which the degree of polymerisation is very high even with a low conversion, the degree of polymerisation in reversible deactivation radical polymerisation increases linearly with conversion.[14, 15, 42, 43]

2.1.2 Photo iniferter RAFT polymerisation via direct photochemical processes

The photo iniferter RAFT process can be separated into three distinct reaction sequences: Reversible initiation, equilibrium, and termination. The proposed mechanism of the photo iniferter RAFT process is depicted in Scheme 2.5.[44, 45] The CTA undergoes bond cleavage under irradiation to generate two radicals and initiates polymerisation. Ideally, this reaction is reversible. Similar to the equilibrium in classical RAFT polymerisation, the propagating radicals can react with a CTA, which has not been cleaved before. The reaction occurs with a degenerative chain transfer between the radical and the CTA. The sulphur radical can also combine with a growing chain to regenerate a dormant species. The dormant species can be reactivated again later with light. The termination works like in the normal RAFT polymerisation: Two chains with a radical will undergo a recombination or a disproportionation.[45]

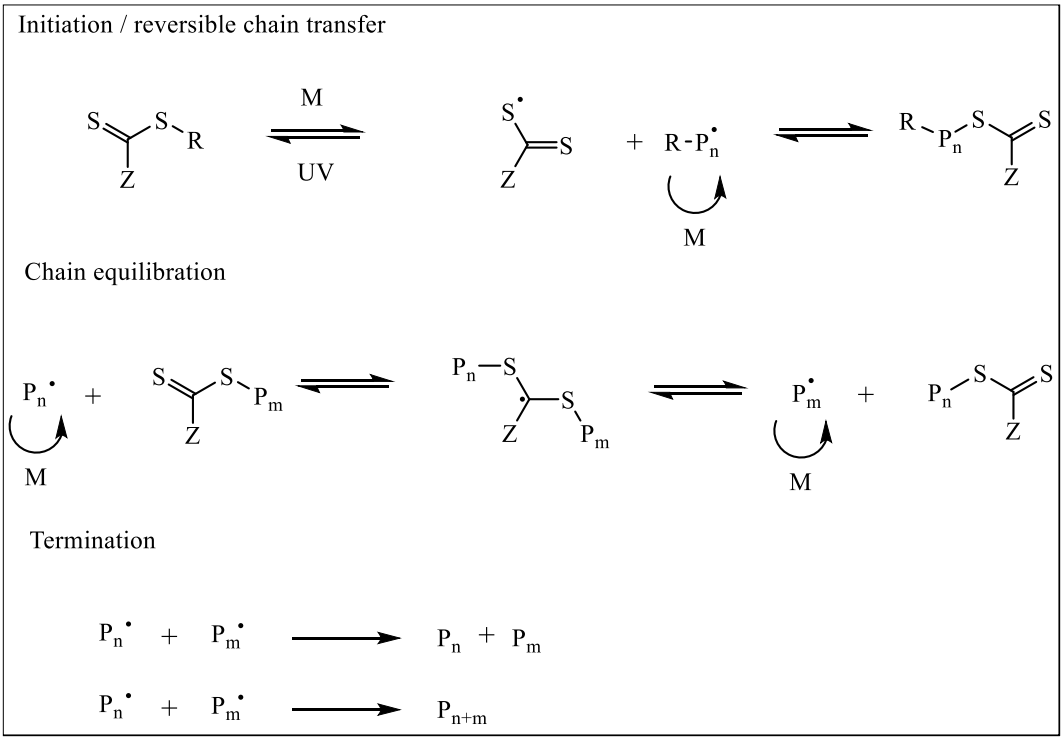

Scheme 2.5. Proposed mechanism of photoiniferter RAFT polymerisation.[45]

The mechanism shows that, in contrast to RAFT polymerisation with an initiator, no external radical initiators are needed. The photo cleavage of the CTA provides the radical source for initiation. It means that there is a distinction between the "classic" photo inducted RAFT polymerisations initiated by an external photoinitiator and polymerisations without external photoinitiator. In the standard photo-initiated RAFT polymerisation, the propagation chain radicals terminate irreversibly and reinitiation can be achieved by adding new initiator After every cycle some chains do not continue to grow. Under perfect conditions, the PI RAFT polymerisation can be cycled infinitely, without using a photoinitiator. However, this is not possible in practice due to undesired side reactions that lead to termination.[45, 46] Especially the procedure from Sumerlin and co-workers seems promising to obtain high molar mass poly(acrylamides) as performed *via* photo induced (PI) RAFT polymerisation,[44] which readily achieves molar masses above $1 \cdot 10^6$ g·mol^{-1}.

2.2 Polymer architecture

An important factor for improving or changing the properties of polymers is their architecture. In general, there are three major pathways to modify the architecture of a polymer (Figure 2.1).[47] First the topology of the polymer can be modified. Examples for modification of different topologies are linear polymers, star polymers or branched polymers. Secondly the composition of the polymer can be modified. Here you can influence, for example, the selection of the monomer and the arrangement of the different units. Examples for polymer architecture with different composition modification are block, gradient, alternating or statistical copolymers. The last modification for polymers is the integration of a functional group. Polymer chains can be functionalised for example at one end of the chain (end functionalisation), at both ends of the chain (telechelic polymers) or at the side chain. Furthermore, it is common to combine multiple modification pathways to design a unique polymer architecture.

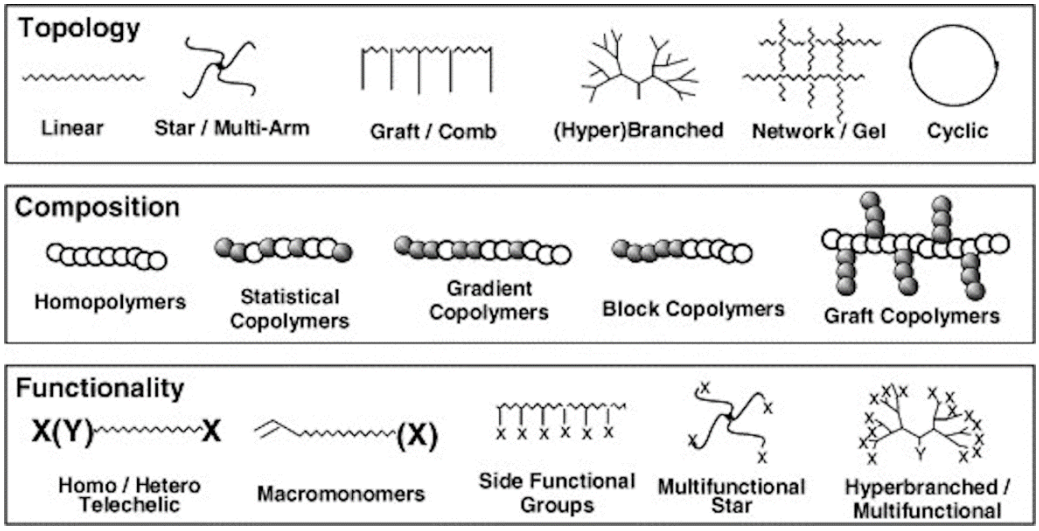

Figure 2.1. Examples of different polymer architectures synthesised via controlled radical polymerisation. Reproduced with permission from reference[47] Copyright Elsevier 2007.

In the following thesis the main focus is on homopolymers, block copolymers and the functionality of the polymers, based on hydrophilic building blocks. RDRP can be used to synthesise a block copolymer in multiple ways. While sequential addition polymerisation makes use of the reversible character of RDRP by conducting two polymerisations in a sequence, coupling reactions make use of the ability to control the end functionality of the polymer to achieve a block copolymer via modular ligation.[48] When employing the sequential addition polymerisation method, two factors must be considered: The macroinitiator should be capable of initiating the second monomer, and the second monomer should be suitable for the same RDRP technique (e.g., RAFT or ATRP). Furthermore, if the functionality or monomer type for the block copolymer is not suitable for certain RDRP technique an initiator-transfer agent-terminator can be used to combine RAFT and ATRP. For the combination of the two RDRP techniques first a RAFT polymerisation is used followed by an ATRP or the other way around to form the final block copolymer.[49, 50] A second strategy utilised controlled polymerisation techniques to introduce designed end group functionalities. As a result, coupling polymers via macromolecular ligation is a common method for forming a block copolymer. The ability to combine different RDRP techniques by polymerising each monomer with the appropriate polymerisation techniques in a suitable solvent and coupling the polymers in a separate step is one of the key features. Therefore, click chemistry is important in modular macromolecular design. One example is copper catalysed alkyne–azide cycloaddition (CuAAc) (1,3-dipolar cycloaddition) first described by Huisgen[51] *et al.* and comparatively by

Kolb and Sharpless[52] described as click chemistry, which could also be used for the preparation of various macromolecular architectures.[53, 54]

An AB block copolymer consisting of two water-soluble polymer building blocks is called double hydrophilic block copolymer (DHBC). In particular, double hydrophilic block copolymers (DHBCs) are interesting for applications in drug delivery or nano reactors, due to their unique self-assembly behaviour.[55, 56] To be applied in biomedical system, the polymer needs to be biodegradable and devoid of metal contamination (e.g. from the catalysts) or toxic contamination (e.g. from an initiator). When using the technique of PI-RAFT polymerisation without an external initiator, these risks are minimised. Previous work on self-assembly of DHBCs[57, 58] focussed on molar masses below 100000 g / mol. The behaviour of DHBCs or hydrophilic polymers with high molar mass has not been investigated so far. Previous studies showed the potential of polysaccharides, like pullulan (Pull) or polyacrylamides like poly(*N*,*N*-dimethylacrylamide) (PDMA) as one polymer for a DHBC self-assembly.[57, 59]

2.3 Phase separation and self-assembly of hydrophilic polymers

Pure water-based polymer systems constitute an important area in biology,[1, 2] medicine[1] or food industry.[60] Especially all aqueous multi-phase systems have attracted a broad interest in recent years, which is mainly due to their applicability in biology for purification and isolation of biomolecules and also for separation of particles as well as environment for enzymatic reactions. Furthermore, self-assembly of block copolymers is an important feature for applications of polymers,[61, 62] which especially counts towards applications in the area of drug delivery and release systems,[16, 63] nano reactors[64] or tissue engineering.[65]

2.3.1 Aqueous two-phase system (ATPS)

An aqueous two-phase system (ATPS) is a liquid-liquid phase separation of two compounds in water *e.g.*, polymer/polymer or polymer/salt. Martinus Beijerinck discovered 1897 a liquid-liquid phase separation during his studies about concentrated starch and gelatin aqueous solution.[66, 67] P.-Å. Albertsson rediscovered ATPSs in the 1950s and used these systems for the separation of bio macromolecules *e.g.* cell fragments or proteins.[68]

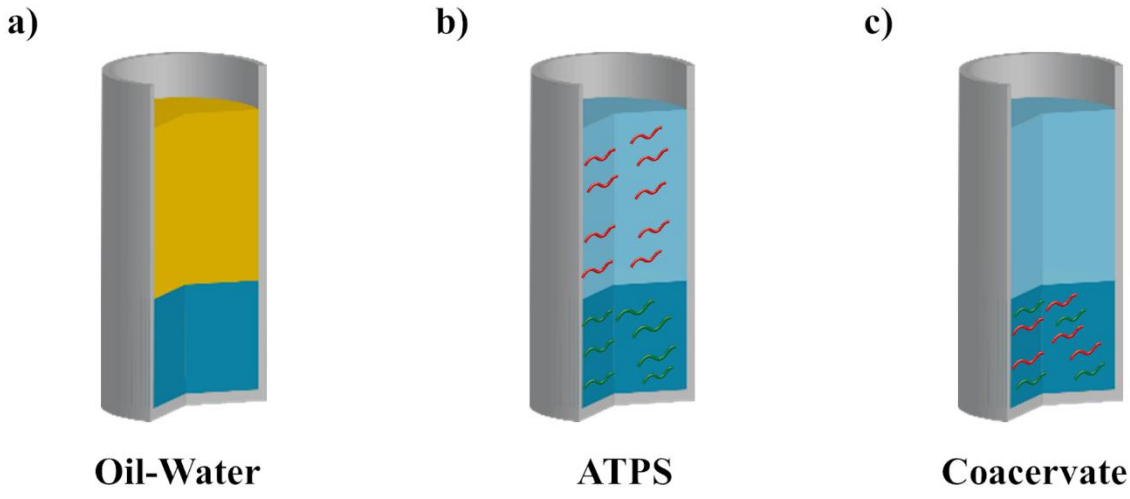

Scheme 2.6. Schematic of different phase separations (a) oil and water phase separation, (b) polymer-polymer ATPS in aqueous solution and (c) polymer-polymer coacervate in aqueous solution.

Similar to the insolubility and phase separation of oil and water (Scheme 2.3a), the phase separation in an aqueous solution containing two hydrophilic polymers is a common phenomenon. A significant number of hydrophilic polymer combinations are incompatible in aqueous solution, which leads to a macroscopic phase separation, with one polymer enriched in one of the phases (Scheme 2.3b).[69, 70] However, it could also associate in a coacervation process, a phase separation with a polymer enriched and a polymer depleted phase (Scheme 2.3c).[71] High polymer concentration leads to phase separation, while at low polymer concentration a single phase is present. The driving force of the demixing process in ATPS is the enthalpy associated with for example water-polymer interaction and the opposing loss of entropy during phase separation. When the entropic contribution favouring mixing becomes smaller relative to the enthalpic contribution opposing it, phase separation occurs.[72] In contrast to oil-water phase separation, the interfacial tension of an ATPS is significantly lower. The stability and required polymer concentration can be influenced with *e.g.* temperature,[73, 74] pH,[73] additives or molecular weight of the used polymers.[73, 74]

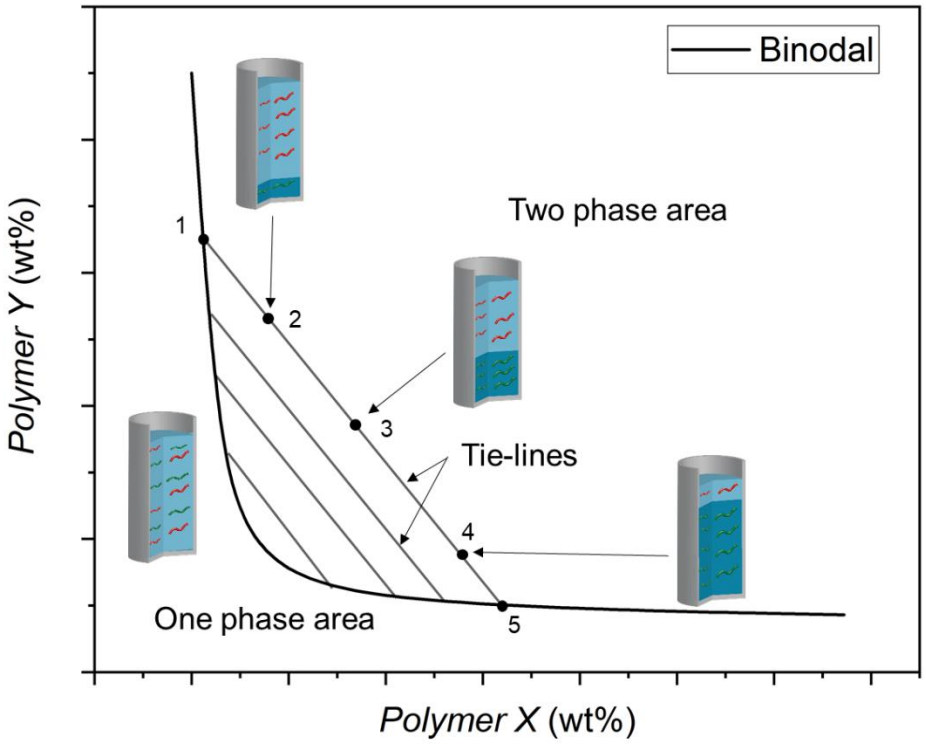

Figure 2.2. Illustration of the phase diagram for an aqueous solution of two neutral polymers.

A phase diagram is one way to characterise an ATPS under set conditions *e.g.,* temperature or pH. The phase diagram provides the information about the concentration of phase-forming components (polymer or salt), necessary to form two phases.[71, 75] The line which separates the one and the two-phase area is the binodal. Tie lines relate the overall components of a solution to the concentration of each of the polymers in the top and bottom phases. The concentration of each polymer is given by the intersection of the tie line on which that composition lies with the coexistence curve. The points (●) 2, 3, and 4 are above the binodal and therefore two phases exist. These points lie on the same tie line and consequently their top and bottom phases compositions are each given by points 1 (top phase) and 5 (bottom phase) but different in the volume. There are three methods for evaluating a binodal.[71] Turbidimetric titration is one avenue to determine a binodal. When two components are immiscible in water, the mixture becomes turbid. During dilution the solution becomes less turbid until it is clear, which will be used as a data point of the binodal. The cloud point method is a similar technique to determine a binodal. A known concentrated stock solution of one component (polymer X) is added dropwise to a known concentrated stock solution of the second component (polymer Y). The mixture is turbid at a critical point (cloud point), an indicator for a two-phase formation. The concentration prior turbidity is the point for the binodal. The last method is the determination of binodal *via* the dilution, mixing and demixing of concentrated ATPSs with different ratios but same total component concentration. The process is repeated, until no phase separation is observed. The concentration at that point is recorded as the data point of the binodal.[69, 76]

In recent years, ATPS have been utilised frequently for the separation of biomacromolecules as well as nanoparticles or as environment for enzymatic catalysis. The most frequently utilised system e.g. for the separation of biomolecules, employing two polymers, makes use of poly(ethylene glycol) (PEG) and dextran (Dex).[70, 77] In order to provide a simple route to the formation of hydrogel microcapsules, a crosslinking technique was explored by Ono and coworkers,[78] namely amide formation via active esters and amines. In a microfluidic avenue, droplets of PEG/Dex were formed in oil. After phase separation, the PEG phase settled as the shell of the aqueous droplets. Notably, the PEG solution was fed into the system via two streams as two PEG species were employed, i.e. tetra-arm PEG with either NH_2 or N-hydroxy succinimide ester functionality that crosslinked immediately after phase separation (Figure 2.3). In such a way, crosslinking was performed directly without light or other stimuli, revealing PEG/Dex capsules

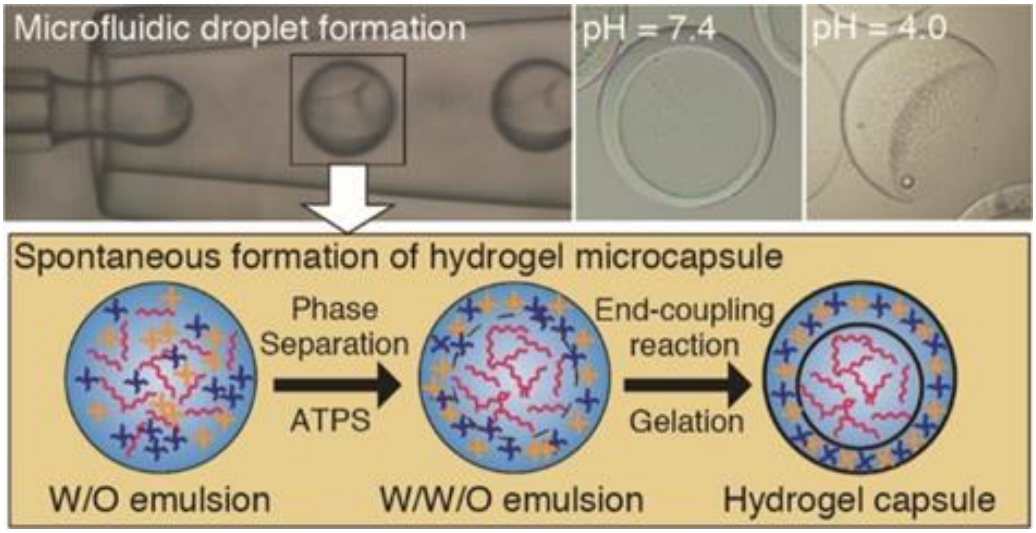

Figure 2.3. Formation of PEG/DEX capsules via ATPS templating in a microfluidic system. (Reproduced with permission from,[78] Copyright American Chemical Society, 2019.)

Regoni and co-workers[79] used the ATPS formed via PEG and Dex to form a ferrofluidic aqueous two-phase system with a significantly low interfacial tension in comparison to regular water based ferrofluidic systems. The ferrofluidic ATPS opens new pathways for example in magnetic-field-enhanced purification of biomolecules such as proteins based on their partitioning in the ATPS The ultralow interfacial tension (about $\gamma \sim 10^{-6}$ N m^{-1}) based on the based on spontaneous phase separation of Dex and PEG and the asymmetric partitioning of superparamagnetic maghemite nanoparticles into the Dex phase.

Besides ATPS, aqueous multi-phase systems featuring more than two phases are under investigation as well.[80-82] Whitesides and co-workers conducted the formation of a plethora of aqueous multi-phase systems based on different hydrophilic polymers[81] and employed them for separation of nanoparticles with different size and shape.[82] Rate-zonal centrifugation was used to accomplish the separation task with an aqueous multi-phase system as the medium, which proved to be stable in the centrifugal field. Furthermore, they investigated the formation of aqueous multi-phase systems in relation to polymer type or surfactant (Figure 2.4). As a consequence, density gradients were precisely designed and adjusted. After phase separation, a mixture of hydrophilic polymers and surfactants could be used to separate beads of varying density. That method could be used to obtain phase separation of mixtures containing two to six components excluding water.

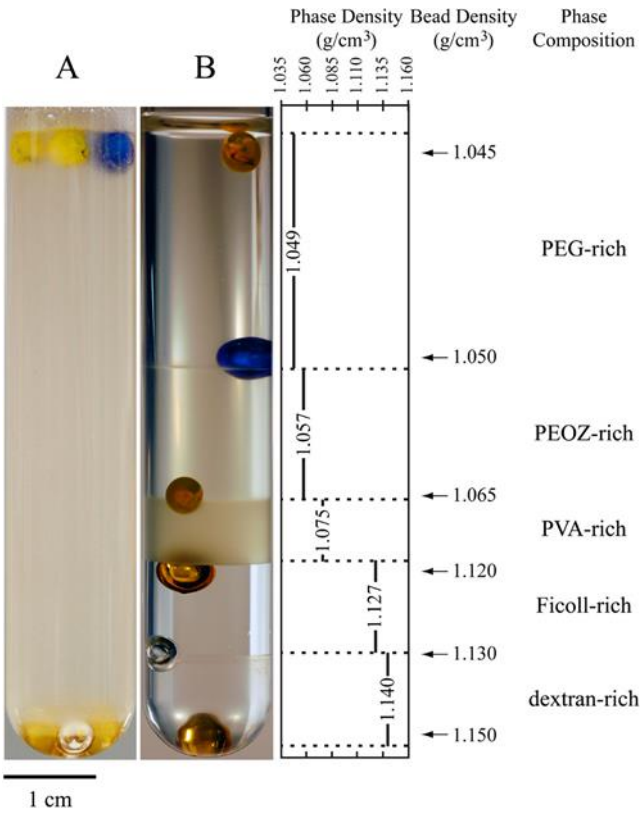

Figure 2.4. Aqueous multi-phase system of various compounds with different density (visualized via polymer beads with different density): (A) after mixing; (B) after phase separation. (Reproduced with permission,[81] Copyright 2012, American Chemical Society)

The macroscopic phase separation of multiple hydrophilic polymers in aqueous solution is one of the important factors for a better understanding of the microscopic self-assembly from hydrophilic polymers and double hydrophilic block copolymers in aqueous solution. A better understanding and new polymer combinations will be a good step to for example to decrease the required concentration for block copolymer microscopic self-assembly. This will be discussed in Chapter 4 and 5.

2.3.2 Water-in-water emulsion (w/w emulsion)

A water-in-water emulsion forms *via* colloidal dispersion of two thermodynamic incompatible aqueous solutions *e.g.*, two hydrophilic polymers in water. The emulsion can be prepared from an ATPS by applying mechanical agitation for example dispersion *via* ultrasound or shaking by hand.

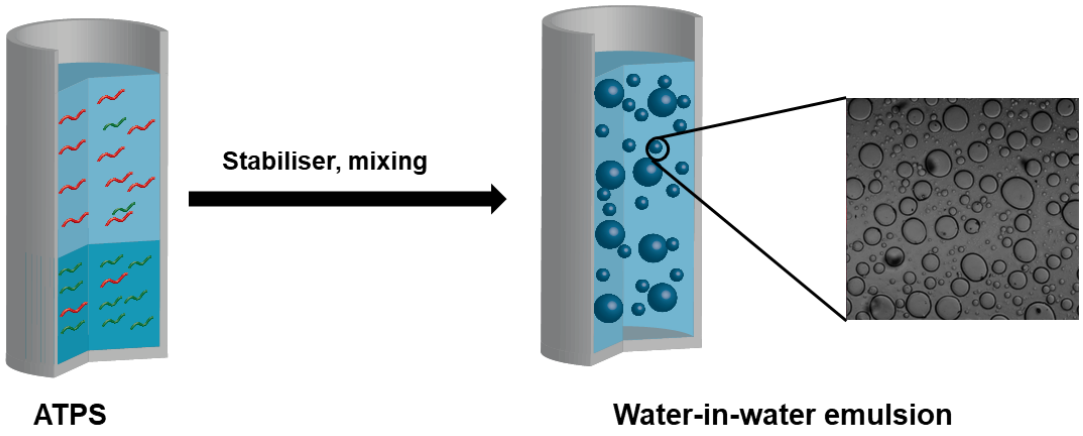

Scheme 2.7. Formation of a w/w emulsion *via* dispersion of an ATPS.

The phase with smaller volume fraction becomes the internal phase. Around approximately equal volume fraction, phase inversion occurs. Close to the 1:1 ratio bicontinuous emulsions can be formed as well.[83] That can be visualised in a similar way to the phase diagram in Figure 2.1. The stability of the droplets in a w/w emulsion is relatively poor because of the significant lower interfacial tension of the ATPS and a very broad interface between the aqueous phases at which small surfactant molecules cannot align properly. Correspondingly, emulsion stabilisation based on surfactants, like in oil-in water or water-in-oil emulsions, is not suitable.[84] However, w/w emulsions can be stabilised *via* various types of particles *e.g.* polydopamine nanoparticles,[85] cellulose nanocrystals,[86] layer double hydroxide (LDH) nanoparticles[87, 88] or graphitic carbon nitride.[89] All these is referring to macroemulsions, micro emulsion were not discussed in this context.

Emulsions stabilised by solid particles rather than surfactants are referred as Pickering emulsion.[90, 91] Pickering emulsions are named after S.U. Pickering, whose publication[92] is widely regarded as the first report of o/w emulsions stabilised by solid particles adsorbed on the surface of oil droplets. The stabilisation mechanisms involved are fundamentally different from conventional emulsifiers, which can be advantageous in terms of emulsion stability.

Especially for w/w emulsion the Pickering emulsion is getting more interesting due to the insufficient stabilisation based on surfactants for w/w emulsion. Pickering emulsions retain the basic properties of classical emulsions stabilised by surfactants (via emulsifiers), so they can be used in most applications in place of a classical emulsions. The high resistance to coalescence is a significant advantage of solid particle stabilisation.[93]

For example, O'Reilly and co-workers showed that 2D diamond-shape poly(lactide) block copolymer nanoplatelets can successfully stabilise w/w emulsions (Figure 2.5). Due to the considerable surface and significant interface to volume ratio, especially larger platelets exhibit strong emulsion stabilisation effect.[94]

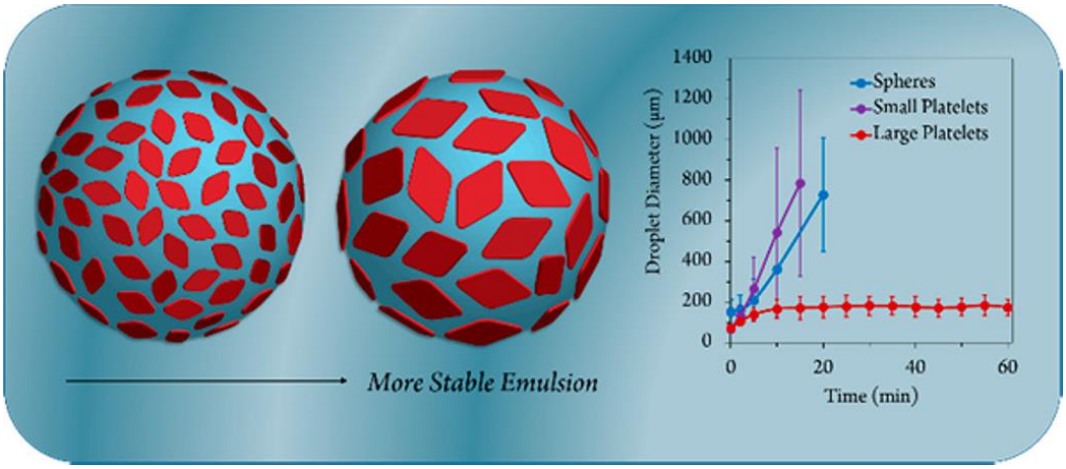

Figure 2.5. Illustration of the w/w emulsion stabilised by 2D diamond-shape poly(lactide) block copolymer nanoplatelets (Reproduced with permission from,[94] reference licensed under CC BY 3.0).

Freitas and co-workers reported a pH-switchable aqueous emulsion of xyloglucan and amylopectin stabilised *via* polysaccharide-coated protein particles.[95] Here, a segregative phase separation could be observed in the mixtures of xyloglucan and amylopectin. A w/w-emulsion of amylopectin droplets in a continuous phase of xyloglucan was stabilised by addition of β-lactoglobulin microgel for pH ≤ 5.0.

Lee and Stebe[96] utilised poly(electrolyte) complexation to form cell-encapsulating compartments in ATPS. Therefore, poly(sodium 4-styrenesulfonate) or poly(diallyldimethylammonium chloride) were dissolved in an aqueous Dex or PEG solution, respectively. If a balanced ratio of poly(electrolyte) equivalents was used, the poly(electrolytes) formed complexes at the interface of the PEG and Dex phase stabilising ATPS droplets. Osmotic (poly(electrolyte) addition) and ionic (salt addition) stress could both disrupt the

capsules. Bacteria were finally introduced into capsule structures and found to grow inside the capsules, with an order of magnitude increase in bacteria counts after 24 hours, indicating that the formed structures are biocompatible.

Overall, w/w emulsion are an important area in chemistry and biology. However, there are some drawbacks using the current systems. The required polymer concentration for a stable ATPS and following a potential w/w emulsion is significantly high. Furthermore, the stabilisation of a w/w-emulsion is challenging and still under investigation.

2.3.3 Self-assembly of block copolymers

The solution of a linear block copolymer forms rarely a homogeneous mixture. In similarity to the mixture of homopolymers, discussed before, the individual polymer blocks are not miscible with each other due to thermodynamic reasons. Therefore, the process can be described with Gibbs free energy of mixing

$$\Delta G_{mix} = \Delta H_{mix} - T\Delta S_{mix} \qquad \text{(Equation 1)}$$

In order to successfully mix the block copolymer, the Gibbs free energy (ΔG_{mix}) has to be negative. A positive Gibbs free energy results in a demixing observed in a phase separation, when the entropic contribution (ΔS_{mix}) favouring mixing becomes smaller relative to the enthalpic contribution (ΔH_{mix}) opposing it. The significant parameter for the phase behaviour of polymers is the enthalpy of mixing.[97]

$$\Delta H_{mix} = k_B\, T\, \chi_{AB}\, n\, \phi_A\, \phi_B \qquad \text{(Equation 2)}$$

The mixing enthalpy depends on two parameters which are independent from the polymer: The Boltzmann constant (k_B) and the temperature (T). Furthermore, the mixing enthalpy depends on three polymer specific parameters: the volume fraction of polymer A and B (ϕ_A, ϕ_B), the total number of polymers (n), and the Flory-Huggins parameter (χ_{AB}).[98, 99] The equation is based on Flory and Huggins' model from the 1940s, and it provides a mathematical approach to determining the segregated block copolymer phases.[98, 99] If n and T are constant, the value of AB and the volume fraction of each polymer are the determining factors in a phase separation process. On the one hand, when both polymers have a high repulsive interaction and are present in a similar volume fraction (χ_{AB}), a high value for ΔH_{mix} is obtained, increasing the probability of phase separation. On the other hand, when both polymers are compatible and the polymers are mixed together in highly different volume fractions e.g. $\phi_A \gg \phi_B$, a relatively small value of ΔH_{mix} results. Additionally, the enthalpy can be increased with the total number of polymers. Therefore, the possibility of a phase separation process increased with the concentration of the polymer. Originally, the Flory-Huggins model was developed to describe

the interaction between polymer and solvent molecules, the model can be used to describe the formation of block copolymer microdomains as well.[100] In order to do so, equation 2 needs to be modified.

$$\Delta H_{mix} = k_B\, T\, \chi_N\, f_A \qquad \text{(Equation 3)}$$

The product of the Flory-Huggins parameter of the segment-segment interaction with the polymerisation index (χ_N) and the fraction f of monomers A in a polymer chain. The monomer fraction f can be calculated by dividing the number of monomers A, N_A by the index of polymerisation.[101, 102]

$$f = \frac{N_A}{N}\ ; \text{with } N = N_A + N_B;\ N_A \gg 1;\ N_B \gg 1 \qquad \text{(Equation 4)}$$

The Flory-Huggins parameter (χ) defines the interaction of a chain segment of polymer A with another polymer B chain segment.[98, 99] A closer look at the fundamentals of a block copolymer melt is required to understand the driving forces of a block copolymer micro phase separation.[100] A molten polymer compressibility is close to zero, and the reduced density of the monomers A and B, although the overall density is constant. Local fluctuations in the reduced density, on the other hand, cause micro phase separation due to the systems attempt to minimise the Gibbs energy ΔG_{mix}. In the case of higher Flory-Huggins parameter (χ), the monomer segments of A and B repel each other to minimise contacts between monomer A and monomer B and to compensate for density fluctuations. The entire system conclusively reduces the mixing energy while decreasing the system's entropy. As a result, the two thermodynamic values ΔG_{mix} and ΔS_{mix} compete, and the mixing or demixing of the polymer blocks is determined by the Flory-Huggins parameter (χ).[103]

Figure 2.6[103] shows a theoretical phase diagram including corresponding morphologies for an AB type block copolymer. Changing the volume fraction of one block, and thus its spatial demand, has an effect on the morphology of the sample. As a consequence, two regions can be

observed: a disordered region where the block copolymer is homogeneously mixed and a region where micro phase separation occurs with a variation of highly ordered morphologies. A homogeneous mixture is formed when the blocks within the block copolymer exhibit compatibility, as indicated by a low value for χ_N. Here, the volume fraction has no effect on morphology change. In contrast, in the cases of extreme incompatibility of the blocks due to a high value for χ_N, the fraction of each building block plays a significant role in the morphology structure. The form of these micro phase domains following demixing of the polymer blocks is highly influenced by the polymer block demands for space. The block copolymer aligns in alternating lamellar structures of segregated polymer fractions if block A has the same spatial requirement as block B ($N_A = N_B$). Because the lamellar phases must be packed as tightly as possible, the section usually comprises two layers of polymer. Whenever the spatial demand of polymer block A increases to the point where the tightest packing no longer fits into a lamellar phase, the phase deforms to keep the tightest packing in a different domain structure (Figure 2.6).[103] The Flory-Huggins theory can be used to describe the morphological outcome of deformation, which is determined by the demand for the tightest packing of the polymer blocks.

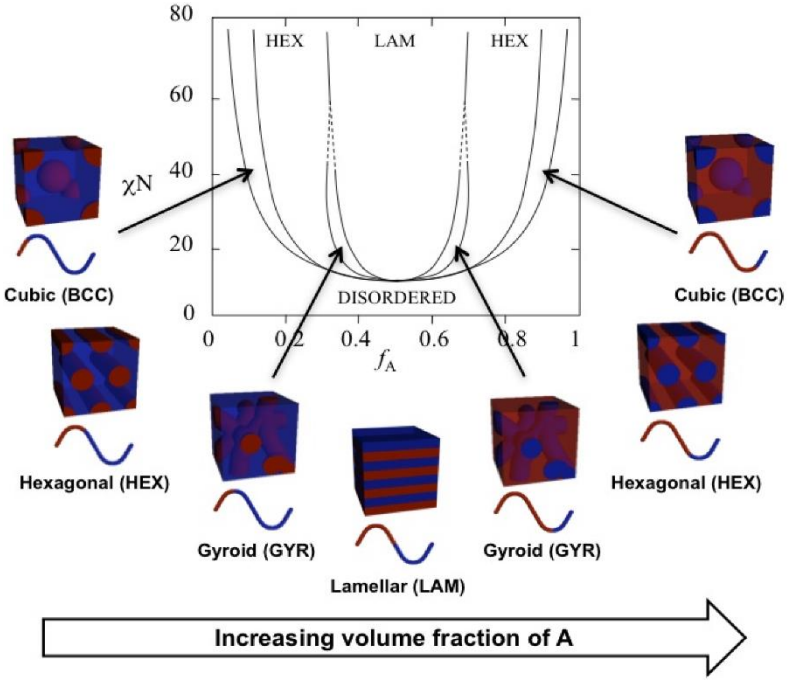

Figure 2.6. Theoretical phase diagram including corresponding morphologies for an AB type block copolymer. Depending on the volume fraction of the building block A f_A the composition shifts between cubic, hexagonal, gyroid and lamellar. (Reproduced with permission from reference,[103] licensed under CC BY 3.0.)

The phase separation behaviour is not limited to bulk block copolymers but can also be observed in block copolymer solutions.[24] Amphiphilic block copolymers with their various structural morphologies are the most prominent examples of phase separation in solution. As known from nature the phase separation of amphiphiles in solution is essential in the majority of organisms on earth. The phase separation of amphiphilic phospholipids in aqueous solutions is a critical component of cell membranes that separate and protect the interior from the environment.[104, 105] A significant impact on polymer science had the potential of synthetic amphiphiles to self-assemble in aqueous solution to mimic and investigate biological systems, as well as their transformation into applications in biomedicine and material science.[106, 107] Amphiphiles are composed of a water-soluble hydrophilic part and a water insoluble hydrophobic part that are connected by a single linkage. The strong difference in solubility between the different parts forces the phase separation of amphiphiles in solution. The amphiphile's water insoluble hydrophobic part attempts to minimise contact with water molecules, resulting in a micro phase separation in which the hydrophobic part is shielded from the aqueous phase by the hydrophilic

head groups.[108, 109] The various morphologies are primarily caused by the inherent molecular curvature and how it influences the packing of the block copolymer chains. In similarity to the phase behaviour of bulk block copolymer, the morphology of the phase separated amphiphiles is dependent on the ratio of the hydrophobic to hydrophilic part.[110] Depending on the volume fraction of the hydrophobic part, various structures can be observed e.g. spherical or cylindrical micelles. As a consequence, the volume ratio of the hydrophobic moiety to the hydrophilic part can be used to describe the self-assembly of block copolymers in solution.

$$p = \frac{v}{a \cdot l} = 1 + Hl + \frac{Kl^2}{3} \qquad \text{(Equation 5)}$$

The Equation of Hyde et al[111] shows the geometrical description of the shape of the amphiphilic block copolymer in a selective solvent can be used to predict the resulting structures. The packing parameter for the possible self-assembly structures (p) is determined by three variables: the volume of the hydrophobic segment (v), the contact area of the head group (a), and the length of the hydrophobic segment (l). Therefore, the packing parameter usually dictates its most likely self-assembled morphology.

$$H = \frac{1}{2}\left(\frac{1}{R_1} + \frac{1}{R_2}\right); K = \frac{1}{R_1 \cdot R_2} \qquad \text{(Equation 6)}$$

The packing parameter can be described as a sum of two curvatures utilising differential geometry: the mean curvature H and the Gaussian Curvature K. Because hydrophobic chains pack as densely as possible to exclude water, the individual curvatures can be described by applying H and K, which are represented by two curvature radii R_1 and R_2. Depending on the packing parameter (p) different self-assembled morphologies can be formed.[112] When $p \leq \frac{1}{3}$, spherical micelles are preferred, followed by cylindrical micelles when $\frac{1}{3} \leq p \leq \frac{1}{2}$, , and enclosed membrane structures (vesicles, also known as polymersomes) when $\frac{1}{2} \leq p \leq 1$ (Figure 2.7).[113]

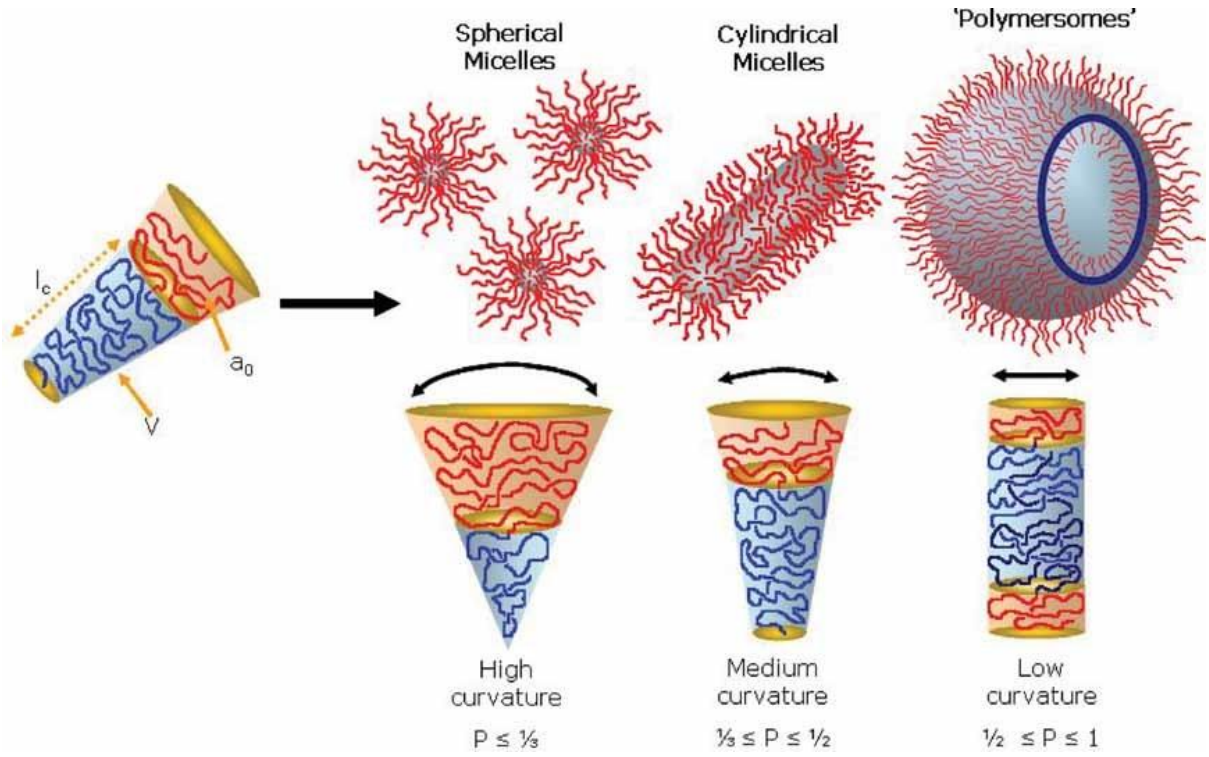

Figure 2.7. Illustration of various self-assembled structures formed by amphiphilic block copolymers. The type of structure formed is due to the molecules inherent curvature, which can be estimated by calculating its dimensionless packing parameter (p). (Reproduced with permission,[113] 2009 WILEY-VCH Verlag GmbH & Co. KGaA)

A significant drawback for the application of amphiphiles e.g. polymersomes in biomedical applications, is their poor biocompatibility and the insufficient permeability of the hydrophobic part of the polymersome membrane.[10] An alternative route to form aggregates, is to use hydrophilic block copolymers *e.g.* double hydrophilic block copolymers (DHBCs).[58] In literature, the most common strategy to form aggregates of DHBCs in aqueous solution is to operate with an external trigger. In a non-selective solvent, aggregates can be formed via external triggers, e.g. frequently with temperature[21] or pH triggers.[114] Scheme 2.8 shows a schematic of a possible self-assembly of a thermo-responsive and pH-responsive building block in DHBCs.

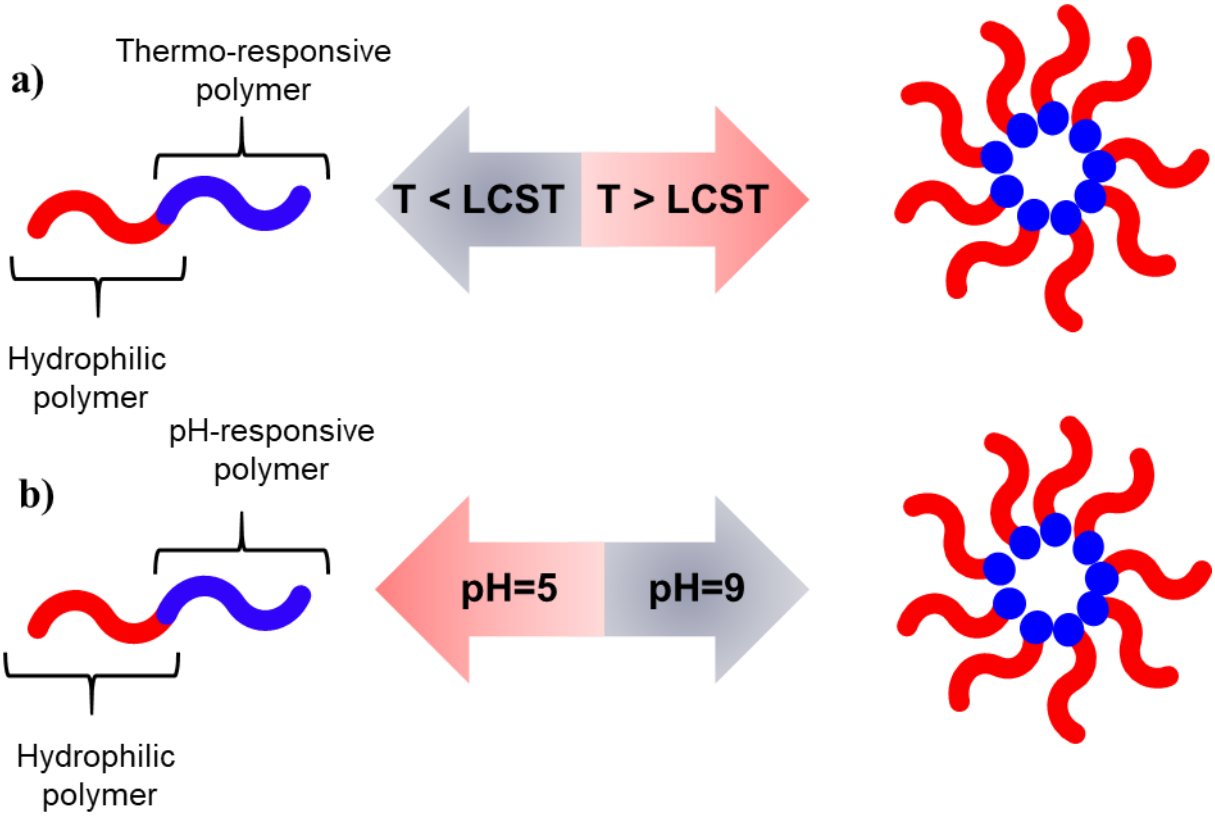

Scheme 2.8. Schematic behaviour of an AB block copolymer upon the external trigger application of leading to micelle formation (a) a block copolymer with a thermo-responsive building block and (b) a pH-responsive building block.

In the case of a temperature trigger, aggregates are formed exploiting a lower critical solution temperature (LCST)[115] or an upper critical solution temperature (UCST)[116] of one of the polymer building segments in the block copolymer. For example, due to a positive contribution to the free energy of mixing ΔG_{mix}, the polymer is capable of forming hydrogen bonds with water molecules below the LCST. When the temperature reaches the point where ΔG_{mix} becomes positive, the hydrophilic polymer prefers polymer-polymer interactions over polymer-solvent contacts, resulting in phase separation of polymer blocks and water and clouding of the solution. However, one of the major driving forces for the phase separation is the entropy of water. These can be expressed with the hydrophobic effect, which described interaction between water and solute. The LCST of poly(*N*-isopropylacrylamide) (PNIPAM)[115] as well as poly(*N*,*N*-diethylacrylamide) (PDEA)[117] in water are well known and exploited to form stimuli-responsive aggregates. A change in pH is another external trigger that can be used to form structures such as micelles or vesicles if one block has a specific pH sensitivity. Polymers such as poly(*N*,*N*-

dimethylaminoethyl methacrylate) (PDMAEMA) and poly(acrylic acid) (PAA) are generally soluble as ionic species but become insoluble when neutralised by a base or an acid, respectively.

Completely water soluble DHBCs show self-assembled structures in aqueous environment as well. The self-assembled structures are formed of DHBCs with specially chosen block combinations in aqueous systems at high concentration. At lower concentration, the formed self-assembled structures are breaking down. The aggregation of DHBCs can be understood from the perspective of aqueous multi-phase systems that feature phase separation of homopolymer mixtures in water at elevated concentration.[81, 85, 118, 119] The different hydrophilic blocks of the DHBC are covalently bound. The covalently binding of the DHBCs blocks results in microscopic self-assembly to compensate the different osmotic pressure hydrophilic polymer domains. Additionally, the self-assembly depends on the Laplace pressure due to the interfacial tension. For a stable aggregate formation, both pressures should be equal. For the self-assembly of DHBCs, the polymer-polymer interaction has a significant influence. According to the studies by Brosnan *et. al.*,[120] the different hydrophilicity of the chosen polymer blocks needs to be significant, to form stable self-assembled structures. Earlier studies have shown that block copolymers like PEO-*b*-poly(2-methyl-2-oxazoline),[121, 122] PEO-*b*-poly(*N*,*N*-dimethylacrylamide) (PEO-*b*-PDMA)[123] or PEO-*b*-poly(2-(methacryloyloxy)ethyl phosphorylcholine)[55] show microphase separation and aggregate formation in the aqueous phase. The research of Brosnan[120] *et. al.* showed the formation of aggregates by different combinations of hydrophilic blocks, *i.e.*, dextran-*b*-PEO, pullulan-*b*-PEO, and dextran-*b*-poly(sarcosine), present in aqueous solution at high concentration (15-25 wt%). Continuing research indicated the self-assembly behaviour of other DHBCs at lower concentration, *e.g.* poly(2-ethyl-2-oxazoline)-*b*-poly(*N*-vinylpyrrolidone) (PEtOx-*b*-PVP),[124] PEO-*b*-PEtOx,[125] pullulan-*b*-PEtOx,[126] pullulan-*b*-PVP[127] or pullulan-*b*-PDMA.[59] Especially glyco polymers were investigated regarding DHBC self-assembly frequently,[128-131] for example poly(2-hydroxyethyl methacrylate)-*b*-poly(2-*O*-(*N*-acetyl-β-D-glucosamine)ethyl methacrylate).[128]

Overall, self-assembly of polymers is a major topic in current polymer chemistry and there is a significant large number of pathways for polymer self-assembly. The following thesis focusses on the phase separation and w/w emulsion of hydrophilic homopolymers (Chapter 4 and 5) as well as of the self-assembly of DHBCs with and without external trigger (Chapter 6 and 7).

Chapter 3

3 Outline and Aims

In the following thesis the phase separation of different hydrophilic homopolymers in aqueous environment as well as the self-assembly of double hydrophilic block copolymers (DHBC) in aqueous and organic solution was investigated. Acrylamides like *N*,*N*-dimethylacrylamide or 4-acryloylmorpholine showed promising potential as monomers for the synthesis of high molar mass homopolymers as wells as building blocks for DHBCs. The polymer synthesis was mostly conducted via reversible addition–fragmentation chain transfer (RAFT) polymerisation, either classical RAFT polymerisation or photoiniferter RAFT (PI RAFT) polymerisation via direct photochemical processes. Due to PI RAFT polymerisation, high molar mass homopolymers and block copolymers could be synthesised. In Chapter 4 the phase behaviour of the combination of the synthesised homopolymers in aqueous solution was investigated. The mixtures of each polymer combination, at low concentrations, were investigated revealing the formation of ATPS or aqueous three phase system (A3PS). Additionally, the phase behaviour of the mixture of poly (*N*,*N*-dimethylacrylamide) (PDMA) and commercial pullulan (Pull) was investigated in Chapter 5. Moreover, the ATPSs were used to form w/w emulsions, stabilised with various stabilisers e.g. Mg/Al-CO_3-LDH nanoparticles. These emulsions were further analysed *via* confocal laser scanning microscopy (CLSM). In order to locate the polymers during the emulsion, each polymer was labelled with a unique dye e.g. Rhodamine B (RhB), or Fluorescein isothiocyanate (FITC). Subsequently, the self-assembly behaviour of the DHBC Pull-*b*-(PDMA-*co*-PDAAM) in aqueous environment was investigated in Chapter 6. Toward this end, alkyne end-functionalised pullulan was coupled via CuAAc with an azide end-functionalised PDMA-*co*-PDAAM. Additionally, the Pull-*b*-(PDMA-*co*-PDAAM) was crosslinked via oxime formation and the aggregation behaviour of Pull-*b*-(PDMA-*co*-PDAAM) and crosslinked Pull-*b*-(PDMA-*co*-PDAAM) was analysed via cryo SEM, dynamic light scattering, and confocal laser scanning microscopy. Additionally, the behaviour of the aggregates in the organic solvent *N*-methyl-2-pyrrolidone (NMP) was studied as well. Furthermore, the self-assembly behaviour of the high molar mass block copolymer poly(*N*,*N*-diethylacrylamide)-*b*-poly(4-acryloylmorpholine) in tetrahydrofuran was investigated in Chapter 7. PDEA-*b*-PAM was analysed via DLS, UV-VIS and cryo TEM, revealing an UCST behaviour of the high molar mass PAM block building block leading to blue dispersion. The main aim of the following thesis is to

decrease the required overall polymer concentration for the phase separation and aggregation of hydrophilic homopolymers and DHBCs.

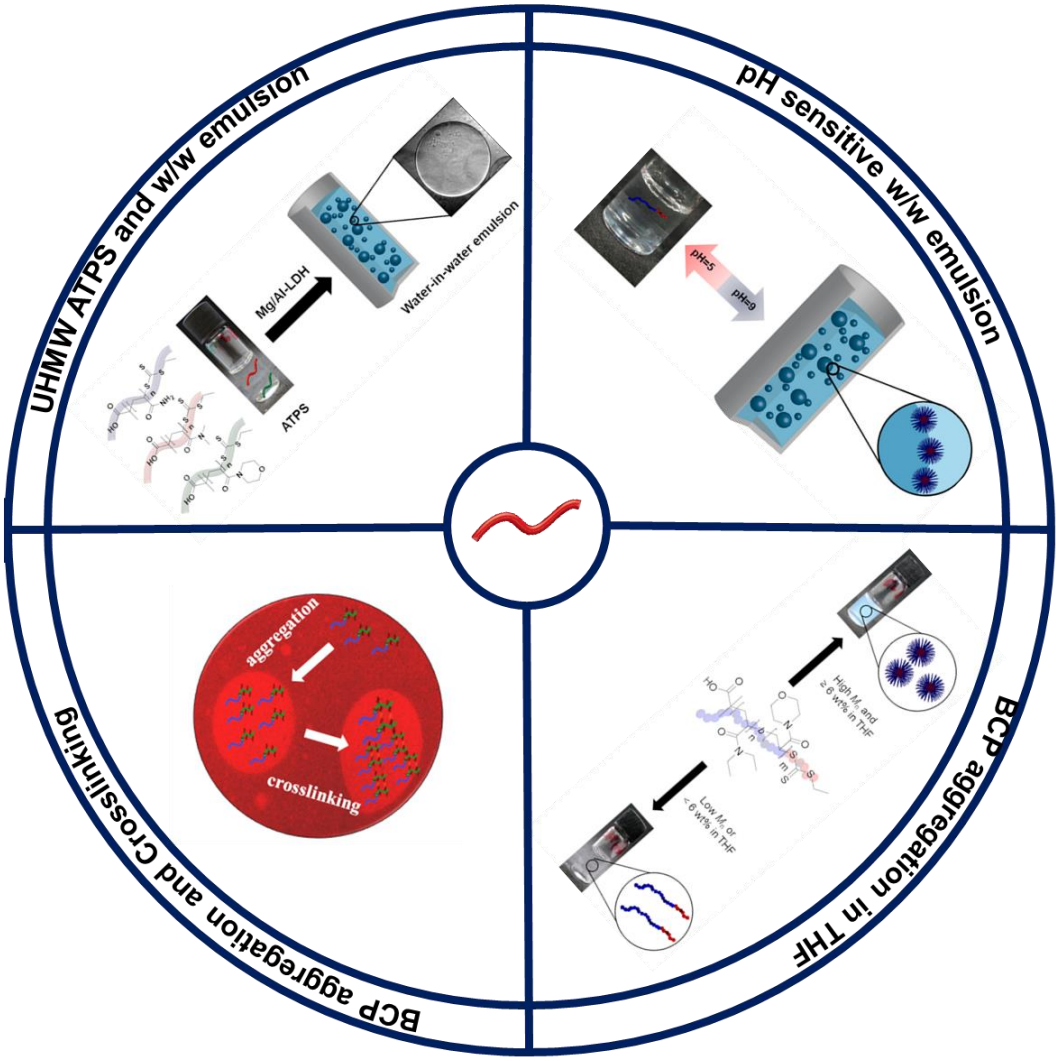

Scheme 3.1. Overview of the different utilisation of hydrophilic polymers for self-assembly or phase separation in this thesis.

Chapter 4

4 Materials and methods

4.1 Abbreviations

^{13}C-NMR	carbon nuclear magnetic resonance
^{1}H-NMR	proton nuclear magnetic resonance
ATPS	Aqueous two-phase system
A3PS	Aqueous three phase system
CL	crosslinker
CLSM	confocal laser scanning microscopy
Cryo	cryogenic
CTA	chain transfer agent
CuAAC	copper(I) catalysed azide alkyne cycloaddition
$Đ$	molecular dispersity
DHBC	double hydrophilic block copolymer
DLS	dynamic light scattering
DOSY-NMR	diffusion ordered spectroscopy NMR
λ	wavelength
LCST	lower critical solution temperature
LDH	layered double hydroxide
M	mol · L^{-1}
MALS	multi angle light scattering
M_n	average number weighted molecular weight

M_w	average mass weighted molecular weight
MWCO	molecular weight cut off
NMRP	nitroxide-mediated radical polymerisation
pH	-log c (H^+)
PI	photo iniferter
RAFT	reversible-addition fragmentation chain transfer
RDPR	reversible deactivation radical polymerisation
RT	room temperature
SEC	size exclusion chromatography
SEM	scanning electron microscopy
TEM	transmission electron microscopy
T_g	glass transition temperature
UCST	upper critical solution temperature
UV	ultraviolet
UV-VIS	ultraviolet to visible light
VIS	visible
wt. %	weight per cent
w/w	water-in-water

4.2 Materials

Materials were used as received unless otherwise noted. Deionised and ultra-pure water were obtained from a Sartorius Arium pro ultrapure water system.

Material	Abbreviation	purity	Vendor
Acetone		analytical grade	Fisher
Acetic acid		1.0 M	VWR chemicals
4-acryloylmorpholine[1]	AM	98 %	Sigma Aldrich
acrylamide	AAM	98 %	Sigma Aldrich
Aluminium oxide	Al_2O_3	basic	Sigma Aldrich
Aluminium nitrate nonahydrate		98%	Sigma-Aldrich
Ascorbic acid		98 %	Alfa Aesar
Azobis(isobutyronitrile)[2]	AIBN	99 %	Sigma Aldrich
1,3-bis(aminooxy)propan dihydrochloride		98 %	Sigma Aldrich
2-bromisobutyric acid		98 %	Sigma Aldrich
3-bromo-1-propanol		97 %	Sigma Aldrich
carbon disulfide	CS_2	99 %	Sigma Aldrich
copper sulfate	$CuSO_4$	99 %	Carl Roth
dichloromethane	DCM	analytical grade	VWR chemicals
***N,N'*-dicyclohexylcarbodiimide**	DCC	99 %	Sigma Aldrich
***N,N*-diethylacrylamide**[1]	DEA	98 %	TCI
***N,N*-dimethylacrylamide**[1]	DMA	99 %	Sigma Aldrich
4-dimethylaminopyridine	DMAP	99 %	Sigma Aldrich
***N,N*-dimethyl formamide**	DMF		SLS

dimethyl sulfoxide	DMSO	analytical grade	VWR chemicals
***N*-(1,1-dimethyl-3-oxobutyl)acrylamide**		99 %	Sigma-Aldrich
dodecanethiol		98 %	Alfa Aesar
ethanethiol		98 %	Alfa Aesar
ethyl acetate		99.5 %	VWR chemicals
Fluorescein isothiocyanate	FITC		Sigma Aldrich
n-hexane		95 %	Sigma Aldrich
hydrochloric acid	HCl	Conc.	Fisher
Magnesium nitrate hexahydrate		99.8 %	Sigma-Aldrich
methanol	MeOH		
***N*-methyl-2-pyrrolidone**	NMP	GC grade	Fluka
Oligo(ethylene glycol methyl ether) methacrylate	OEGMA	M_n= 500 g mol^{-1}	Sigma-Aldrich
poly(styrene) latex nanoparticles negatively charged		0.1 µm, 10 wt % aqueous suspension	Sigma-Aldrich
potassium phosphate	K_3PO_4		Sigma Aldrich
propagylamine		98 %	Sigma Aldrich
pullulan	Pull	pure	TCI
Rhodamine B isothiocyanate	RITC	98 %	Sigma Aldrich
sodium azide		99 %	Fluka
sodium acetate		anhydrous 98 %	Fisher
sodium cyanoborohydride	$NaCNBH_3$	95%,	Sigma Aldrich
Sodium hydroxide	NaOH		Fisher
Sulforhodamine B			Sigma Aldrich
tetrahydrofuran	THF		
triethylamine	Et_3N	99.5 %	Sigma Aldrich
7-[4-(trifluoromethyl)coumarin]acrylamide		98 %	Sigma Aldrich

[1] Monomer was passed over a column of basic aluminium oxide

[2] AIBN was recrystallized from MeOH at 50 °C.

Photo iniferter RAFT (PI-RAFT) polymerisation was initiated with two 50 W LED chips (Foxpic High Power 50 W LED Chip Bulb Light DIY White 3800LM 6500 K) or with UV-light (UV nail-light-curing-lamp, λ = 365 nm).

4.3 Applied methods

Nuclear magnetic resonance (NMR) spectroscopy

^{1}H-NMR spectra were recorded in deuterium oxide (D_2O, Aldrich) at ambient temperature at 400 MHz with a Bruker Ascend400 or at 600 MHz with an Agilent600. ^{13}C spectra were recorded in deuterium oxide (D_2O, Aldrich) at 600 MHz with an Agilent600. DOSY was performed in deuterium oxide (DMSO-d_6, Aldrich) at 600 MHz with an Agilent600 using the Dbppste_CC pulse sequence.

Bright field microscopy

Bright field microscopy was performed on Zeiss LSM710 confocal microscope (Zeiss, Göttingen, Germany) and software Carl Zeiss ZEN 2011 v7.0.3.286. LD EC Epiplan NEUFLUAR 50X, 0.55 DIC (Carl Zeiss, White Plains, NY, USA), NEUFLUAR 20X, 0.55 DIC (Carl Zeiss, White Plains, NY, USA) and N-Achroplan 10x/0.25 Ph 1 (Carl Zeiss, White Plains, NY, USA) objectives were used. All samples were prepared in a CELLview (Greiner Bio-One, Stonehouse, UK) 35 mm plastic cell culture dish with a borosilicate glass bottom.

Cryogenic scanning electron microscopy (cryo SEM)

Cryo SEM was conducted with a Jeol JSM 7500 F and the cryo-chamber from Gatan (Alto 2500).

Cryogenic transmission electron microscopy (cryo TEM)

Cryo TEM was performed under following conditions: 3.6 μL of polymer solution were loaded onto freshly glow discharged Quantifoil 1.2/1.3 holey carbon support film, grids were blotted for 3 seconds and plunged into a bath of liquid nitrogen cooled liquid ethane. Specimen vitrification was performed in a Vitrobot Mark 4 from Thermo Fisher held at 22 °C and 95% humidity. Vitrified samples were held in a Gatan 626 cryostage and imaged in a JEOL F200 cryo transmission electron microscope equipped with a Direct Electron DE20 detector. Images were recorded at an accelerating voltage of 200 keV.

Confocal laser scanning microscopy (CLSM)

CLSM was performed on Zeiss LSM710 confocal microscope (Zeiss, Göttingen, Germany) and software Carl Zeiss ZEN 2011 v7.0.3.286. LD EC Epiplan NEUFLUAR 50X, 0.55 DIC (Carl Zeiss, White Plains, NY, USA), NEUFLUAR 20X, 0.55 DIC (Carl Zeiss, White Plains, NY, USA) and N-Achroplan 10x/0.25 Ph 1 (Carl Zeiss, White Plains, NY, USA) objectives were used. All samples were prepared in a CELLview (Greiner Bio-One, Stonehouse, UK) 35 mm plastic cell culture dish with a borosilicate glass bottom. The images were taken with three different channels for the particular dyes (RITC, FITC or coumarin) and for a bright field image.

Differential Scanning Calorimetry (DSC)

DSC was measured on a DSC 204 by Netzsch in the range from -100 °C to 220 °C. The results from the second cycle were used for data evaluation.

Dynamic light scattering (DLS)

DLS in Chapter 6 was performed using an ALV-7004 Multiple Tau Digital Correlator in combination with a CGS-3 Compact Goniometer and a HeNe laser (Polytec, 34 mW, λ = 633 nm at θ = 90° setup for DLS). Toluene was used as immersion liquid and sample temperatures were adjusted to 25 °C. Apparent hydrodynamic radii (R_{app}) were determined from fitting autocorrelation functions using the CONTIN algorithm.

DLS in Chapter 4,5 and 7 was performed on a ZetaSizer by Malvern with water or THF as solvent.

Size exclusion chromatography (SEC)

Multi angle light scattering (MALS) Detection

SEC of UHMW PDMA and PAAM were conducted in 0.1 M aqueous $NaNO_3$ buffer at 25 °C using a column system with a PL Aquagel-OH Guard and PL Aquagel-OH MIXED-H and Viscotek VE 3580 RI detector and Viscotek SEC-MALS 20 for the molar mass determination. The system was calibrated with pullulan standards.

SEC of UHMW PAM was conducted in THF at 25 °C using a PSS SD guard column, a PSS SDV-Linear-M column, Wyatt Optilab DSP RI detector and a Wyatt DAWN EOS detector.

A Brookhaven differential refractometer was used for the determination of d*n*/d*c*

Standard calibration

SEC of PAM was conducted in NMP and 0.005 mol · L^{-1} LiBr with methyl benzoate as internal at 70 °C using a column system with a PSS GRAM VS; PSS GRAM 7 µm 100 A; PSS GRAM 7 mm, 1000 A and PSS SECurity Refractive Index-1260 RID and calibration with polystyrene (PS) standards.

SEC of $PDEA_{98}$ and $PDEA_{98}$-*b*-PAM_{387} were conducted in THF at 35 °C using a column system with an Agilent PL Gel Guard Column (5 µm) and an Agilent PL Gel Mixed-D Column (5 µm) as well as an Agilent Infinity1260 II RID and calibration with PS standards.

SEC of $PDEA_{1850}$ and $PDEA_{1850}$-*b*-PAM_{1380} was conducted in THF at 25 °C using a PSS SD guard column, a PSS SDV-Linear-M column, Wyatt Optilab DSP RI detector and a Wyatt DAWN EOS detector.

SEC of pullulan and acrylamides were conducted in acetate buffer containing 20% methanol with the salt peak as internal standard at 25 °C using a column system with a PSS Suprema VS; PSS Suprema 10 µm, 30 A; PSS Suprema 10 µm and PSS SECurity Refractive Index-1260 RID and calibrated with pullulan standards.

UV-VIS

Cloud point (Tcp) measurements were performed with a Shimadzu UV-3600 UV-Vis-NIR spectrometer and a Shimadzu TCC-100 temperature-controlled cell holder. Sample in glass cuvette was placed in the sample holder and equilibrated and held at 50 °C for 5 min. Afterwards, the samples were cooled down manually in 5 or 2 °C steps and held at each temperature for 2 min. Over the entire time, transmittance at 450 nm was recorded and plotted as a function of temperature. Tcp was determined as the temperature at which samples exhibit half of the initial transmittance.

Chapter 5

5 All-Aqueous Multi-Phase Systems and Emulsions Formed *via* Low-Concentrated Ultra-High-Molar Mass Polyacrylamides

5.1 Introduction[a]

A key factor for the self-assembly or dispersion of multiple hydrophilic polymers in aqueous solution e.g., aggregation of block copolymers or in w/w emulsions, is the phase separation of different hydrophilic polymers in an aqueous mixture. A liquid-liquid phase separation of two compounds e.g., polymer/polymer, is driven by the enthalpy associated with for example water-polymer interaction and the opposing loss of entropy during phase separation process.[69, 132] If hydrophilic polymers form an aqueous multi-phase system, it is more likely the corresponding block copolymers aggregate as well.

Due to the high biocompatibility, w/w-emulsions[83, 133] are an interesting application for water-based polymer systems like ATPSs. However, in contrast to oil/water or water/oil emulsions, the interfacial tension of an ATPS is significantly lower and the interface between the aqueous phases is very wide. Therefore, stabilisation based on surfactants or larger particles is not suitable for w/w emulsions.[84, 134, 135] One avenue to stabilise w/w emulsions or suspensions is via platelets like layered double hydroxide (LDH) particles.[87, 88] For example, O'Reilly and co-workers showed that 2D diamond-shape poly(lactide) block copolymer nanoplatelets can successfully stabilise w/w emulsions. Due to the considerable surface and significant interface to volume ratio, especially larger platelets exhibit strong emulsion stabilisation effect.[94]

In the literature a significant number of studies were presented regarding the influence of molar mass on the formation of ATPS.[73, 74, 136, 137] These studies showed that the location of the binodal, which is the line that separates one- and two-phase region of the phase diagram, strongly depends on the molar mass of the used polymers. In the example for the system PEG and Dex, the higher the molar mass, the lower the required concentration for ATPS formation.[74, 136] However, most frequently ATPS are formed with a polymer concentration above 4 wt%,

[a] Terms of use: This chapter was adapted with permission from: A. Plucinski, M. Pavlovic, B. V. K. J. Schmidt, *Macromolecules* **2021**, 54, 12, 5366–5375, Copyright © 2021, American Chemical Society. Contribution by A. Plucinski in the following chapter about 90%.

which is a considerable issue for applications due to increased viscosity, costs, and often unspecific interaction with the surrounding medium. In order to decrease the required amount of polymer material for a stable ATPS and in correlation for a w/w emulsion, increased molar mass of the employed polymers could be a useful development for the field.

Due to their aggregation behaviour in water as part of DHBCs, shown in former studies in our group,[58, 59] poly(acrylamides) represent a good choice for an ATPS and the formation of w/w emulsions. To investigate novel high molar mass poly(acrylamide) based ATPS, reversible-deactivation radical polymerisation like reversible addition fragmentation chain transfer (RAFT) polymerisation, is a good approach for polymer synthesis.[44, 138-140] Especially the procedure from Sumerlin and co-workers seems promising to obtain high molar mass poly(acrylamides) as performed *via* photo iniferter (PI) RAFT polymerisation, which readily achieves molar masses above $1 \cdot 10^6$ g·mol^{-1}.[44, 140]

This chapter will focus on the phase behaviour of three different high molar mass hydrophilic polymers in ATPS formation. Therefore three polymers with high molar mass, i.e. poly(*N*,*N*-dimethylacrylamide) (PDMA), poly(acrylamide) (PAAM), and poly(4-acryloylmorpholine) (PAM), were synthesised *via* PI-RAFT polymerisation. Subsequently, the polymers were analysed by ^{1}H-NMR spectroscopy and size exclusion chromatography (SEC). Additionally, the mixtures of each polymer combination, at low concentrations, were investigated revealing the formation of ATPS or aqueous three phase system (A3PS). Moreover, the ATPSs were used to form w/w emulsions, stabilised with Mg/Al-CO_3-LDH nanoparticles.[b] These emulsions were further analysed *via* confocal laser scanning microscopy (CLSM). In order to localise the polymer in the emulsion, Rhodamine B (RhB), fluorescein and Coumarin labelled hydrophilic polymers were employed.

[b] LDH nanoparticles were synthesised by M. Pavlovic

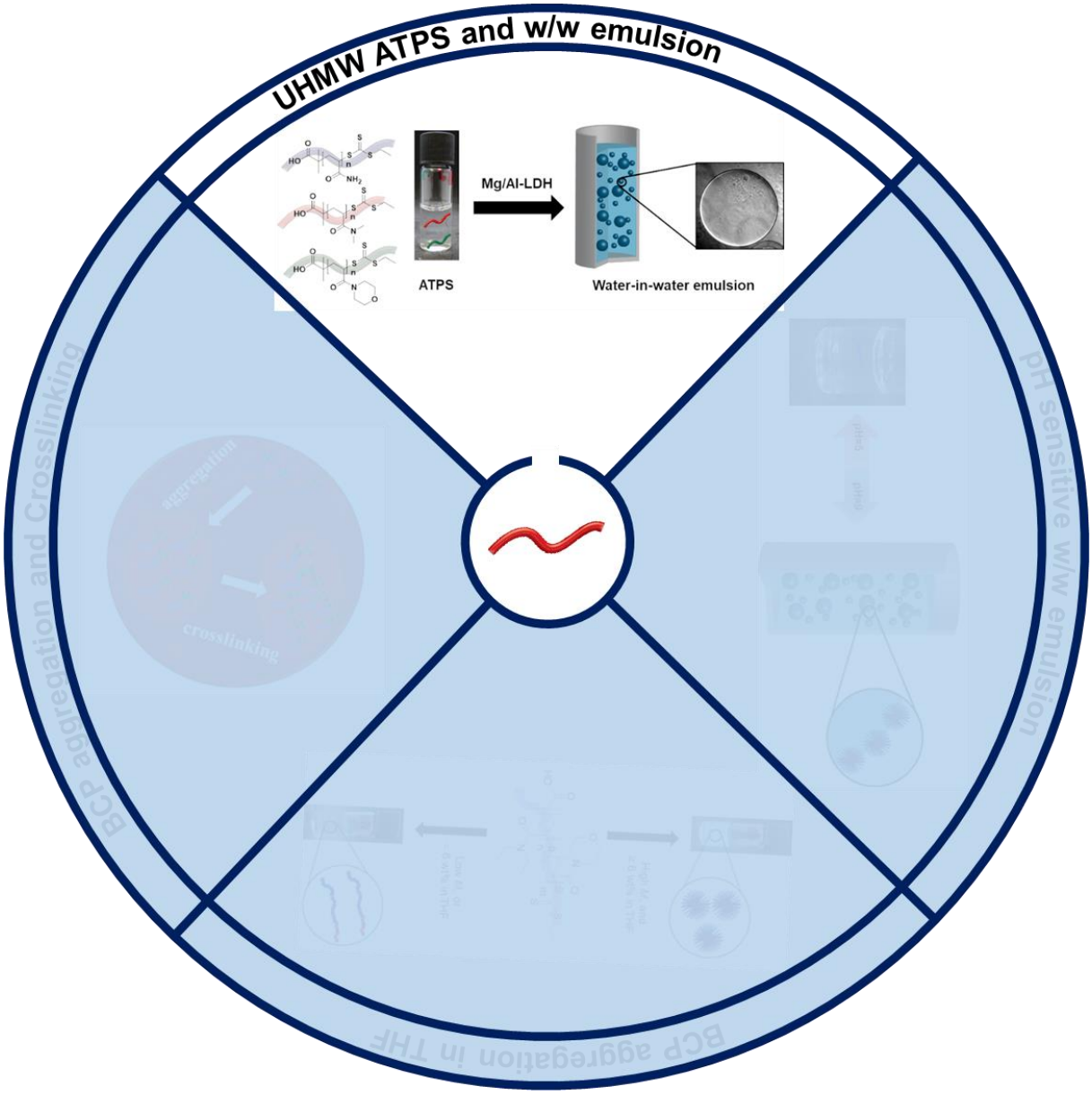

Scheme 5.1. Overview of the different utilisation of hydrophilic polymers for self-assembly or phase separation, higlighted the part of the current chapter: UHMW ATPS and w/w emuslion.

5.2 Synthesis of Poly(acrylamides) via PI RAFT polymerisation

In order to analyse the self-assembly and phase separation of ultra-high molar mass poly(acrylamides) in aqueous solution, the polymers poly(*N*,*N*-dimethylacrylamide) (PDMA), poly(acrylamide) (PAAM) and poly(4-acryloylmorpholine) (PAM) were synthesised *via* PI RAFT polymerisation and the phase behaviour in aqueous solution was investigated.

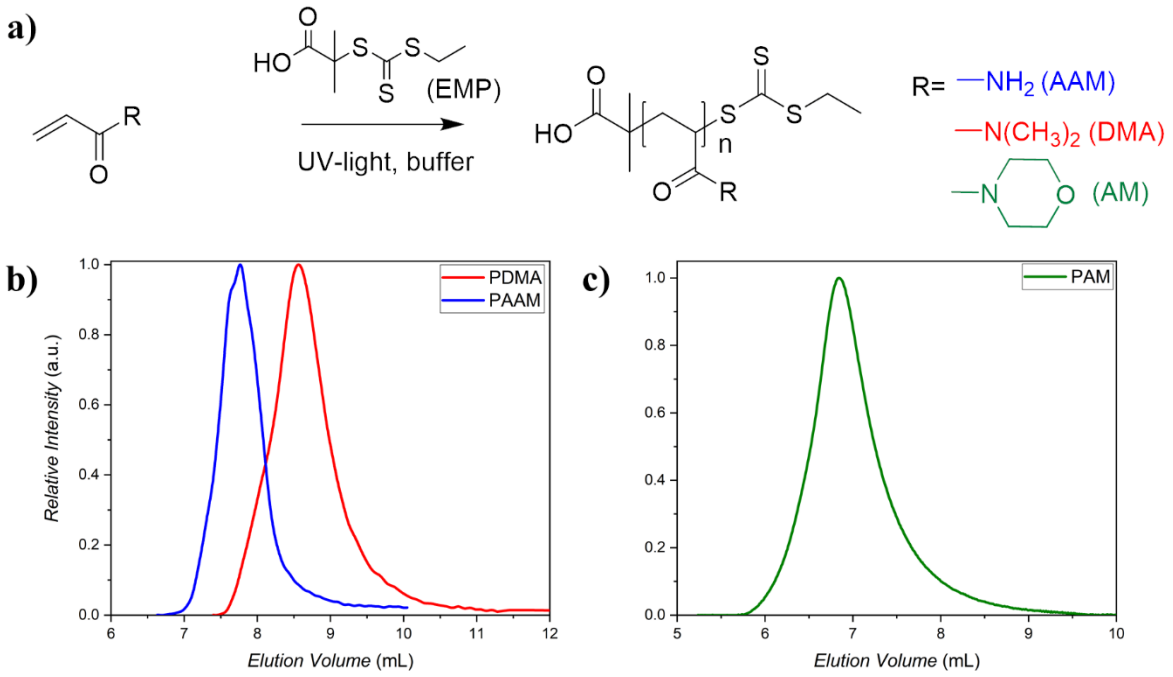

Figure 5.1. (a) Reaction scheme of the PI RAFT-polymerisation of acrylamides with EMP as chain transfer agent, (b) Results of Multi-Angle Light Scattering (SEC-MALS) of PDMA and PAAM measured in 0.1 N $NaNO_3$ buffer, (c) result of SEC-MALS measurement of PAM measured in THF.

Table 5-1. Results of SEC-MALS measurement of PDMA and PAAM measured in 0.1 N $NaNO_3$ buffer and SEC-MALS measurement of PAAM measured in THF.

Polymer	M_n **(kg·mol^{-1})**	$Đ$	**d*n*/d*c* (mL g^{-1})**
PDMA	1070	1.4	0.1728 ± 0.0039
PAAM	730	1.7	0.2005 ± 0.0005
PAM	1040	1.1	0.1957 ± 0.0008

RAFT polymerisation is a well-known avenue to synthesise polymers like PDMA, PAAM and PAM. In order to synthesise high molar mass poly(acrylamides) the procedure of Sumerlin and co-workers was employed.[44] 2-(((Ethylthio)carbonothioyl)thio)-2-methylpropanoic acid (EMP) was used as chain transfer agent and the reaction was initiated in acetate buffer *via* UV-light (nail-lamp, λ=365 nm). A high concentrated solution of monomer (> 7 M) was utilised and the ratio between monomer and EMP was adjusted to 10,000-21,000 (depending on the monomer): 1 to obtain a theoretical molar mass of around $1.5 \cdot 10^6$ g·mol^{-1}. To obtain a high molar mass a low amount of EMP was employed, and the reaction was initiated by UV-light, in order to decrease the number of radicals in the reaction and enable fast initiation, in comparison to the thermal RAFT-polymerisation with exogenous radical initiation. All conversions were determined by ^{1}H-NMR (Figure 5.12 -14), which revealed a quantitative monomer conversion for all polymerisations. The poly(acrylamide) products were analysed *via* SEC-MALS revealing ultra-high molar masses and rather broad molar mass distributions with M_n= 1.07 · 10^6 g · mol^{-1} and $Đ$ = 1.4 for PDMA, M_n= 730,000 g · mol^{-1} and $Đ$ = 1.7 for PAAM, and M_n= 1.04· 10^6 g · mol^{-1} and $Đ$ = 1.5 for PAM (Figure 5.1 and Table 5.1). Although RAFT polymerisation was employed, rather high $Đ$ were observed which might be due to a low efficiency of initiation, *i.e.* radical termination and low initiation rate, as also obvious by the tailing of the polymer related peaks in SEC towards lower molar masses. Additionally, the PI-RAFT polymerisation was conducted in high concentrated solution, which leads to increasing of the viscosity during the polymerisation. The significantly increase of viscosity could have an influence on the conversion of the polymerisation and the termination processes.

5.3 ATPS of ultra-high molar mass acrylamides

In order to elucidate the phase behaviour of the different ultra-high molar mass poly(acrylamide) mixtures in aqueous solution, ATPS formation of the three poly(acrylamides) was investigated. For that, a phase diagram was assembled for each combination (PDMA/PAAM, PDAM/PAM, and PAAM/PAM). To analyse the phase behaviour of the ATPSs, five differently concentrated stock solutions were prepared for all combinations (9, 7.5, 5, 2.5, and 1 (w/w)). Two different stock solutions were mixed together to obtain a total polymer concentration of 5 wt% (4.5/0.5, 3.75/1.25, 2.5/2.5, 1.25/3.75 and 0.5/4.5 (w/w)). Subsequently, the solutions were mixed, equilibrated at ambient temperature to demix, investigated, and diluted to find the concentration at which only one phase is observed (Figure 5.2 a). To generate the phase

diagram, the last concentration, where a phase separation was observed was used as data point in the binodal, which is the line that separates one- and two-phases in the graph.

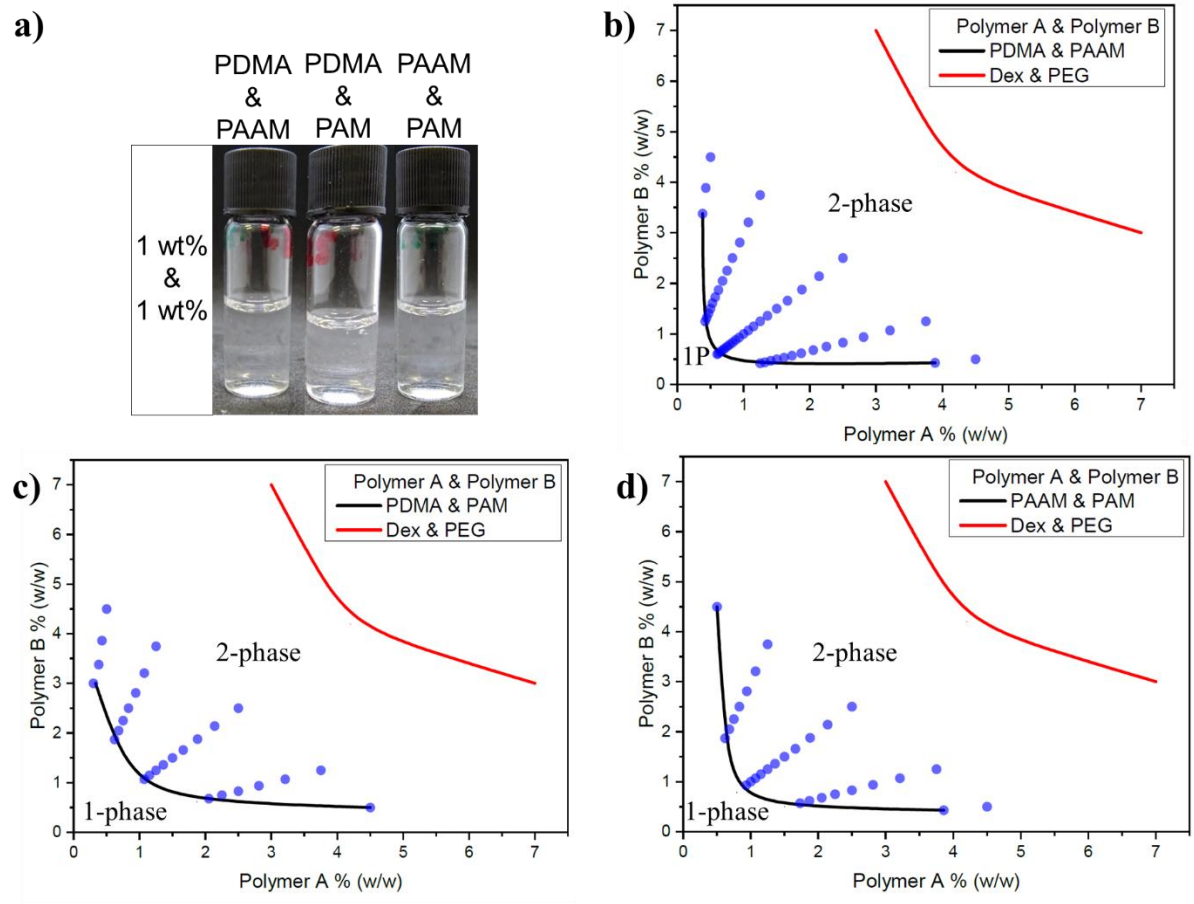

Figure 5.2. ATPS of each combination at a total polymer concentration of 2 wt% (1wt%/1wt%). (b-d) Phase diagrams of the ATPS for all polymer combinations showing the experimental binodals (black curves) and the dilution steps (blue dots): (b) PDMA and PAAM, (c) PDMA and PAM, (d) PAAM and PAM, in comparison to the ATPS of Dextran (M_n=40,000 g·mol^{-1}) and PEG (M_n=35,000 g·mol^{-1}) (red curve).

The binodal was located at significantly lower concentrations for the combination of PDMA and PAAM, in comparison to the commonly used ATPS formed by commercial Dex/PEG.[70, 75, 77] It should be noted the comparison ATPS formed by Dex and PEG are at lower molar mass, which is the commonly used system. The lowest concentration for an observed ATPS, for the equal concentration of the polymers was 0.56 wt% (Figure 5.2b). The phase diagram indicates that for a stable ATPS of PDMA/PAAM the concentration of polymers could be seven times lower compared to the common Dex/PEG system. For the ATPS formed by PDMA and PAM (Figure 5.2c), the slope of the binodal was more flat than for PDMA/PAAM. In comparison to Dex/PEG, the binodal was again at significant lower concentration. The lowest concentration

for an observed ATPS, for the equal concentration of the polymers, was 0.9 wt%. For the polymer combination of PDMA and PAAM the required concentration for a stable ATPS is around four times lower, in contrast to Dex/PEG. The phase diagram for the combination of PAAM and PAM (Figure 5.2 d) is similar to the phase diagrams of the previous combinations. The minimal concentration for a stable ATPS was found to be at 0.79 wt%. In comparison to the ATPS, formed by Dex/PEG, the concentration for a stable ATPS of PAAM and PAM could be five times lower. Surprisingly the results show that the mixtures of the most hydrophilic polymers (PDMA & PAAM) require the lowest concentration for phase separation. This in contrast to our expectation that for the formation of a macroscopic phase separation, the combination featuring the most different hydrophilicity should form the most stable phase separation. One reason for that could be the influence of the high hydration enthalpies of PDMA and PAAM, which equalise the loss of entropy during the phase separation.

In order to understand these differences, the location of each polymer was detected *via* ^{1}H-NMR of each phase (Figure 5.16 - 18) with DMF as internal standard. The results showed for the combination of PDMA and PAAM a clear separation of the polymers in the phases after 24 hours (Figure 5.3 a). PDMA was located in the upper and PAAM in the lower phase, which is similar to the most studied ATPS formed by PEG and Dex.[141] In here, the PEG is enriched in the upper phase and Dex is enriched in the lower phase. The combination of PDMA and PAM showed a less clear separation after 24 hours. PAM was located in the lower phase but PDMA is present in both phases (Figure 5.3 b). In the case of PAAM and PAM, the polymers are clearly separated in different phases.

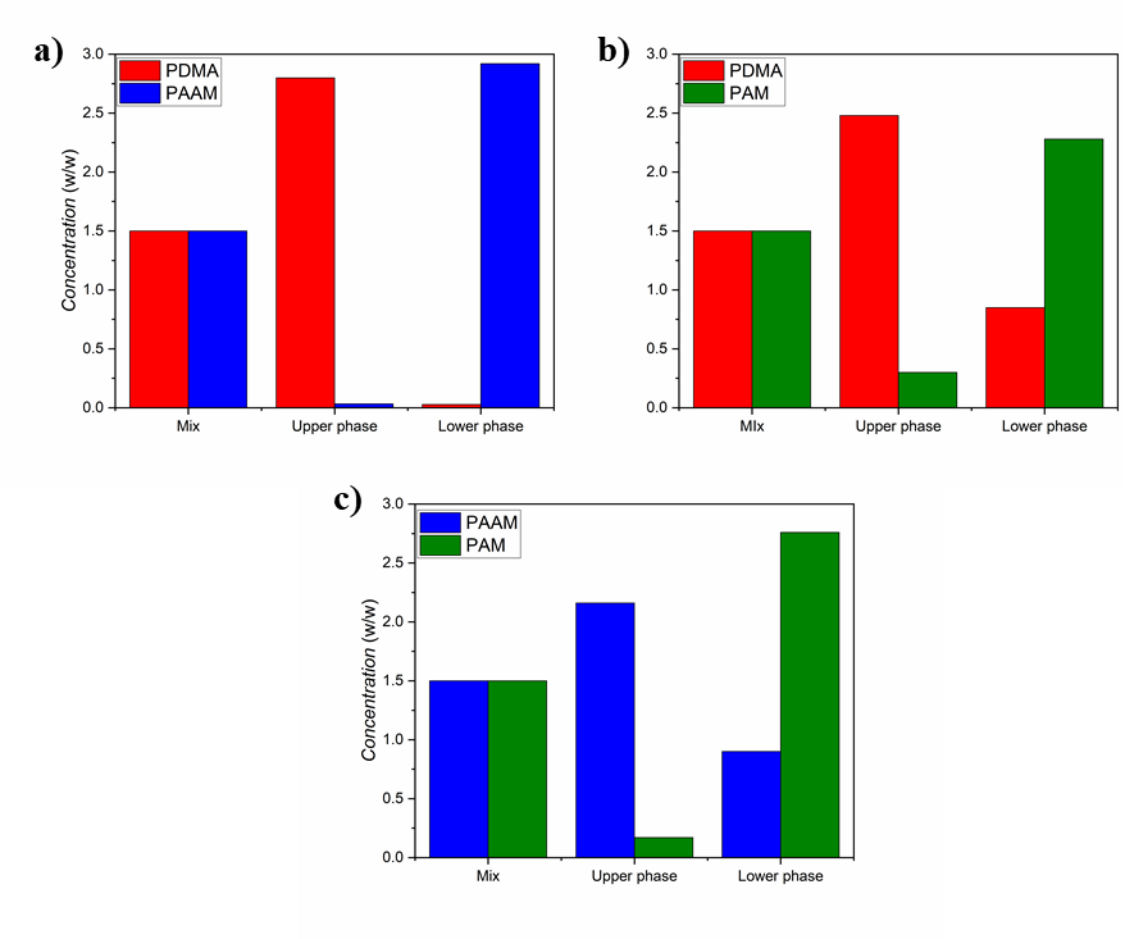

Figure 5.3. (a-c) Concentration before and after observed phase separation (24 h), detected via ^{1}H-NMR in D_2O using DMF as internal standard, of PDMA (red), PAAM (blue) and PAM (green) for (a) ATPS PDMA & PAAM, (b) ATPS PDMA & PAM and (c) ATPS PAAM & PAM.

However, in both phases, a small amount of the other polymer is present as well (Figure 5.3 c). The NMR results show that the combination with the best separation of the polymers also features the lowest concentration required for phase separation (PDMA and PAAM). One reason for the good phase separation of PDMA and PAAM, could be because of the high hydrophilicity of both polymers and thereby significant water polymer interaction. Apparently, the extent of separation of the polymers in different phases is an important parameter to lower the concentration required for ATPS formation. Furthermore, the concentration for a successful phase separation is dependent on the molar mass of the poly(acrylamides) (Figure 5.19).

5.4 Water-in-water emulsions of ultra-high molar mass poly(acrylamides)

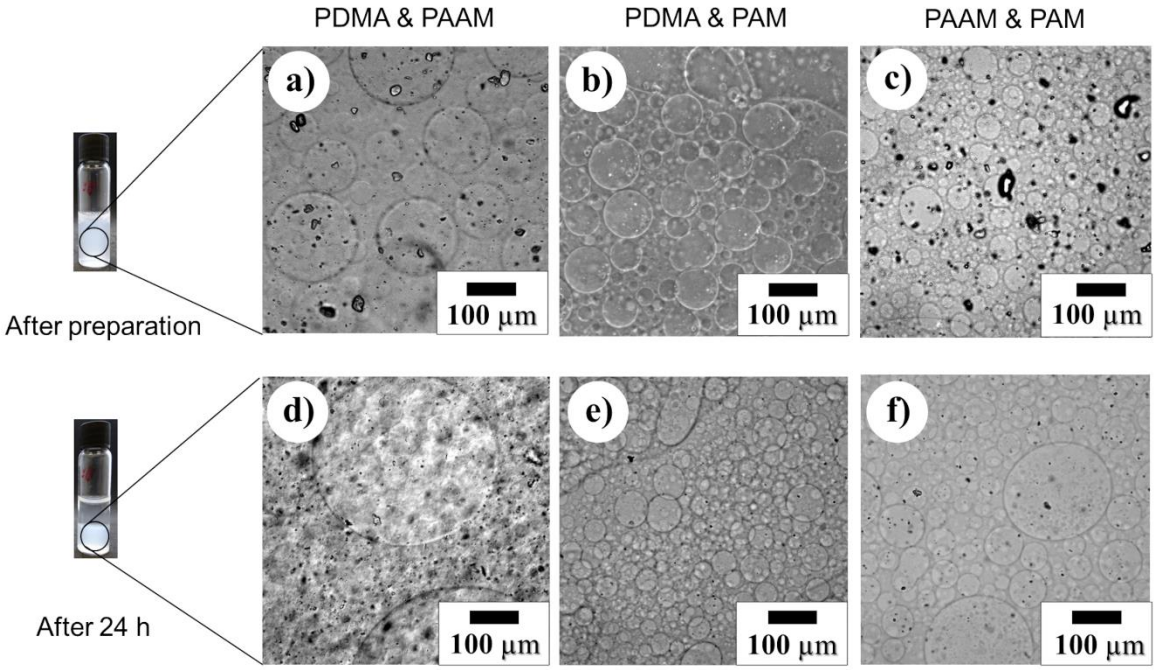

Figure 5.4. (a-c) Bright field microscopy images of the water-in-water emulsion of each ATPS (1.5 wt%/1.5 wt%) stabilised with Mg/Al-CO_3-LDH (0.1 wt%) (a) PDMA and PAAM, (b) PDMA and PAM, (c) PAAM and PAM, (d-f) bright field images of the cloudy phase after 24 h for (d) PDMA and PAAM, (e) PDMA and PAM, (f) PAAM and PAM.

In order to form w/w emulsions, an ATPS for all three polymer combinations (PDMA & PAAM, PDMA & PAM and PAAM & PAM) was prepared at 1.5/1.5 wt%. The concentration was chosen to be placed well in the two-phase region of the phase diagram to obtain a stable ATPS. In order to stabilise the w/w emulsion, a 0.2 wt% aqueous dispersion of Mg/Al-CO_3-LDH nanoparticles[142-144] with 100 nm diameter were added to the ATPS to give a final concentration of 0.1 wt%. Subsequently, the mixture was subjected to ultrasonic treatment for two minutes as well as shaking by hand for one minute. In all three combinations the mixture turned cloudy, which is an indicator for formation of an emulsion. Next, the emulsions were analysed directly *via* bright field microscopy (Figure 5.4 a-c). After approximately two hours the dispersions started to phase separate, which was completed after around 24 hours. The lower phase remained cloudy for all combinations. Both phases were analysed *via* bright field microscopy to identify the composition of the phases (Figure 5.4 d-f). It should be noted that in the bright field images of all combinations aggregated stabiliser particles were visible in the

background of the emulsion (black particles). To investigate the stability of the emulsion, the phase separation was analysed *via* bright field microscopy after 4 weeks again (Figure 5.21). Therefore, the size of the emulsion droplets of all combinations were determined from bright field images and averaged (Table 5.2), which revealed slight changes of droplet size with time after phase separation.

Bright field microscopy shows droplet formation for the emulsion based on PDMA and PAAM with an average droplet size around 82 ± 58 µm (Figure 5.4 a). For the w/w emulsion of PDMA and PAAM the phase separation begins to start after around two hours and a completely visible phase separation was observed after 24 hours. The upper phase was clear, while the lower phase was cloudy indicating the presence of droplets. In order to confirm the presence or absence of droplets both phases were analysed *via* bright field microscopy after phase separation (Figure 5.4 d). In the clear upper phase, the bright field images show no presence of droplets, while the images of the cloudier lower phase show droplets featuring an increased size compared to the emulsion before phase separation. The average droplet size after phase separation, in the cloudy phase was around 122 ± 120 µm. Long-term stability was probed as well, which confirmed that phase separation after four weeks was similar to the phase separation after 24 hours. Also, bright field imaging shows the presence of droplets in the cloudy phase with droplets larger than 100 µm after four weeks (Figure 5.21).

For the system of PDMA and PAM, bright field imaging displayed the presence of droplets in the w/w emulsion as well (Figure 5.4 b). The average droplet size was slightly higher, with around 101 ± 33 µm in comparison to the PDMA and PAAM system. As with all investigated emulsions, phase separation was observed and both phases were analysed *via* bright field microscopy after 24 h (Figure 5.4 e). In the images of the clear upper phase, no droplets were visible, while the bright field images of the lower cloudy phase revealed droplets. The average droplet size is around 63 ± 24 µm and smaller in comparison to the emulsion before the phase separation, which might be due to an incomplete phase separation after 24 hours. This reason is supported by the observed droplet size >100 µm after four weeks.

Table 5-2. Average droplet size of 1.5/1.5 wt% ATPS and 0.1 wt% LDH additive before phase separation, after 24 hours of phase separation and after four weeks of phase separation, averaged over 30 particles.

ATPS	Droplet Size Emulsion [µm]	Droplet size after phase separation (24h) [µm]	Droplet size after phase separation (4 weeks) [µm]
PDMA & PAAM	82.0 ± 58.3	122.4 ± 119.8	134.9 ± 93.5
PDMA & PAM	101.2 ± 33.5	63.0 ± 24.2	125.4 ± 45.9
PAAM & PAM	64.4 ±16.2	98.3 ± 39.7	99.3 ± 48.1

The bright field measurement of the emulsion formed by the ATPS PAAM and PAM, displayed droplets with a size between 30 and 100 µm and an average droplet size of around 64 ± 16 µm (Figure 5.4 c), which is the smallest amongst the studied emulsions. After 24 hours and phase separation, droplets between 50 and 200 µm and an average droplet size of around 98 ± 40 µm were observed *via* bright field microscopy in the emulsion phase (Figure 5.4 f), while the upper clear phase showed no droplets. After four weeks of phase separation, the emulsion phase displayed droplets in the range of 60 and 150 µm, which is similar to the droplets after 24 hours of phase separation. The high standard deviation is due to the presence of larger and smaller droplets. High dispersity in the samples was the result of the mixing method (shaking and ultrasonic bath). One way to produce emulsion droplets with lower dispersity is for example the use of microfluidic devices.

Overall, for all three ATPS combinations with Mg/Al-CO_3-LDH as additive, an emulsion could be observed at low concentration (1.5/1.5 wt%). After 24 hours of phase separation, in two of the three combinations the droplet sizes increased significantly. The droplet size increases most likely due to the phase separation and Ostwald ripening during the phase separation process until an equilibrium is reached. Furthermore, the emulsion was only stable in the lower phase of the ATPS, which is presumably due to the enrichment of LDH particles in the lower phase after phase separation. For the combination of PDAM and PAM the droplet sizes of the emulsion decrease. After four weeks of phase separation, all three combinations display similar droplet sizes >100 µm. Obviously, the prepared w/w emulsions feature a broad dispersity of droplet sizes, which is mainly due to the preparation process. As such, the droplet size and dispersity could mostly likely be tailored via a different preparation method *e.g.*, microfluidics or further optimisation in mixing *via* vortex and subsequently ultrasound treatment.

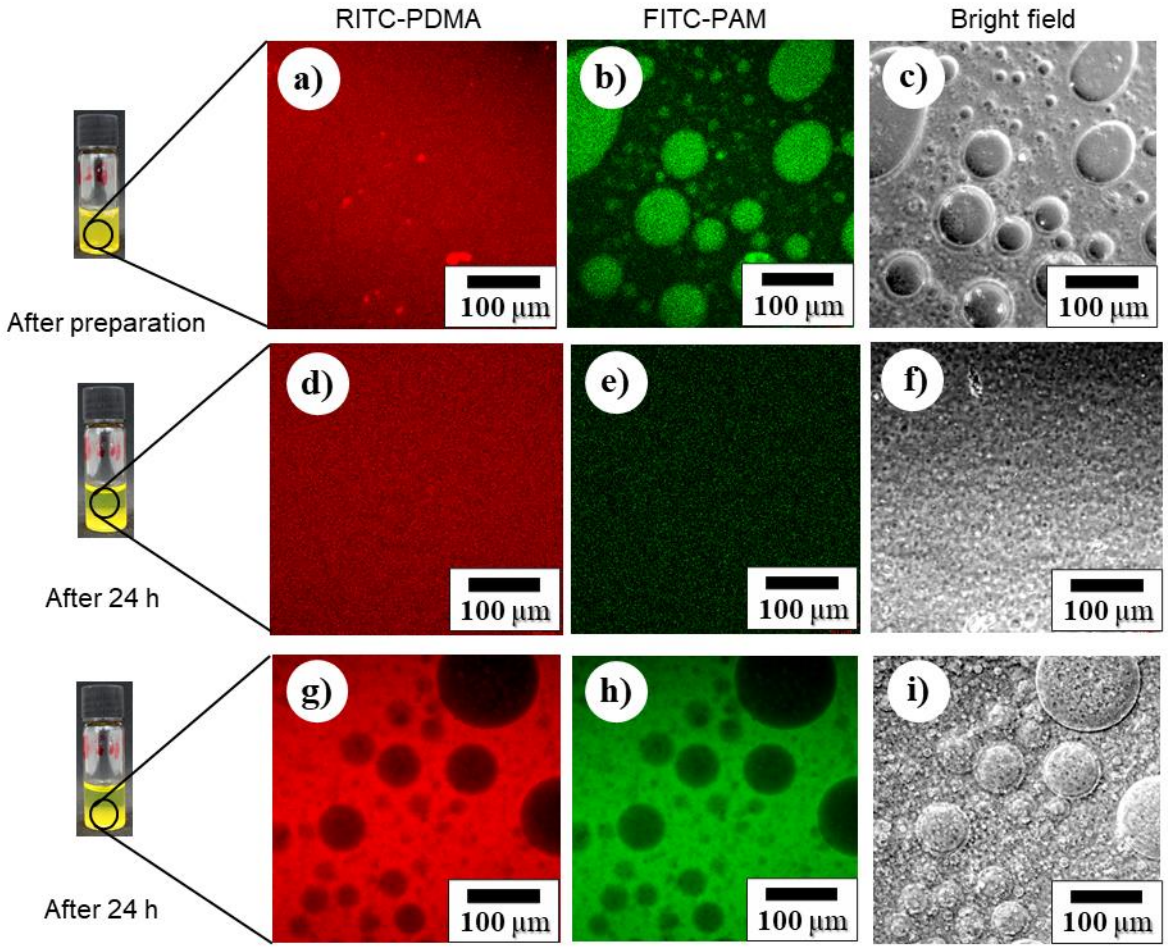

Figure 5.5. CLSM images of the w/w emulsion of RTIC-PDMA and FTIC-PAM (a) RITC-PDMA (b) FITC-PAM (c) bright field image and (g-h) CLSM images of the lower phase after 24 h (g) RITC-PDMA (h) FITC-PAM (i) bright field image.

In order to localise the polymer type in the emulsion, each polymer type was labelled with a different dye (RTIC, FTIC and coumarin) and the emulsions were analysed *via* confocal laser scanning microscopy (CLSM) (Figure 5.5). The emulsions were prepared with a polymer concentration of 1.5/1.5 wt% and stabilised with 0.1 wt% Mg/Al-CO_3-LDH. via ultrasonic treatment for two minutes as well as shaking by hand for one minute. In the CLSM images for some combinations the stabiliser particles were visible in the background of the emulsion. Especially for the images with coumarin labelled PAAM, due to the similar emission region of LDH particles and coumarin labelled PAAM. For the system PDMA and PAM (Figure 5.5 a-f) the CLSM images show that PDMA is located over the entire sample (Figure 5.5 a) and PAM is enriched in the emulsion droplets (Figure 5.5 b) for the emulsion direct after preparation. After 24 hours and phase separation each phase was analysed *via* CLSM again. In the upper

phase similar to the bright field results, no droplets were visible and both polymers were located over the entire sample (Figure 5.5 d-f). In the CLSM images of the lower phase, droplets were visible and both polymers were located outside the droplets (Figure 5.5 g-i).

In the system PDMA and PAAM, the CLSM images showed that both polymers were primary located inside the droplet (Figure 5.6 a-c) directly after preparation. After phase separation, no droplets were visible in the upper phase (Figure 5.6 d-f) and in the lower phase, both polymers were located outside the observed droplets (Figure 5.6).

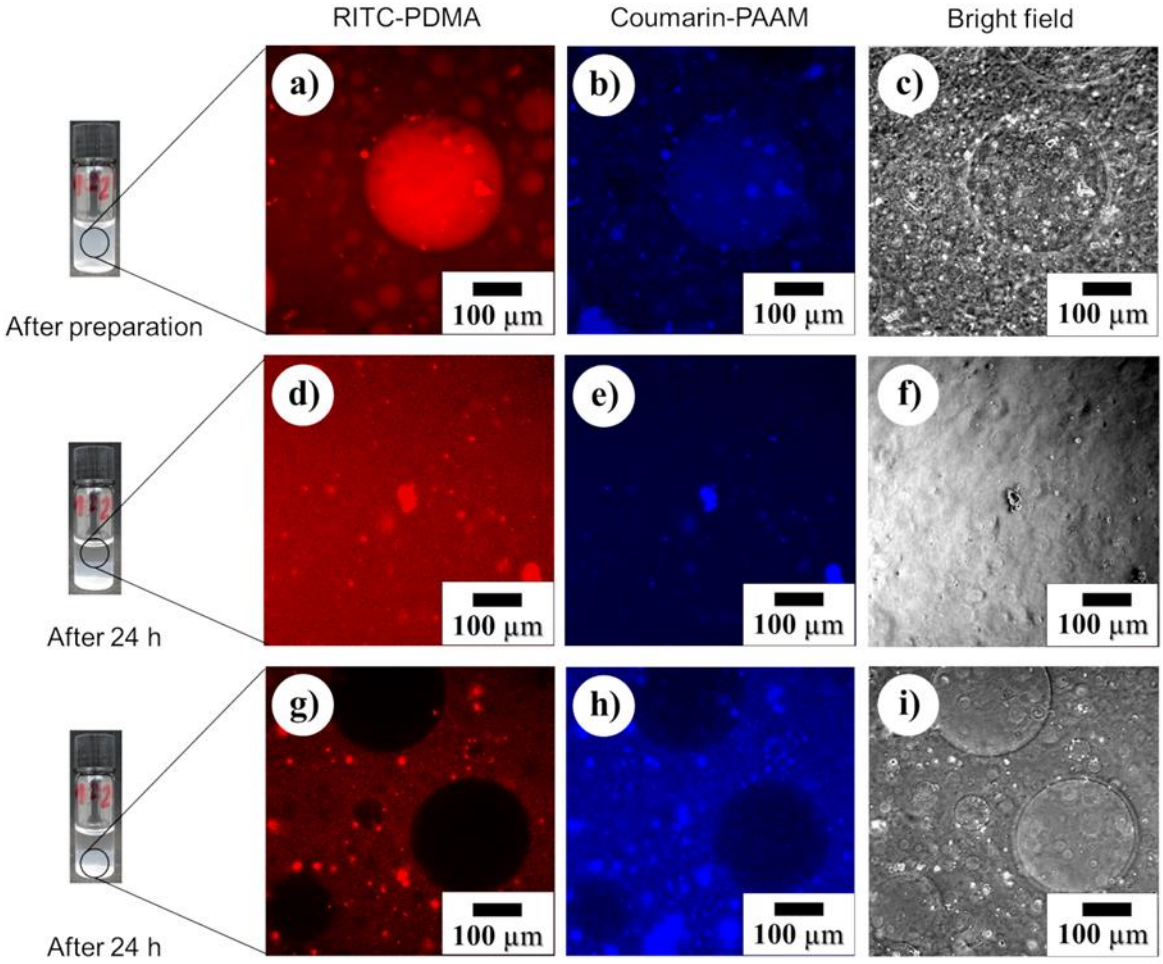

Figure 5.6. (a-c) CLSM images of the w/w emulsion after preparation of RTIC-PDMA and Coumarin-PAAM (a) RITC-PDMA (b) Coumarin-PAAM (c) bright field image, (d-f) CLSM images of the upper phase of RTIC-PDMA and Coumarin-PAAM after 24 h (d) RITC-PDMA, (e) Coumarin-PAAM and (f) bright field. and (g-i) CLSM images of the lower phase after 24 h (g) RITC-PDMA, (h) Coumarin-PAAM and (i) bright field image.

The CLSM images of the emulsion formed by the ATPS PAAM and PAM (Figure 5.7 a-c), displayed polymer located inside the droplets after preparation. Similar to the other cases, after 24 hours and observation of phase separation, no droplets are visible in the upper phase and the polymers are located over the entire phase (Figure 5.7 d-f). The droplet containing lower phase featured both polymers located outside the droplets (Figure 5.7 g-i).

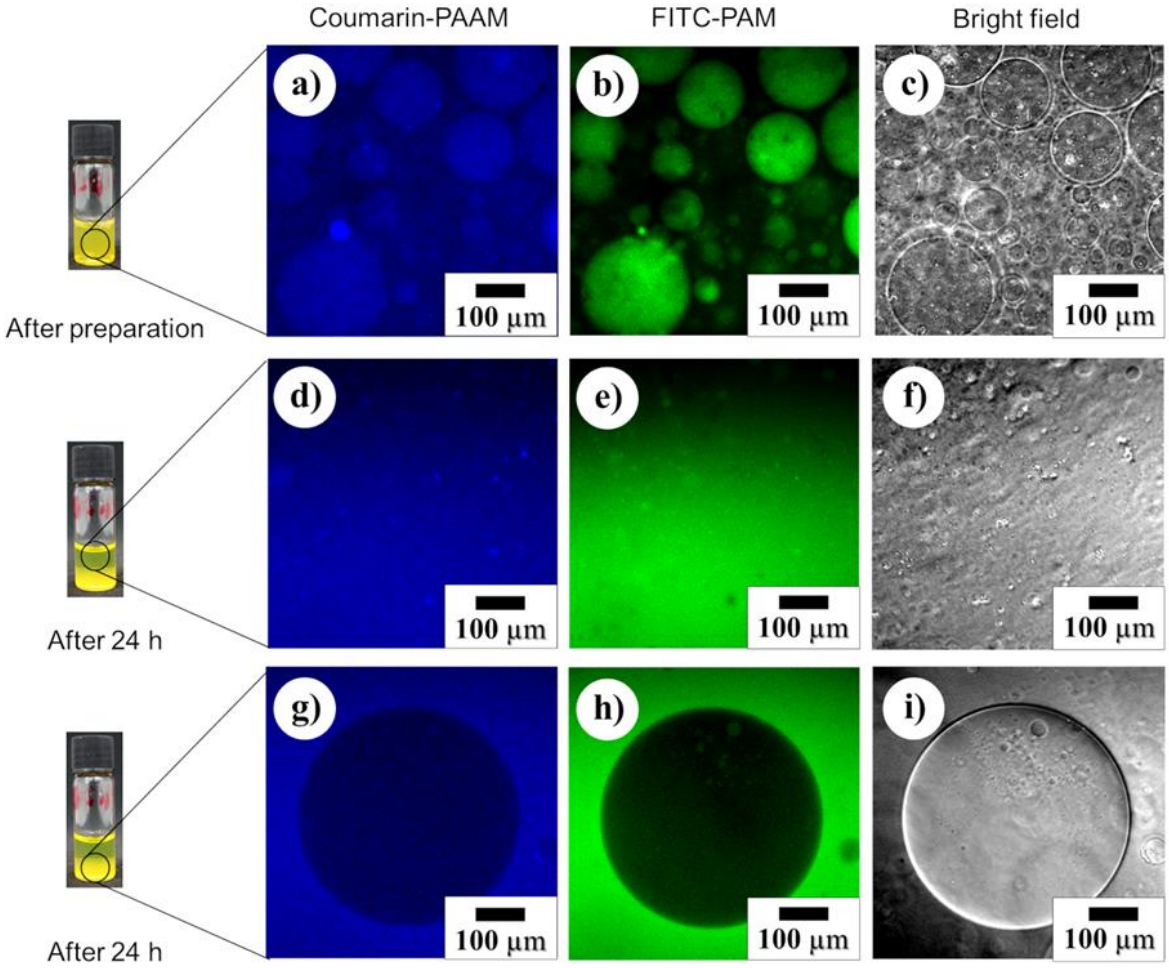

Figure 5.7. (a-c) CLSM images of the w/w emulsion after preparation of Coumarin-PAAM and FTIC-PAM a) Coumarin-PAAM b) FITC-PAM c) bright field image, (d-f) CLSM images of the upper phase of Coumarin-PAAM and FTIC-PAM after 24 h (d) Coumarin-PAAM, (e) FTIC-PAM and (f) bright field. and (g-i) CLSM images of the lower phase after 24 h (g) Coumarin-PAAM, (h) FITC-PAM and (i) bright field.

Overall, the results show that right after emulsion formation only in the case of PDMA and PAM both polymers are present in different phases (droplet and continuous phase), while for the other cases both polymers are located in the continuous phase. However, after phase separation in all cases the polymers are present in the continuous phases. The location of both polymer types in one phase is unexpected as it opposes the situation found for the non-dispersed

ATPS. The partitioning of both polymers into the continuous phase is most likely not due to the formation of a coacervate as both polymers tend to demix in the common ATPS system. Thus, we assume that the reason for the uncommon partitioning lies in the emulsion formation itself, *i.e.*, the addition of stabiliser and dispersion of the phases.

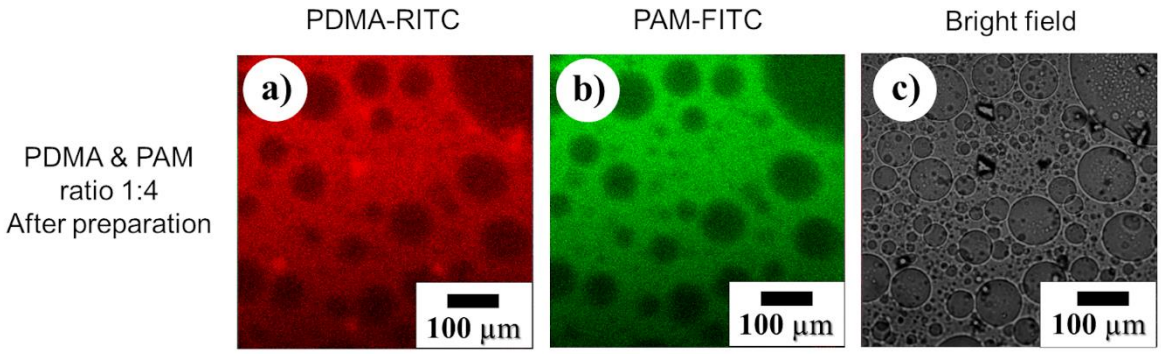

Figure 5.8. (a-c) CLSM images of the w/w emulsion of RITC-PDMA and FITC-PAM directly after preparation with the ratio PDMA:PAM 1: 4: (a) RITC-PDMA, (b) FITC-PAM, (c) bright field image.

One reason is the change of the polymer ratio after phase separation. An experiment with different polymer ratio (1:4) shows a similar partitioning of both polymers directly after preparation, in comparison to the partitioning after phase separation for the 1:1 ratio (Figure 5.8). The dyes have not an influence on the phase behaviour of the polymers in the emulsion. The partitioning of both polymers is the same with only one dye present at the time (Figure 5.22). Furthermore, the large number of hydroxyl groups in the LDH nanoparticles could also influence the polymer separation. In addition, the amount of stabiliser is important. At low stabiliser concentration the polymers are present inside the droplet.

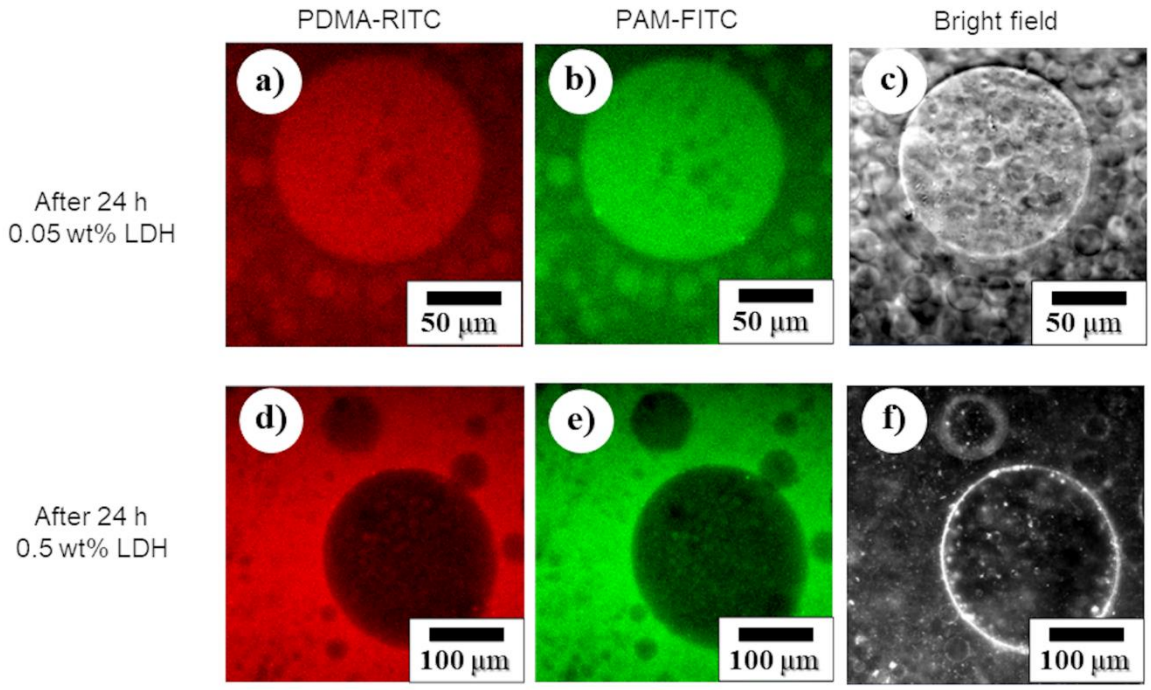

Figure 5.9. (a-c) CLSM images of the w/w emulsion of RITC-PDMA and FITC-PAM after 24 h, using 0.05 wt% LDH nanoparticles (a) RITC-PDMA, (b) FITC-PAM, (c) bright field image, (d-f) CLSM images of the w/w emulsion of RITC-PDMA and RITC-PDMA, using 0.5 wt% LDH nanoparticles (d) RITC-PDMA, (e) FITC-PAM and (f) bright field image.

However, at higher stabiliser concentration both polymers are a present in the continuous phase (Figure 5.9). Moreover, DLS measurements of the LDH nanoparticles in combination with the polymer in aqueous solution showed a formation of larger aggregates (Figure 5.23 and Table 5.4), which indicates an interaction between polymer and nanoparticles. The formation of nanocomposites from LDH nanoparticles and polymers is described for various polymers *e.g.* polyacrylamide[145-147] or double hydrophilic block copolymers.[148]

5.5 A3PS of ultra-high molar mass poly(acrylamides)

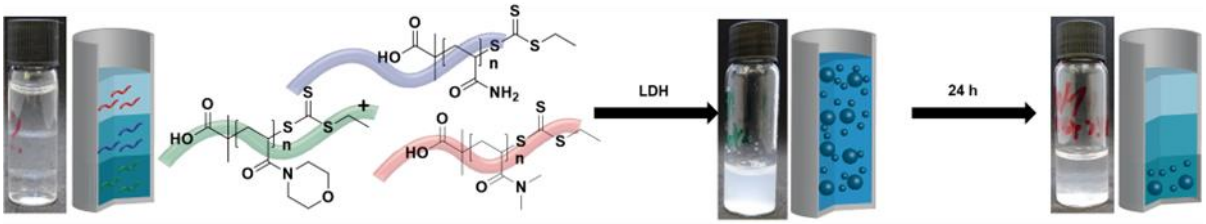

Scheme 5.2. Schematics of the water-in-water emulsion of the A3PS (PAAM, PAM and PDMA) stabilised by Mg/Al-LDH nanoparticles.

In order to test the limitations of the system, an aqueous three phase system (A3PS) of the three poly(acrylamides) was investigated. Therefore, polymer solutions with different concentrations were prepared *e.g.*, 6 wt% total polymer concentration (2 wt% PDMA/2 wt% PAAM/2 wt% PAM). The solution was mixed, equilibrated at ambient temperature to demix, investigated and diluted. Upon dilution the A3PS turned into an ATPS and finally into an one phase system. In order to receive an in-depth look into the A3PS, the phase diagram was prepared. The phase diagram (Figure 5.11 a) shows two phase transitions, one for the three phase/two phase border and one for the two phase/one phase border. The three phase/two phase border for the equal starting concentration of all polymers (2/2/2) was observed around a total polymer concentration of 2.1 wt% (0.7 wt% PDMA/ 0.7 wt% PAAM/ 0.7 wt% PAM) and the two phase/one phase border around a total polymer concentration of 1.5 wt% (0.5/0.5/0.5). The presence of the polymers in the individual phases were detected *via* ^{1}H-NMR in D_2O with DMF as internal standard after the phase separation and the polymer concentration detected (Figure 5.10). The ^{1}H-NMRs showed that every phase of the three phases was enriched with one polymer (Figure 5.24).

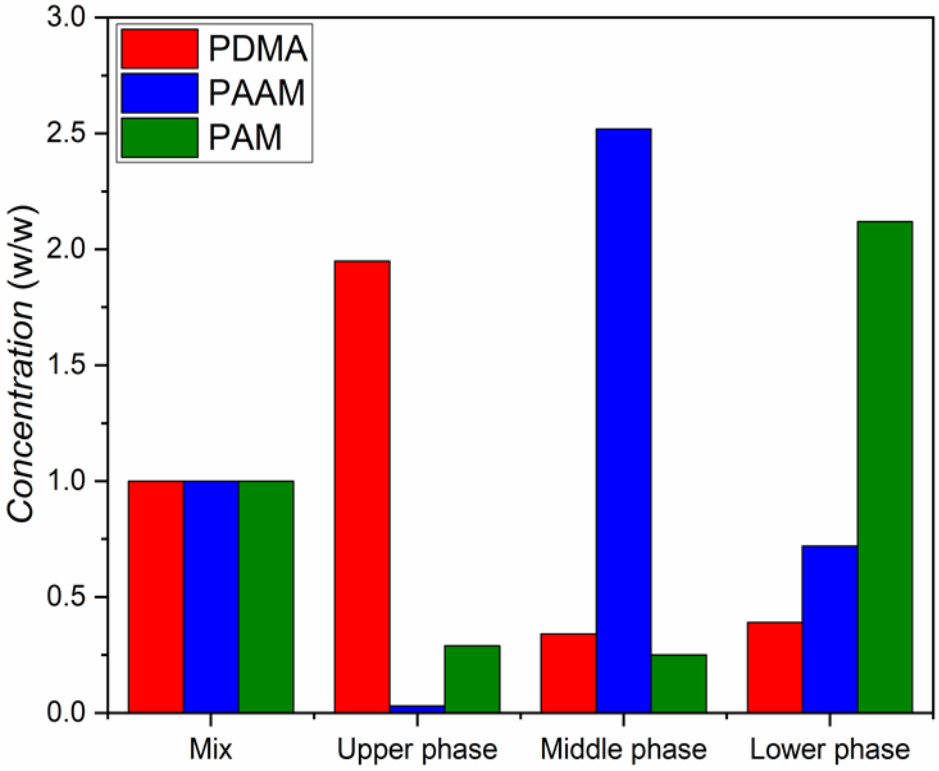

Figure 5.10. Concentration changes before and after observed phase separation (24 h), detected *via* ^{1}H-NMR in D_2O using DMF as internal standard, PDMA (red), PAAM (blue) and PAM (green) for the A3PS.

Additionally, a w/w emulsion was prepared with the A3PS and Mg/Al-CO_3-LDH as additive. In comparison to the w/w emulsion formed by the different ATPSs the total polymer concentration was set to 3 wt% (1/1/1) and the LDH concentration to 0.1 wt%. The w/w emulsion was analysed *via* bright field microscopy (Figure 5.11 b) revealing droplets with a diameter between 50 and 250 µm with an average particle size around 184.2 ± 70.9 µm indicating a successful w/w emulsion formation. In order to locate the polymers in the emulsion, the labelled polymers were added in the preparation of the emulsion and the emulsion was analysed *via* CLSM before and after phase separation after 24 h. Similar to the two polymer systems, the CLSM images of the mixture showed water droplets in a polymer-enriched matrix. After phase separation (24 h) the upper and the middle phase of the A3PS did not display droplets. In contrast, the lower phase contained droplets, where the polymers are located outside of the emulsion droplet (Figure 5.11 c-f).

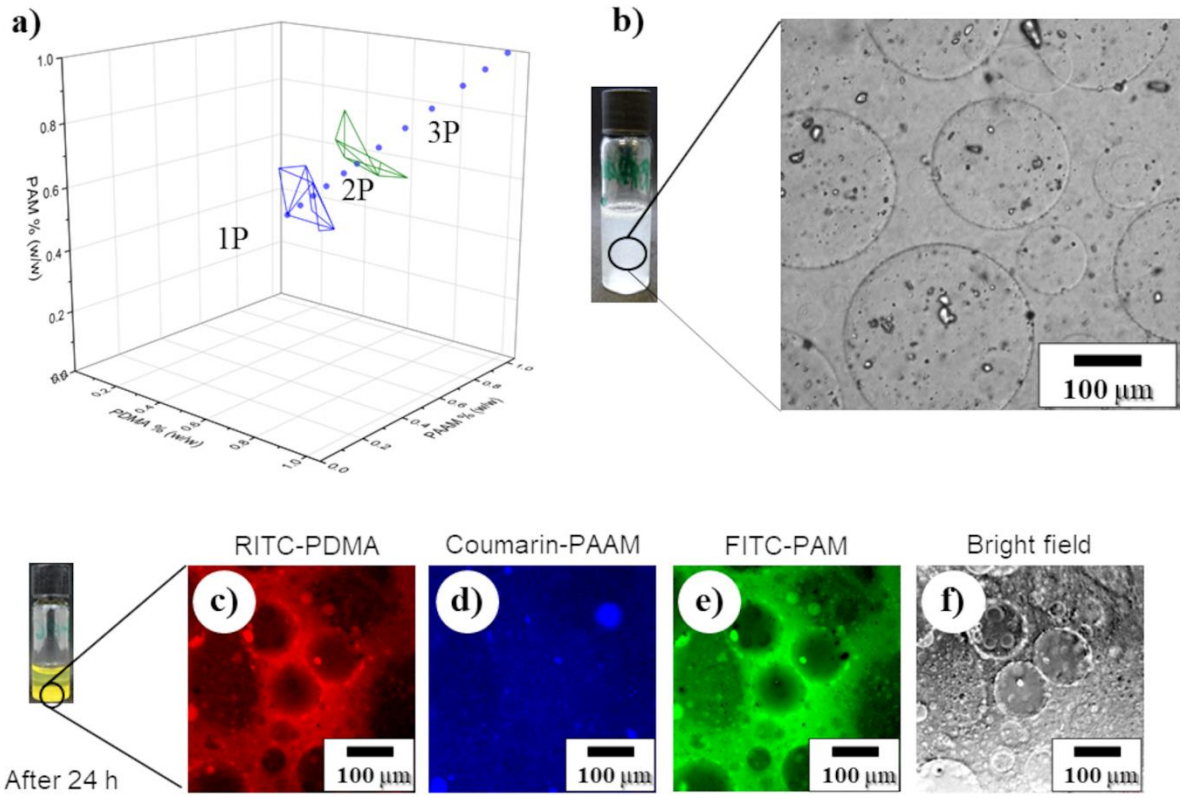

Figure 5.11. (a) Phase diagram of the A3PS of PDMA, PAAM and PAM with one-phase/two-phase (1P/2P) border (blue line) and two-phase/three-phase (2P/3P) border (green line), (b) Bright field image of the w/w emulsion of A3PS with Mg/Al-LDH, (c-f) CLSM images of the w/w emulsion of A3PS after 24 hours and phase separation (c) RITC-PDMA, (d) coumarin-PAAM, (e) FITC-PAM and (f) bright field.

Overall, the aqueous solution of the three polyacrylamides, leads to A3PS. Upon dilution the A3PS turns into an ATPS around a total polymer concentration of 2.1 wt% and into an one phase system around a total polymer concentration of 1.5 wt%. Furthermore, the A3PS can form, stabilised by LDH particles, a w/w emulsion before and after phase separation as well. Similar to the two-polymer system, the polymers are located outside the emulsion droplets in the lower phase. After phase separation the emulsion was again only stable in the lower phase presumably, due to the enrichment of LDH particles in the lower phase.

5.6 Conclusion

The three ultra-high molar mass polyacrylamides PDMA, PAAM and PAM were synthesised *via* PI RAFT polymerisation and were subjected to ATPS formation, which is stable at significantly lower concentration in comparison to the system Dex/PEG. In addition, the ATPSs were used to form w/w emulsions, stabilised with Mg/Al-CO_3-LDH nanoparticles. The emulsion was stable in the mixture and after phase separation, in the lower phase for at least four weeks. The polymers were located in the emulsion via CLSM, showing that at first polymer-containing droplets in water were formed directly after dispersion and water droplets in polymer matrix after phase separation. Furthermore, the solution of all three polymers in water, revealed the formation of an A3PS, which is stable at low concentration as well. The emulsion formed by the A3PS was indicated as water droplets in polymer matrix for the emulsion before and after phase separation. Interestingly, in most cases polymers were enriched in the same phase, which has several implications for future applications. The enrichment of polymers and the requirement of low polymer concentrations might be useful for bio molecule separation or the compartmentalisation of aqueous environments in catalysis in the future.

The following chapter will focus on the ATPS formed by PDMA and the polysaccharide pullulan. The influence of molar mass on the ATPS and polymer ratio for the emulsion will be analysed more in detail. Furthermore, the possibility of pH switchable w/w emulsion, using the PDMA & Pull ATPS, will be tested.

5.7 Experimental Part

PI-RAFT-polymerisation of DMA_{10}[6]

Destabilised DMA (1.0 g, 10 mmol, 15151 eq.), EMP (146 µL, 0.06 µmol, 1.0 eq. from a DMSO stock solution 1 mg · mL^{-1}), and acetate buffer (1 mL, 0.2 M, pH=5) were mixed in a vial (7 mL) containing a stirring bar and sealed with a septum. The solution was bubbled for 30 min with nitrogen and the polymerisation was initiated by an UV-lamp (nail-lamp). The polymerisation was stopped after 24 h. Subsequently, the polymer was dialysed against deionised water (Spectra/Por 3500 Da) for 3 days. Finally, the sample was freeze-dried, and a white solid (780 mg, M_n= 1.07 · 10^6 g · mol^{-1}) was obtained.

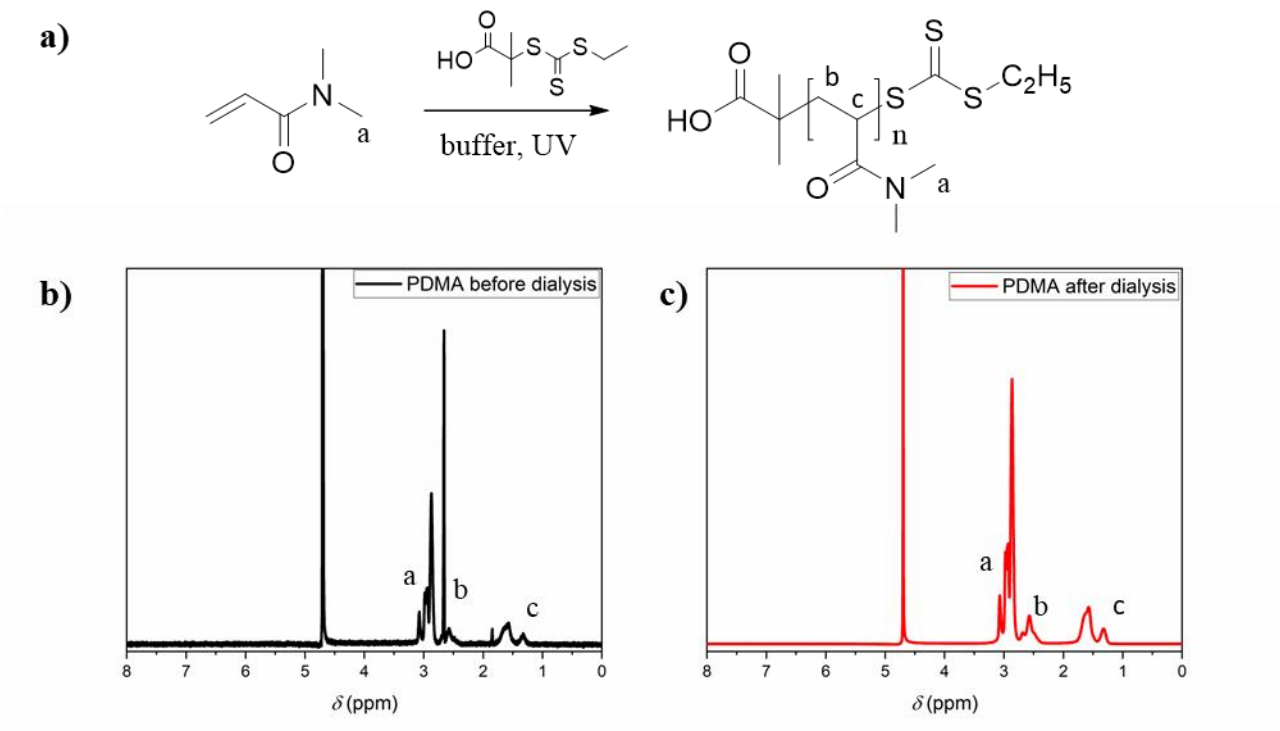

Figure 5.12. (a) Reaction scheme of the photo induced RAFT-polymerisation of *N*,*N*-dimethylacrylamide (DMA), (b and c) ^{1}H-NMR measurement of PDMA in D_2O (b) before dialysis and (c) after dialysis.

PI-RAFT-polymerisation of AAM$_{730k}$

In a glass vial (7 mL) AAM (1.0 g, 14 mmol, 21,000 eq.) was dissolved under stirring in acetate buffer (1 mL, 0.2 M, pH=5). Subsequently, EMP (146 µL, 0.06 µmol, 1.0 eq. from a DMSO stock solution 1 mg · mL^{-1}) was added and the vial (7 mL) containing a stirring bar was sealed with a septum. The solution was bubbled for 30 min with nitrogen and the polymerisation was initiated by an UV-lamp (nail-lamp). The polymerisation was stopped after 24 h. Subsequently, the polymer was dialysed against deionised water (Spectra/Por 3500 Da) for 3 days. Finally, the sample was freeze-dried, and a white solid (995 mg, M_n= 730,000 g · mol^{-1}) was obtained.

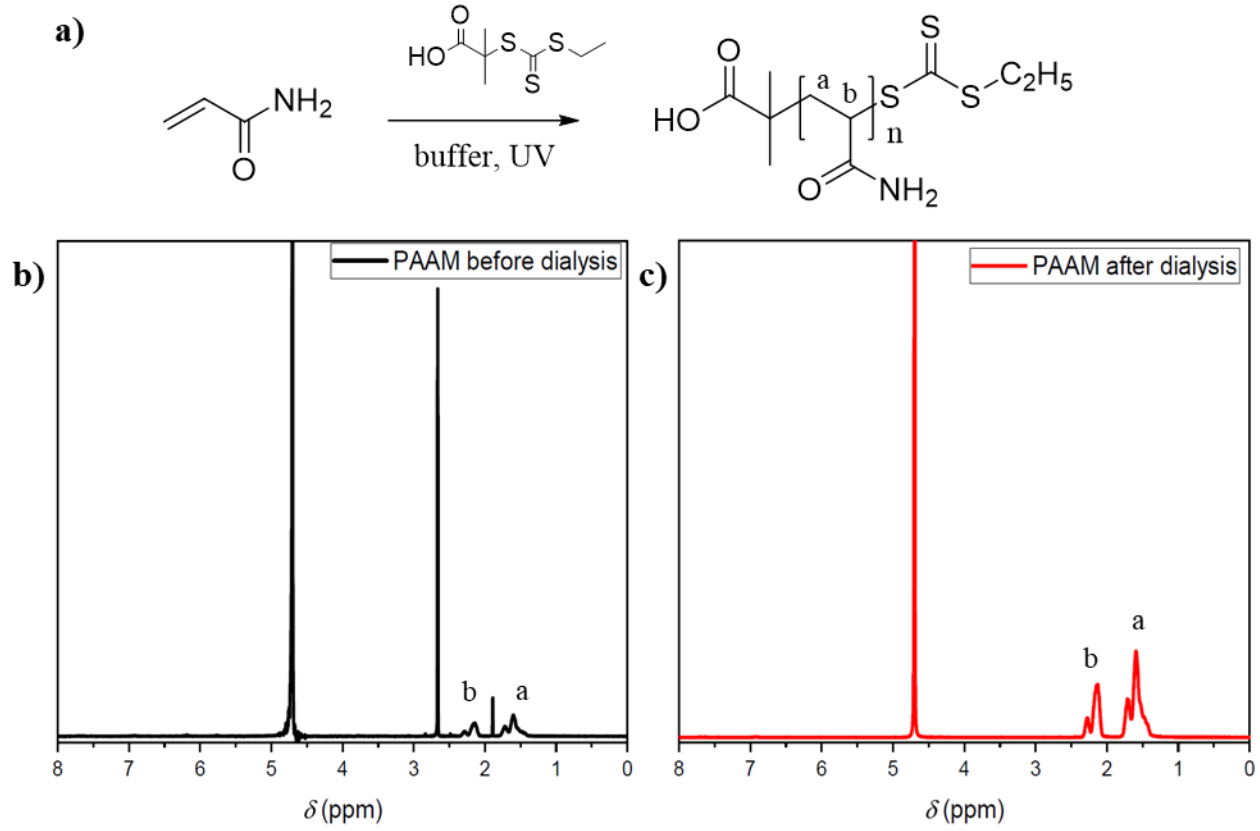

Figure 5.13. (a) Reaction scheme of the photo induced RAFT-polymerisation of acrylamide (AAM), (b and c) ^{1}H-NMR measurement of PAAM in D_2O (b) before dialysis and (c) after dialysis.

PI-RAFT-polymerisation of AM_{10}^6

Destabilised AM (1.0 g, 7.0 mmol, 10640 eq.), EMP (146 µL, 0.06 µmol, 1.0 eq. from a DMSO stock solution 1 mg · mL^{-1}), and acetate buffer (1 mL, 0.2 M, pH=5) were mixed in a vial (7 mL) containing a stirring bar and sealed with a septum. The solution was bubbled for 30 min with nitrogen and the polymerisation was initiated by an UV-lamp (nail-lamp). The polymerisation was stopped after 24 h. Subsequently, the polymer was dialysed against deionised water (Spectra/Por 3500 Da) for 3 days. Finally, the sample was freeze-dried, and a white solid (990 mg, M_n= 1.04· 10^6 g · mol^{-1}) was obtained.

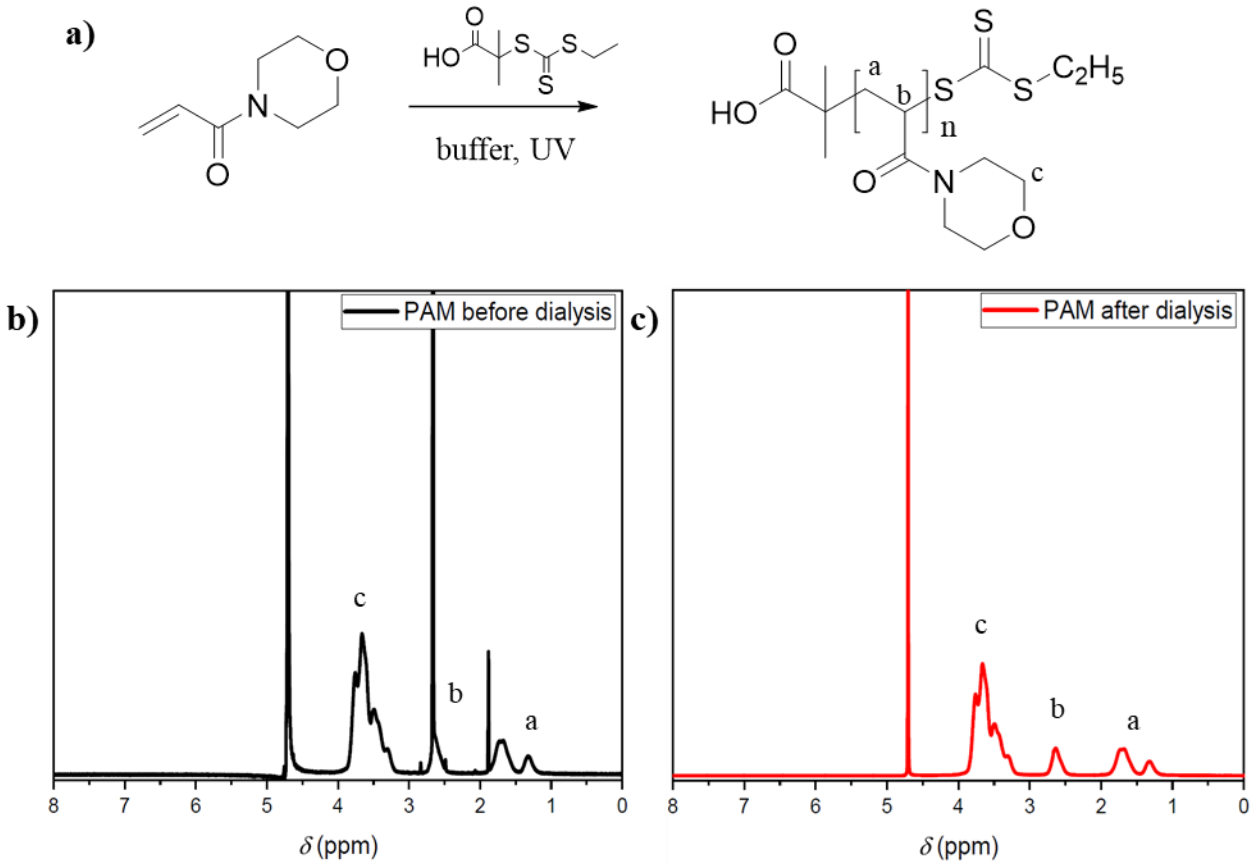

Figure 5.14. (a) Reaction scheme of the photo induced RAFT-polymerisation of AM, (b and c) ^{1}H-NMR measurement of PAM in D_2O (b) before dialysis and (c) after dialysis.

Formation of Rhodamine B labelled PDMA

In a dry, argon purged 100 mL round bottom Schlenk flask, PDMA (0.05 g, 0.0001 mmol, 1.0 eq.) was dissolved in dry DMSO (5 mL). Hexylamine (53 µg, 0.00026 mmol 2.5 eq.) was added, placed in a pre-heated oil bath (50 °C) and stirred overnight. Afterwards, the reaction mixture was cooled down to ambient temperature, Rhodamine B ITC (0.42 mg, 0.0008 mmol, 7.5 eq.) was added and the solution stirred over night at 50 °C. The mixture was cooled down to ambient temperature and diluted with deionised water. Afterwards, the polymer was dialysed against deionised water (Spectra/Por 3500 Da) for three days, freeze-dried, and a purple solid (45.7 mg) was obtained.

Formation of Fluorescein labelled PAM

In a dry, argon purged 100 mL round bottom Schlenk flask, PAM (0.1 g, 0.00023 mmol, 1.0 eq.) was dissolved in dry DMSO (5 mL). Hexylamine (58 µg, 0.00057 mmol, 2.5 eq.) was added, placed in a pre-heated oil bath (50 °C) and stirred overnight. Afterwards, the reaction mixture was cooled down to ambient temperature, Fluorescein ITC (0.67 mg, 0.0017 mmol, 7.5 eq.) was added and the solution stirred over night at 50 °C. The mixture was cooled down to ambient temperature and diluted with deionised water. Afterwards, the polymer was dialysed against deionised water (Spectra/Por 3500 Da) for three days, freeze-dried, and a yellow solid (98.2 mg) was obtained.

Formation of Coumarin labelled $PAAM_{730k}$

In a glass vial, the dried PAAM (100 mg, 0.0003 mmol, 1.0 eq.) was dissolved in an acetate buffer (5 mL). After the polymer was dissolved, the 7-[4-(trifluoromethyl)coumarin]acrylamide (0.5 mg, 0.0015 mmol, 5.0 eq. in 0.5ml DMF) and 4,4'-azobis(4-cyanovaleric acid) (19 µL from an acetate stock solution 1 mg mL^{-1}) was added. Subsequently, the vial was sealed with a septum and bubbled for 30 min with Nitrogen. The polymerisation was stopped after 24h. After that, the polymer was dialysed against de-ionised water (Spectra/Por 3500 Da). Finally, the sample was freeze-dried, and a white solid (99.2 mg) was obtained.

Synthesis of Mg/Al-CO_3-LDH

Utilised LDH (layered double hydroxide) material (Mg/Al-CO_3-LDH) was prepared by coprecipitation method,[142, 143] followed by subsequent hydrothermal treatment for narrowing of the size distribution.[144] Appropriate masses of $Mg(NO_3)_2 \cdot 6H_2O$ (2.5641 g) and $Al(NO_3)_3 \cdot 9H_2O$ (1.8757 g) were dissolved in 100 ml MilliQ water in order to obtain 2:1 molar ration of $Mg^{2+}Al^{3+}$ cations. Another solution was prepared by dissolving 1.0599 g of Na_2CO_3 in 1M NaOH. Two solutions were mixed under vigorous stirring and kept during 24 h at pH 9.0 ± 0.5 at room temperature. Obtained white precipitate was washed 5 times by employing centrifuge at 10000 rpm during 10 min. Powder was afterwards left in oven to dry overnight at 60°C. Synthesised dried powder was dispersed at 4 wt% and placed in autoclave which was sealed in order to perform hydrothermal treatment at 120 °C for 24 hours. Eventually, final product was again washed several times, dried and redispersed at 10 wt% as a stock solution. Successful synthesis was confirmed by XRD and TEM (Figure 5.15). Prior to usage, stock solution was diluted to desired concentration and treated by ultrasonication for 10 min.

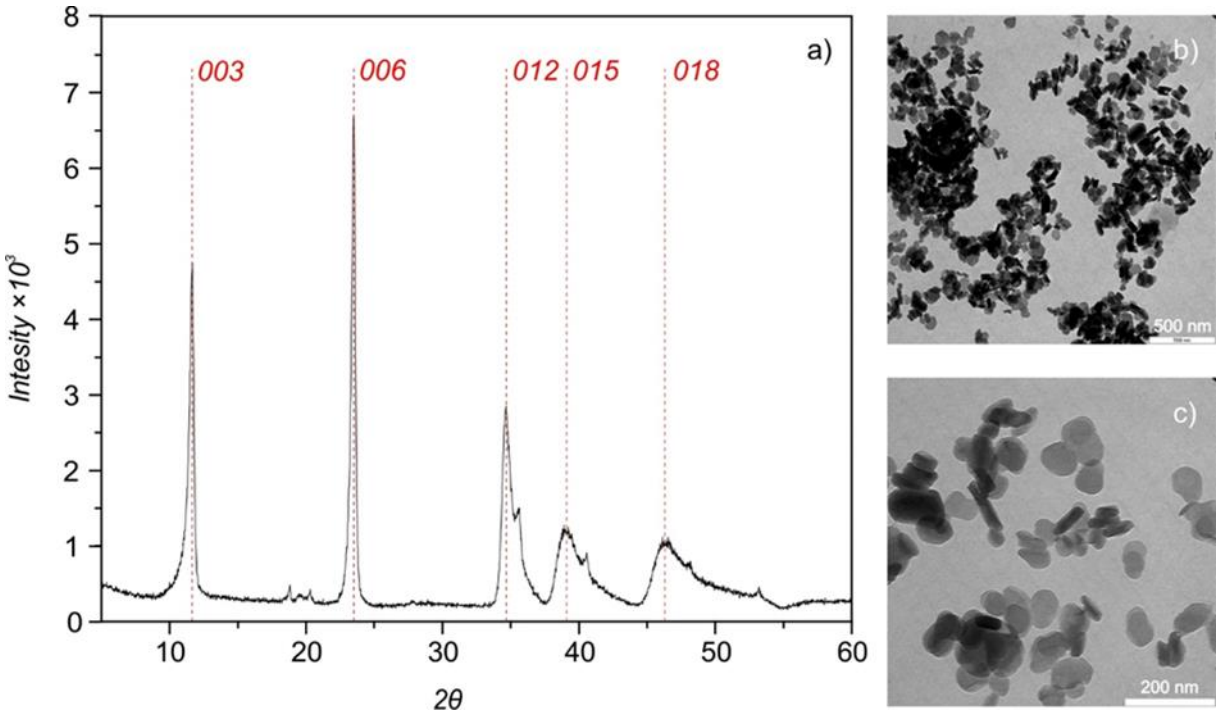

Figure 5.15. LDH characterisation was performed by XRD experiments (a), in combination with TEM micrographs at two different magnification (b) and (c).

Preparation of ATPS and phase diagram

Dried PDMA (25 mg) was dissolved in deionised water (475 mg), to obtain a 5 wt% solution. A 5 wt% solution of PAAM was prepared in the same way. Afterwards both solutions were mixed to receive a 2.5 wt% / 2.5 wt% mixture. Subsequently, the solution was equilibrated at ambient temperature in order to demix, investigated and diluted (100 mg of deionised water each cycle). The process was repeated, until no phase separation was observed, which was recorded as the data point of the binodal curve. All other concentration combinations were conducted in a similar way.

Preparation of A3PS and phase diagram

Dried PDMA (20 mg), PAAM (20 mg), and PAM (20 mg) were dissolved in deionised water (940 mg) to obtain a 2 wt% / 2 wt% / 2 wt% mixture. Subsequently, the solution was mixed, equilibrated at ambient temperature in order to demix, investigated and diluted (100 mg of deionised water each cycle). The process was repeated, until no phase separation was observed, which was recorded as the data point of the binodal curve. All other concentration combinations were conducted in a similar way.

Preparation of w/w emulsions

Dried PDMA (30 mg) and PAAM (30 mg) were dissolved in water (940 mg) to form a 3.0/3.0 wt% solution. LDH particles (2.0 mg) were dispersed in water (998 mg) to generate a 0.2 wt% dispersion. Both solutions were combined to obtain 1.5/1.5 wt% polymer and 0.1 wt% LDH particles in the mixture. The mixture was subjected to ultrasonic treatment for two minutes as well as shaking by hand for one minute and subsequently analysed *via* CLSM. The sample was again analysed *via* CLSM after 24 h and phase separation observed. All other concentration combinations were conducted in a similar way.

Preparation of w/w emulsions with additional labelled poly(acrylamides)

Dried PDMA (12 mg), RITC-PDMA (3 mg), PAM (12 mg) and FITC-PAM (3 mg) were dissolved in water (470 mg) to form a 3.0/3.0 wt% solution. LDH particles (1.0 mg) were dispersed in water (499 mg) to generate a 0.2 wt% dispersion. Both mixtures were combined to obtain 1.5/1.5 wt% polymer and 0.1 wt% LDH particles in the mixture. The mixture was subjected to ultrasonic treatment for two minutes as well as shaking by hand for one minute and subsequently analysed via CLSM. The sample was again analysed *via* CLSM after 24 h and phase separation observed. All other combinations were conducted in a similar way.

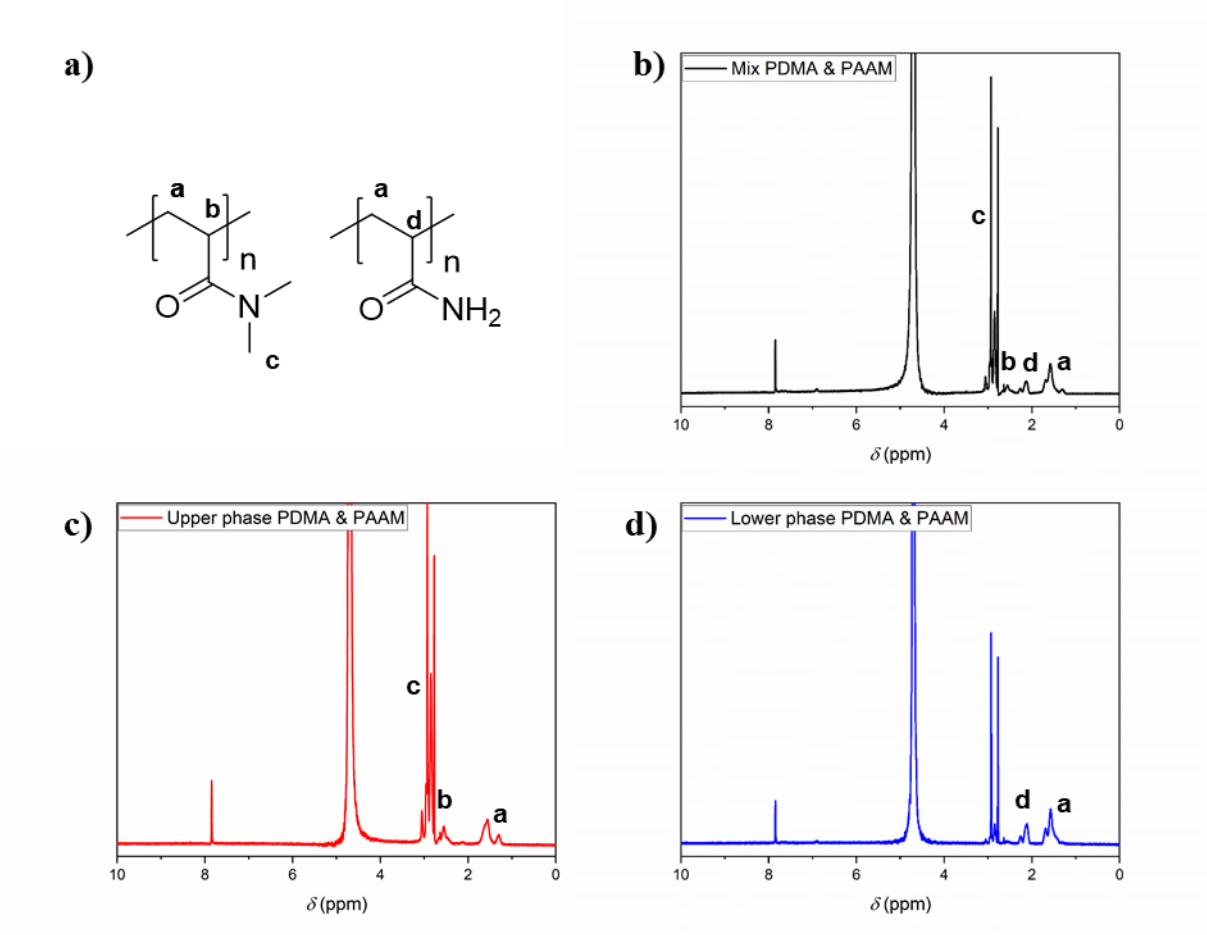

Figure 5.16. (a) Structures of PDMA and PAAM and (b-d) ^{1}H-NMR in D_2O of the (b) mixture, (c) upper and (d) lower phase after 24 h for the combination PDMA & PAAM using DMF as internal standard.

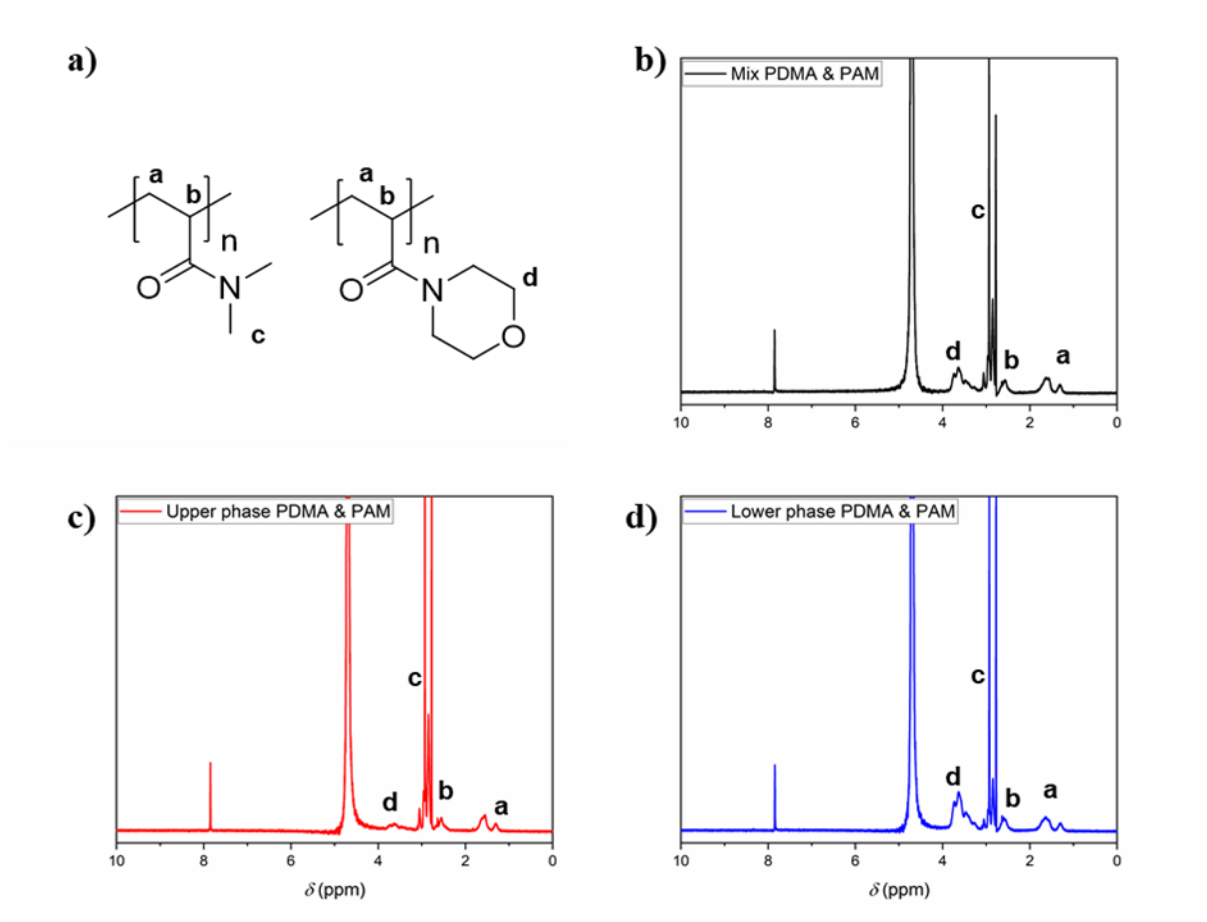

Figure 5.17. (a) Structures of PDMA and PAM and (b-d) ^{1}H-NMR in D_2O of the (b) mixture (c) upper and (d) lower phase after 24 h and observed phase separation for the combination PDMA & PAM using DMF as internal standard.

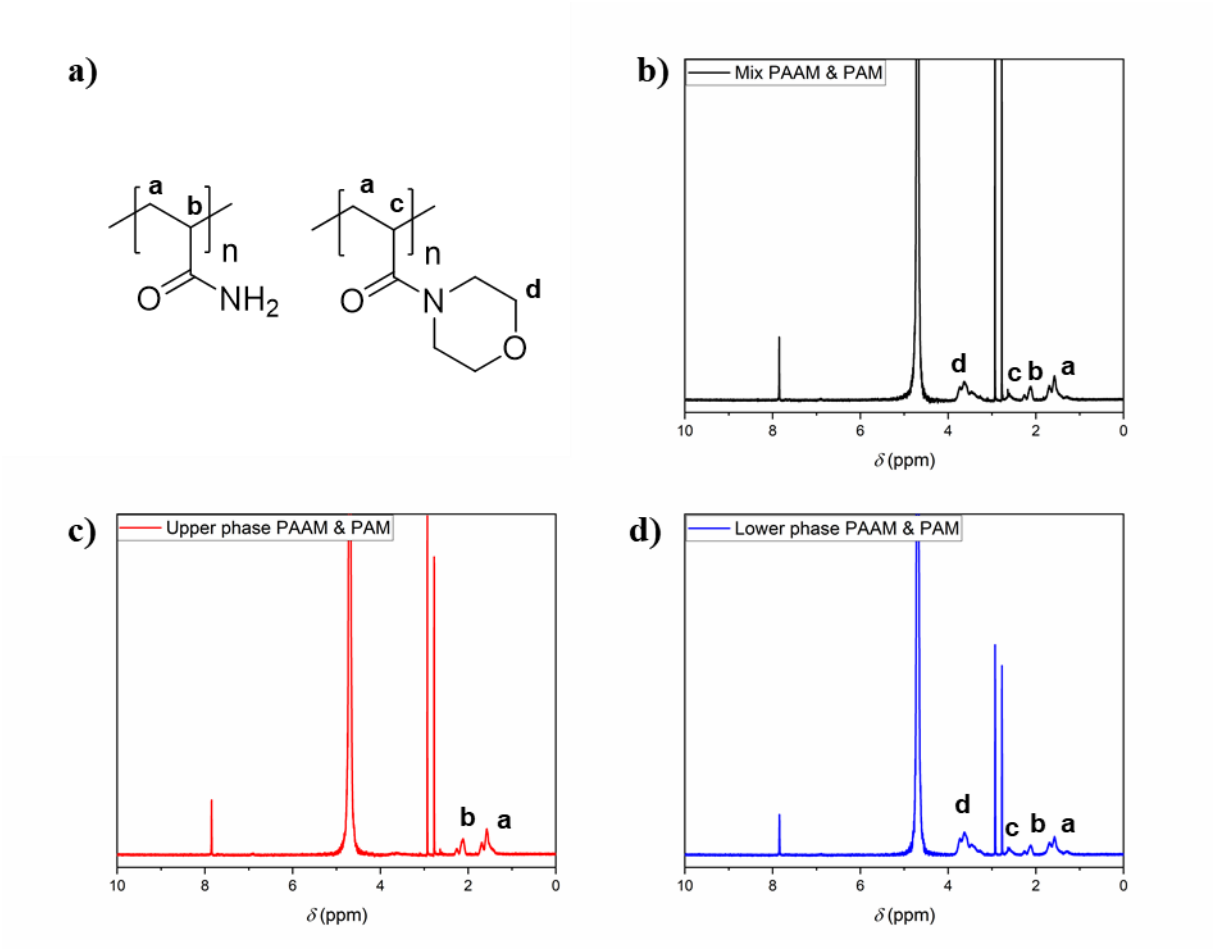

Figure 5.18. (a) Structures of PAAM and PAM and (b-d) ^{1}H-NMR in D_2O of (b) the mixture, (c) upper and (d) lower phase after 24 h for the combination PAAM & PAM using DMF as internal standard.

$$P_{P_x} = \frac{c_{P_x L_1}}{c_{P_x L_2}}$$

Equation 5.1. For the calculation of the partition coefficient for each polymer in the ATPS with P_{Px}-partition coefficient, c_{PxL1}-concentration of the polymer in the upper phase (L1) and c_{PxL2}- concentration of the polymer in the lower phase (L2).

Table 5-3. Partition coefficients of the three combinations ATPS from PDMA & PAAM, ATPS from PDMA & PAM and ATPS from PAAM & PAM after phase separation.

Combination (P_1 & P_2)	$P_{P1, L1, L2}$	$P_{P2, L1, L2}$
PDMA & PAAM	100	0.01
PDMA & PAM	2.91	0.13
PAAM & PAM	2.4	0.06

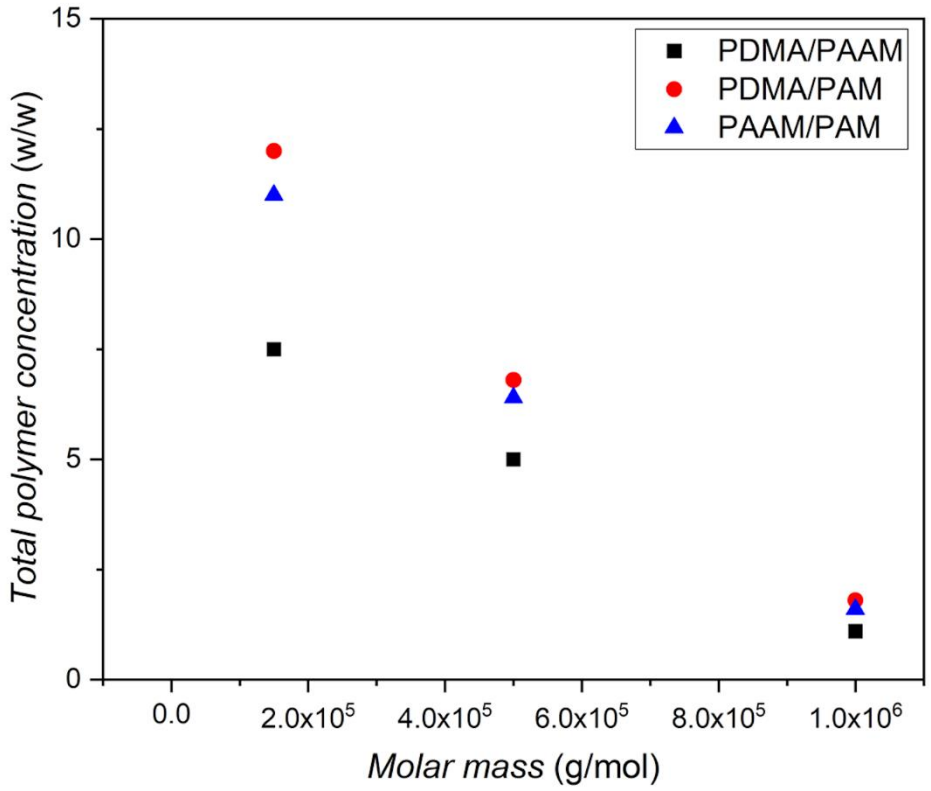

Figure 5.19. Minimum total polymer concentration required for a stable ATPS for different molar masses of PDMA & PAAM (black), PDMA & PAM (red) and PAAM & PAM (blue).

It should be noted, all molar masses for that experiment were determined with SEC in N-methyl-2-pyrrolidone (NMP) with PS calibration.

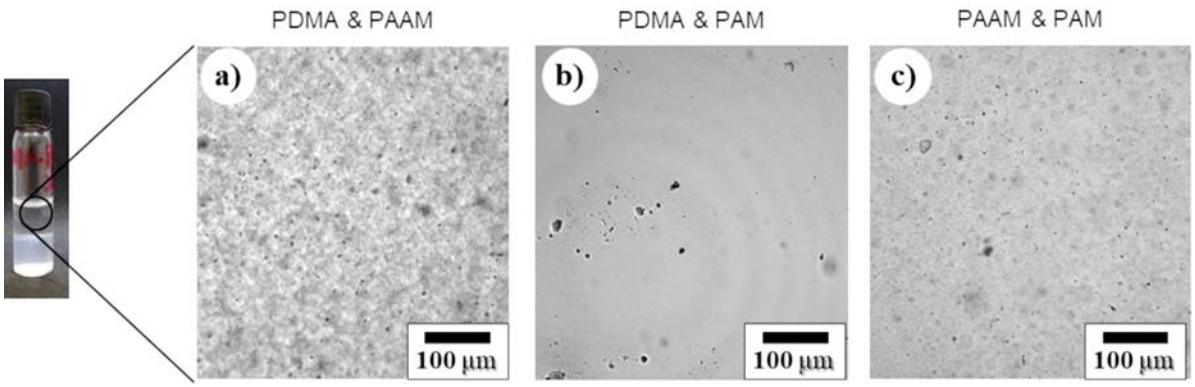

Figure 5.20. Bright field images of the upper clear phase after 24 h for (a) PDMA and PAAM, (b) PDMA and PAM, (c) PAAM and PAM.

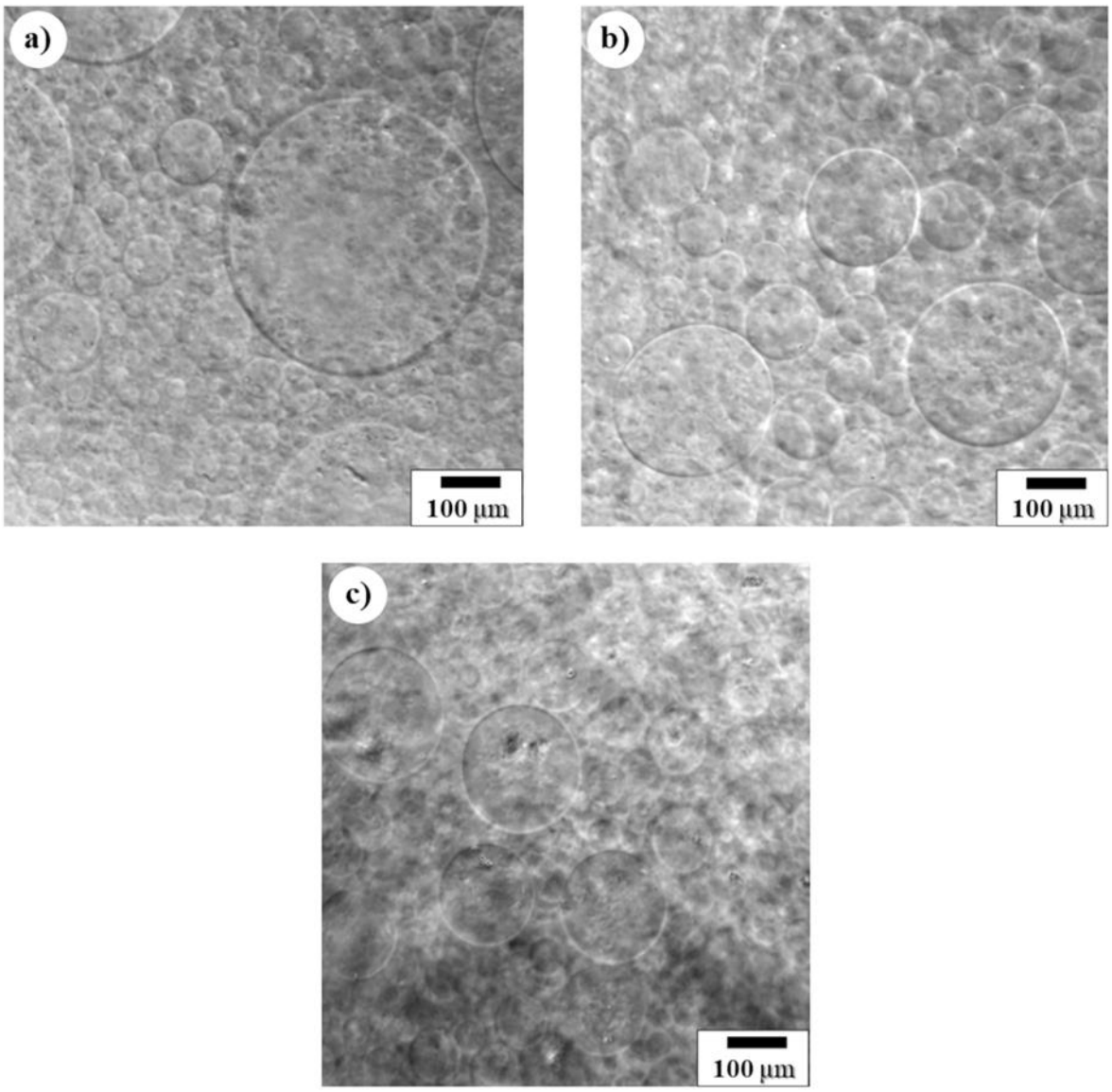

Figure 5.21. Bright field microscopy images of the emulsion phase after four weeks of phase separation (a) PDMA and PAAM, (b) PDMA and PAM and (c) PAAM and PAM.

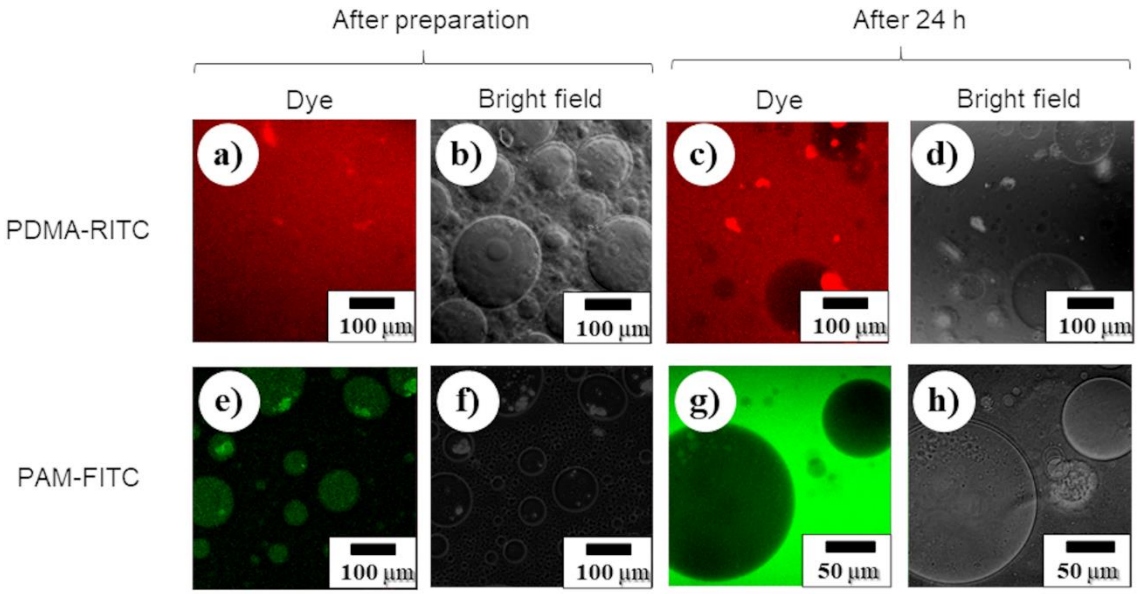

Figure 5.22. (a-d) CLSM images of the w/w emulsion of PDMA-RITC and PAM (a and b) after preparation and (c and d) after 24 h (a, c) PDMA-RITC, (b, d) bright field image, (e-h) CLSM images of the w/w emulsion of PAM-FITC and PDMA (e and f) after preparation and (g and h) after 24 h (e, g) PAM-FITC, (f, h) bright field image.

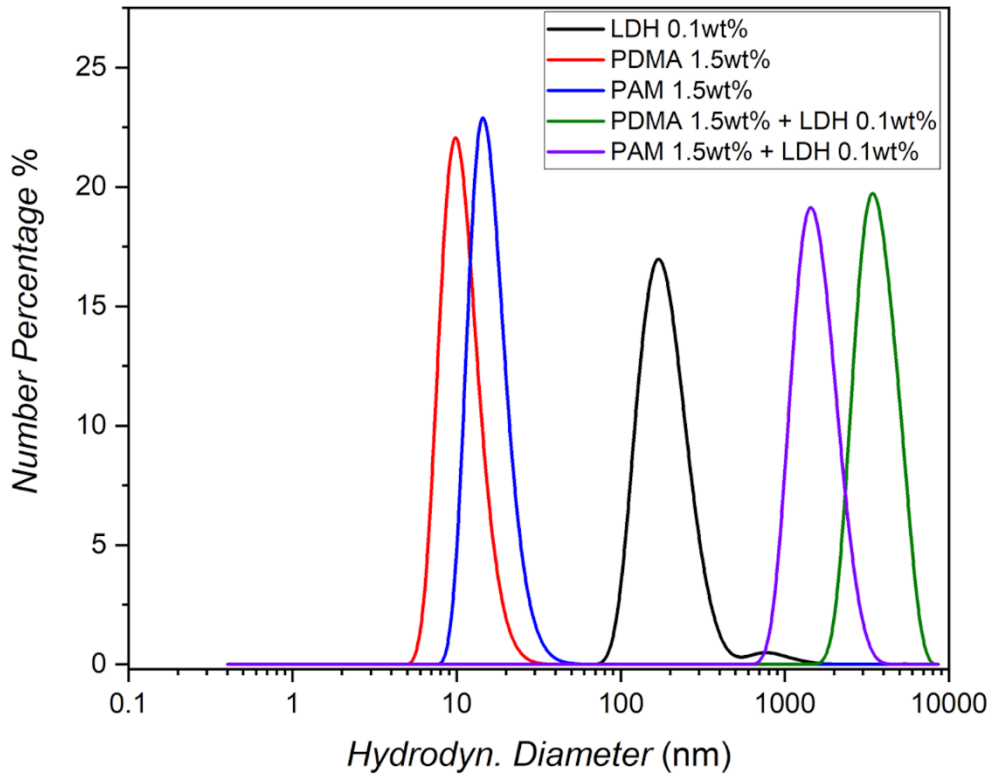

Figure 5.23. Comparison of number weighted particle size distribution of LDH nanoparticles (0.1 wt%, black curve), PDMA (1.5 wt%, red curve), PAM (1.5 wt%, blue curve), PDMA + LDH (1.5 wt%/0.1 wt%, green curve) and PAM + LDH (1.5 wt%/0.1 wt%, purple curve) in aqueous solution at ambient temperature.

Table 5-4. Summary of hydrodynamic diameter of LDH nanoparticles (0.1 wt%), PDMA (1.5 wt%), PAM (1.5 wt%), PDMA + LDH (1.5 wt%/0.1 wt%) and PAM + LDH (1.5 wt%/0.1 wt%) in aqueous solution at ambient temperature.

Compound	Concentration	Hydrodynamic diameter [nm]
LDH	0.1 wt%	164
PDMA	1.5 wt%	10
PAM	1.5 wt%	16
PDMA + LDH	1.5 wt% / 0.1wt%	3090
PAM + LDH	1.5 wt% / 0.1wt%	1480

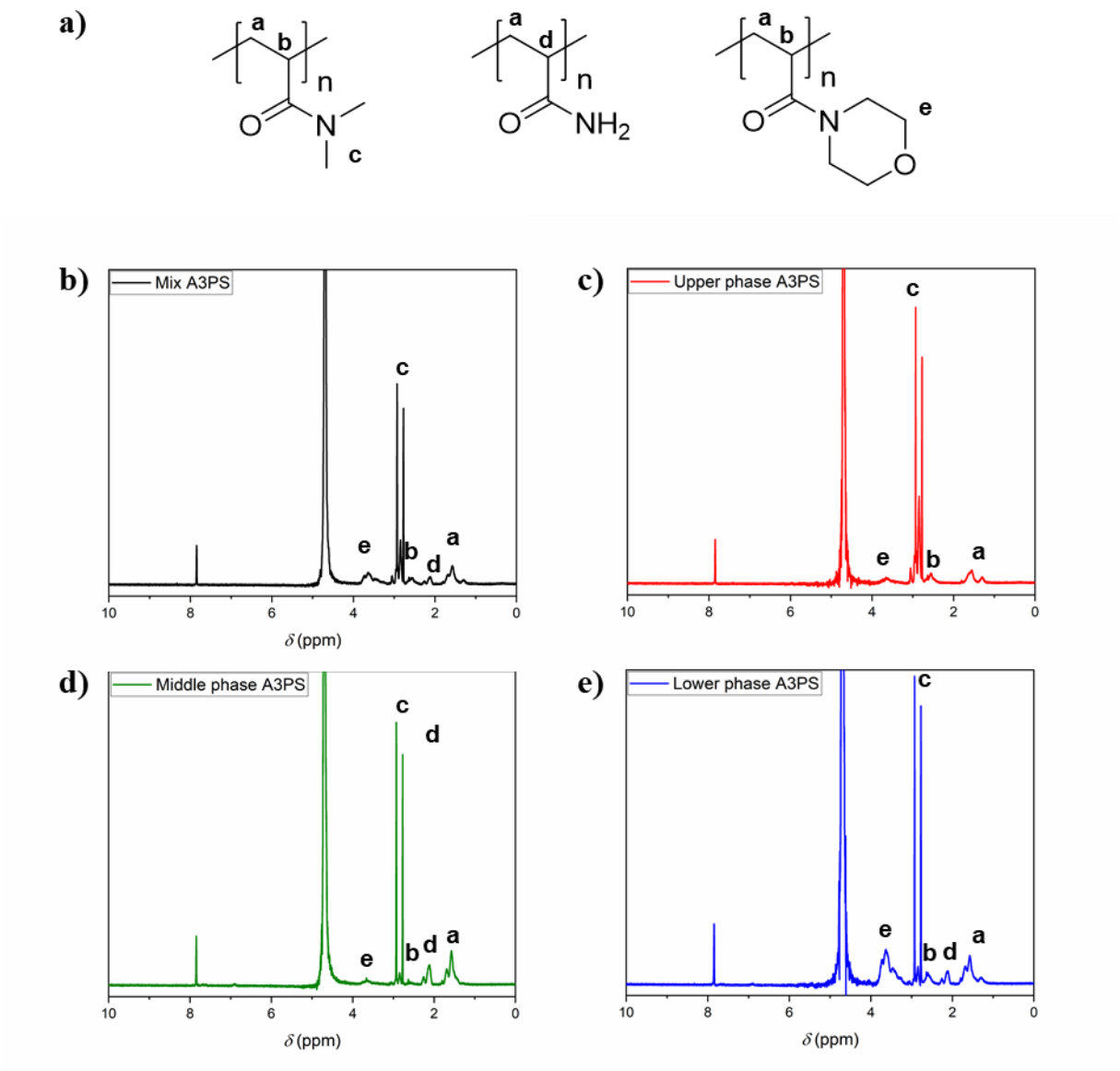

Figure 5.24. (a) Structures of PDMA, PAAM and PAM, (b-d) ^{1}H-NMR in D_2O of (b) the mixture, (c) upper phase, (d) middle phase and (e) lower phase after 24 h.

$$P_{P_x} = \frac{c_{P_xL_x}}{c_{P_xL_1} + c_{P_xL_2} + c_{P_xL_3}}$$

Equation 5.2. For the calculation of the partition coefficient for each polymer in the A3PS with P_{Px}-partition coefficient, c_{PxL1}-concentration of the polymer in the upper phase (L1), c_{PxL2}-concentration of the polymer in the middle phase (L2) and, c_{PxL3}- concentration of the polymer in the lower phase (L3)

Chapter 6

6 pH sensitive water-in-water emulsions based on the pullulan and poly(*N*,*N*-dimethylacrylamide) aqueous two-phase system

6.1 Introduction[c]

In the previous chapter the formation of ATPS and w/w emulsions of UHMW poly(acrylamides) was discussed. The results showed the required concentration for a stable ATPS and w/w emulsion decreases significantly by using UHMW poly(acrylamides). As mentioned in Chapter 5 an increase of the molar mass will result in a decrease of the critical polymer concentration.[74, 75] However, most commonly used systems for an ATPS and a w/w emulsion are formed by one synthetic polymer e.g. poly(ethylene glycol) (PEG) and one polysaccharide e.g. dextran (Dex).[25, 83] Therefore, here one poly(acrylamide) will be replaced with the polysaccharide pullulan to form an ATPS of poly(acrylamide) and Pull.

As described in the previous chapter, the stabilisation of w/w emulsions can be challenging, due to the low interfacial tension ATPS and a very wide interface between the aqueous phases.[84, 134, 135] The literature showed that w/w emulsions can be designed to be responsive to external triggers. Especially the use of defined polymer-based stabilisers with integrated pH or temperature switchable blocks enables a considerable control of the emulsion state. That avenue leads to sensitive w/w emulsions, depending on a defined temperature or pH-value. For example Nicolai and co-workers introduced linear polyelectrolytes, such as diethyl aminoethyl dextran to stabilise a PEG and Dex w/w emulsion using different pH-values.[149] Freitas and co-workers reported a pH-switchable aqueous emulsion of xyloglucan and amylopectin stabilised *via* polysaccharide-coated protein particles.[95] Furthermore, previous studies in our group

showed successfully stabilisation of w/w emulsion via block copolymers, designed with a temperature switchable block.[150]

In analogy to Chapter 5, RAFT polymerisation is a good avenue for the synthesis of a variation of poly(acrylamides) with access to a broad range of molar masses. As shown in the previous chapter, photo iniferter (PI) RAFT polymerisation is a simple way to reach UHMW ($M_n > 10^6$ g·mol^{-1}) for the synthesis of poly(acrylamides) e.g. poly(*N*,*N*-dimethylacrylamide) (PDMA).[44, 140]

In the following chapter, the ATPS formation of commercial Pull and PDMA featuring three different molar masses is investigated. The different PDMAs were synthesised *via* RAFT polymerisation and molar masses were varied between lower molar mass of 24k g mol^{-1}and UHMW > $1 \cdot 10^6$ g·mol^{-1}. The mixtures of PDMA with Pull were analysed and revealed ATPS formation. Additionally, the ATPS formed by UHMW PDMA and Pull was used to form w/w emulsions stabilised with polystyrene (PS) nanoparticles or the pH responsive block copolymer poly(2-(dimethylamino)ethyl methacrylate)-*b*-poly(oligo(ethylene glycol) methyl ether methacrylate) (PDMAEMA-*b*-POEGMA).[151] The emulsions were further analysed *via* bright-field microscopy and confocal laser scanning microscopy (CLSM). In order to localise the polymer in the emulsion, rhodamine B (RhB)- and fluorescein-labelled polymers were employed.

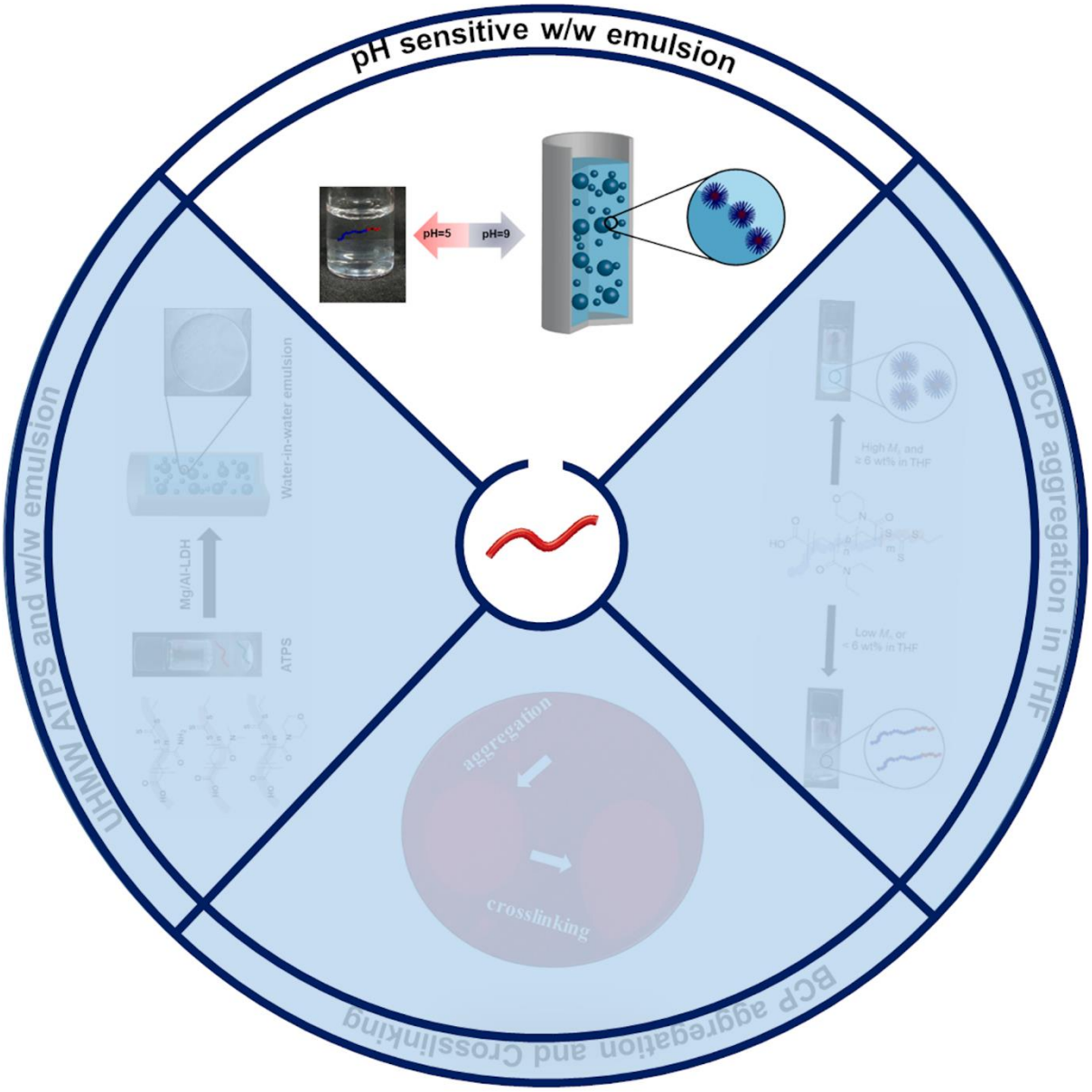

Scheme 6.1. Overview of the different utilasation of hydrophilic polymers for self-assembly or phase separation, higlighted the part of the current chapter: hydrophilc polymers utilised for the formation of pH sensitive w/w emulsion.

6.2 Synthesis of poly(*N*,*N*-dimethylacrylamides) *via* RAFT polymerisation

For ATPS formation, PDMA with various molar masses was synthesised at first. RAFT polymerisation is a superb avenue for the synthesis of polyacrylamides such as PDMA. For the lower and medium molar mass range, PDMA was synthesised *via* classical RAFT polymerisation. EMP was used as the chain transfer agent and the reaction was performed at 65 °C with AIBN as initiator in DMF. In the case of UHMW PDMA, EMP was used as photoiniferter in acetate buffer *via* UV light (nail lamp, λ = 365 nm). Conversions were determined by ^{1}H-NMR (Figure 6.9-11) revealing quantitative monomer conversion for low molar mass PDMA, 75% monomer conversion for medium molar mass PDMA and quantitative monomer conversion for UHMW PDMA. The low and medium molar mass PDMAs were analysed *via* SEC in NMP against PS standards **(**Figure 6.1 b and Table 6.1) indicating a molar mass of M_n = 23900 g·mol^{-1} and M_n = 80000 g·mol^{-1} and a dispersity of $Đ$ = 1.11 and $Đ$ = 1.06, respectively. UHMW PDMA was obtained with a molar mass of $M_n = 1.07 \cdot 10^6$ g·mol^{-1} and a dispersity of $Đ$ = 1.40, as analysed *via* MALS-SEC in 0.1N $NaNO_3$ (Figure 6.1 c and Table 6.1).

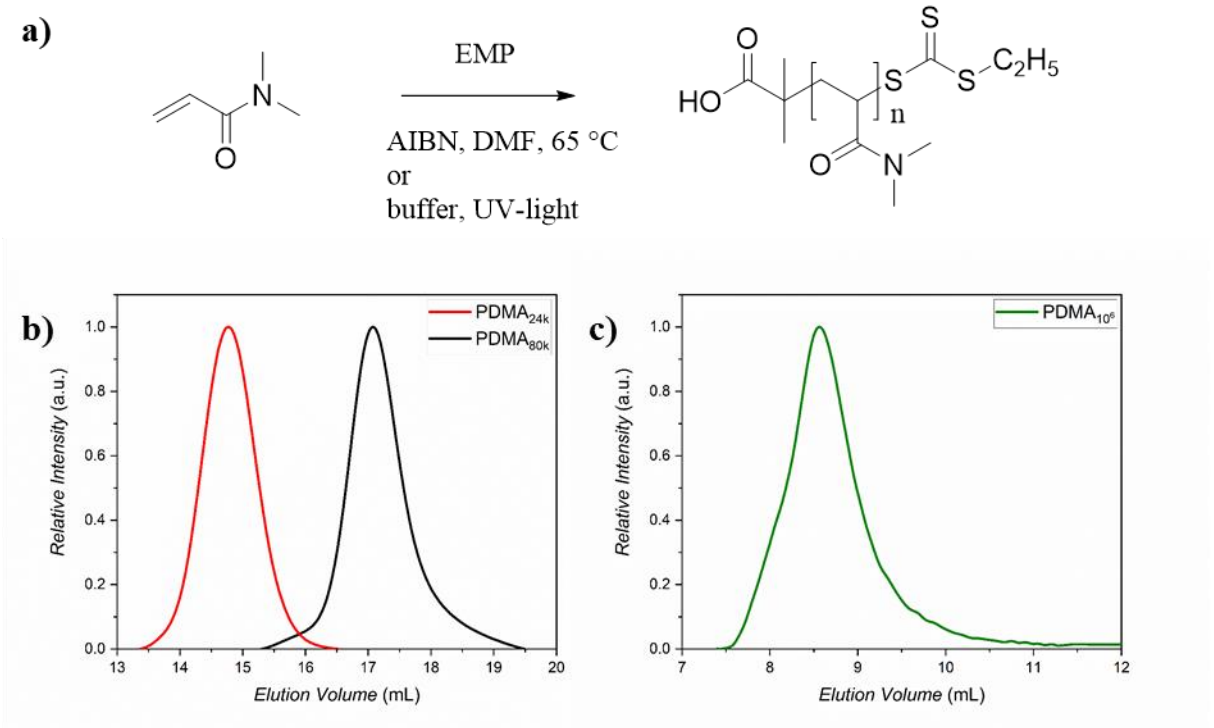

Figure 6.1. (a) Reaction scheme of the RAFT-polymerisation of DMA with EMP as chain-transfer agent, (b) results of SEC measurement of low and medium molar mass PDMA measured in NMP against PS standards and (c) result of SEC-MALS measurement of UHMW PDMA measured in 0.1 N $NaNO_3$ buffer.

Table 6-1. Results of SEC measurements.

Polymer	$M_{n,\,theory}$ (g·mol^{-1})	$M_{n,\,SEC}$ (g·mol^{-1})	$Đ$	dn/dc (mL g^{-1})
PDMA$_{24k}$[a]	**24,500**	**23,900**	**1.11**	**-**
PDMA$_{80k}$[a]	**118,800**	**80,000**	**1.06**	**-**
PDMA$_{10^6}$[b]	**1.5 · 10^6**	**1.07 · 10^6**	**1.40**	**0.1728 ± 0.0039**

a) low and medium molar mass PDMA measured in NMP against PS standards, b) SEC-MALS measurement of UHMW PDMA measured in 0.1 N $NaNO_3$ buffer.

6.3 ATPS of PDMA and pullulan

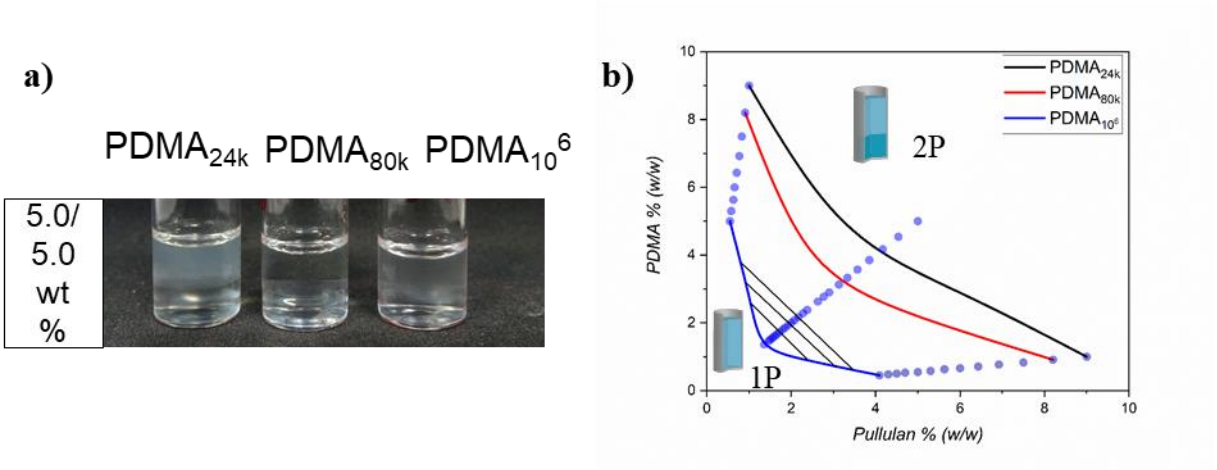

Figure 6.2. **(**a**)** ATPS of each combination at a total polymer concentration of 10 wt% (5 wt%/5 wt%). (b) Phase diagrams of the ATPS for all polymer combinations showing the experimental binodal (black, red and blue curve, respectively) and the dilution steps (blue dots) for the combination PDMA$_{10^6}$ & Pull.

In order to elucidate the phase behaviour of PDMA and pullulan in water and the influence of different molar mass, ATPS formation of pullulan and PDMA of different molar mass in aqueous solution were investigated. For that, phase diagrams were assembled for three different molar masses of PDMA (24k, 80k and 1· 10^6) with commercial pullulan. To develop the ATPS phase diagram, start solutions of total 10 wt% polymer concentration (9/1, 7.5/2.5, 5/5, 2.5/7.5, 1/9) were prepared. Subsequently, the solutions were mixed, equilibrated at ambient temperature to demix, investigated, and diluted to find the concentration at which only one phase is observed (Figure 6.2 a). The last concentration with visible phase separation, was used

as a data point for the binodal, which is the line separating the one- and two-phase area in the phase diagram (Figure 6.2 b). A shift of the binodal was observed depending on PDMA molar mass. For the combination with low and medium molar mass PDMA the binodal is located at higher concentration. The lowest concentration for an observed phase separation on equal polymer concentration were at 4.0/4.0 wt% for $PDMA_{24k}$ and 3.1/3.1 wt% for $PDMA_{80k}$. However, for the ATPS using UHMW PDMA the binodal is located at significantly lower concentrations with a lowest concentration for an observed phase separation on equal concentrations of polymer of 1.25/1.25 wt%. The results show the significant influence of the molar mass of the polymers for the minimum required polymer content for a phase separation. The higher the molar mass, the lower the required concentration for a stable ATPS, which is an effect known from literature.[74, 75]

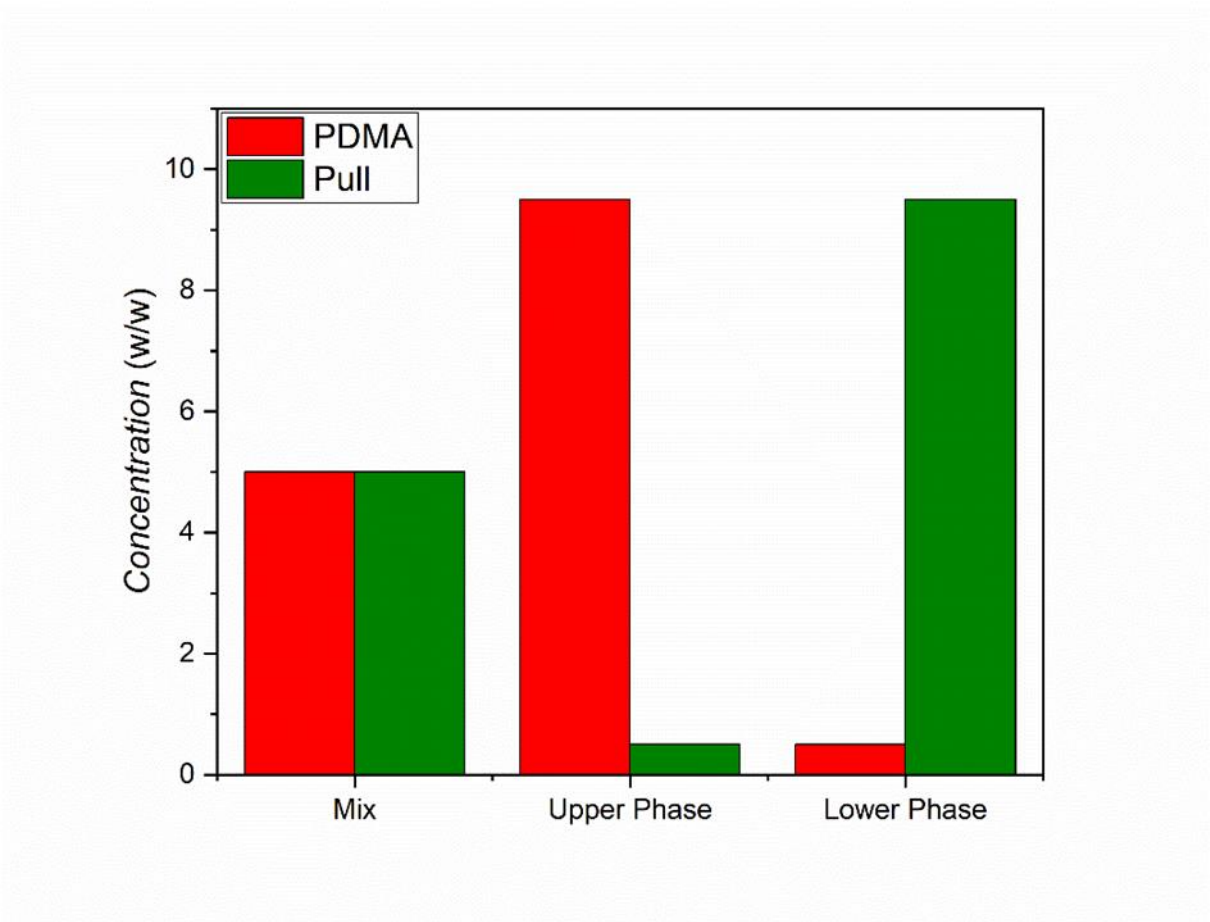

Figure 6.3. Concentration change directly after mixing and after phase separation (24 h), detected *via* ^{1}H-NMR in D_2O using DMF as internal standard, of $PDMA_{10}{}^6$ (red), Pull (green) for the ATPS of UHMW PDMA and Pull.

In order to quantify the demixing of the individual polymer types in the ATPS, the location and concentration of each polymer was detected via ^{1}H-NMR of each phase (Figure 6.13)

employing DMF as internal standard. The results showed a clear separation of the polymers after 24 h. PDMA was enriched in the upper phase and pullulan was enriched in the lower phase of the ATPS. However, in each phase a residual amount of the opposite polymer was present in the respective depleted phases. After 24 h the partition coefficients (Equation 6.1) for the ATPS of $PDMA_{10}^{6}$ and Pull were for 17.9 for $PDMA_{10}^{6}$ and 0.067 for Pull in the upper phase.

6.4 W/W emulsion stabilised by PDMAEMA-*b*-POEGMA

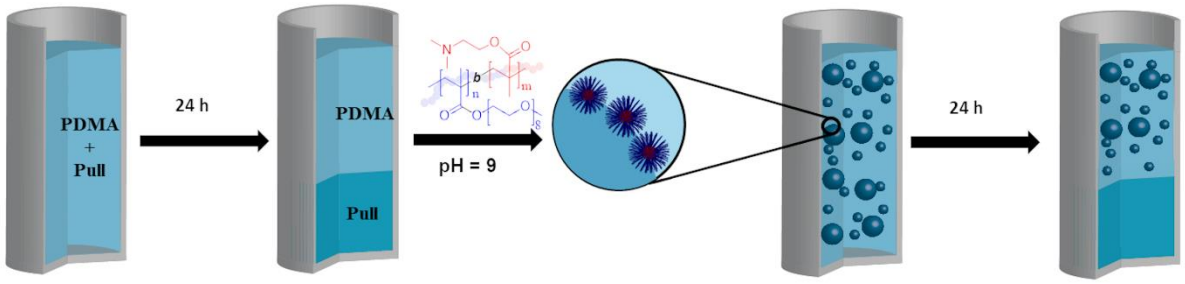

Scheme 6.2. ATPS formation of PDMA and Pullulan and w/w-emulsion stabilised with the block copolymer PDMAEMA-*b*-POEGMA at pH = 9.

To form a w/w emulsion the ATPS of UHMW PDMA and pullulan was chosen due to the low required polymer concentration for formation of a stable ATPS. An ATPS of UHMW PDMA and commercial pullulan was prepared at a concentration of 1.5/1.5 wt%, which was chosen because it is placed far enough in the two-phase area of the phase diagram to assure a stable ATPS. In order to stabilise the w/w emulsion, PS latex nanoparticles and poly(2-(dimethylamino)ethyl methacrylate)-*b*-poly(oligo(ethylene glycol) methyl ether methacrylate) (PDMAEMA-*b*-POEGMA) were used (Scheme 6.2).

In order to form w/w emulsions, PS latex nanoparticles with around 100 nm diameter were added to the ATPS to give a final stabiliser concentration of 0.1 wt%. Subsequently, the mixture was subjected to ultrasonic treatment for 2 min and shaken by hand for 1 min. The mixture turned cloudy, which indicated the formation of an emulsion stabilised with PS nanoparticles. In the following, the emulsion was analysed directly after preparation *via* bright-field microscopy displaying droplet formation (Figure 6.4a). The average droplet size directly after preparation was 32 ± 5 µm at pH=6 and 76 ± 26 µm at pH=9. After approximately 3 h the mixture started to phase-separate, which was completed after 24 h. The upper phase remained

cloudy, and the lower phase turned clear. Both phases were analysed *via* bright-field microscopy (Figure 6.4c and 6.14), revealing droplets in the upper phase and no droplets in the lower phase. The average droplet size after phase separation, in the cloudy phase was around 49 ± 22 µm at pH=6 and 118 ± 53 µm at pH=9. The results revealed droplet size increase during phase separation for the emulsion stabilised by PS. The droplet size increases most likely due to the phase separation and Ostwald ripening during the phase separation process until an equilibrium is reached. Additionally, the average droplet size of the emulsion in basic solution was significantly higher in comparison to the emulsion in acidic solution. One key factor for the droplet size is the preparation of the emulsion as it was treated ultrasound and shaken by hand only. More defined droplets could be generated e.g., via microfluidics.

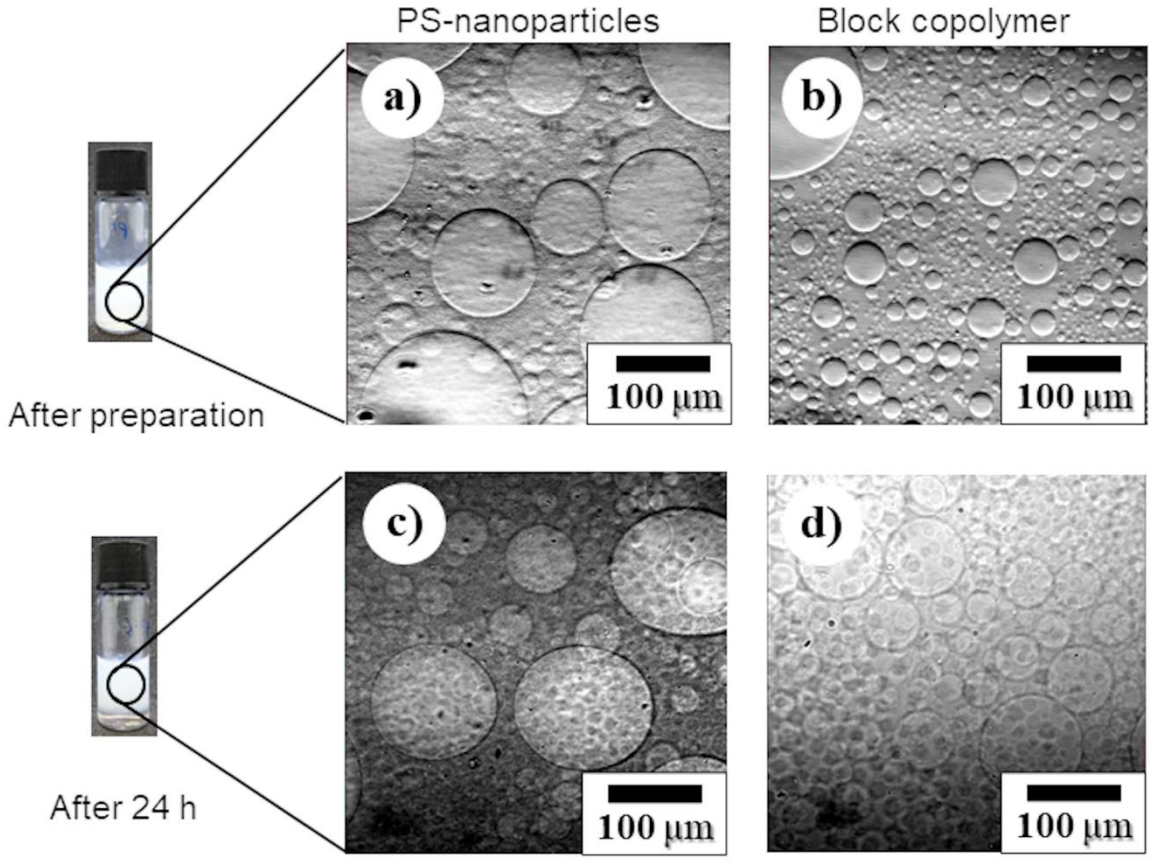

Figure 6.4. (a−d) Bright-field microscopy images of the w/w emulsion of UHMW PDMA and commercial Pullulan (1.5 wt%/1.5 wt%) stabilised with PS-nanoparticles and PDMAEMA-*b*-POEGMA at pH=9 (a, b) after preparation (a) stabilised with PS-nanoparticles, (b) stabilised with PDMAEMA-*b*-POEGMA, (c, d) upper phase after 24 h (c) stabilised with PS-nanoparticles and (d) stabilised with PDMAEMA-*b*-POEGMA.

In order to investigate a pH sensitive w/w emulsion stabiliser, PDMAEMA-*b*-POEGMA was employed. PDMAEMA-*b*-POEGMA was synthesised *via* RAFT polymerisation using 4-

cyano-4-(phenylcarbonothioylthio)pentanoic acid as a chain transfer agent. The block copolymer was obtained with a molar mass of 108000 g·mol^{-1} and a dispersity of $Đ$=1.37 (Figure 6.5). The block copolymer PDMAEMA-*b*-POEGMA was employed due to the pH sensitivity of the DMAEMA block leading to aggregate formation under basic conditions.[151] The formation of the block copolymer PDMAEMA-*b*-POEGMA is indicated by the increase of the molar mass from the first block to the block copolymer as well as the decrease of the elution volume. However, even after dialysis a shoulder is present around the area of the first block in the elugram of the block copolymer sample indicating a residual amount of the first block in the block copolymer. Dynamic-light scattering (DLS) revealed aggregates with a hydrodynamic diameter of 20 nm in basic aqueous solution (pH=9) and a hydrodynamic diameter of 3 nm in acidic aqueous solution indicating micelle formation and free block copolymer chains, respectively (Figure 6.12).

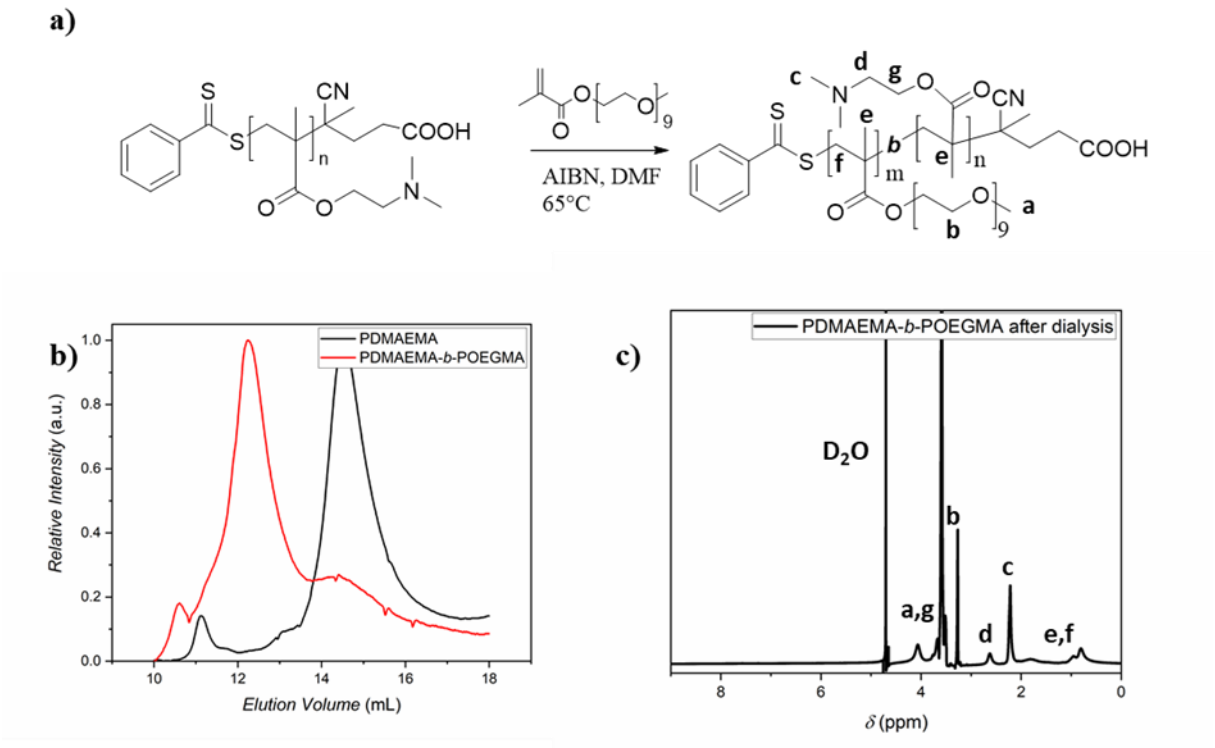

Figure 6.5. (a) Reaction scheme of the synthesis of the block copolymer PDMAEMA-*b*-POEGMA *via* RAFT polymerisation, (b) SEC measurement of PDMAEMA-*b*-POEGMA measured in DMF against PEG standards and (c) ^{1}H-NMR of PDMAEMA-*b*-POEGMA after dialysis.

For emulsion formation, PDMAEMA-*b*-POEGMA was dissolved at pH=9 and used at a concentration of 1 wt% in combination with the ATPS formed by $PDMA_{10}^{6}$ and Pull at a

concentration of 1.5/1.5 wt%. Afterwards, the mixture was treated like the PS nanoparticle stabilised emulsion employing ultrasound and shaking by hand.

Table 6-2. Average droplet size of 1.5/1.5 wt% ATPS formed by $PDMA_{10}^{6}$ and Pull and 0.1 wt% PS nanoparticles or 1 wt% PDMAEMA-*b*-POEGMA additive before phase separation and after 24 h of phase separation, measured over 30 particles.

ATPS	Droplet Size Emulsion [µm]	Droplet size after phase separation (24 h) [µm]
PDMA & Pull + PS at pH =6	**32 ± 5**	**49 ± 22**
PDMA & Pull + PS at pH =9	**76 ± 27**	**118 ± 53**
PDMA & Pull + BCP at pH =9	**86 ± 56**	**107 ± 31**

In contrast to the PS nanoparticle stabilised emulsion, the mixture stayed clear, which might be explained with the difference in stabiliser particle size (100 nm vs. 20 nm). Similar to the PS nanoparticle stabilised emulsion the phase separation started after around 3 h, which was complete after 24 h. The mixture was analysed directly after preparation and after 24 h *via* bright-field microscopy. Bright-field microscopy showed droplets direct after preparation and in the upper phase after 24h (Figure 6.4). No droplets were observed in the lower phase. The bright field microscopy and CLSM images indicate successful w/w emulsion formation from the ATPS formed by UHMW PDMA and pullulan using PS nanoparticles or PDMAEMA-*b*-POEGMA as stabiliser at pH=9. The average droplet size directly after preparation was 86 ± 56 µm at pH=9 and after 24 h, in the cloudy phase the average droplet size was around 107 ± 31 µm at pH=9.

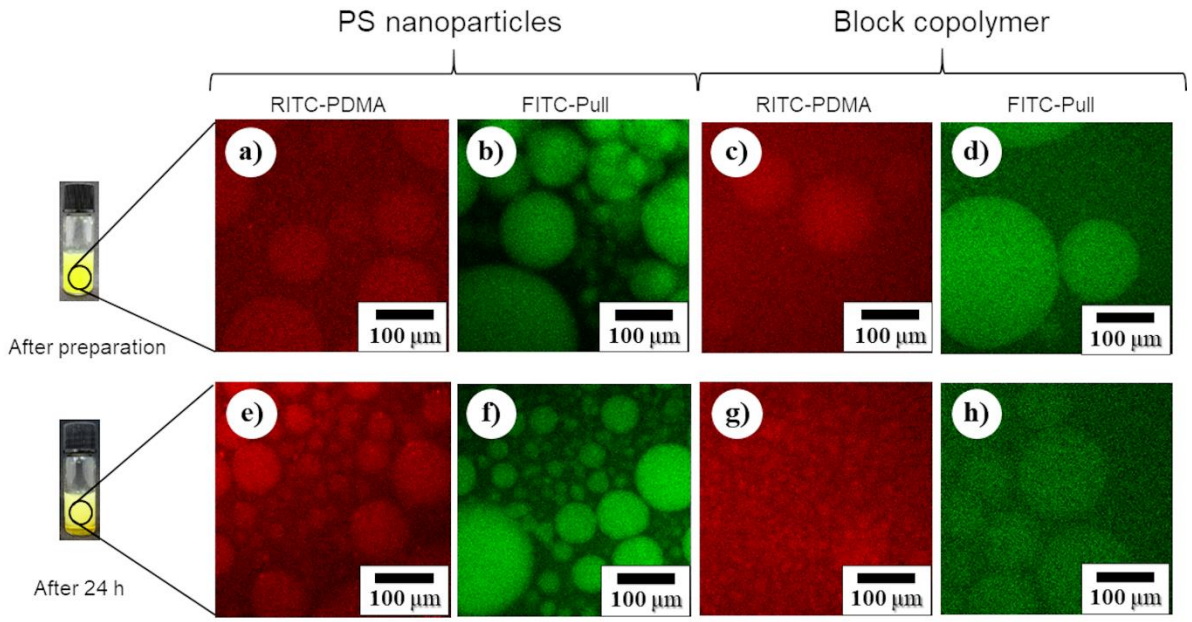

Figure 6.6. (a−b, e-f) CLSM images of the w/w emulsion of RITC−PDMA and FITC−Pullulan stabilised with PS-nanoparticles at pH = 9: (a-b) after preparation and (e-f) upper phase after 24 h, (c−d, g-h) CLSM images of the w/w emulsion of RITC-PDMA and FITC-Pullulan stabilised with PDMAEMA-*b*-POEGMA at pH = 9: (c-d) after preparation and (g-h) upper phase after 24h.

In order to localise the polymers in the emulsion, PDMA was labelled with RITC and pullulan was labelled with FITC. The emulsions were prepared for both stabilisers as described before and analysed *via* CLSM directly after preparation and after 24h (Figure 6.6). For the system stabilised with PS nanoparticles, the PDMA was located over the entire sample directly after the preparation. However, the pullulan was only present inside the emulsion droplets. After 24 h, similar to the bright field images, emulsion droplets were observed only in the upper phase of the two-phase system (Figure 6.6 a and b). In the upper phase PDMA was located again over the entire sample and pullulan was enriched inside the droplets (Figure 6.6 e and f). The CLSM images for the system stabilised with PDMAEMA-*b*-POEGMA displayed, directly after preparation, PDMA located over the entire sample and pullulan enriched inside the droplets (Figure 6.6 c and d). After 24 h emulsion droplets were observed in the upper phase only. Similar to the w/w emulsion stabilised with PS-nanoparticles, PDMA was located over the entire sample and the pullulan enriched inside the droplets (Figure 6.6 g and h). Overall, the CLSM results showed that for both stabilisers the polymers PDMA and pullulan are predominately present in different phases. The pullulan enriched inside the droplet and the UHMW PDMA enriched outside the droplets.

Especially the CLSM images of the PS nanoparticle system, indicate the presence of PDMA inside the droplets as well. The reason for the increased amount of PDMA in the Pull enriched droplets after phase separation could be the higher concentration of the PDMA in the upper phase and shift of the polymer ratio after phase separation. Another reason could be the non-perfect phase separation of the ATPS system PDMA and pullulan. Even after a period of 24 h there are approximately 10% of each polymer present in the opposite enriched phase. All CLSM images were prepared with only one dye present at a time. Furthermore, the results indicate the dye functionalisation does not have an influence on the partitioning of the polymers in the emulsion. In comparison to the w/w emulsions shown in Chapter 5 the emulsion was only stable in the upper phase after 24 h instead of be stable in the lower phase after 24 h. A significant influence for the location of the emulsion is the stabiliser. In all cases, including the stabiliser used in Chapter 5 (all three stabilisers: LDH nanoparticles, PS-nanoparticles and PDMAEMA-*b*-POEGMA), the stabiliser was enriched in a phase with an enriched poly(acrylamide).

6.5 pH-sensitive w/w emulsions

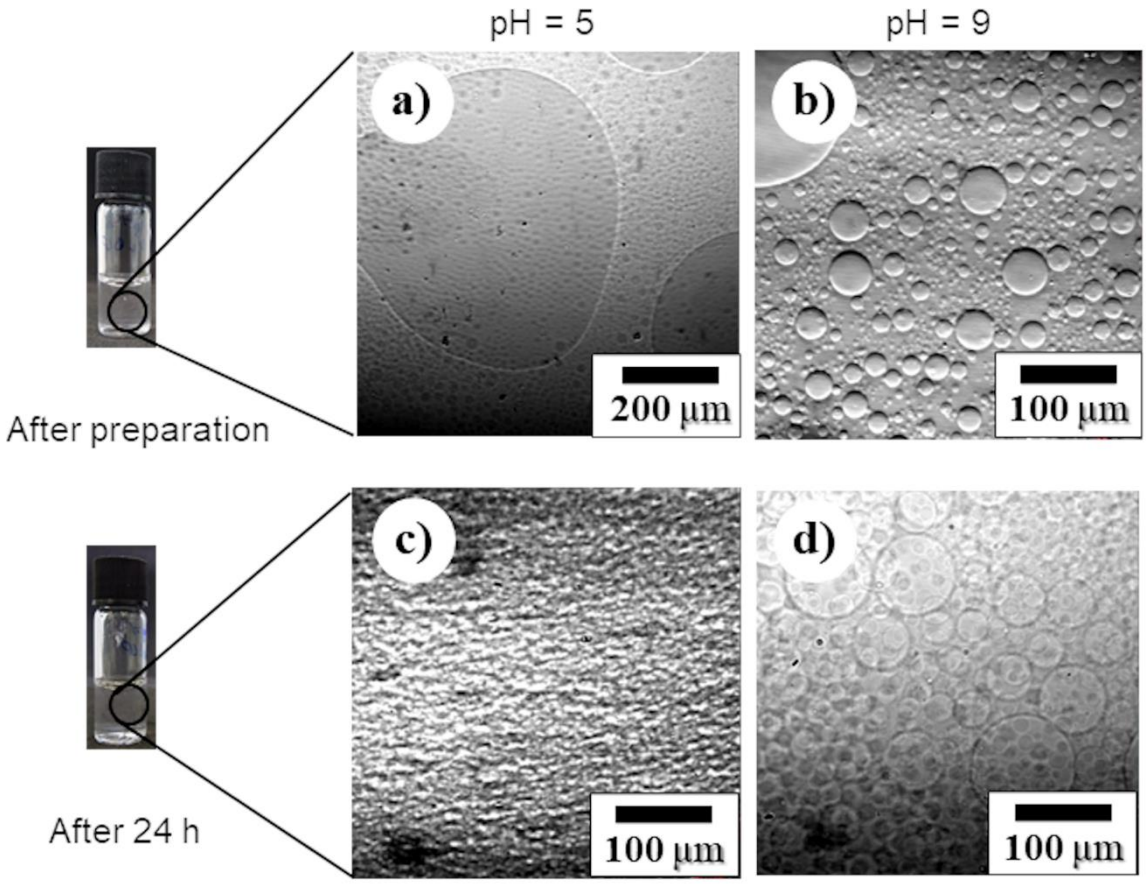

Figure 6.7. (a−d) Bright-field microscopy images of the w/w emulsion of UHMW PDMA and commercial Pullulan (1.5 wt%/1.5 wt%) stabilised with PDMAEMA-*b*-POEGMA (1 wt%) (a) after preparation at pH = 5, (b) after preparation at pH = 9, (c) upper phase after 24 h at pH =5 and (d) upper phase after 24 h at pH = 9.

In order to prove the pH influence and sensitivity of the emulsion stabilised by PDMAEMA-*b*-POEGMA, the emulsion was prepared under acidic and basic conditions. The emulsions were prepared with a polymer concentration of 1.5/1.5 wt% and stabilised with 1.0 wt% PDMAEMA-*b*-POEGMA. Two different emulsions were prepared, one at pH=5 and one at pH=9. The mixture was subjected to ultrasonic treatment for 2 min and shaken by hand for 1 min. The emulsion was analysed direct after preparation *via* bright-field microscopy (Figure 6.7 a and b). Furthermore, both samples were analysed by bright-field microscopy after 24 h. For the mixture prepared at pH=5 bright-field microscopy shows the formation of large droplets (>200 µm) directly after preparation. The significant larger droplets indicate that PDMAEMA-*b*-POEGMA could not successfully stabilise the w/w emulsion at pH=5. The larger droplets

show coalescence on the way to a complete phase separation of the mixture. The bright-field images after 24 h showed no droplets at all, which substantiate the unsuccessful stabilisation of the emulsion. The insufficient stabilisation is indicated by DLS showing only small particle diameters of the block copolymer under acidic conditions, due to the protonated form of DMAEMA, according to single polymer coils (Figure 6.12) that are not capable of w/w emulsion stabilisation. However, at pH=9 the block copolymer shows small aggregate formation due to the deprotonated DMAEMA at higher pH. The aggregate formation was confirmed in the DLS results (Figure 6.12) The bright-field images at pH=9, display droplet formation directly after preparation, which indicates a presence of an emulsion stabilised by PDMAEMA-*b*-POEGMA micelles. Furthermore, after 24 h droplet formation could only be observed in the upper phase (Figure 6.7 d).

Overall, the w/w emulsion using the ATPS of UHMW PDMA and pullulan could be stabilised using the block copolymer PDMAEMA-*b*-POEGMA. The emulsion is only stable in basic aqueous solution (pH=9), due to the aggregation of the block copolymer under those conditions. In acidic solution however, the emulsion could not be stabilised by the block copolymer PDMAEMA-*b*-POEGMA. In contrast, non-pH responsive PS nanoparticles were capable of stabilising the w/w emulsion in basic and acidic medium (Figure 6.14).

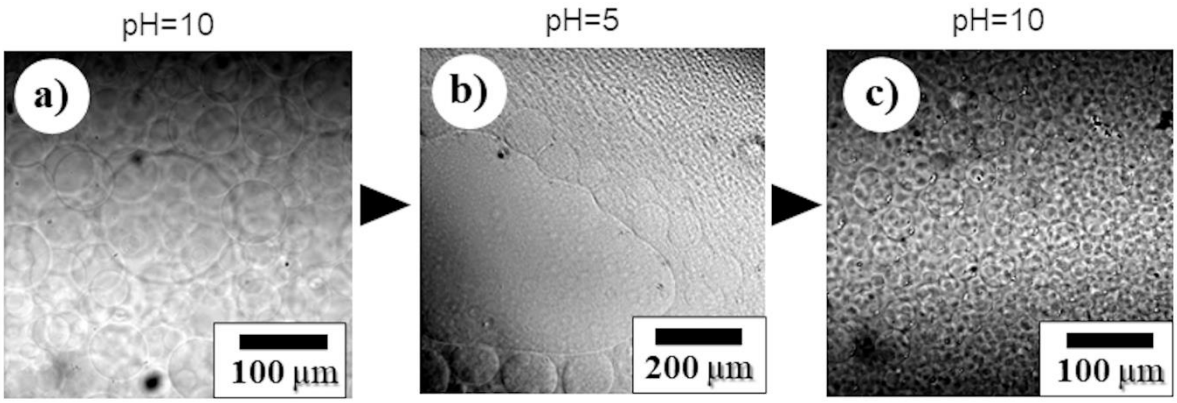

Figure 6.8. (a−c) Bright-field microscopy images of the pH-sensitive w/w emulsion of UHMW PDMA and commercial pullulan (1.5 wt%/1.5 wt%) stabilised with PDMAEMA-b-POEGMA (1 wt%) (a) at pH=10 (b) at pH=5 after pH change with HCl and redispersion and (c) at pH=10 after pH change with NaOH and redispersion.

The results before showed the influence of the pH value on the stabilisation of the w/w emulsion of UHMW PDMA and pullulan stabilised by PDMAEMA-*b*-POEGMA. In order to

prove the sensitivity and switchability of stabilisation using PDMAEMA-*b*-POEGMA, the pH value was switched in the mixture multiple times. The emulsion was prepared with a polymer concentration of 1.5/1.5 wt%, a block copolymer concentration of 1.0 wt% and a start pH value of pH=10. The mixture was subjected to ultrasonic treatment for 2 min and shaken by hand for 1 min. A small sample was taken for analysis. Afterwards, the pH was changed to pH=5 using conc. HCl, and the sample subjected to ultrasonic treatment and shaking by hand again. A sample was retrieved for analysis and the pH was changed to pH=10 using NaOH solution, and the sample was redispersed. All samples were analysed *via* bright-field microscopy (Figure 6.8). For the first sample at pH=10 the microscope images showed droplet formation (Figure 6.8 a). After the pH change to acidic, the displayed droplets were significantly larger, due to an unstable w/w emulsion and onset of phase separation in the sample (Figure 6.8 b). However, after a pH change to basic, the emulsion droplets were stable again (Figure 6.8 c). Overall, the results show that the w/w emulsion of the UHMW PDMA and pullulan, stabilised by PDMAEMA-*b*-POEGMA is pH sensitive. In basic aqueous solution the emulsion is stable. If the pH value is changed to acidic, the block copolymer is not stabilising the emulsion anymore. The w/w emulsion can be stabilised again with a change of the pH back to basic. However, pH switches are limited by concentration as the sample is diluted by a small amount during the pH switch. If the polymer concentration will drop under the limit of the ATPS binodal the emulsion is not stable anymore.

6.6 Conclusion

ATPS and w/w emulsions are a major topic in current polymer chemistry research. In here, a new ATPS consisting of PDMA, and pullulan was investigated. The stability of the PDMA/pullulan ATPS is depending on the molar mass of the polymers. As such, the required concentration for a stable ATPS can be decreased significantly with an increase of the molar mass of one of the polymers. In addition, the ATPS was used to form w/w emulsions, stabilised by PS nanoparticles or the block copolymer PDMAEMA-*b*-POEGMA in basic aqueous solution. The emulsion was stable in the mixture and after phase separation in the upper phase. Pullulan was enriched inside the droplets and PDMA was located all over the sample. Furthermore, w/w emulsions stabilised by PDMAEMA-*b*-POEGMA was pH sensitive, i.e., depending on the pH the emulsion could be stabilised or not stabilised by the block copolymer.

The next chapter will be focusing on the self-assembly and crosslinking of a block copolymer formed with Pull and poly(acrylamides) in aqueous solution.

6.7 Experimental Part

RAFT-polymerisation of DMA_{24k}

In a dry and nitrogen purged 50 mL Schleck tube, destabilised DMA (1.0 g, 10 mmol, 250 eq.), EMP (9.0 mg, 0.04 mmol, 1.0 eq.), AIBN (1.3 mg, 0.008 mmol, 0.2 eq.) were dissolved in DMF (3 mL). The solution was degassed by three freeze-pump-thaw cycles and placed in a pre-heated oil bath (65 °C). Subsequently, the reaction mixture was stirred for 24 h, stopped by cooling down with liquid nitrogen and exposure to air. Afterward, the polymer was dialysed against deionised water (Spectra/Por 3500 Da) for three days, freeze-dried and a yellow solid (992 mg, Mn = 23,918 g·mol^{-1}, $Đ$ = 1.11 measured in NMP against PS standards) was obtained.

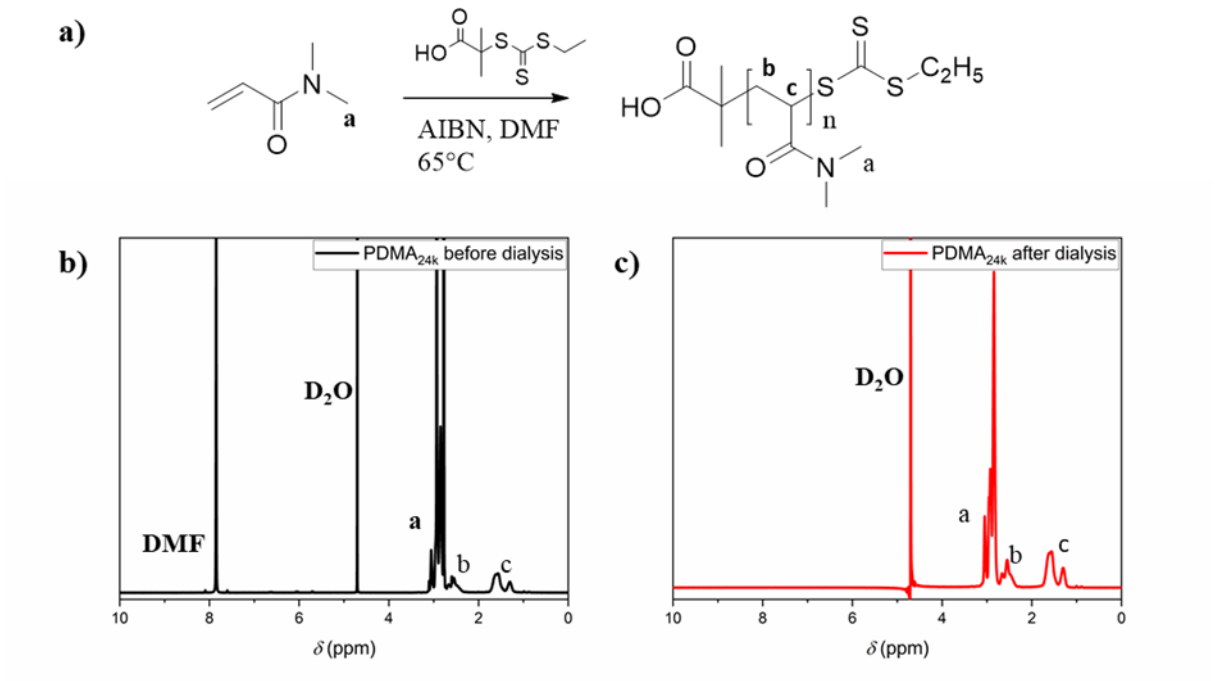

Figure 6.9. (a) Reaction scheme of the RAFT-polymerisation of DMA, (b and c) ^{1}H-NMR of $PDMA_{24k}$ in D_2O (b) before dialysis and (c) after dialysis.

RAFT-polymerisation of DMA_{80k}

In a dry and nitrogen purged 50 mL Schlenk tube, EMP (9.4 mg, 0.042 mmol, 1.0 eq.), and AIBN (1.4 mg, 0.0085 mmol, 0.2 eq.) were dissolved in DMF (300 µL) and DMA (5.0 g, 10 mmol, 1200 eq.) added. The solution was degassed by three freeze-pump-thaw cycles and placed in a pre-heated oil bath (65 °C). Subsequently, the reaction mixture was stirred for 19 h, stopped by cooling with liquid nitrogen and exposure to air. Afterwards, the polymer was dialysed against deionised water (Spectra/Por 3500 Da) for three days, freeze-dried and a white solid (4.25 g, M_n = 80,000 g·mol^{-1}, $Đ$ = 1.06 measured in NMP against PS standards) was obtained.

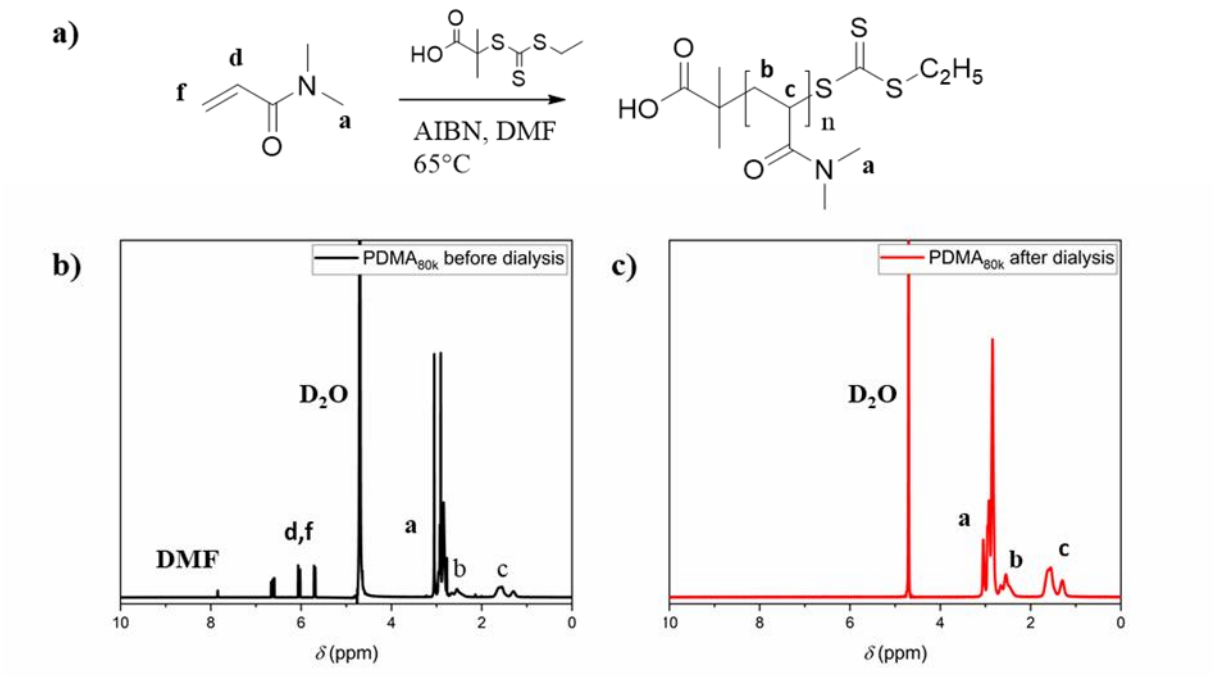

Figure 6.10. (a) Reaction scheme of the RAFT-polymerisation of DMA, (b and c) ^{1}H-NMR of $PDMA_{24k}$ in D_2O (b) before dialysis and (c) after dialysis.

PI-RAFT-polymerisation of DMA_{10}^{6}

Destabilised DMA (1.0 g, 10 mmol, 15151 eq.), EMP (146 µL, 0.06 µmol, 1.0 eq. from a DMSO stock 1 mg mL^{-1} DMSO), and acetate buffer (1 mL, 0.2 M, pH=5) were mixed in a vial (7 mL) containing a stirring bar and sealed with a septum. The solution was bubbled for 30 min with nitrogen and the polymerisation was initiated by an UV-lamp (nail-lamp). The polymerisation was stopped after 24 h. Subsequently, the polymer was dialysed against deionised water (Spectra/Por 3500 Da) for 3 days. Finally, the sample was freeze-dried, and a white solid (780 mg, $M_n = 1.07 \cdot 10^6$ g · mol^{-1}) was obtained.

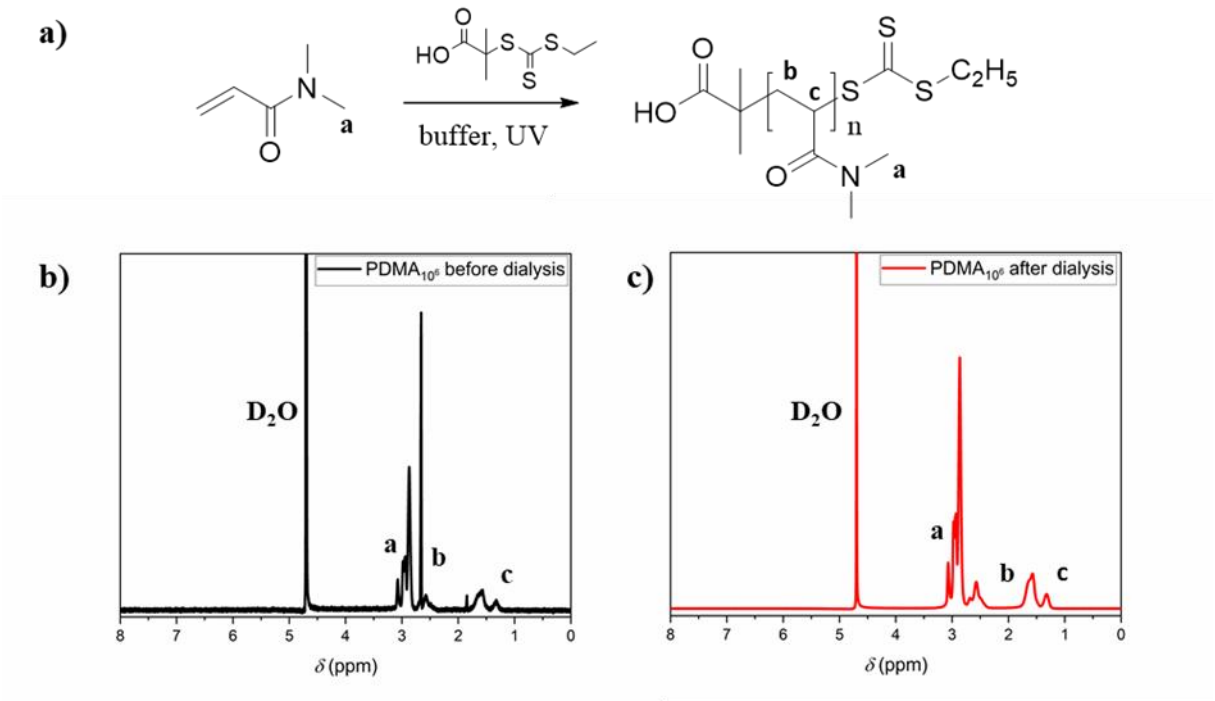

Figure 6.11. (a) Reaction scheme of the photo induced RAFT-polymerisation of DMA, (b and c) ^{1}H-NMR of $PDMA_{10}^{6}$ in D_2O (b) before dialysis and (c) after dialysis.

Formation of Rhodamine B labelled PDMA

In a dry, argon purged 100 mL round bottom Schlenk flask, PDMA (0.05 g, 0.0001 mmol, 1.0 eq.) was dissolved in dry DMSO (5 mL). Hexylamine (53 µg, 0.00026 mmol 2.5 eq.) was added, placed in a pre-heated oil bath (50 °C) and stirred overnight. Afterwards, the reaction mixture was cooled down to ambient temperature, Rhodamine B ITC (0.42 mg, 0.0008 mmol, 7.5 eq.) was added and the solution stirred over night at 50 °C. The mixture was cooled down to ambient temperature and diluted with deionised water. Afterwards, the polymer was dialysed against deionised water (Spectra/Por 3500 Da) for three days, freeze-dried and a purple solid (45.7 mg) was obtained.

Formation of FITC labelled pullulan

Pullulan (300 mg) was dissolved in DMSO (3 mL) containing pyridine (50 µL). Subsequently, FITC (30 mg, 0.077 mmol, 1.0 eq.) and dibutyltin dilaurate (6 mg, 0.0095 mmol, 0.12 eq.) were added to the solution and the mixture was heated up for 2 h at 95 °C. Afterwards, the mixture was cooled down to ambient temperature and precipitated several times in ethanol, followed by dialysis against deionised water (Spectra/Por 3500 Da) for five days. Finally, the product was freeze-dried and an orange solid (302 mg) was obtained.

RAFT-polymerisation of DMAEMA

In a dry and nitrogen purged 50 mL Schlenk tube, destabilised DMAEMA (2.0 g, 12.7 mmol, 130 eq.), 4-cyano-4-(phenylcarbonothioylthio)pentanoic acid (27.0 mg, 0.097 mmol, 1.0 eq.) and AIBN (3.1 mg, 0.019 mmol, 0.2 eq.) were dissolved in DMF (5 mL). The solution was degassed by three freeze-pump-thaw cycles and placed in a pre-heated oil bath (65 °C). Subsequently, the reaction mixture was stirred for 24 h, stopped by cooling with liquid nitrogen and exposure to air. Afterwards, the polymer was dialysed against deionised water (Spectra/Por 3500 Da) for three days, freeze-dried and a yellow solid (1.4 g, M_n = 13900 g·mol^{-1}, $Đ$ = 1.2 measured in DMF against PEG standards) was obtained.

Formation of PDMAEMA-*b*-POEGMA via RAFT-polymerisation

In a dry and nitrogen purged 50 mL Schlenk tube, destabilised OEGMA (1.5 g, 3.0 mmol, 84 eq.), PDMAEMA (500 mg, 0.035 mmol, 1.0 eq.) and AIBN (1.1 mg, 0.007 mmol, 0.2 eq.) were dissolved in DMF (5 mL). The solution was degassed by three freeze-pump-thaw cycles and placed in a pre-heated oil bath (65 °C). Subsequently, the reaction mixture was stirred for 24 h, stopped by cooling with liquid nitrogen and exposure to air. Afterwards, the polymer was dialysed against deionised water (Spectra/Por 3500 Da) for three days, freeze-dried and a yellow solid (1.99 g, M_n = 108,000 g·mol^{-1}, $Đ$ = 1.37 measured in DMF against PEG standards) was obtained.

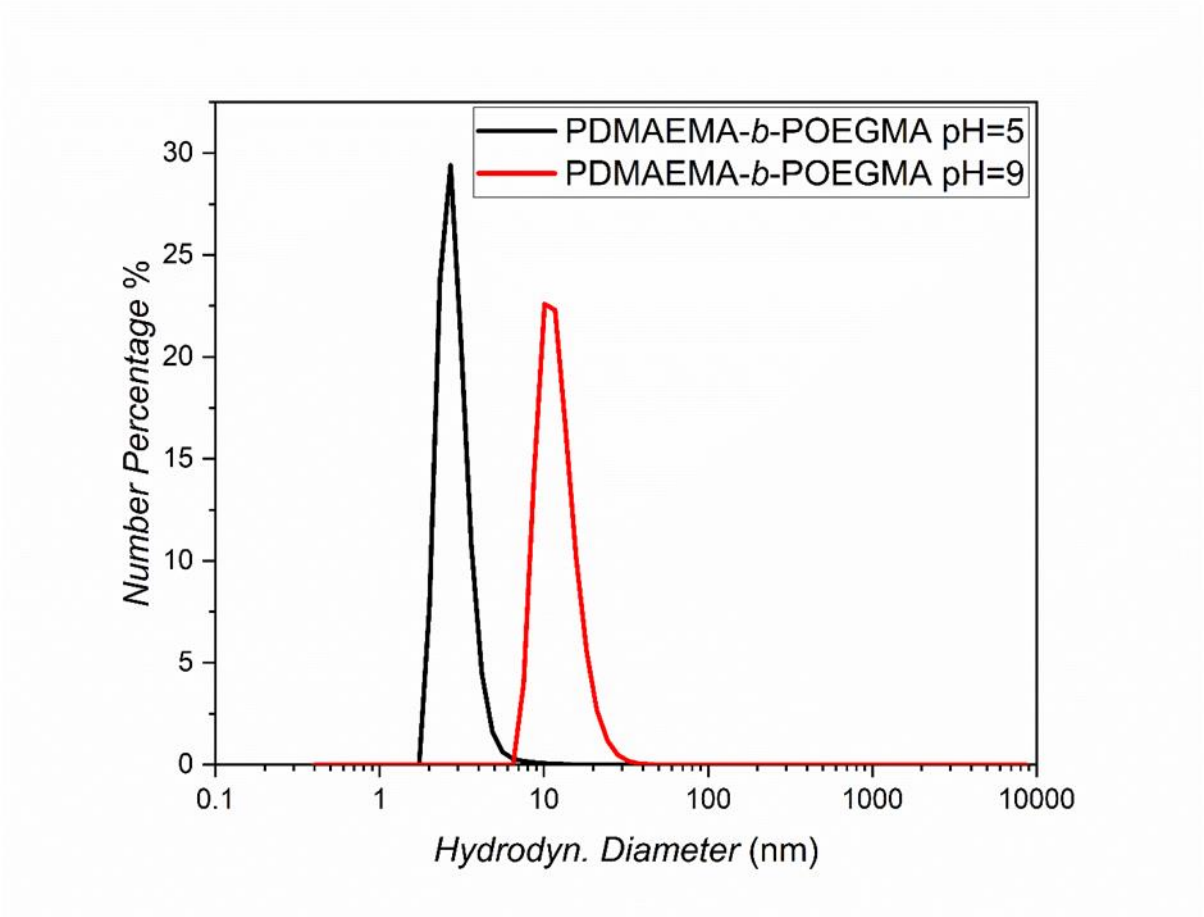

Figure 6.12. Comparison of number weighted particle size distribution of PDMAEMA-*b*-POEGMA in aqueous solution at pH=5 (1.0 wt%, black curve) and PDMAEMA-*b*-POEGMA in aqueous solution at pH=10 (1.0 wt%, red curve) at ambient temperature.

Preparation of ATPS and phase diagram

PDMA (50 mg) was dissolved in deionised water (450 mg) to obtain a 10 wt% solution. A 10 wt% solution of pullulan was prepared in the same way. Afterwards both solutions were mixed to receive a 5.0 wt% / 5.0 wt% mixture. Subsequently, the solution was equilibrated at ambient temperature in order to demix, investigated and diluted (100 mg of deionised water each cycle). The process was repeated, until no phase separation was observed, which was recorded as the data point of the binodal curve. All other concentration combinations were conducted in a similar way.

Preparation of w/w emulsions using PDMAEMA-*b*-POEGMA

UHMW PDMA (15 mg) and Pull (15 mg) were dissolved in water (470 mg, pH = 5 or 9) to form a 3.0/3.0 wt % solution. PDMAEMA-*b*-POEGMA (10 mg) was dispersed in water (490 mg, pH = 5 or 9) to generate a 2.0 wt % dispersion. Both solutions were combined to obtain a concentration of 1.5/1.5 wt % polymer and 1.0 wt % PDMAEMA-*b*-POEGMA in the mixture. The mixture was subjected to ultrasonic treatment for 2 min, shaken by hand for 1 min, and subsequently analysed via CLSM. After 24 h, phase separation was observed and the sample was analysed again via CLSM. All other concentration combinations were prepared in a similar way.

Preparation of w/w emulsions using PS latex nanoparticles

UHMW PDMA (15 mg) and pullulan (15 mg) were dissolved in water (470 mg, pH = 5 or 9) to form a 3.0/3.0 wt % solution. PS latex nanoparticles (10 µL of a 10% stock solution) were dispersed in water (490 mg, pH = 5 or 9) to generate a 0.2 wt % dispersion. Both solutions were combined to obtain a concentration of 1.5/1.5 wt % polymer and 0.1 wt % PS nanoparticles in the mixture. The mixture was subjected to ultrasonic treatment for 2 min, shaken by hand for 1 min, and subsequently analysed via CLSM. After 24 h, phase separation was observed, and the sample was analysed again via CLSM.

Preparation of w/w emulsions with addition of labelled PDMA and Pull

PDMA (12 mg), RITC−PDMA (3 mg), pullulan (12 mg), and FITC−Pullulan (3 mg) were dissolved in water (470 mg, pH = 5 or 9) to form a 3.0/3.0 wt % solution. PDMAEMA-*b*-POEGMA (10 mg) were dispersed in water (490 mg, pH = 5 or 9) to generate a 2.0 wt % dispersion. Both mixtures were combined to obtain a concentration of 1.5/1.5 wt % polymer and 1.0 wt % PDMAEMA-*b*-POEGMA in the mixture. The mixture was subjected to ultrasonic treatment for 2 min, shaken by hand for 1 min, and subsequently analysed *via* CLSM. After 24 h, phase separation was observed and the sample was analysed again via CLSM. All other concentration combinations were prepared in a similar way.

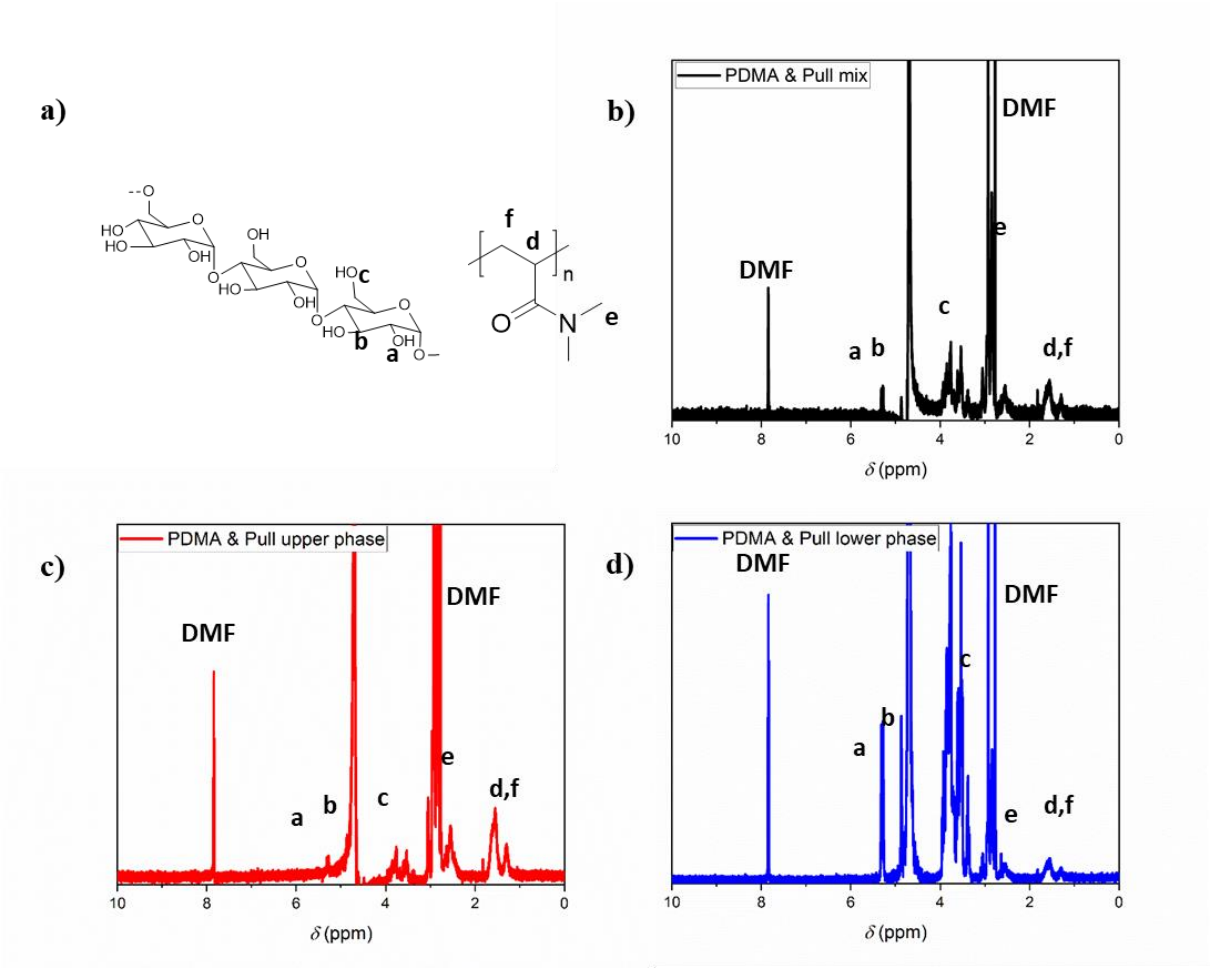

Figure 6.13. (a) Structures of Pull and PDMA and (b-d) ^{1}H-NMR in D_2O of the (b) mixture, (c) upper and (d) lower phase after 24 h for the combination $PDMA_{10}^{6}$ & Pull using DMF as internal standard.

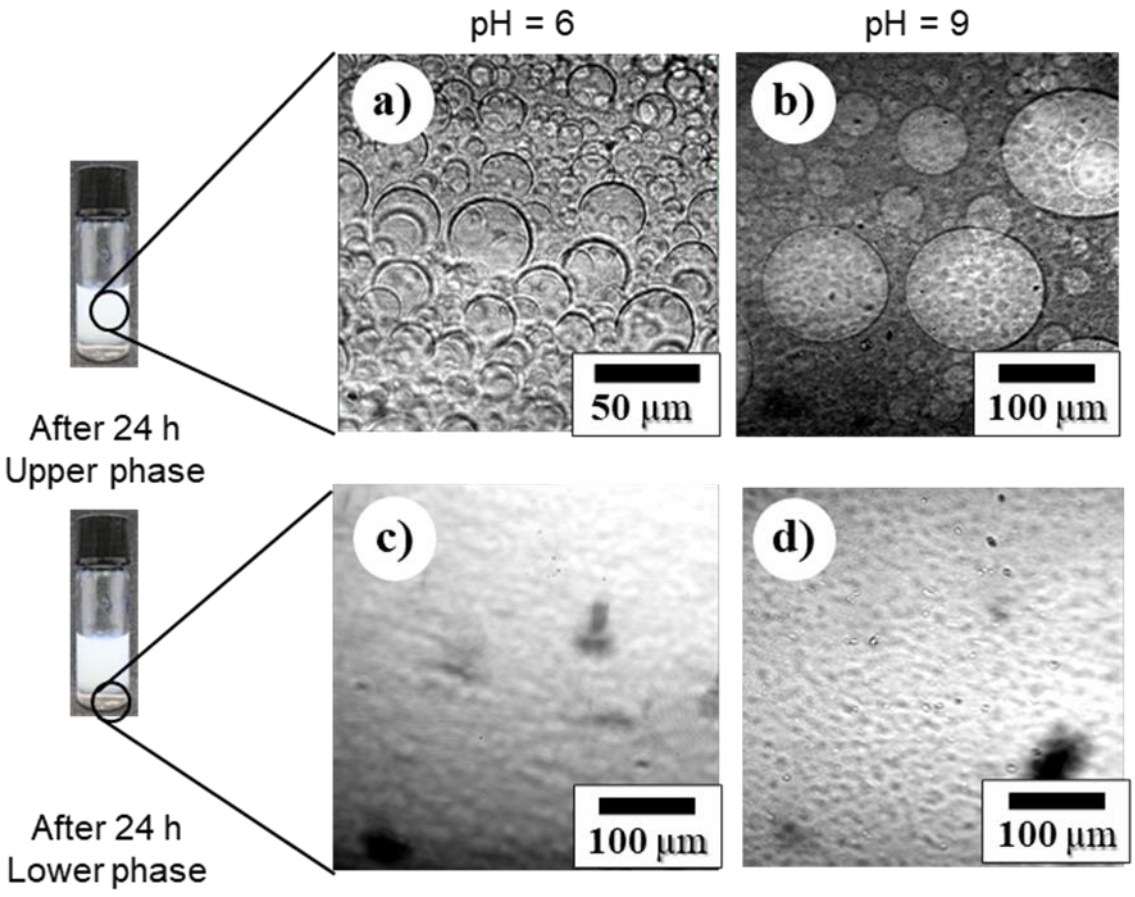

Figure 6.14. (a−d) Bright-field microscopy images of the w/w emulsion of UHMW $PDMA_{10}^{6}$ and Pull (1.5 wt %/1.5 wt %) stabilised with PS nanoparticles (0.1 wt%) after 24 h (a) upper phase at pH = 6, (b) upper phase at pH = 9, (c) lower phase at pH =6 and (d) lower phase at pH = 9.

Chapter 7

7 Aggregation and Crosslinking of Poly(*N*,*N*-dimethylacrylamide)-b-pullulan Double Hydrophilic Block Copolymers

7.1 Introduction [d]

The previous chapters discussed the phase separation of different hydrophilic polymers in aqueous solution. Aggregation for pure hydrophilic DHBCs can be established *via* the different degree of hydrophilicity of the different blocks.[6, 152] At high concentration the pure hydrophilic DHBCs showed self-assembly structures with specially chosen block combinations in aqueous solution. However, during dilution the formed self-assembly structures start to break down. Similar to Chapter 5 and 6, the self-assembly of the DHBCs can be understood from the perspective of aqueous multi-phase systems that feature phase separation of homopolymer mixtures in water at elevated concentration.[81, 85, 118, 153] According to the previous chapters, the combination of the polysaccharide pullulan and polyacrylamides are a good choice for a novel DHBC. The homopolymers showed, depending on the concentration, a stable ATPS and a stable w/w emulsion. The previous results indicate the difference in the hydrophilicity of Pull and PDMA is potentially high enough for a successful DHBC self-assembly. Moreover, previous studies showed the potential of pullulan as one polymer for a DHBC self-assembly.[57, 59, 154]

As described in the previous chapter, the synthesis of DHBCs can be conducted via reversible addition–fragmentation chain transfer (RAFT) polymerisation. An alternative route to form DHBCs is *via* copper catalysed alkyne–azide cycloaddition (CuAAc) (1,3-dipolar cycloaddition) first described by Huisgen[51] *et al.* and comparatively by Kolb and Sharpless[52] described as click chemistry, which could also be used for the preparation of various macromolecular architectures.[53, 54] For the formation of a novel block copolymer, one homopolymer needs to be alkyne end-functionalised and the second polymer should be azido end-functionalised. One route to form alkyne end-functionalised polymer is to functionalise

[d] Terms of use: This chapter was adapted with permission from: A. Plucinski, J. Willersinn, R. B. Lira, R. Dimova, B. V. K. J. Schmidt, *Macromol. Chem. Phys.* **2020,** 221, 2000053. reference licensed under CC BY 3.0, Contribution by A. Plucinski in the following chapter about 75%.

bio-based polymers, *e.g.*, pullulan[155] or synthetic polymers, *e.g.*, poly(2-hydroxyethyl methacrylate) (PHEMA)[156] with an alkyne end group. For hydrophilic azido end-functionalised polymers, RAFT polymerisation[157] is a technique to synthesise functionalised poly(acrylamides), *e.g.*, PDMA.[158] Consequently, a large pool of possible block copolymer combinations formed by CuAAC is available. Starting from a small number of building blocks, it is possible to form a significant number of different block copolymers.

A significant factor for future applications of DHBC aggregation is a high stability. One method to improve the stability is crosslinking of the DHBCs aggregates.[159] For pullulan based DHBCs, crosslinking of the pullulan block was investigated in the past to improve aggregate stability in aqueous solution, *e.g.*, *via* sodium trimetaphosphate (STMP)[57] or *via* cystamine forming dynamic covalent imine linkages with aldehyde groups after pullulan oxidation.[127] Moreover, there are many different options from supramolecular chemistry to crosslink DHBCs, *e.g.*, via hydrogen bonds or host-guest inclusion complexes.[160, 161] An alternative avenue for crosslinking of polymers is the reaction of primary amines or hydroxylamine with aldehydes or ketones to generate an oxime or imine bond, which was already used to form biocompatible hydrogels.[162] As such, the formation of a reversible oxime bond is an efficient technique to modify the structure of macromolecules.[163, 164] For example, oxime formation was used by Sumerlin and co-workers for the crosslinking of polymers containing diacetone acrylamide (DAAM) as repeating unit in aqueous solution.[165]

In the current chapter, the self-assembly behaviour of the DHBC Pull-*b*-(PDMA-*co*-PDAAM) in aqueous environment is investigated. Toward this, alkyne end-functionalised pullulan is coupled *via* CuAAc with an azide end-functionalised PDMA-*co*-PDAAM. Subsequently, Pull-*b*-(PDMA-*co*-PDAAM) is analysed via ^{1}H-NMR, ^{13}C-NMR spectroscopy, and size exclusion chromatography (SEC). Additionally, the Pull-*b*-(PDMA-*co*-PDAAM) is crosslinked via oxime formation (Scheme 7.1), which is investigated *via* ^{1}H-NMR and ^{13}C-NMR spectroscopy. Moreover, the aggregation behaviour of Pull-*b*-(PDMA-*co*-PDAAM) and crosslinked Pull-*b*-(PDMA-*co*-PDAAM) is analysed *via* cryo SEM, dynamic light scattering (DLS), and confocal laser scanning microscopy (CLSM). Additionally, the behaviour of the aggregates in the organic solvent *N*-methyl-2-pyrrolidone (NMP) is studied as well.

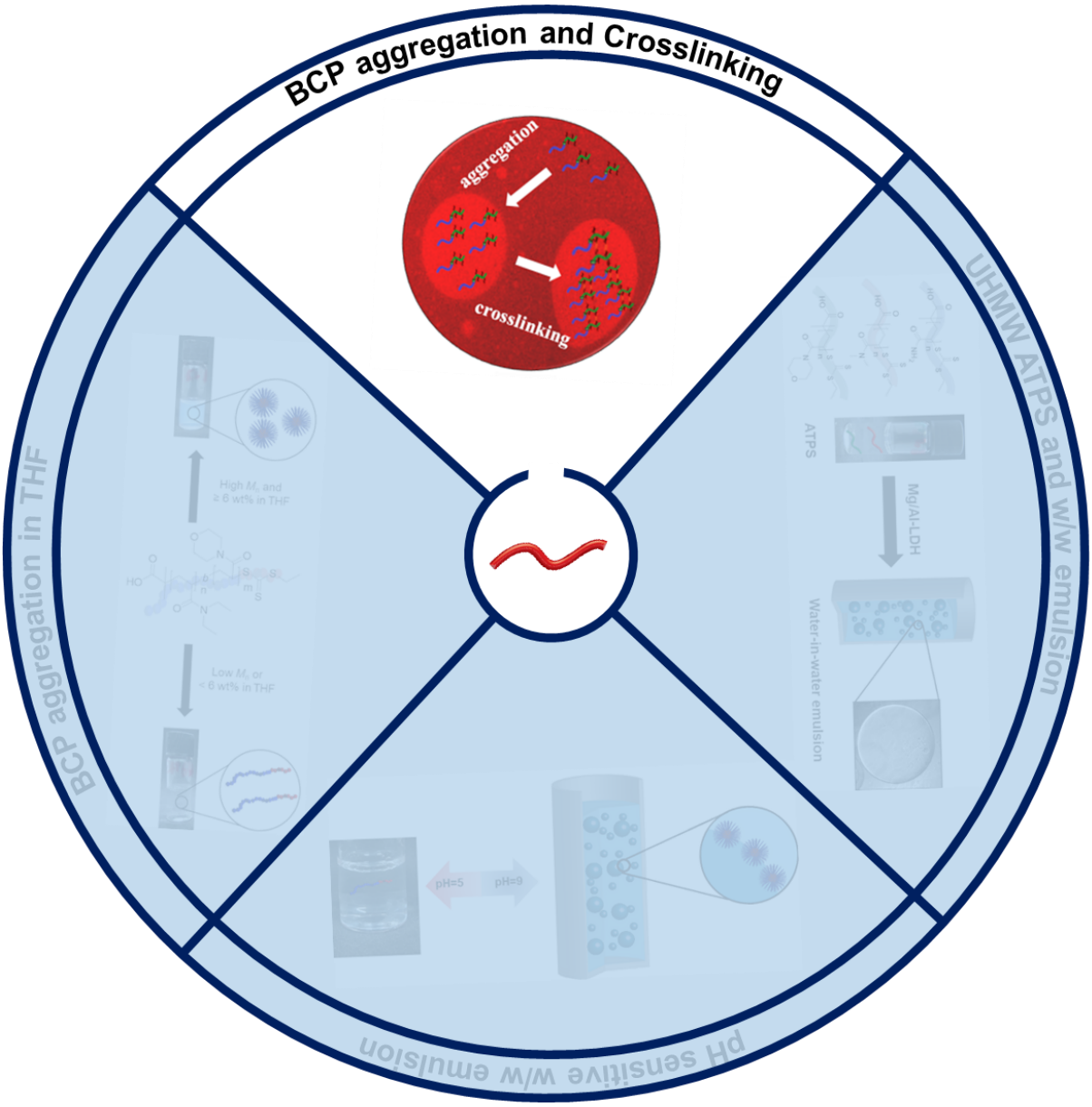

Scheme 7.1. Overview of the different utilisation of hydrophilic polymers for self-assembly or phase separation, highlighted the part of the current chapter: DHBC aggregation and crosslinking.

7.2 Synthesis of end functionalised PDMA-*co*-PDAAM and pullulan[e]

Copolymers like PDMA-*co*-PDAAM are easily formed via reversible deactivation radical polymerisation *e.g.* RAFT polymerisation. Dodecylthiocarbonylthio-2-methylpropanoic acid 3'-azido propyl ester was used as chain transfer agent based on the procedure from literature.[158] The ratio between DMA and DAAM was adjusted to 1:4, to introduce a ratio of 20 % of DAAM in the final copolymer. PDMA-*co*-PDAAM was obtained as copolymer with molar mass of 27,800 g · mol^{-1} and a Đ of 1.9 (Scheme 7.2a). The presence of both monomers in the azido functionalised polymer was proven by ^{1}H-NMR spectroscopy that shows the peaks for PDMA and PDAAM at 3.0 ppm and 2.1 ppm. The integral ratio between the peak at 3.0 ppm for the two methyl groups (PDMA) and the terminal single methyl group (PDAAM) at 2.1 ppm is around 8:1. According to the integration the content of PDAAM is 20%.

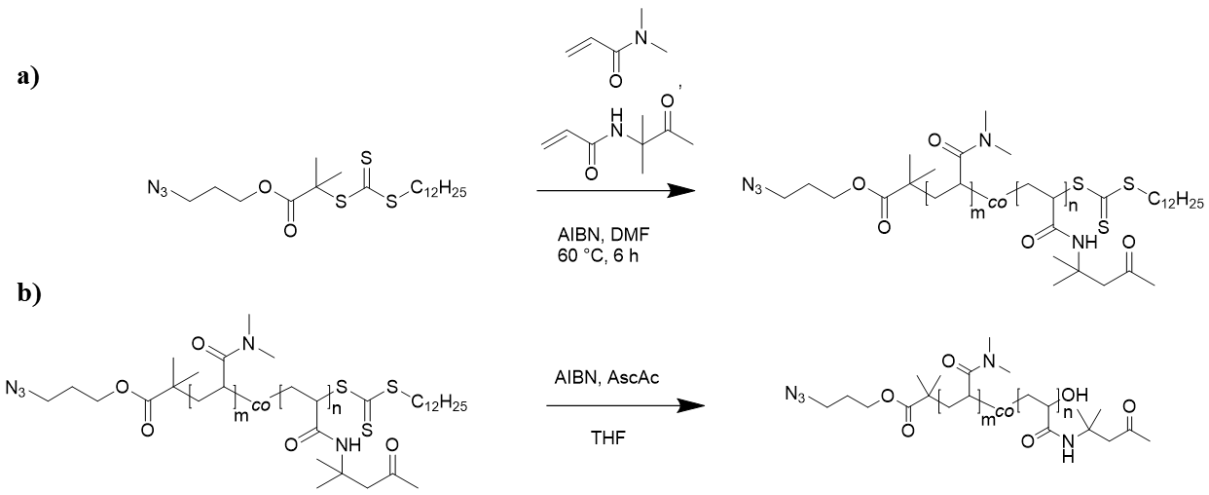

Scheme 7.2. Reaction scheme for the (a) formation of the copolymer PDMA-*co*-PDAAM via RAFT polymerisation and (b) RAFT group removal from the copolymer PDMA-*co*-PDAAM.

The azido functional group was introduced to react with alkyne end-functionalised Pull. In order, to avoid side reactions in the following CuAAc reaction and side effects caused by hydrophobic moieties during self-assembly, the RAFT-group was converted to a hydroxyl group (Scheme 7.2 b). For that, the PDMA-*co*-PDAAM was reacted with tetrahydrofuran peroxide and ascorbic acid.[166] Finally, azido functionalised PDMA-*co*-PDAAM was obtained

[e] End functionalised polymers, block copolymer and RhB labelled polymers were synthesised by Jochen Willersinn at the Max-Planck Institute for Colloid and Interfaces.

with a molar mass of 22,000 g · mol^{-1} and *Đ* of 1.9 (Figure 7.1 and Table 7.1). Moreover, the hydroxy functionalised copolymer was characterised via ^{1}H-NMR.

The linear polysaccharide pullulan is produced by fermentation of starch with a fungus *e.g. Aureobasidium pullulans* to act like a protective layer. Therefore, commercial pullulan possesses a high average molar mass between a M_w of 300,000 and 500,000 g·mol^{-1} and broad molar mass weight distribution of *Đ* between 2 and 4. In order to obtain lower molar mass Pull with a more defined *Đ*, commercial pullulan has to undergo depolymerisation prior the formation of block copolymers. Pull consist predominantly α-(1,6) linked maltotriose units and the most accessible point for the depolymerisation is that α-(1,6) bond connecting the maltotriose units. Ilic *et al.* described a controlled method to depolymerise pullulan, using 0.025 M HCl at 85 °C (Scheme 7.3 a).[167] Based on that literature, commercial Pull was depolymerised to a M_n = 14,800 g·mol^{-1} and *Đ* = 2.1.

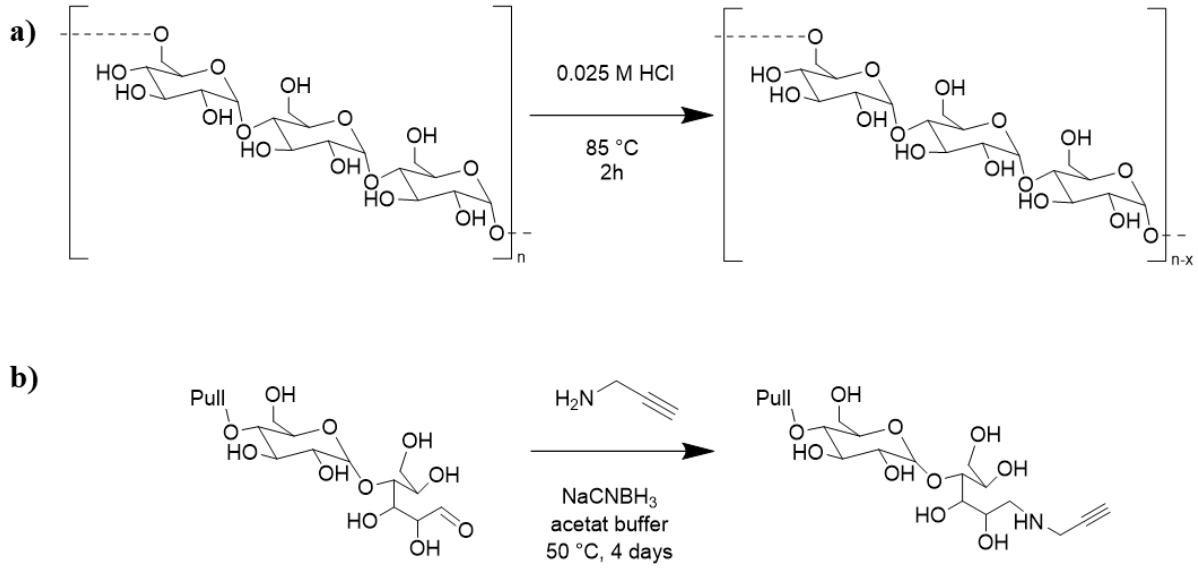

Scheme 7.3. Reaction scheme of the (a) depolymerisation of Pull and (b) the alkyl end functionalisation via reductive amination.

For application as a building block in the formation of block copolymers, pullulan has to be further functionalised with an alkylne group. Following the procedure of Schatz *et al.*,[168] Pull was end functionalised in an acetate buffer solution with propargylamine and sodium cyanoborohydride ($NaCNBH_3$) (Scheme 7.3 b). To ensure full conversion and diminish undesired side reactions *e.g.,* further depolymerisation propargylamine and $NaCNBH_3$ was applied in a significant high excess. The end functionalised Pull was obtained with M_n= 19,400 g·mol^{-1} and *Đ* = 2.0.

7.3 Synthesis of Pull-*b*-(PDMA-*co*-PDAAM) *via* copper catalysed azide alkyne cycloaddition

CuAAc is an alternative avenue to form new block copolymers.[51] Azido end-functionalised PDMA-*co*-PDAAM and alkyne end-functionalised pullulan were conjugated under copper catalysis via a triazole as linker (Figure 7.1 a).[156] For the cycloaddition of two hydrophilic block copolymers, the reaction was carried out in a mixture of DMSO and water. To ensure full conversion of the reaction, an excess of alkyne end-functionalised pullulan was present. Azide functionalised polystyrene-resin (PS-resin) was added after the reaction to bind unreacted pullulan. After the reaction, the PS-resin was removed easily by filtration.

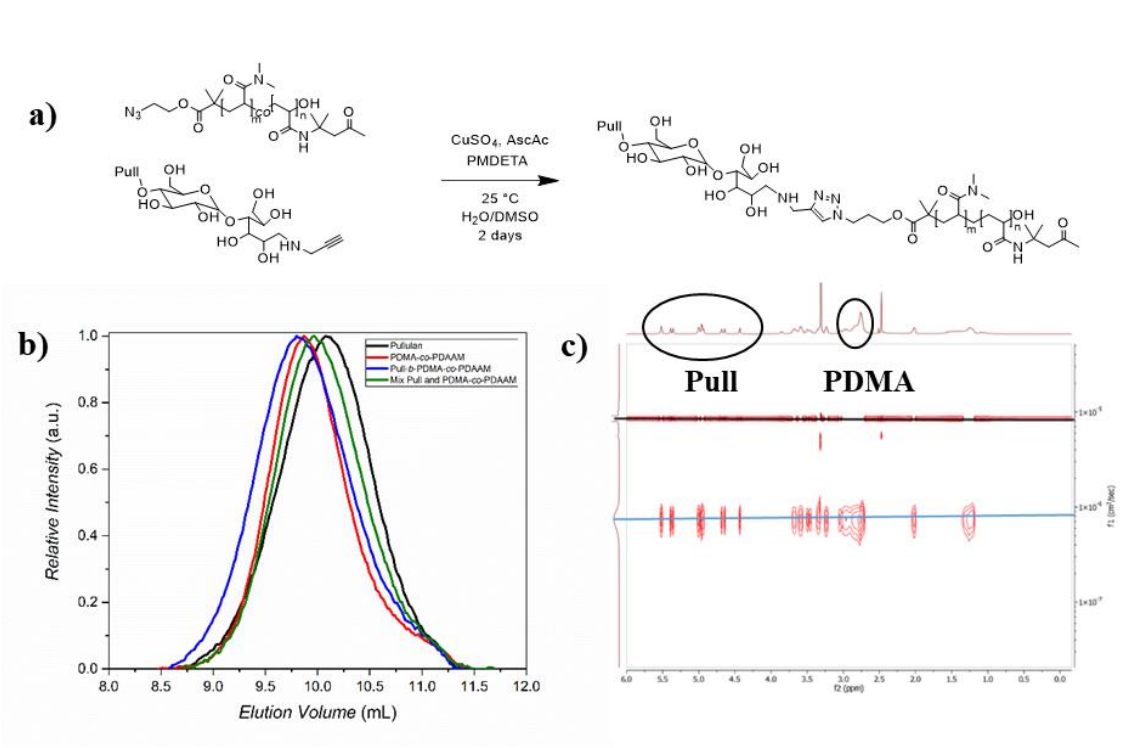

Figure 7.1. (a) Reaction scheme for the formation of Pull-*b*-(PDMA-*co*-PDAAM), (b) SEC measurement of depolymerised pullulan (black curve), PDMA-*co*-PDAAM (red curve), mixture of depolymerised pullulan and PDMA-*co*-PDAAM (green curve), and Pull-*b*-(PDMA-*co*-PDAAM) (blue curve) measured in acetate buffer against pullulan standards and (c) DOSY measurement of Pull-*b*-(PDMA-*co*-PDAAM) (measured in DMSO-d_6) with the diffusion coefficient of DMSO-d_6 (black line) and Pull-*b*-(PDMA-*co*-PDAAM) including all ^{1}H-NMR peaks from all individual blocks (blue line).

Table 7-1. Results of SEC measurements of depolymerised pullulan (black curve), PDMA-*co*-PDAAM (red curve), mixture of depolymerised pullulan and PDMA-*co*-PDAAM (green curve) and Pull-*b*-(PDMA-*co*-PDAAM) (blue curve) measured in acetate buffer against pullulan standards.

Polymer	M_n **(kg·mol^{-1})**	$Đ$
Pullulan	19.4	2.0
PDMA-*co*-PDAAM	22.0	1.9
Mix Pull and PDMA-*co*-PDAAM	20.0	1.9
Pull-*b*-(PDMA-*co*-PDAAM)	25.8	2.0

The formed block copolymer was analysed via SEC, ^{1}H-NMR, ^{13}C-NMR, and DOSY-NMR. ^{1}H-NMR and ^{13}C-NMR show the presence of pullulan and PDMA-*co*-PDAAM in the copolymer, *e.g.,* the signal for protons of pullulan around 3.4 to 3.7 ppm, the signal from the two methyl groups of PDMA around 3.0 ppm and terminal methyl group of the PDAAM around 2.1 ppm. In order to prove the successful block copolymer formation, the block copolymer was analysed via DOSY-NMR. The DOSY-NMR measurement (Figure 7.1 c) showed two species. A species with high diffusion coefficient, which belongs to the solvent d-DMSO. The second, at a lower diffusion coefficient included all ^{1}H-NMR peaks, from the individual blocks in the block copolymer, which confirms block copolymer formation. Moreover, SEC measurements indicate block copolymer formation via a shift in the elugram towards shorter retention times. Additionally, a comparison of elugrams between Pull-*b*-PDMA-*co*-PDAAM and the mixture of pullulan and PDMA-*co*-PDAAM showed a significant difference. According to pullulan calibration a molar mass of 25,800 g · mol^{-1} was obtained (Figure 7.1 b and Table 7.1).

7.4 Aggregation behaviour of Pull-*b*-(PDMA-*co*-PDAAM) in aqueous solution

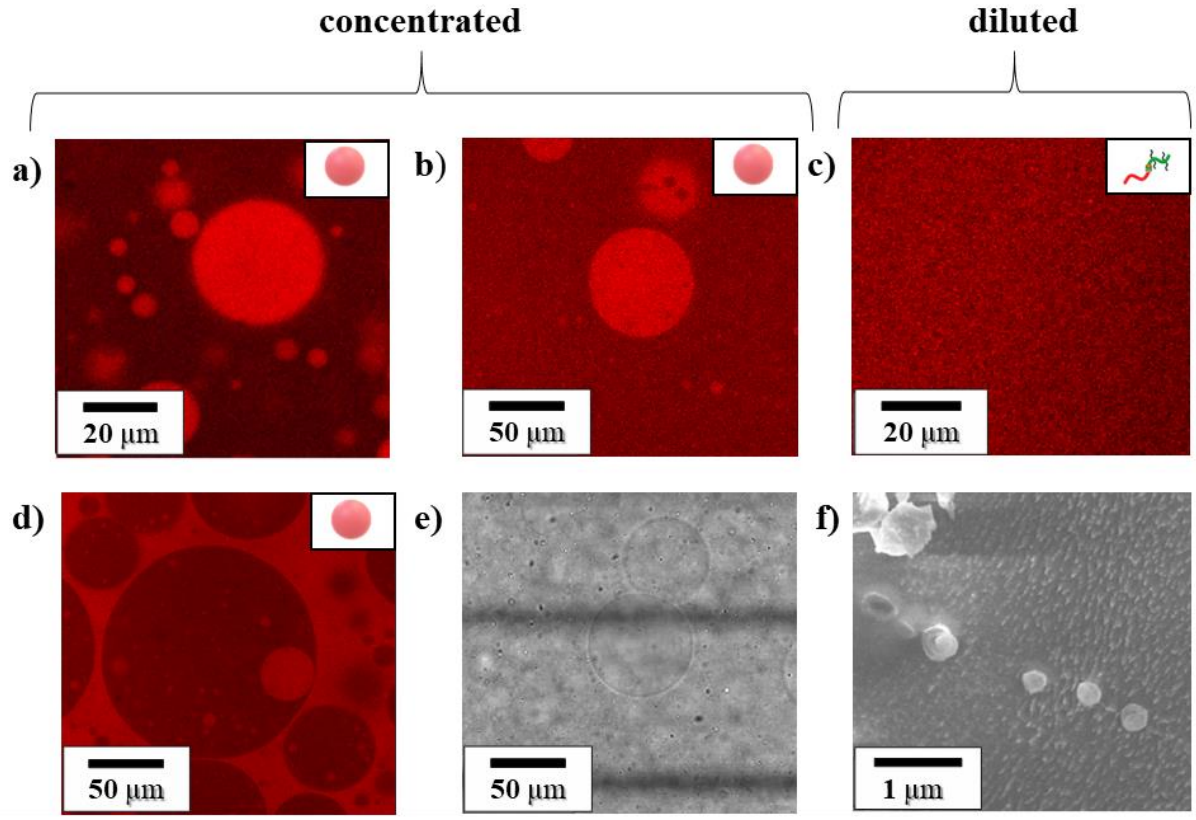

Figure 7.2. (a-e) CLSM[f] images of Pull-*b*-(PDMA-*co*-PDAAM): (a) mixture of Pull-*b*-(PDMA-*co*-PDAAM) and RhB labelled Pull-*b*-(PDMA-*co*-PDAAM) at 20 wt%, (b) Pull-*b*-(PDMA-*co*-PDAAM) at 20 wt% stained with Sulforhodamine B (SRB), (c) Pull-*b*-(PDMA-*co*-PDAAM) at 15 wt%, (d) inverse phase of Pull-*b*-(PDMA-*co*-PDAAM) at 20 wt% stained with SRB, (e) bright field images of Pull-*b*-(PDMA-*co*-PDAAM) at 20 wt%, (f) cryo SEM images of Pull-*b*-(PDMA-*co*-PDAAM) at 0.6 wt%.

Aggregation of DHBCs in aqueous solution without external triggers, such as pH change or temperature, demand specific properties of block copolymers and particular conditions. One of the most important conditions is concentration.[58, 121, 122] For the analysis of the aggregation of Pull-*b*-(PDMA-*co*-PDAAM), a 20 wt% solution was investigated via CSLM, which revealed the presence of giant polymer enriched droplets in water (Figure 7.2 a). The 20 wt% polymer solution was observed under bright field (Figure 7.2 e) and confocal with SRB as additive. In both cases, the presence of polymer droplets in a polymer / water matrix with sizes between 10 and 50 µm is visible on the time scale of the experiment. In order to investigate the position of

[f] CLSM and bright field images were conducted by Dr. Rafael Lira at the Max-Planck Institute for Colloid and Interfaces.

the polymer, the polymer was labelled, and the concentrated solution was analysed via CLSM (Figure 7.2 a). The image with the labelled polymer displays a higher concentration of the polymer in the droplet, indicating that the polymer is enriched in this phase. Interestingly, the phases can be inverted as well, *e.g.*, at high concentration two kinds of droplets were observed via CSLM: In one case the polymer is more concentrated in the droplet, in the other case the polymer is more concentrated outside the droplet (Figure 7.2 d). The result of inverted droplets indicates that the formation of polymer-rich droplets in water or water in polymer-rich matrix is a very sensitive system. However, the droplets are only stably formed at high polymer concentrations. Notice that the phases are metastable; upon contact, the droplets fuse, demonstrating their liquid-like behaviour. Upon dilution with water, the droplets destabilise, until they start to dissolve (around 15 wt%) (Figure 7.2 c).

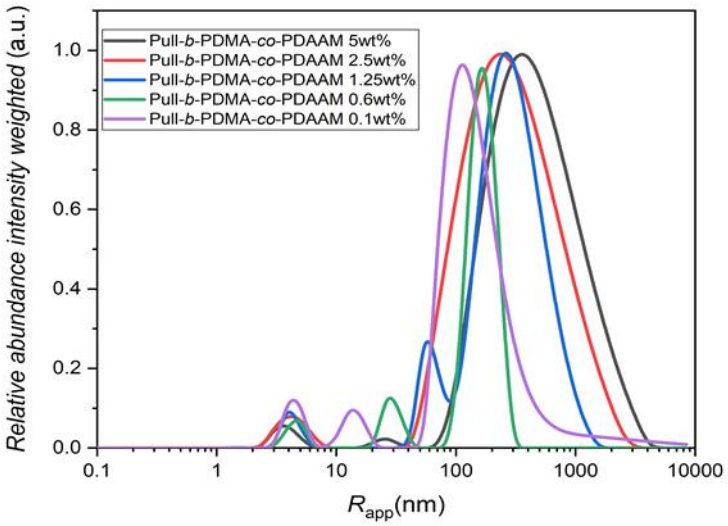

Figure 7.3. Intensity weighted particle size distribution of 5.0, 2.5, 1.25, 0.6, and 0.1 wt% solution of Pull-*b*-(PDMA-*co*-PDAAM) in water measured via DLS at 25 °C.

Table 7-2. Summary of apparent average hydrodynamic radii of Pull-*b*-(PDMA-*co*-PDAAM) in water.

Polymer	concentration	1st Peak (nm)	Rel. abund.	2nd Peak (nm)	Rel. abund.	3rd Peak (nm)	Rel. abund.
Pull-*b*-(PDMA-*co*-PDAAM) before CL	5 wt%	3.7	0.06	25.5	0.02	448	1.0
	2.5 wt%	4.2	0.08	-	-	284	1.0
	1.25 wt	4.2	0.08	58.6	0.27	260	1.0
	0.6 wt%	4.5	0.08	29.2	0.13	165	1.0
	0.1 wt%	4.4	0.12	13.8	0.1	159	1.0

In order to investigate the aggregation behaviour of Pull-*b*-(PDMA-*co*-PDAAM) in aqueous solution at lower concentrations, the aqueous solution was analysed by DLS at 25 °C. Therefore, 5.0, 2.5, 1.25, 0.6, and 0.1 wt % solution of Pull-*b*-(PDMA-*co*-PDAAM) block copolymer was prepared and analysed to determine apparent hydrodynamic radii (R_{app}) for the formed aggregates at each concentration (Figure 7.3). The intensity weighted particle size distribution of Pull-*b*-(PDMA-*co*-PDAAM) shows a dependency on concentration (Table 6.2). At all concentrations, bi- or trimodal particle size distributions are observed. The first peak lies around 4 nm for all concentrations, which can be assigned to free polymer chains in the solution.[121] For higher concentration, the intensity of small components around 4 nm is lower. The main peak is above 100 nm at all concentrations. The peak over 100 nm indicates the formation of larger aggregates by Pull-*b*-(PDMA-*co*-PDAAM). The size of these larger particles depends on the block copolymer concentration, *i.e.*, the aggregate size increases with increasing concentration. It should be noted though that the mentioned results are extracted from intensity weighted particle size distributions that overestimate larger structures. The 0.6 wt% solution was analysed via cryo SEM, to investigate the aggregate structure at low concentration. The cryo SEM images of 0.6 wt% solution of Pull-*b*-(PDMA-*co*-PDAAM) display a significant number of spherical aggregates with a particle size between 200 and 600 nm (Figure 7.2 f). For a concentration of 0.6 wt% of block copolymer, the apparent average hydrodynamic radius was around 165 nm as determined by DLS, which is in the range of the observed diameter by cryo SEM measurements. From the cryo SEM images, the average particle size in 0.6 wt% solution was calculated and confirmed the DLS results. A particle size

calculation of 50 particles, revealed an average particle size is 355 nm with standard deviation of 165 nm for the block copolymer Pull-*b*-(PDMA-*co*-PDAAM).

7.5 Crosslinking of Pull-*b*-(PDMA-*co*-PDAAM) via oxime formation

To improve the stability of the phase separation during dilution and at lower concentration, crosslinking of Pull-*b*-(PDMA-*co*-PDAAM) was considered. An avenue to crosslink Pull-*b*-(PDMA-*co*-PDAAM) is the click reaction of aldehydes or ketones with primary amines or hydroxylamines to generate imine or oxime bonds, respectively (Figure 7.4 a).[165, 169] As such, the carbonyl group of the DAAM repeating units is a position for crosslinking via oxime formation with a suitable dihydroxylamine. Therefore, the block copolymer was dissolved in water, at a concentration of 20 wt%, the crosslinker a hydroxylamine dihydrochloride, 3,5-diaminobenzoic acid dihydrochloride as a catalyst[169] and a base namely triethylamine were added. The ratio between keto groups and crosslinker was adjusted to [keto]: [crosslinker] 2:1. As the crosslinker, 1,3-bis(aminooxy)propane dihydrochloride can react with two keto groups of Pull-*b*-(PDMA-*co*-PDAAM) in order to form a crosslinking point. The oxime was formed by direct condensation of the hydroxylamine with the carbonyl group of the PDAAM at 35 °C.

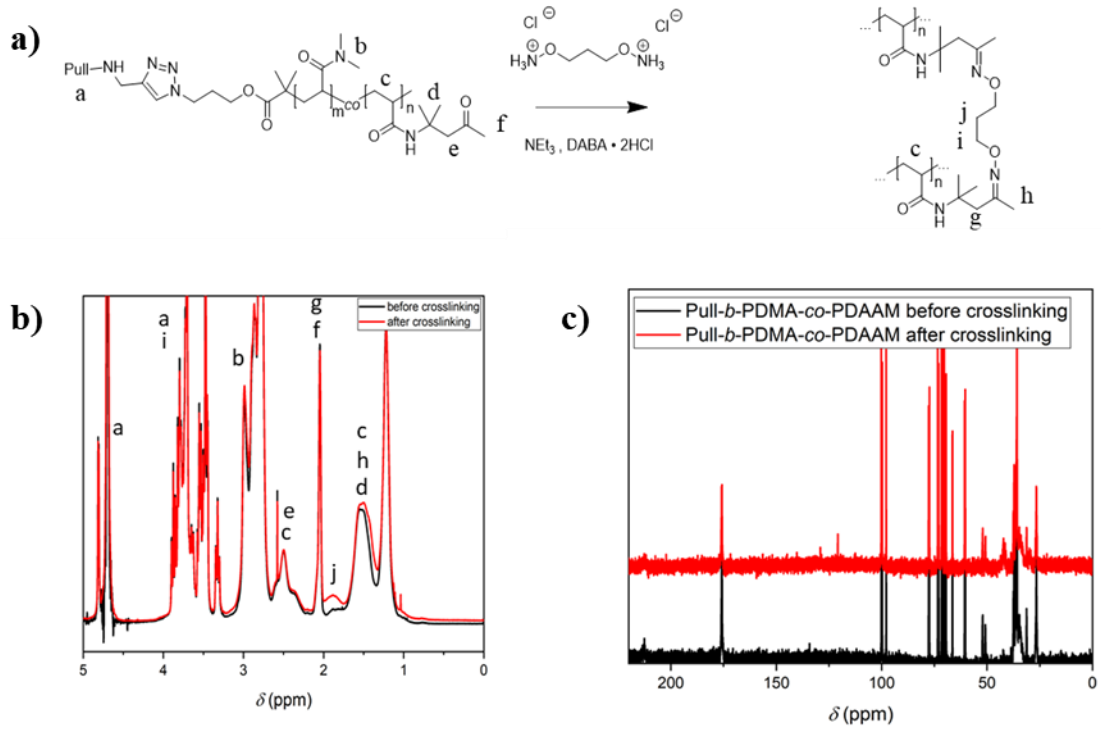

Figure 7.4. (a) Reaction scheme for crosslinking of Pull-*b*-(PDMA-*co*-PDAAM) with 1,3-bis(aminooxy)propan dihydrochloride *via* oxime formation in water employing 3,5-diaminobenzoic acid dihydrochloride (DABA) as catalyst, (b) ^{1}H-NMR of Pull-*b*-(PDMA-*co*-PDAAM) before (black) and after (red) crosslinking in D_2O, (c) ^{13}C-NMR of Pull-*b*-(PDMA-*co*-PDAAM) before (black) and after (red) crosslinking in D_2O.

Oxime formation was investigated via ^{1}H-NMR (Figure 7.4 b) and ^{13}C-NMR (Figure 7.4 c) at first. For ^{1}H-NMR, the presence of the crosslinker is indicated with the typical signal around 1.7-2.0 ppm. Moreover, in ^{13}C-NMR, the switch of the quaternary carbon with two methyl groups in PDAAM from about 52 ppm to 42 ppm after crosslinking is visible, which indicates that the oxime formation was successful, and the product is not a mixture of block copolymer and crosslinker. Furthermore, the carbonyl group at 220 ppm is not clearly visible after crosslinking. Additionally, the carbons of the crosslinker are observable around 30 to 32 ppm. The analytical results of the hydroxylamine-treated Pull-*b*-(PDMA-*co*-PDAAM) are similar to the results for oxime crosslinking, in literature.[165]

For a successful oxime formation, the ratio of DAAM to DMA in the copolymer PDMA-*co*-PDAAM should be high enough, which was determined to be 20%. For a content of 10 and 5% PDAAM in the block copolymer, successful oxime formation could not be verified, for example via ^{1}H- and ^{13}C NMR measurement (Figure 7.13).

7.6 Aggregation behaviour of crosslinked Pull-*b*-(PDMA-*co*-PDAAM) in aqueous solution

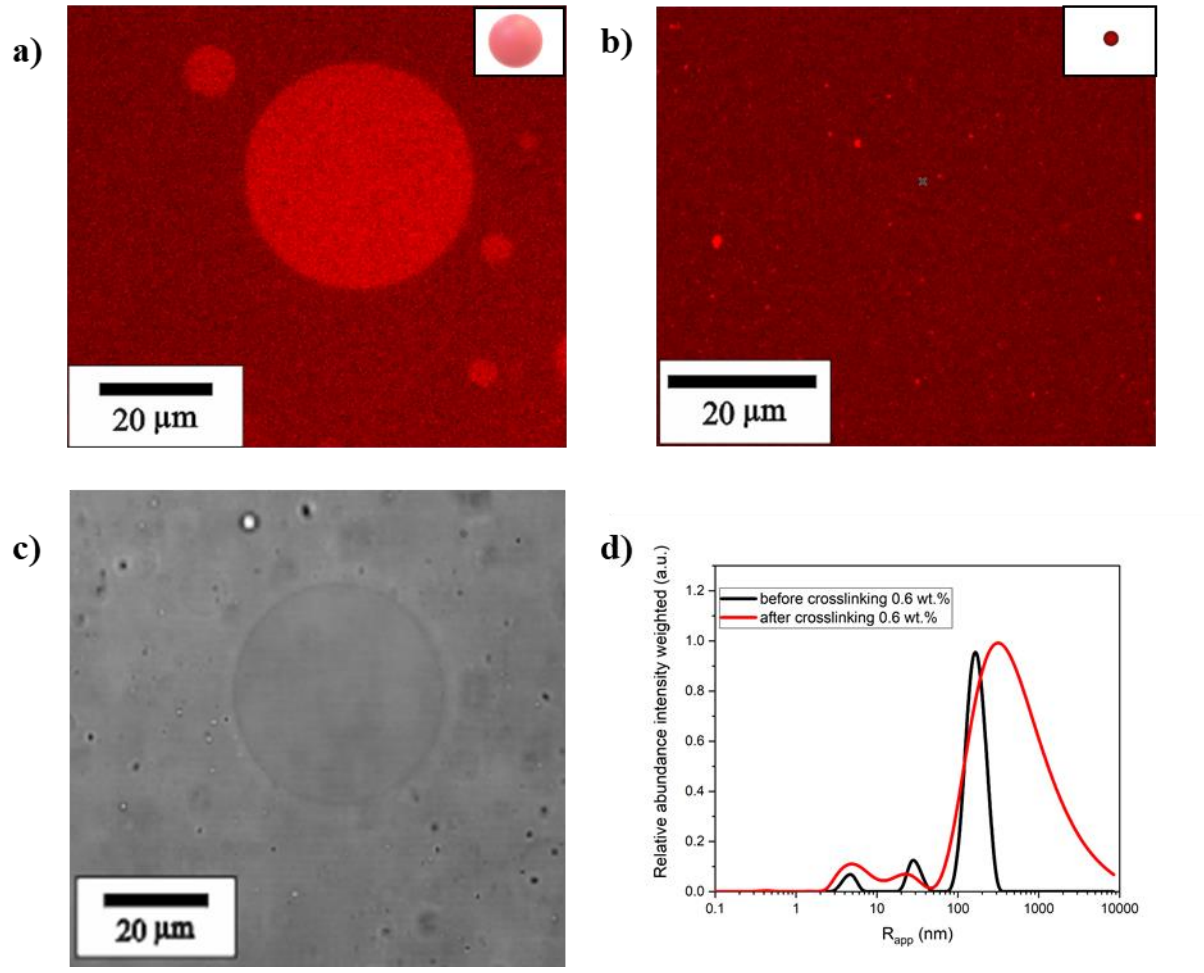

Figure 7.5. a) CLSM images of crosslinked Pull-*b*-(PDMA-*co*-PDAAM) at 20 wt% stained with Sulforhodamine B (SRB), (b) CLSM images of crosslinked Pull-*b*-(PDMA-*co*-PDAAM) at 10 wt% stained with SRB, (c) Bright field images of a 20 wt% solution of Pull-*b*-(PDMA-*co*-PDAAM) in water after crosslinking, (d) Intensity weighted particle size distribution of 0.6 wt% solution of Pull-*b*-(PDMA-*co*-PDAAM) before (black curve) and after crosslinking (red curve) measured in water via DLS at 25 °C.

After the verification of the formation of oximes via addition of dihydroxyl amines, in the next step the actual formation of crosslinked structures was investigated. Initially, CLSM was studied similar to pure Pull-*b*-(PDMA-co-PDAAM) DHBC. For the 20 wt% solution of crosslinked copolymer, droplets (between 10 and 50 µm) are present and visible in bright field (Figure 7.5 c) and with the additive SRB (Figure 7.5 a) in CLSM. However, the droplets are again only stable at high concentration, as the droplets dissolved upon dilution with water even though crosslinking was attempted. Nevertheless, in comparison to the non-crosslinked Pull-*b*-(PDMA-*co*-PDAAM), the crosslinked block copolymer features a high amount of small

fluorescent particles even at lower concentration (at 10 wt%, Figure 7.5 b). Thus, the crosslinking was not successful to stabilise the large, separated phases. Albeit, the presence of smaller particles of lower concentration for crosslinked copolymer, signifies that crosslinking for Pull-*b*-(PDMA-*co*-PDAAM) takes place in a small area and not over the whole phase leaving crosslinked particles behind. Overall, even after crosslinking the phase separation at higher concentration is unstable.

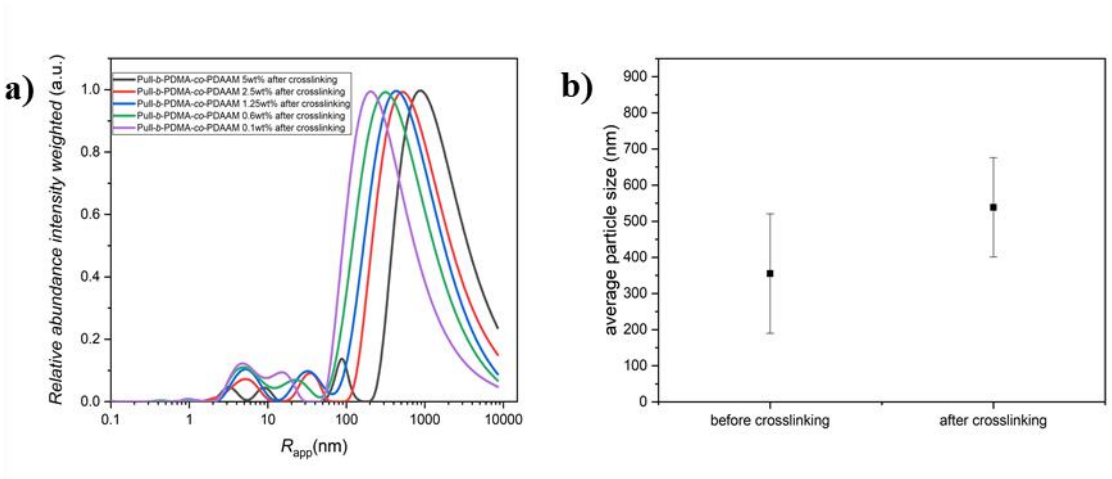

Figure 7.6. (a) Intensity weighted particle size distribution of 5.0, 2.5, 1.25, 0.6, and 0.1 wt% solution of crosslinked Pull-*b*-(PDMA-*co*-PDAAM) in water measured via DLS at 25 °C. (b) average particle size of 0.6 wt% solution of Pull-*b*-(PDMA-*co*-PDAAM) before and after crosslinking, measured over 50 particles.

Table 7-3. Summary of apparent average hydrodynamic radii of crosslinked Pull-*b*-(PDMA-*co*-PDAAM) in water.

Polymer	concentration	1st Peak (nm)	Rel. abund.	2nd Peak (nm)	Rel. abund.	3rd Peak (nm)	Rel. abund.
Pull-*b*-(PDMA-*co*-PDAAM) after CL	5 wt%	8.7	0.04	86.9	0.14	1324	1.0
	2.5 wt%	4.2	0.07	33.6	0.09	820	1.0
	1.25 wt	5.2	0.10	31.7	0.10	575	1.0
	0.6 wt%	4.9	0.11	22.1	0.07	366	1.0
	0.1 wt%	4.7	0.12	15.3	0.09	348	1.0

As the state of phase separation could not be locked via crosslinking, the formed particle structures were investigated in more detail. In order to do so, the crosslinked Pull-*b*-(PDMA-*co*-PDAAM) was analysed at lower concentration via DLS and cryo SEM (Figure 7.6 a and 7.7 c). An aqueous solution of 5.0, 2.4, 1.25, 0.6, and 0.1 wt% was investigated by DLS and the 0.6 wt% solution was analysed via cryo SEM. The intensity weighted particle size distribution of crosslinked Pull-*b*-(PDMA-*co*-PDAAM) is dependent on the concentration (Figure 7.7 and Table 7.3), which is similar to the non-crosslinked Pull-*b*-(PDMA-*co*-PDAAM). All concentrations show a trimodal particle size distribution. For higher concentrated solutions, larger aggregates are visible. The small particles, with a peak around 5 nm for nearly all concentrations, can be attributed to the free block copolymer chains in solution. The intensity of the free block copolymer chains increases, if the concentration decreases. The main peak is situated, dependent on the concentration, between 350 nm and 1.3 µm, which can be attributed to aggregate formation. In case of crosslinked block copolymer, the aggregates have a significant higher hydrodynamic radius than for non-crosslinked Pull-*b*-(PDMA-*co*-PDAAM). Depending on the concentration, the hydrodynamic radius is two to four times larger than for the non-crosslinked Pull-*b*-(PDMA-*co*-PDAAM). Especially for the higher concentrated solutions (5.0 and 2.5 wt%), the hydrodynamic radius for the observed aggregates is larger *e.g.* for 5 wt% solution (450 nm for non-crosslinked and 1.3 µm for crosslinked Pull-*b*-(PDMA-*co*-PDAAM)).

In order to underpin the results of DLS measurement, cryo SEM images of the 0.6 wt% solution of crosslinked block copolymer was recorded. The cryo SEM images display a significant amount of aggregates with a particle size in the rage of 400 and 700 nm (Figure 7.7 c). The average particle size, measured over 50 particles observed in the cryo SEM images (Figure 7.7 b), is 581 nm with a standard deviation of 171 nm, which confirm the DLS results with a hydrodynamic radius of 367 nm for the larger aggregates in the 0.6 wt% solution. In comparison to the non-crosslinked Pull-*b*-(PDMA-*co*-PDAAM), the average particle size of the aggregates at a concentration of 0.6 wt% is around 60 % higher for the crosslinked block copolymer. According to results of the DLS and cryo SEM measurements, it seems like the crosslinking of Pull-*b*-(PDMA-*co*-PDAAM) stabilised the aggregates of the block copolymer and further shifts the equilibrium to aggregates.

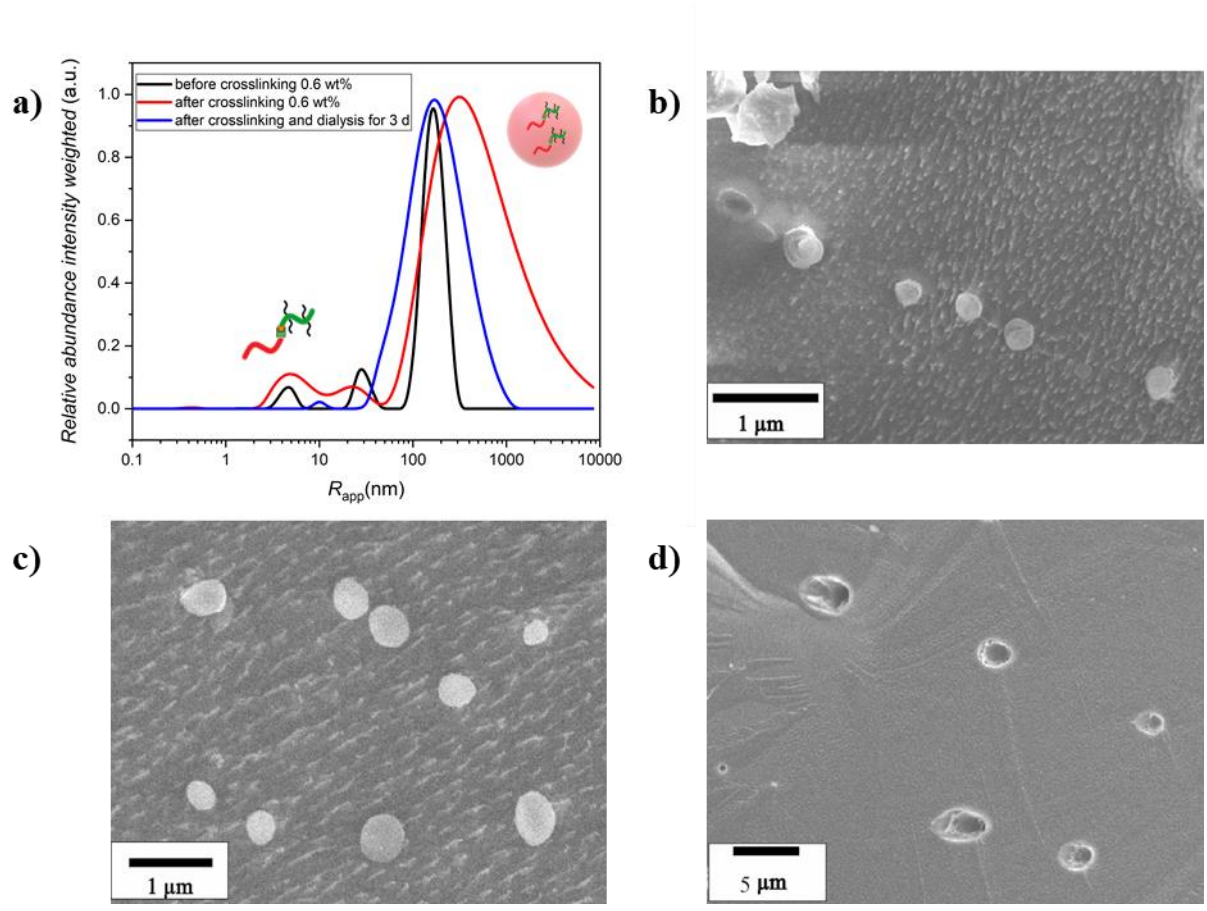

Figure 7.7. (a) Intensity weighted particle size distribution of 0.6 wt% solution of Pull-*b*-(PDMA-*co*-PDAAM) before (black curve) and after crosslinking (red curve), and crosslinked Pull-*b*-(PDMA-*co*-PDAAM) after dialysis against water for 3 days (blue curve) measured in water *via* DLS at 25 °C, (c-d) cryo SEM images of (b) Pull-*b*-(PDMA-*co*-PDAAM) before crosslinking (c) Pull-*b*-(PDMA-*co*-PDAAM) after crosslinking and (d) Pull-*b*-(PDMA-*co*-PDAAM) after crosslinking and dialysis against water for 3 days.

In order to remove free block copolymer chains in solution, the crosslinked Pull-*b*-(PDMA-*co*-PDAAM) was dialysed against Millipore water for 3 days with MWCO 1000kD. The dialysed crosslinked block copolymer was analysed via cryo SEM (Figure 7.7 d) and DLS (Figure 7.7 a). The results of DLS measurement possess a small peak around 10 nm. That peak could be derived from remaining free block copolymer chains in solution. Furthermore, the DLS measurement shows the main peak at 178 nm, which belongs to the larger aggregates. However, the results for the cryo SEM measurement display aggregates, which correspond with the particle size to the DLS results. In addition, it shows aggregates, which are considerably larger than 1 µm (Figure 7.7 d) and significantly larger than the DLS results indicate, which could be due to considerable swelling of the particles at very low concentrations after dialysis. These

structures resemble the structures observed by Brosnan *et al*. via cryo SEM.[120] Thus, the crosslinking stabilised the aggregates at lower concentration and these aggregates are lager in comparison to the non-crosslinked block copolymer. Overall, the crosslinking was successful to stabilise the aggregates at lower concentration but not strong enough to stabilise the polymer phase separation when larger phases were formed. A reason for that could be that the crosslinking does not take place over a longer distance in spare and significant number of particles to stabilise the polymer phase separation but in a smaller area, therefore only small aggregates are observed at lower concentrated solution.

7.7 Aggregates of crosslinked and non-crosslinked Pull-*b*-(PDMA-*co*-PDAAM) in NMP

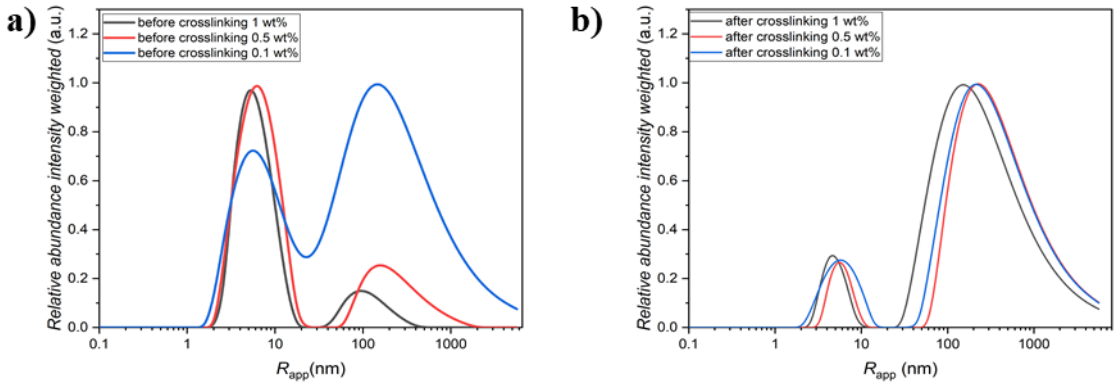

Figure 7.8. (a, b) Comparison of intensity weighted particle size distribution of Pull-*b*-(PDMA-*co*-PDAAM) at different concentrations before (a) and after crosslinking (b) measured *via* DLS in NMP at 25 °C.

Table 7-4. Summary of apparent average hydrodynamic radii of Pull-*b*-(PDMA-*co*-PDAAM) before and after crosslinking for 1.0, 0.5, and 0.1 wt% solution in *N*-methyl-2-pyrrolidone (NMP).

Polymer	concentration	1st Peak (nm)	Rel. abund.	2nd Peak (nm)	Rel. abund.
Before crosslinking	1 wt%	5.7	1.0	93	0.15
	0.5 wt%	6.2	1.0	174	0.25
	0.1 wt%	6.2	0.72	147	1.0
After crosslinking	1 wt%	4.8	0.30	252	1.0
	0.5 wt%	5.8	0.27	375	1.0
	0.1 wt%	5.6	0.27	350	1.0

In order to prove the successful crosslinking of Pull-*b*-(PDMA-*co*-PDAAM) and the influence of the crosslinking for the stability of the aggregates in organic solvent, the block copolymer was analysed via DLS at 25 °C in *N*-methyl-2-pyrrolidone (NMP). For that, 1.0, 0.5, and 0.1 wt% solutions of the non-crosslinked and crosslinked block copolymer were investigated by DLS (Figure 7.8 and Table 7.4) in NMP. For the non-crosslinked Pull-*b*-(PDMA-*co*-PDAAM), the results show a considerable dependency of stability on the polymer concentration. In the case of a low concentration, more lager particles are present in the solution and the intensity of smaller particles decreases for low concentration.

In contrast, the results for the crosslinked Pull-*b*-(PDMA-*co*-PDAAM) display no dependency on concentration. For all concentrations, the results are similar. Only the hydrodynamic radius of the larger aggregates increased at lower concentrated solutions, probably due to the swelling of the aggregates in the organic solvent. The smaller particles are all around 6 nm, with a similar intensity. The larger particles show an apparent average hydrodynamic radius between 252 and 375 nm. Especially for the low concentration, the results are similar to the DLS results for the crosslinked Pull-*b*-(PDMA-*co*-PDAAM) in water. In comparison to the non-crosslinked block copolymer, the crosslinked block copolymer shows no dependency on the concentration in an NMP solution. The significant difference of the DLS measurement shows that the crosslinking was successful, and it can stabilise the aggregates in low concentrated NMP solutions.

7.8 Conclusion

The DHBC Pull-*b*-(PDMA-*co*-PDAAM) was synthesised *via* CuAAc. The block copolymer shows mesoscale phase separation at high concentrations of 20 wt%, which is reversible upon dilution. In lower concentrated solution, Pull-*b*-(PDMA-*co*-PDAAM) displayed, dependently on the concentration, aggregates with sizes between 160 and 450 nm. Additionally, the Pull-*b*-(PDMA-*co*-PDAAM) was crosslinked *via* oxime formation. The crosslinked block copolymer induced droplet formation at high concentration of 20 wt% similar to the non-crosslinked polymer. For lower concentrations, the crosslinked block copolymer featured aggregates with sizes between 350 nm and 1.3 µm. Furthermore, the crosslinked Pull-*b*-(PDMA-*co*-PDAAM) shows aggregates of around 1 µm, after dialysis against water. Studies in organic solvent showed an increased stability of the crosslinked aggregates of Pull-*b*-(PDMA-*co*-PDAAM) in low concentrated NMP solutions. By increasing of the stability of the aggregates *via* crosslinking, DHBCs might be interesting for biomedical application. The next chapter will focus on the synthesis as well as the temperature and concentration dependent self-assembly of the high molar mass block copolymer PDEA-*b*-PAM.

7.9 Experimental part

Depolymerisation of pullulan

Based on the literature, [167] pullulan (3.0 g) was placed in an argon purged 100 mL round bottom Schlenk flask and dissolved in an aqueous hydrochloric acid solution (60 mL, 0.025 mol·L^{-1}). The solution was placed in a pre-heated oil bath (85 °C) and stirred for 2.5 hours. The depolymerisation was stopped by cooling down with liquid nitrogen. After that, the polymer was dialysed against deionised water (Spectra/Por 10.000 Da) for three days, freeze-dried and a colourless solid was obtained (2.11 g, $M_{n,SEC}$ = 14,800 g · mol^{-1} measured in acetate buffer against pullulan standards).

Alkyne end-functionalised pullulan

According to literature,[168] depolymerised pullulan (2.0 g, 0.135 mmol, 1 eq.) was placed in a dry argon purged 100 mL round bottom Schlenk flask and dissolved in acetate buffer solution (67 mL). Propargyl amine (0.74 g, 13.5 mmol, 100 eq.) was added and placed in a pre-heated oil bath. Sodium cyanoborohydride (0.21 g, 3.4 mmol, 25.0 eq.) was added and the reaction mixture was stirred for four days. Every 24 h, a new portion of sodium cyanoborohydride (0.21 g, 3.4 mmol, 25.0 eq.) was added to the reaction. After that, the polymer was dialysed against deionised water (Spectra/Por 3500 Da) for three days, freeze-dried and a colourless solid was obtained (1.25 g, M_n =19,400 g · mol^{-1} measured in acetate buffer against pullulan standards).

Formation of PDMA-*co*-PDAAM

In a dry, argon purged 100 mL round bottom Schlenk flask, dodecylthiocarbonylthio-2-methylpropanoic acid 3'-azidopropylester (40.8 mg, 0.1 mmol, 1 eq.), AIBN (3.0 mg, 0.018 mmol, 0.2 eq.), DMA (1.8 g, 18.16 mmol, 181.6 eq.) and *N*-(1,1-dimethyl-3-oxobutyl)acrylamide (0.77 g, 4.54 mmol, 45.4 eq.) were dissolved in DMF (5.6 mL). The solution was degassed by three freeze-pump-thaw cycles and placed in a pre- heated oil bath (60 °C). Subsequently, the reaction mixture was stirred for six hours, stopped by cooling down with liquid nitrogen and exposure to air. Afterwards, the polymer was dialysed against

deionised water (Spectra/Por 3500 Da) for three days, freeze-dried and a yellow solid (2.14 g, M_n =21,800 g · mol^{-1}, $Đ$ = 1.9 measured in acetate buffer against pullulan standards) was obtained.

Formation of RhB labelled PDMA-*co*-PDAAM

In a dry, argon purged 100 mL round bottom Schlenk flask, PDMA-*co*-PDAAM (0.3 g, 0.014 mmol, 1.0 eq.) was dissolved in dry DMSO (30 mL). Hexylamine (3.5 mg, 0.035 mmol 2.5 eq.) was added, placed in a pre-heated oil bath (50 °C) and stirred overnight. Afterwards, the reaction mixture was cooled down to ambient temperature, Rhodamine B ITC (5.6 mg, 0.105 mmol, 7.5 eq.) was added and the solution stirred over night at 50 °C. The mixture was cooled down to ambient temperature and diluted with deionised water. Afterwards, the polymer was dialysed against deionised water (Spectra/Por 3500 Da) for three days, freeze-dried and a purple solid (0.36 g, M_n =23,200 g · mol^{-1}) was obtained.

RAFT group removal of PDMA-*co*-PDAAM

According to the literature,[166] in a 100 mL round bottom flask, AIBN (0.364 g, 2.15 mmol, 40 eq.) was dissolved in destabilised THF (120 mL). The solution was stirred vigorously for 30 min at 60 °C under air. After a positive peroxide test, PDMA-*co*-PDAAM (1.5 g, 0.054 mmol, 1.0 eq.) was added. The reaction mixture was stirred at 60 °C, until the yellow colour vanished. Subsequently, the reaction was cooled down to ambient temperature and the THF was removed under reduced pressure. The remaining crude product was dissolved in deionised water, dialysed against deionised water (Spectra/Por 3500 Da) for three days, freeze-dried and a slightly greenish solid (1.32 g, M_n =21,800 g · mol^{-1} measured in acetate buffer against pullulan standards) was obtained.

Formation of Pull-*b*-(PDMA-*co*-PDAAM)

Pullulan (0.52 g, 0.028 mmol, 1.2 eq.) was dissolved in Millipore water (7.5 mL). $CuSO_4$ (2.4 mg, 0.015 mmol, 0.65 eq.), DMSO (10 ml), ascorbic acid (8.1 mg, 0.046 mmol, 2 eq. in 2.5 mL water), PMDETA (6 mg, 0.035 mmol, 1.5 eq. in 5 mL DMSO) and PDMA-*co*-PDAAM (0.5 g, 0.023 mmol, 1eq.) were added to the solution. The reaction mixture was stirred for two days at ambient temperature. Ascorbic acid (8.1 mg) and azido functionalised PS-resin (16 mg) was added to the reaction mixture and was stirred for two days at ambient temperature. Subsequently, the polymer was dialysed against deionised water (Spectra/Por 3500 Da). Finally, the sample was freeze-dried and a white solid (0.98 g, M_n= 25,300 g· mol^{-1} measured in acetate buffer against pullulan standards) was obtained. For Rhodamine B labelled Pull-*b*-(PDMA-*co*-PDAAM), the copolymer PDMA-*co*-PDAAM was synthesised in a similar way and subsequently conjugated with RITC.

Crosslinking of Pull-*b*-(PDMA-*co*-PDAAM)

Pull-*b*-(PDMA-*co*-PDAAM) (0.1 g, 0.004 mmol, 1.0 eq.) was dissolved in Millipore water (0.4 mL, all used Millipore water was filtered with a 0.45 µm CA syringe filter). 1,3-bis(aminooxy)propan dihydrochloride (26 µL, 0.0002 mmol, 0.05 eq. from a aqueous stock solution 1.4 mg in 1 mL Millipore water), 3,5-diaminobenzoic acid dihydrochloride (1 µL, from an aqueous stock solution 1 mg in 1 mL Millipore water) and triethylamine (23 µL, 0.008 mmol, 0.2 eq. from a aqueous stock solution 1 µL in 200 µL Millipore water) was added to the polymer solution. The reaction mixture was placed in a 35 °C oil-bath overnight.

Formation of RhB labelled Pull-*b*-PDMA-*co*-PDAAM

Alkyne end-functionalised pullulan (0.16 g, 0.0082 mmol, 1.2 eq.) was dissolved in Millipore water (3 mL). $CuSO_4$ (0.7 mg, 0.0044 mmol, 0.65 eq.), DMSO (5 ml), ascorbic acid (2.5 mg, 0.0136 mmol, 2.0 eq. in 1.5 mL water), PMDETA (2.4 mg, 0.01 mmol, 1.5 eq.) and RhB labelled PDMA-*co*-PDAAM (0.15 g, 0.0068 mmol, 1.0 eq.) were added to the solution. The reaction mixture was stirred for two days at ambient temperature. Ascorbic acid (8.1 mg) and azido functionalised PS-resin (16 mg) was added to the reaction mixture and was stirred for two days at ambient temperature. Subsequently, the polymer was dialysed against deionised water (Spectra/Por 3500 Da). Finally, the sample was freeze-dried and a purple solid (0.25 g, M_n = 22,300 g· mol^{-1} measured in acetate buffer against pullulan standards) was obtained.

Analysis of Pull-*b*-(PDMA-*co*-PDAAM)

A 5 wt% solution of Pull-*b*-(PDMA-*co*-PDAAM) was diluted with Millipore water (filtered with a 0.45 µm CA syringe filter) to 2.5 wt%, 1.25 wt%, 0.6 wt% and 0.1 wt% for DLS characterisation. Cryo SEM was performed with a 0.6 wt% solution. ^{1}H-NMR and ^{13}C-NMR were conducted with freeze dried samples.

Analysis of crosslinked Pull-*b*-(PDMA-*co*-PDAAM)

A 5 wt% solution of crosslinked Pull-*b*-(PDMA-*co*-PDAAM) was diluted with Millipore water (filtered with a 0.45 µm CA syringe filter) to 2.5 wt%, 1.25 wt%, 0.6 wt% and 0.1 wt% for DLS characterisation. 2.5 wt% (2 mL) and 1.25 wt% (2 mL) polymer solution were combined and dialysed against Millipore water (Spectra/Por 1000 kDa) and analysed *via* DLS and cryo SEM. The 0.6 wt% solution was analysed *via* cryo SEM. ^{1}H-NMR and ^{13}C-NMR were conducted with freeze dried samples.

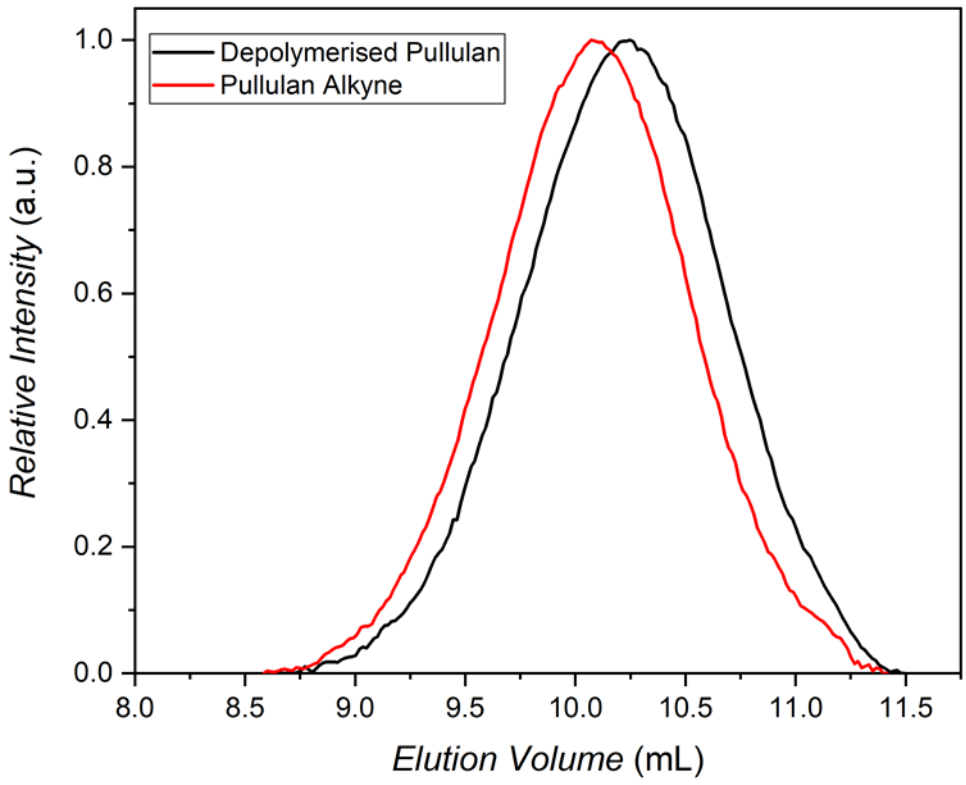

Figure 7.9. SEC measurement of depolymerised pullulan (black curve) and pullulan alkyne (red curve) measured in acetate buffer against pullulan standards.

Table 7-5. Results of SEC measurements of depolymerised pullulan (black curve) and pullulan alkyne (red curve) measured in acetate buffer against pullulan standards

Polymer	M_n **(kg·mol^{-1})**	$Đ$
Depolymerised pullulan	14.8	2.1
Pullulan alkyne	19.4	2.0

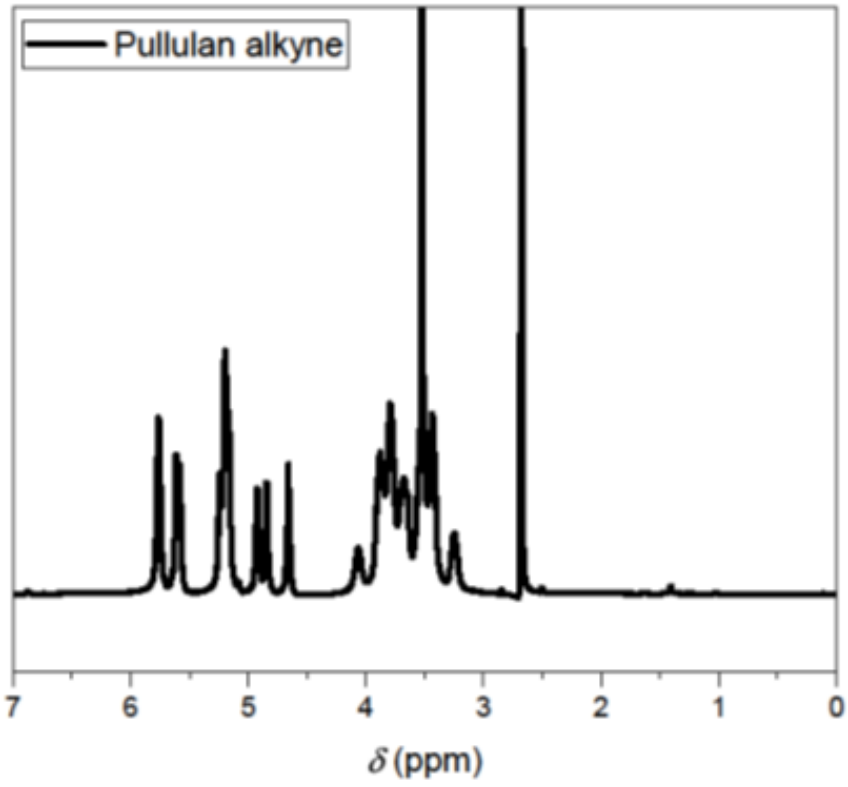

Figure 7.10. ^{1}H-NMR of the alkyne endfunctionalised pullulan measured in D_2O.

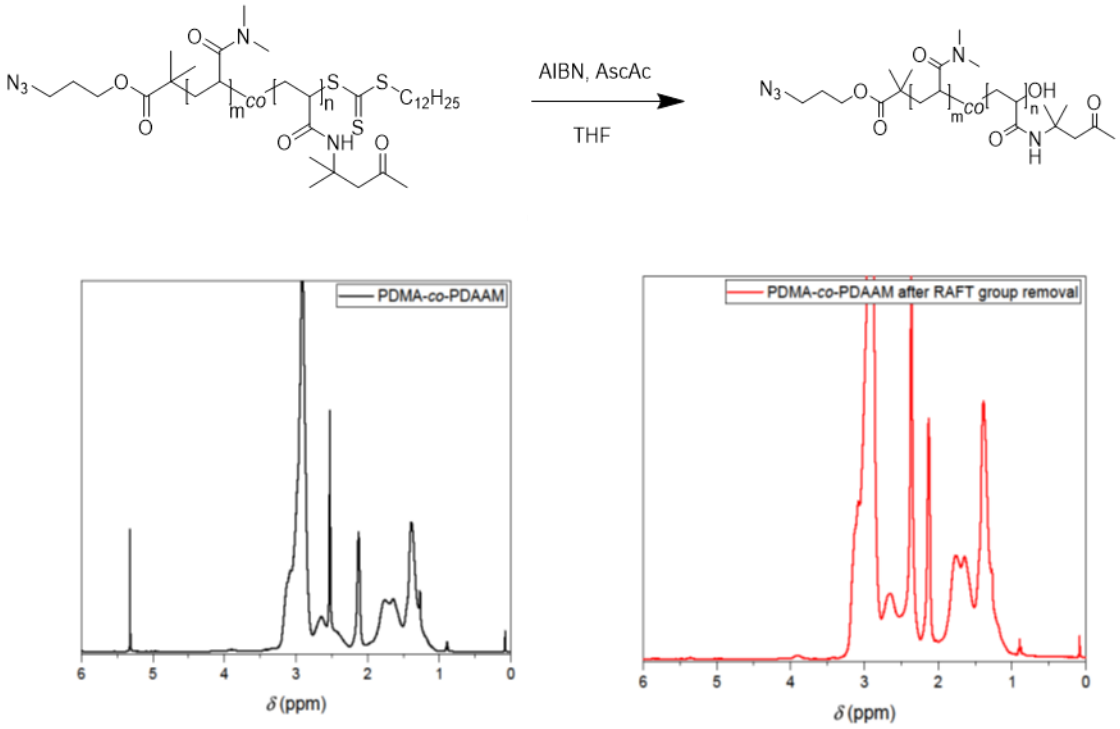

Figure 7.11. ^{1}H-NMR measurement of the statistical copolymer PDMA-*co*-PDAAM before (black curve) and after (red curve) the RAFT group removal (measured in $CDCl_3$).

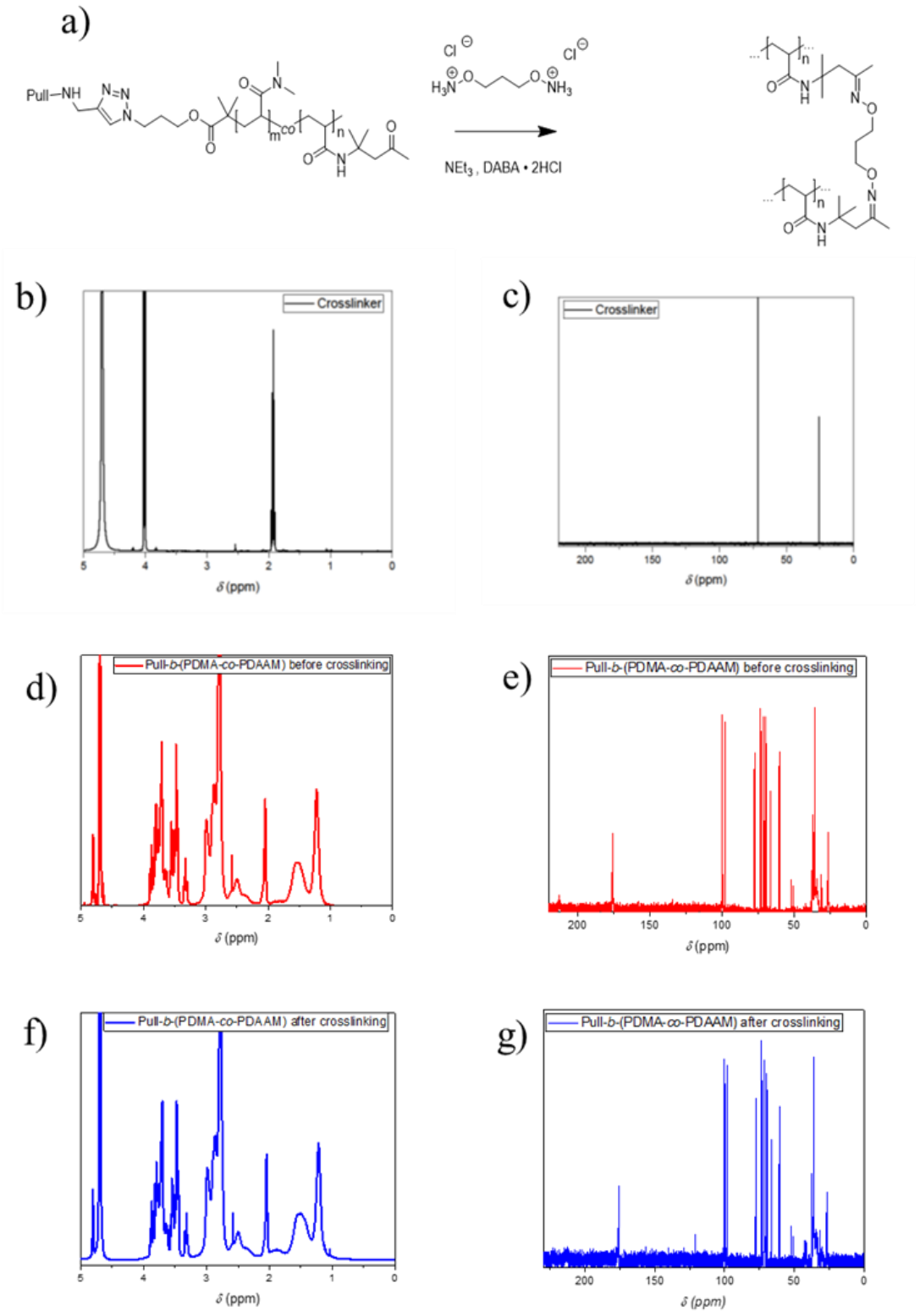

Figure 7.12. (a) Reaction scheme for crosslinking of Pull-*b*-(PDMA-*co*-PDAAM) containing 20% of DAAM with 1,3-bis(aminooxy)propan dihydrochloride via oxime formation in water; (b, d and f) ^{1}H-NMR and (c, e and g) ^{13}C-NMR of the crosslinker 1,3-bis(aminooxy)propan dihydrochloride (black curve) Pull-*b*-(PDMA-*co*-PDAAM) before (red) and after (blue) crosslinking in D_2O.

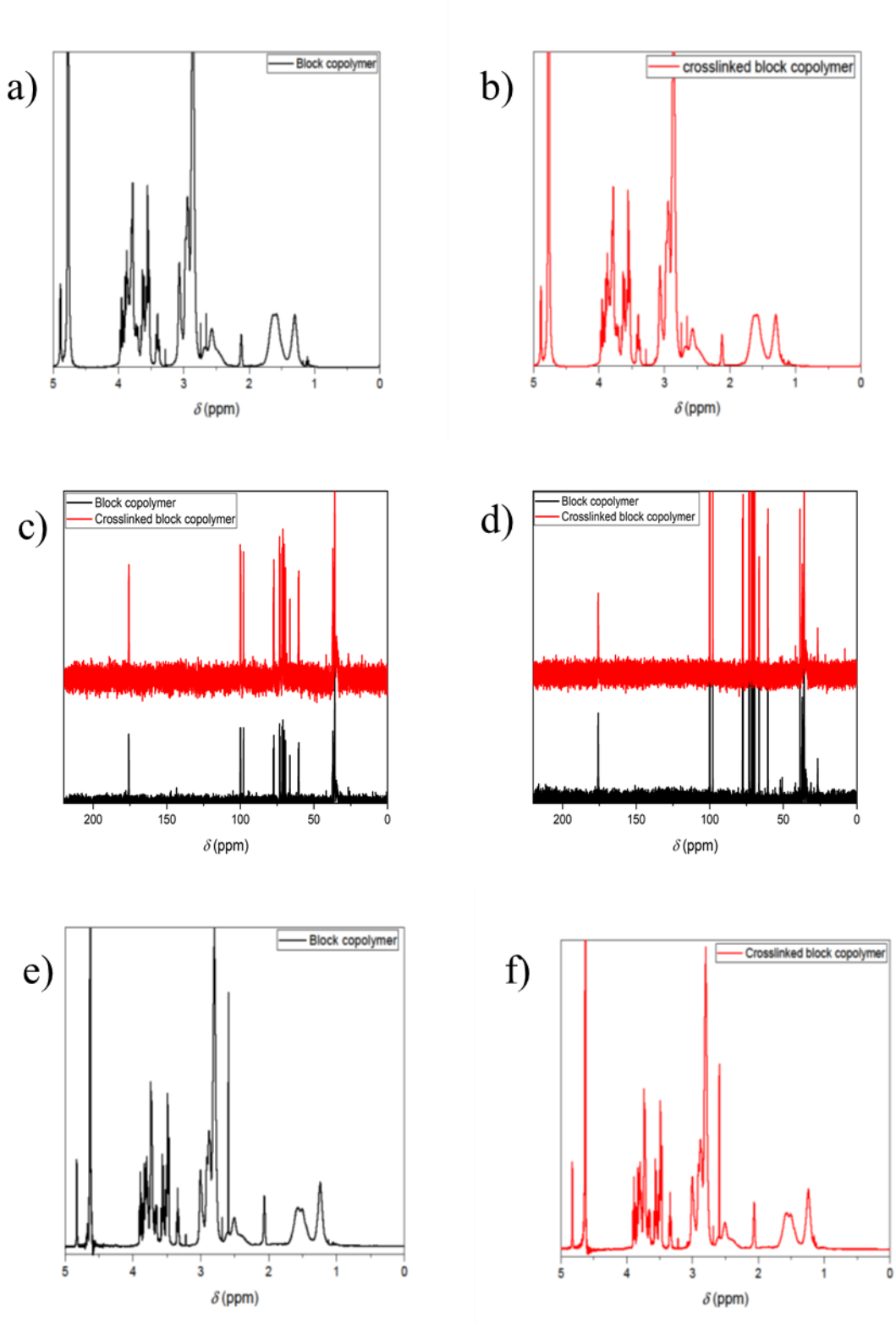

Figure 7.13. ^{1}H and ^{13}C-NMR spectra measured in D_2O before (black curve) and after crosslinking (red curve) of Pull-*b*-(PDMA-*co*-PDAAM) with 1,3-bis(aminooxy)propan dihydrochloride *via* oxime formation in water containing 5% of PDAAM (a-c) and 10% PDAAM (d -f).

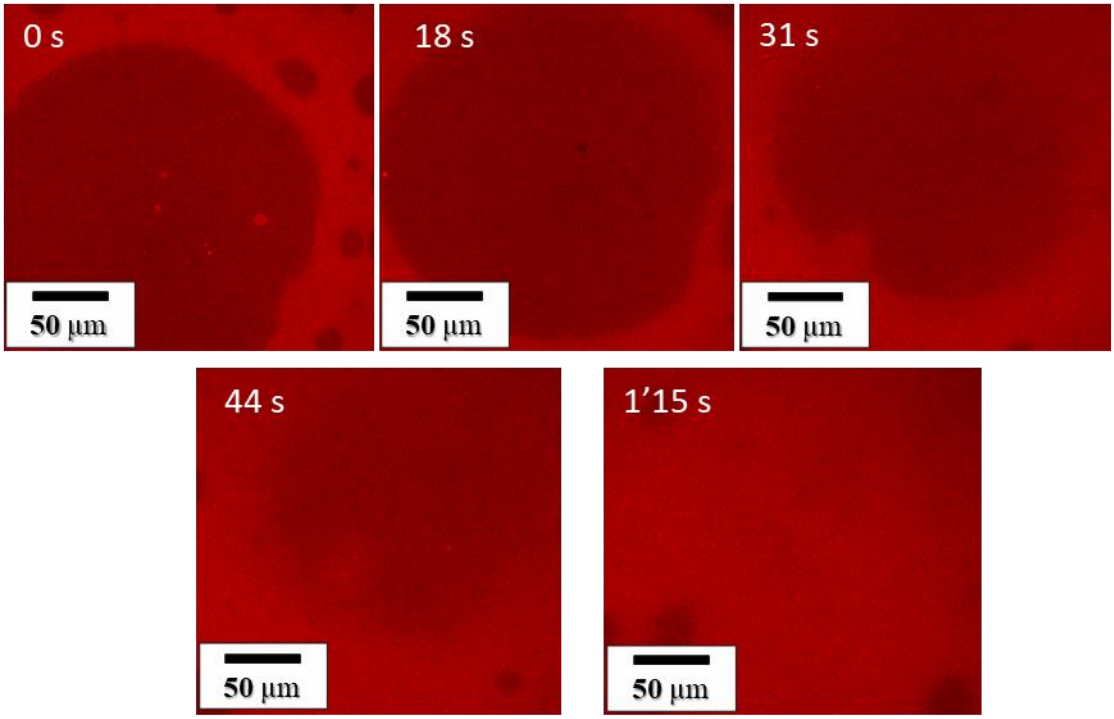

Figure 7.14. CLSM image series of the time lapse dilution video of crosslinked Pull-*b*-(PDMA-*co*-PDAAM), starting at 20 wt%, in water stained with sulforhodamine B.

Chapter 8

8 Stimuli-Responsive Aggregation of High Molar Mass Poly(*N*,*N*-Diethylacrylamide)-*b*-Poly(4-Acryloylmorpholine) in Tetrahydrofuran

8.1 Introduction[g]

The previous chapter discussed the aggregation of double hydrophilic block copolymers (DHBC) based on pullulan and acrylamides in aqueous and organic environment. The following chapter will, based on that knowledge, focus on the phase behaviour and self-assembly of double hydrophilic block copolymers (DHBC) in organic environment. Based on the results of the previous Chapters, poly(acrylamides) seem a good choice to constitute one or two blocks in novel DHBCs. An important factor for the self-assembly and aggregation of polymers is the molar mass of the block copolymers. One strategy in formation of well-defined aggregates is the utilisation of block copolymer (BCPs) self-assembly. In a selective solvent for one of the polymer blocks, aggregates like micelles[170] or vesicles[9] are formed. Furthermore, in a non-selective solvent, aggregates can be formed via external triggers, *e.g.* with temperature[171] or pH[114] as common triggers. In the case of a temperature trigger, aggregates are formed exploiting a lower critical solution temperature (LCST)[172] or an upper critical solution temperature (UCST)[116] of one of the polymer building segments in the block copolymer.

Besides self-assembly in aqueous environment, organic solvents and solvent mixtures are of interest as well,[173, 174] *e.g.* as a stabiliser for oil-in-oil emulsions[175, 176] or in the formation of micellar photonic crystals.[177] The group of Urban formed thermochromic inverse polymeric micelles in toluene, using ultra-high molar mass poly(2-(*N*,*N*-dimethylamino)ethyl methacrylate)-*b*-poly(*n*-butyl acrylate).[178] Gröschel and co-workers used block copolymer

[g] Terms of use: This chapter was adapted with permission from: A. Plucinski, M. Pavlovic, M. Clarke, D. Bhella, B. V. K. J. Schmidt, *Macromol. Rapid Commun*. **2022**,43, 210065, reference licensed under CC BY 3.0 Contribution by A. Plucinski in the following chapter about 90%.

micelle formation in combination with solvent exchange and following dilution to generate photonic fluids and crystals.[179]

In order to synthesise novel high molecular weight block copolymers and in analogy to Chapter 4 and 5, RAFT polymerisation is a facile avenue.[180, 181] In similarity to Chapter 5 and 6, at first primarily homopolymers or chain extensions were investigated, *e.g.* PDMA and PDMA-*b*-PDMA.[44] Additionally Sumerlin and co-workers utilised PI-RAFT polymerisation for the synthesis of ultra-high molecular weight block copolymers *e.g*. poly(*N*,*N*-dimethylacrylamide-*b*-*tert*-butyl acrylate) (PDMA-*b*-PtBA), which form assemblies upon solvent switch from THF to H_2O.[140]

A significant part of this thesis is the phase separation and self-assembly of hydrophilic polymers in aqueous environment. The block copolymer PDEA-*b*-PAM also shows aggregation at high concentration (> 20 wt%) at ambient temperature in aqueous solution. Aggregation of the block copolymer leads to a high viscous blue solution. Due to the high viscosity of the solution, detailed characterisation like DLS or cryo TEM is certainly challenging. However, during the search for other characterisation methods, PDEA-*b*-PAM revealed a blue dispersion in tetrahydrofuran (THF) at lower concentration. First tests revealed the formation of the blue dispersion depends on temperature, concentration and molar mass. Due to the unique behaviour in the organic solvent THF, the aggregation was analysed further.

In the following chapter the high molecular weight double hydrophilic block copolymer poly(*N*,*N*-diethylacrylamide)-*b*-poly(4-acryloylmorpholine) (PDEA-*b*-PAM) was synthesised *via* PI-RAFT polymerisation. The block copolymer showed unprecedented temperature-responsive aggregation in THF. The aggregation behaviour in THF was analysed at different concentrations and temperatures *via* dynamic light scattering (DLS), cryo TEM and temperature-controlled UV-VIS.

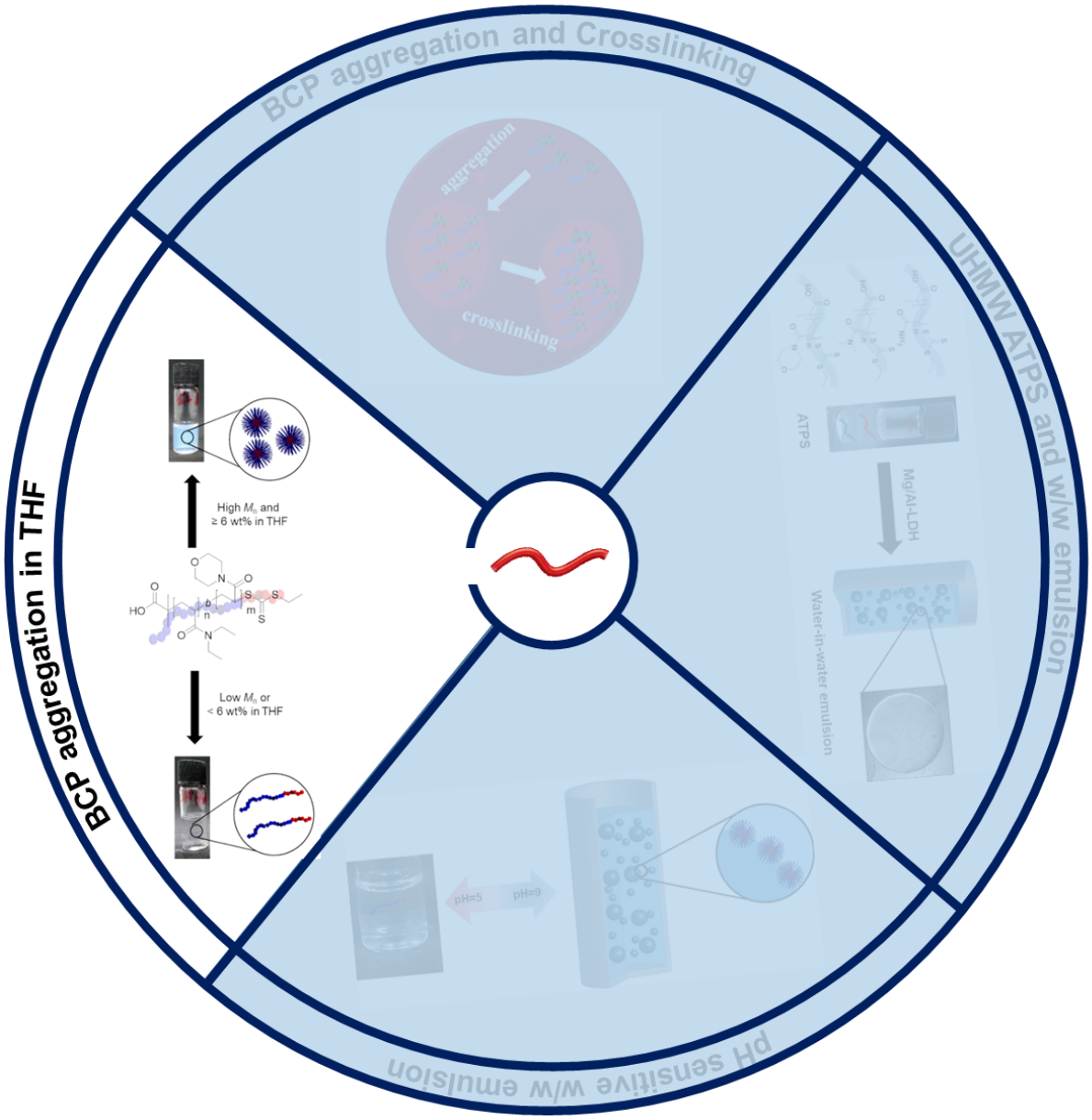

Scheme 8.1. Overview of the different utilisation of hydrophilic polymers for self-assembly or phase separation, highlighted the part of the current chapter: DHBC utilised for an aggregation in the organic solvent THF.

8.2 Block copolymer formation and self-assembly

PDEA-*b*-PAM was synthesised via RAFT polymerisation. At first, the PDEA block was synthesised, yielding PDEA with a molar mass of M_n= 203,000 g·mol^{-1} and a molecular dispersity of (*Đ)* of 1.3 according to SEC-MALS (Figure 8.1 and Table 8.1). Following on the literature,[44] the block copolymer was synthesised *via* visible light mediated PI-RAFT polymerisation of AM in high concentrated buffer solution (Figure 8.1 a). PDEA-*b*-PAM was obtained with a molar mass of M_n= 403,000 g·mol^{-1} and *Đ* of 1.5 according to SEC-MALS. The increment of absolute molar mass (Figure 8.1 b) and the signals for both polymers, around 3.5 ppm for PAM and around 3.0 ppm for PDEA, in the ^{1}H-NMR (Figure 8.9), indicate the successful formation of the block copolymer. Additionally, the synthesis of the high molecular weight block copolymer was confirmed via diffusion ordered NMR spectroscopy (DOSY) that revealed signals at a diffusion coefficient of 7.5 10^{-7} cm^2·s^{-1} for both block types (Figure 8.10). Moreover, the block copolymer formation was confirmed *via* differential scanning calorimetry (DSC), as observed by two glass transition temperatures (T_g) corresponding to the individual polymer blocks (Figure 8.11).

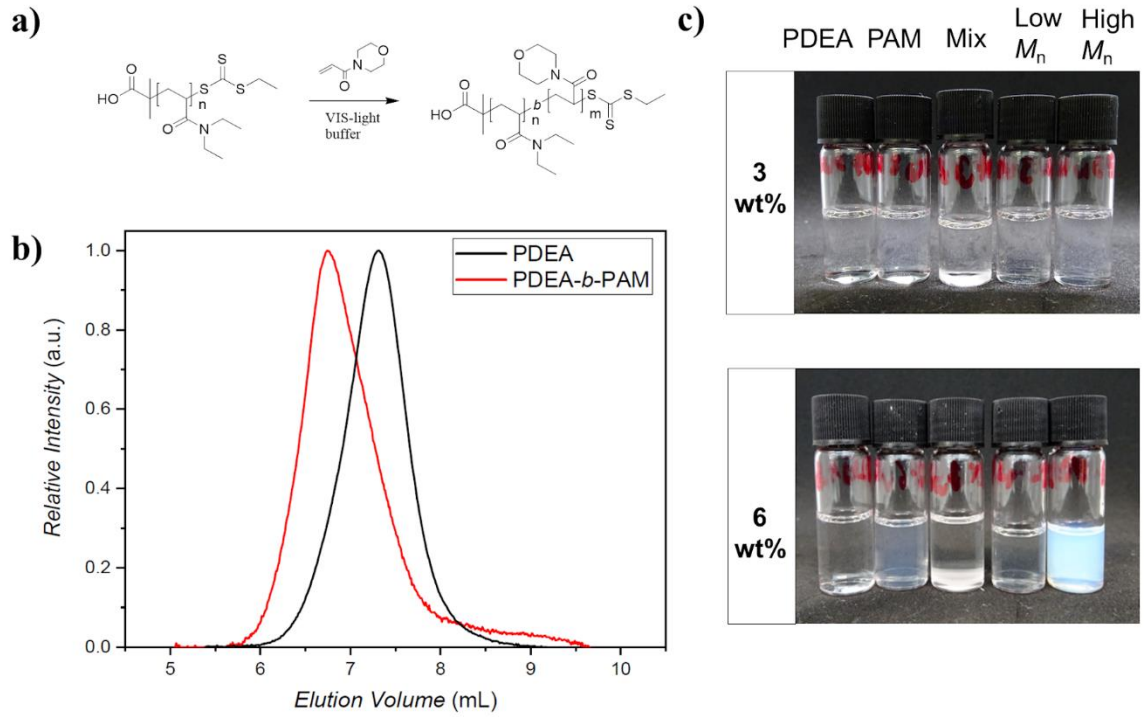

Figure 8.1. (a) Reaction scheme of PDEA-*b*-PAM formation *via* visible light photo induced RAFT-polymerisation, (b) SEC-MALS traces of PDEA and PDEA-*b*-PAM in THF, (c)

solubility behaviour of $PDEA_{1850}$, PAM_{830}, $PDEA_{1850}/PAM_{830}$ mix, $PDEA_{98}$-*b*-PAM_{387} and $PDEA_{1850}$-*b*-PAM_{1380} in THF at 3 and 6 wt%.

Table 8-1. Results of SEC measurements of PDEA, PAM and PDEA-*b*-PAM with $PDEA_{98}$ and $PDEA_{98}$-*b*-PAM_{387} measured in THF against PS standards, PAM_{830} measured in NMP against PS standards, $PDEA_{1850}$ and $PDEA_{1850}$-*b*-PAM_{1380} measured in THF with MALS detection (d*n*/d*c* ($PDEA_{1850}$): 0.090 ± 0.031 $mL \cdot g^{-1}$; d*n*/d*c*($PDEA_{1850}$-*b*-PAM_{1380}): 0.105 ± 0.038 $mL \cdot g^{-1}$).

Polymer	M_n **(kg·mol^{-1})**	$Đ$
$PDEA_{98}$[a]	12.4	1.1
$PDEA_{1850}$[c]	235.1	1.3
PAM_{830}[b]	117.3	1.6
$PDEA_{98}$-*b*-PAM_{387}[a]	67.2	1.3
$PDEA_{1850}$-*b*-PAM_{1380}[c]	403.5	1.5

Unexpectedly, $PDEA_{1850}$-*b*-PAM_{1380}, forms blue dispersions at high concentration in THF, i.e. above 6 wt% (Figure 8.1 c). To verify the influence of the molar mass and to compare the block copolymer to the homopolymers, solubility behaviour of $PDEA_{1850}$, PAM_{830}, $PDEA_{1850}/PAM_{830}$ mix, $PDEA_{98}$-*b*-PAM_{387} and $PDEA_{1850}$-*b*-PAM_{1380} was analysed at 3 and 6 wt% in THF. A colour change could be observed only for $PDEA_{1850}$-*b*-PAM_{1380} above 6 wt% (Figure 8.1 c) indicating aggregation of the block copolymer in THF.

8.3 Particle formation and UCST in tetrahydrofuran

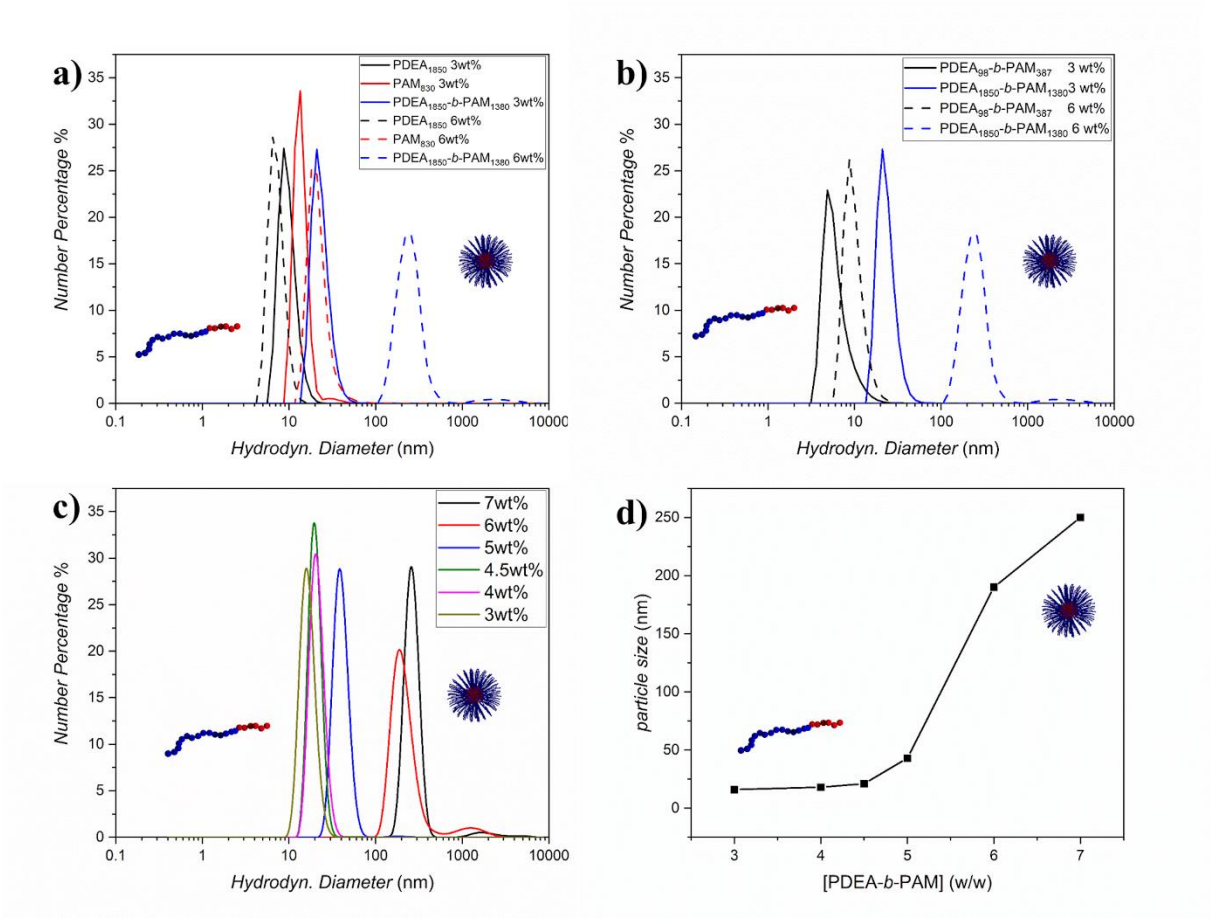

Figure 8.2. (a) Comparison of number weighted particle size distribution of $PDEA_{1850}$ (black curve), PAM_{830} (red curve) and $PDEA_{1850}$-*b*-PAM_{1380} (blue curve) at different concentration, measured in THF at ambient temperature, (b) $PDEA_{98}$-*b*-PAM_{387} (black curve) and $PDEA_{1850}$-*b*-PAM_{1380} (blue curve) at different concentration measured in THF at ambient temperature, (c) number weighted particle size distribution of $PDEA_{1850}$-*b*-PAM_{1380} at different concentration measured in THF at ambient temperature and (d) particle size change at different concentration in THF at ambient temperature.

In order to analyse the aggregation behaviour of $PDEA_{1850}$-*b*-PAM_{1380} in THF, $PDEA_{1850}$, PAM_{830}, $PDEA_{98}$-*b*-PAM_{387} and $PDEA_{1850}$-*b*-PAM_{1380} were dissolved in THF at different concentrations (3 and 6 wt%). The hydrodynamic diameter was monitored for all concentrations *via* dynamic light scattering (DLS) at 25 °C (Figure 8.2 a and b). The DLS results show for all polymers at 3 wt% a hydrodynamic diameter between 10 and 30 nm, which can be most likely assigned to free polymer chains in the solution. The difference in the hydrodynamic diameter at 3 wt% can be the explained with the different molar masses of the respective polymers. At a concentration of 6 wt%, the hydrodynamic diameter was in a similar

range (around 8 to 30 nm) for both homopolymers ($PDEA_{1850}$ and PAM_{830}) and the low molar mass block copolymer $PDEA_{98}$-*b*-PAM_{387} (10 to 20 nm). In contrast, the hydrodynamic diameter of $PDEA_{1850}$-*b*-PAM_{1380} increased significantly to 230 nm at 6 wt%, confirming the presence of aggregates for the high molar mass block copolymer in THF at higher concentration. Thus, the concentration dependence of the aggregation of $PDEA_{1850}$-*b*-PAM_{1380} in THF was further analysed via DLS between 3 and 7 wt% (Figure 8.2 c). The concentration dependent DLS measurement shows that $PDEA_{1850}$-*b*-PAM_{1380} has a critical aggregation concentration around 6 wt%. As such, the turbidity of the dispersion can be explained with the high molar mass of the bock copolymer, which leads to the formation of large aggregates leading to refraction.

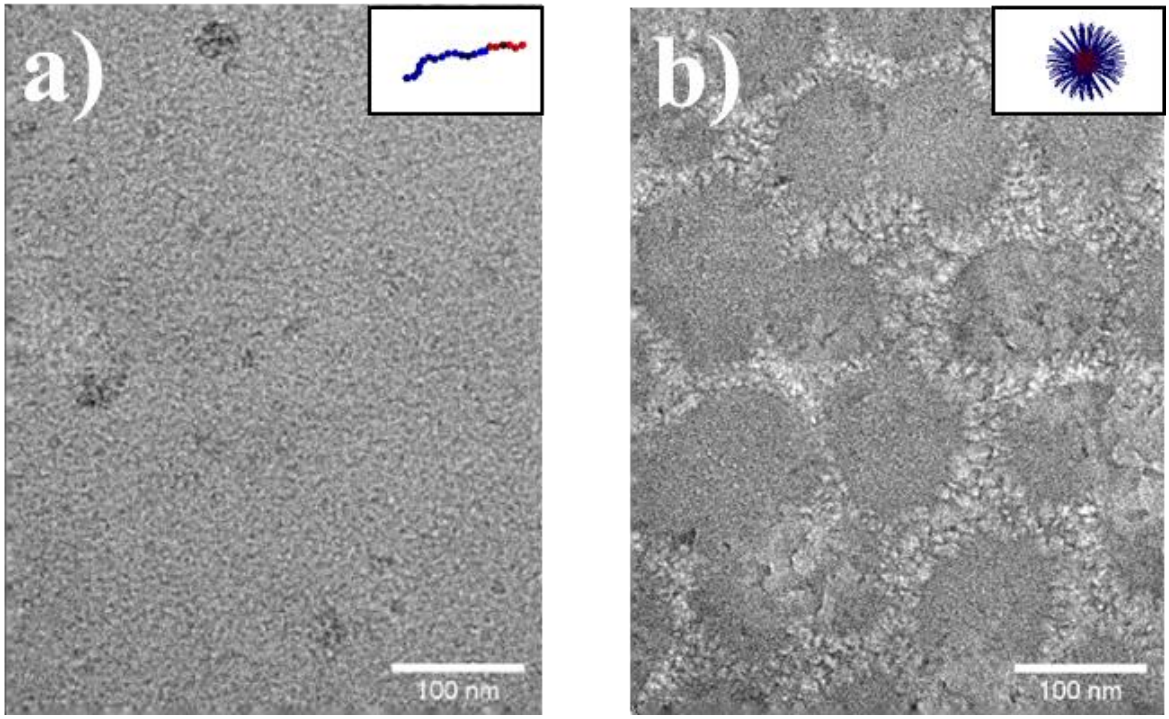

Figure 8.3. (a,b) Cryo TEM images of PDEA-*b*-PAM at a concentration of 6 wt% in THF (a) $PDEA_{98}$-*b*-PAM_{387} and (b) $PDEA_{1850}$-*b*-PAM_{1380}.

To further characterise the formed aggregates, the block copolymers were analysed *via* cryo TEM. Two samples were analysed, one block copolymer with lower molar mass ($PDEA_{98}$-*b*-PAM_{387}) and one with higher molar mass ($PDEA_{1850}$-*b*-PAM_{1380}) at a concentration of 6 wt% in THF. The cryo TEM image of $PDEA_{98}$-*b*-PAM_{387} (Figure 8.3 a) displays no visible aggregation at a magnification of 50k. In contrast, the cryo TEM image of $PDEA_{1850}$-*b*-PAM_{1380} shows aggregates with sizes between 80 and 120 nm (Figure 8.3 b) and an average particle size of 105 ± 15 nm. The results of the cryo TEM measurement confirm the molar mass

influence of PDEA-*b*-PAM on the formation of aggregates in THF. In comparison to the DLS measurement the particle size in the cryo TEM images is slightly lower. The difference could be due to imaging of denser aggregate cores in cryo TEM compared to the full particles including corona in DLS.

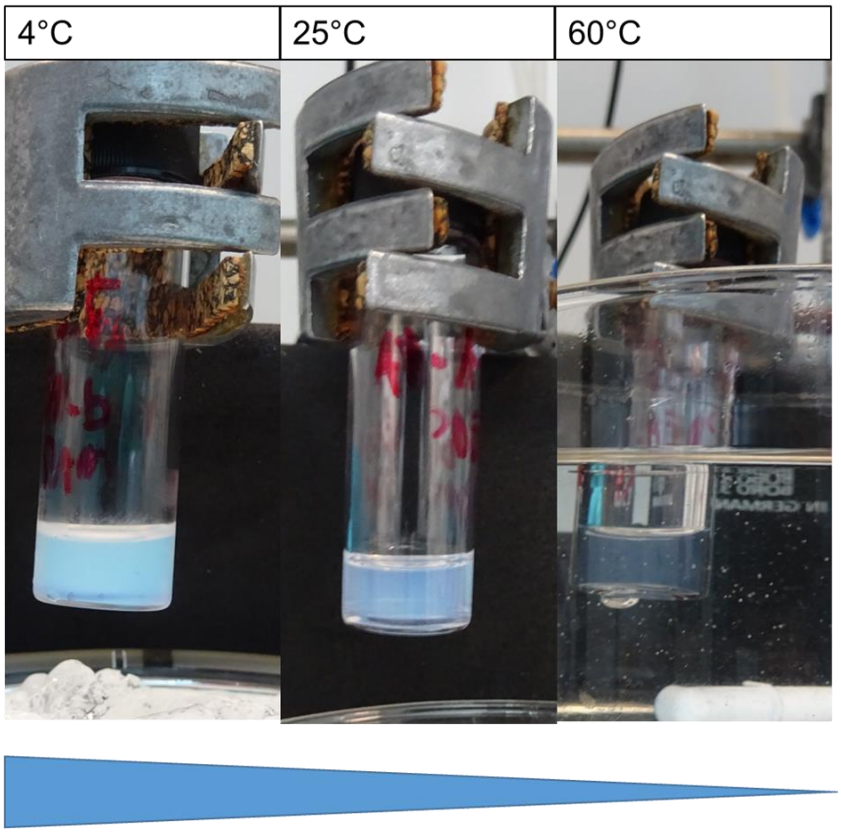

Figure 8.4. Intensity of the blue coloured dispersion of $PDEA_{1850}$-*b*-PAM_{1380} at 6 wt% in THF depending on the temperature.

After analysis of the formed aggregates the underlying driving force was investigated. It was noticed that the aggregation of $PDEA_{1850}$-*b*-PAM_{1380} depends on the temperature and is related to an UCST of PAM in THF. For example, the intensity of the blue colour increases at lower temperatures (Figure 8.4). In order to analyse the UCST of PAM_{830} in THF, the cloud point (T_{cp}) of PAM_{830}, and $PDEA_{1850}$-*b*-PAM_{1380}, were measured *via* turbidimetry (Figure 8.5 c). At 3 wt%, the T_{cp} was around 10 °C for PAM_{830} and 12 °C for the block copolymer. The increase of the T_{cp} can be explained by the connected THF-soluble PDEA block. As expected, the

exhibited T_{cp} increased by 5 °C for PAM_{830} at 6 wt%. In the case of $PDEA_{1850}$-*b*-PAM_{1380} no explicit T_{cp} was detected but rather a transition range from 20 to 40 °C.

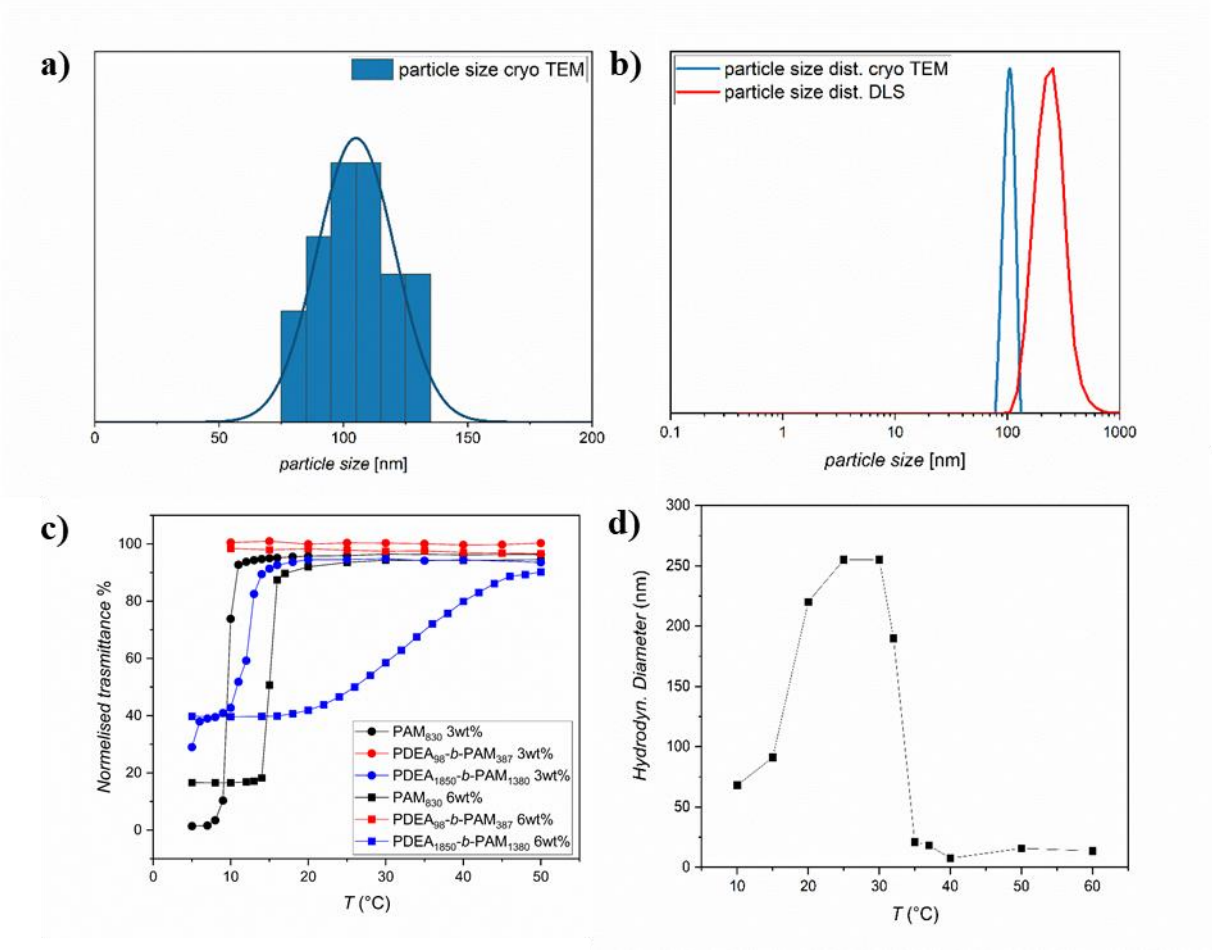

Figure 8.5. (a, b) Particle size distribution of PDEA-*b*-PAM at 6 wt% in THF (a) measured over 30 particles in cryo TEM images including normal distribution and (b) comparison of the particle size distribution measured with cryo TEM images (blue curve) and DLS (red curve), (c) turbidimetry of PAM_{830} (black curves), $PDEA_{98}$-*b*-PAM_{387} (red curves) and $PDEA_{1850}$-*b*-PAM_{1380} (blue curves), (d) particle size change at different temperatures of $PDEA_{1850}$-*b*-PAM_{1380} at 6wt% in THF.

The change in transmittance was significantly lower in comparison to PAM at 6 wt% and both polymers at 3 wt%, which is due to the presence of the PDEA block hindering the formation of large aggregates and a sudden aggregation via steric stabilisation. It should be noted that the gradual change in transmittance was not depending on cooling time. Additionally, the particle size depends on the temperature as shown in DLS measurements of $PDEA_{1850}$-*b*-PAM_{1380} at a concentration of 6 wt% (Figure 8.5 d and Figure 8.6).

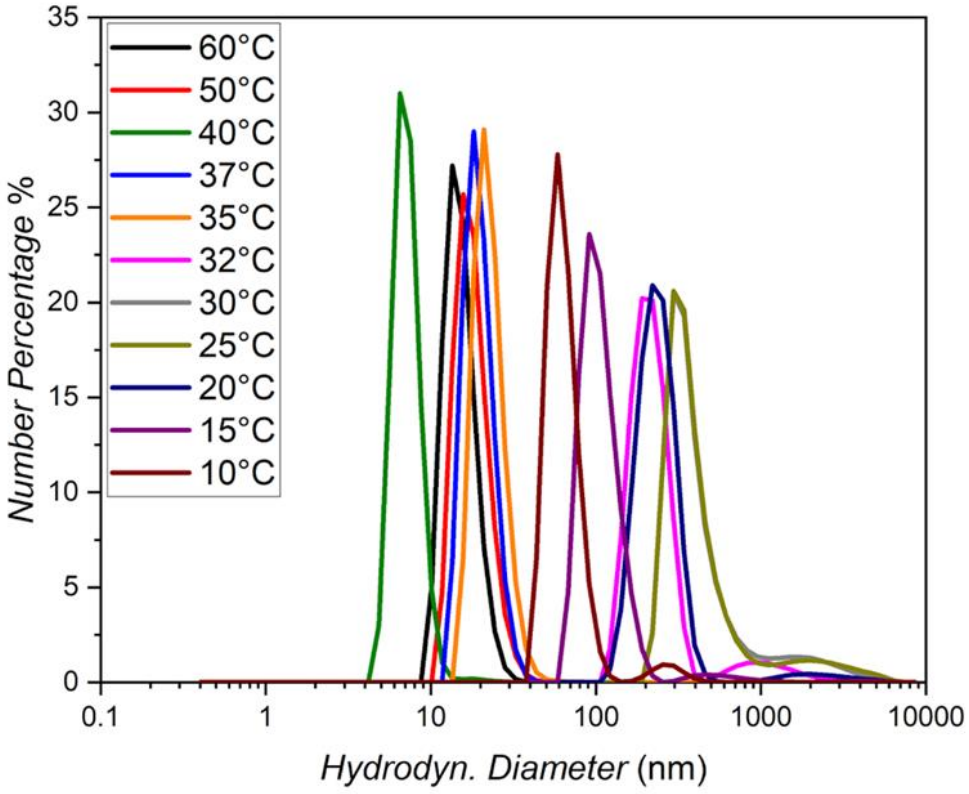

Figure 8.6. Comparison of number weighted particle size distribution of $PDEA_{1850}$-*b*-PAM_{1380} in THF at 6 wt.% measured via DLS at different temperatures (10-60 °C).

Table 8-2. Comparison of number weighted particle size distribution of $PDEA_{1850}$-*b*-PAM_{1380} in THF at 6 wt.% measured via DLS at different temperatures (10-60 °C).

T (°C)	**10**	**15**	**20**	**25**	**30**	**32**	**35**	**37**	**40**	**50**	**60**
Particle size (nm)	70	91	220	255	255	190	21	18	8	16	14

Above 35 °C the particle size is around 15 nm which is similar to the free chain polymer at 3 wt%. In the range of 20 to 32 °C the particle size stabilises around 190-260 nm and the hydrodynamic diameter decreases to 70 nm between 10 and 20 °C. As such, the DLS results (Figure 8.6 and Table 8.2) for $PDEA_{1850}$-*b*-PAM_{1380} in THF confirm the result of the turbidimetry that aggregation starts around 40 °C. Overall, the temperature-dependent measurements show that the aggregation of $PDEA_{1850}$-*b*-PAM_{1380} is due to an UCST of the PAM block in THF. Interestingly, aggregate formation strongly depends on concentration and

molar mass. The initially observed aggregates at ambient temperature and high concentration are formed due to the presence of the UCST at temperatures under 40 °C, which leads to a blue coloured dispersion, in contrast to homo polymer and low molar mass block copolymer.

8.4 Conclusion

Chapter 8 described the UCST behaviour of PAM in THF, which was further utilised to form thermo-responsive block copolymer aggregates via the high molecular weight (HMW) block copolymer $PDEA_{1850}$-*b*-PAM_{1380}. The formed aggregates feature a particle size of around 200 nm in high concentrated THF solution leading to a blue coloured dispersion. The aggregation depends on molar mass and concentration of the block copolymer as well as temperature.

8.5 Experimental Part

Synthesis of low molar mass $PDEA_{98}$

In a dry, argon purged 100 mL round bottom Schlenk flask, destabilised DEA (1.0 g, 7.9 mmol, 118.0 eq.), EMP (15.0 mg, 0.067 mmol, 1.0 eq.), AIBN (2.1 mg, 0.013 mmol, 0.2 eq.) were mixed together with a stirring bar and sealed. The solution was degassed by three freeze-pump-thaw cycles and placed in a pre-heated oil bath (65 °C). The polymerisation was stopped after 24 h. Subsequently, the polymer was dialysed against deionised water (Spectra/Por 3500 Da). Finally, the sample was freeze-dried and a white solid (0.8 g, M_n =12,400 g · mol^{-1}, $Đ$ = 1.1) was obtained.

Synthesis of PAM_{830}

In a dry, argon purged 100 mL round bottom Schlenk flask, destabilised AM (1.0 g, 7.1 mmol, 1800 eq.), EMP (0.88 mg, 0.0039 mmol, 1.0 eq.), AIBN (0.13 mg, 0.0007 mmol, 0.2 eq.), and DMF (3 mL) were mixed together with a stirring bar and sealed. The solution was degassed by three freeze-pump-thaw cycles and placed in a pre-heated oil bath (60 °C). The polymerisation was stopped after 24 h. Subsequently, the polymer was dialysed against deionised water (Spectra/Por 3500 Da). Finally, the sample was freeze-dried and a white solid (0.9 g, M_n= 117,300 g · mol^{-1}, $Đ$ = 1.6) was obtained.

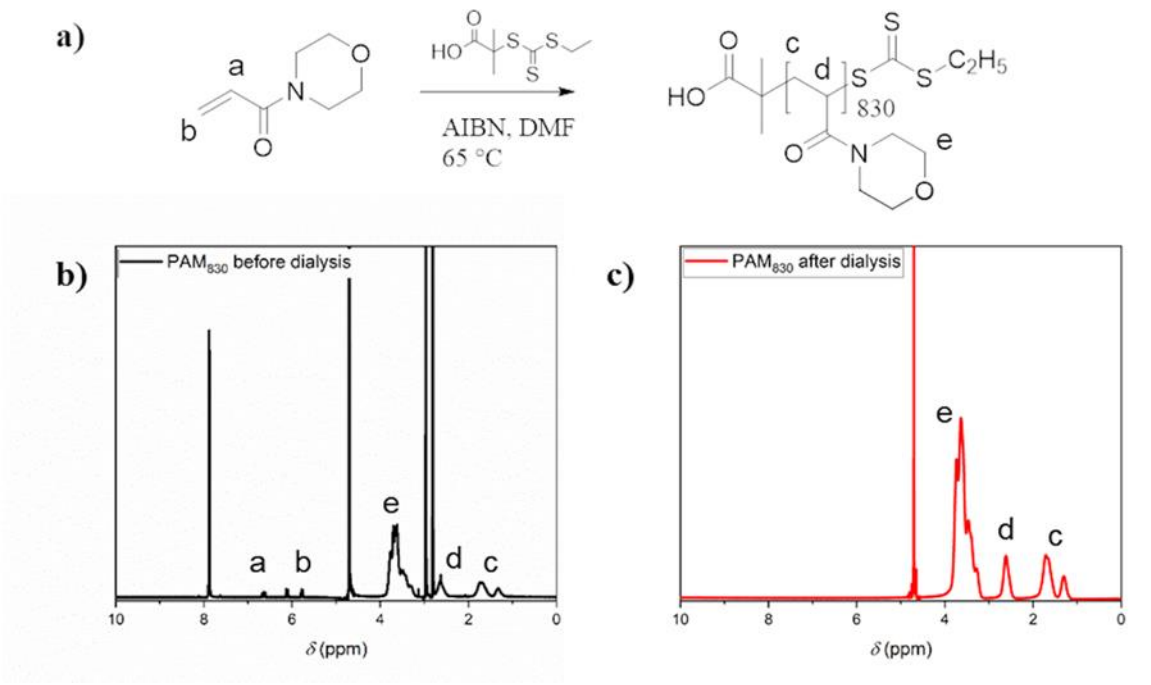

Figure 8.7. (a) Reaction scheme of the photo induced RAFT-polymerisation of AM, (b and c) ^{1}H-NMR measurement of PAM_{830} in D_2O (b) before dialysis and (c) after dialysis.

Formation of low molar mass PDEA$_{98}$-*b*-PAM$_{387}$

Destabilised AM (300 mg, 2.1 mmol, 260 eq.), PDEA (100 mg, 0.0081 mmol, 1.0 eq.), and acetate buffer (0.5 mL, 0.2 M, pH=5) were mixed together with a stirring bar in a glass vial (14 mL) and sealed with a septum. The solution was bubbled with nitrogen for 30 min and the polymerisation was initiated by a VIS-light-lamp. The polymerisation was stopped after 24 h. Subsequently, the polymer was dialysed against deionised water (Spectra/Por 3500 Da). Finally, the sample was freeze-dried and a white solid (357 mg, M_n= 67,200 g · mol^{-1}, $Đ$ = 1.3) was obtained.

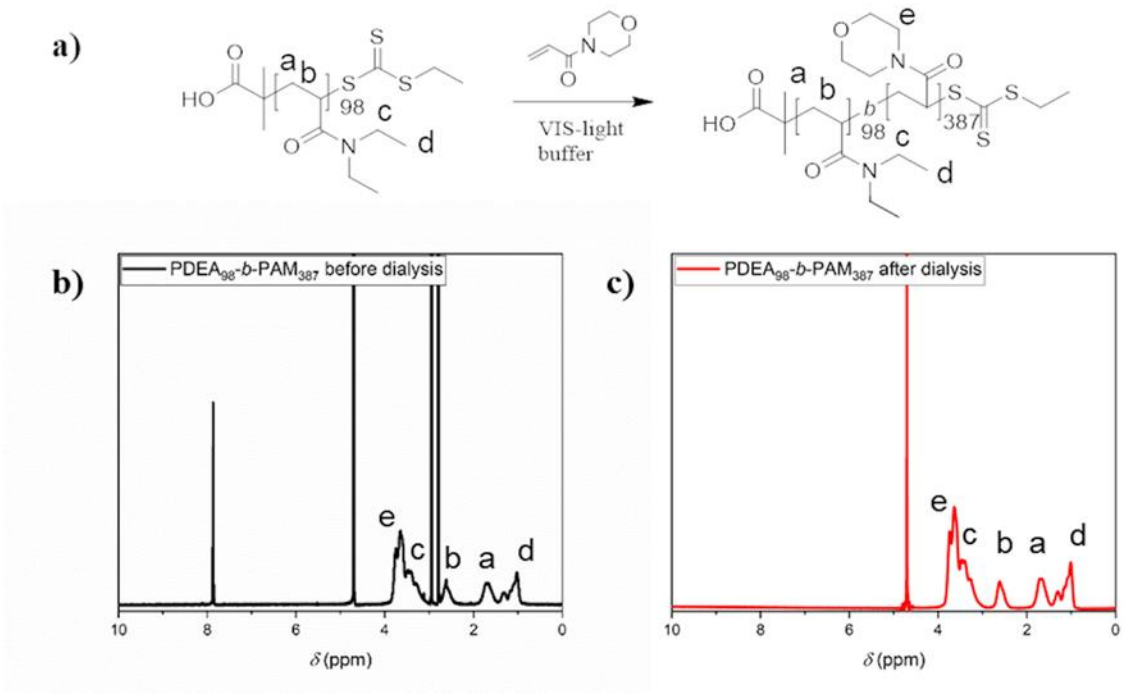

Figure 8.8. (a) Reaction scheme of the photo induced RAFT-polymerisation for PDEA-*b*-PAM synthesis, (b and c) ^{1}H-NMR measurement of PDEA$_{98}$-*b*-PAM$_{387}$ in D_2O (b) before dialysis and (c) after dialysis.

Synthesis of high molar mass PDEA$_{1850}$

In a dry, argon purged 100 mL round bottom Schlenk flask, destabilised DEA (5.0 g, 39.0 mmol, 2000 eq.), EMP (4.4 mg, 0.0197 mmol, 1.0 eq.), and AIBN (0.65 mg, 0.0039 mmol, 0.2 eq.) were mixed together with a stirring bar and sealed. The solution was degassed by three freeze-pump-thaw cycles and placed in a pre- heated oil bath (65 °C). The polymerisation was stopped after 24 h. Subsequently, the polymer was dialysed against deionised water (Spectra/Por 3500 Da). Finally, the sample was freeze-dried and a white solid (4.3 g, M_n= 235,100 g · mol^{-1}, $Đ$ = 1.3) was obtained.

Formation of high molar mass PDEA$_{1850}$-*b*-PAM$_{1380}$

Destabilised AM (300 mg, 2.1 mmol, 4883 eq.), PDEA$_{1850}$ (100 mg, 0.00043 mmol, 1.0 eq.), and acetate buffer (0.7 mL, 0.2 M, pH=5) were mixed together with a stirring bar in a glass vial (14 mL) and sealed with a septum. The solution was bubbled with nitrogen for 30 min and the polymerisation was initiated by a VIS-light-lamp. The polymerisation was stopped after 24 h. Subsequently, the polymer was dialysed against deionised water (Spectra/Por 3500 Da). Finally, the sample was freeze-dried and a white solid (320 mg, M_n= 403,500 g · mol^{-1}, $Đ$ = 1.5) was obtained.

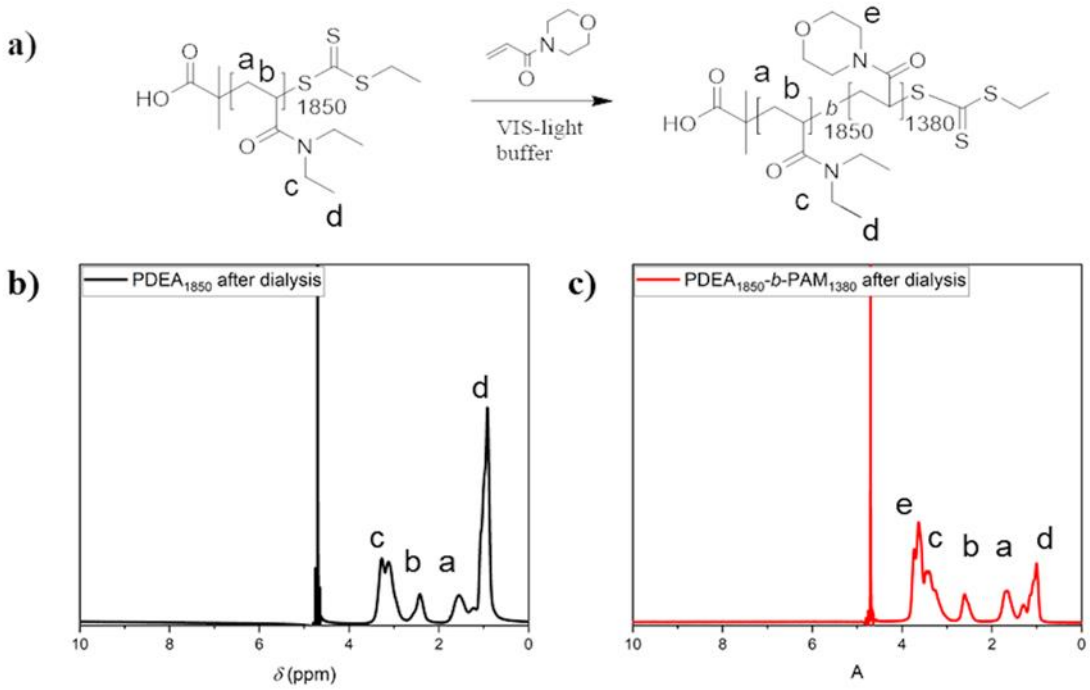

Figure 8.9. (a) Reaction scheme of the photo induced RAFT-polymerisation of PDEA-*b*-PAM, (b) ^{1}H-NMR measurement of $PDEA_{1850}$ in D_2O and (c) ^{1}H-NMR measurement of $PDEA_{1850}$-*b*-PAM_{1380} after dialysis in D_2O.

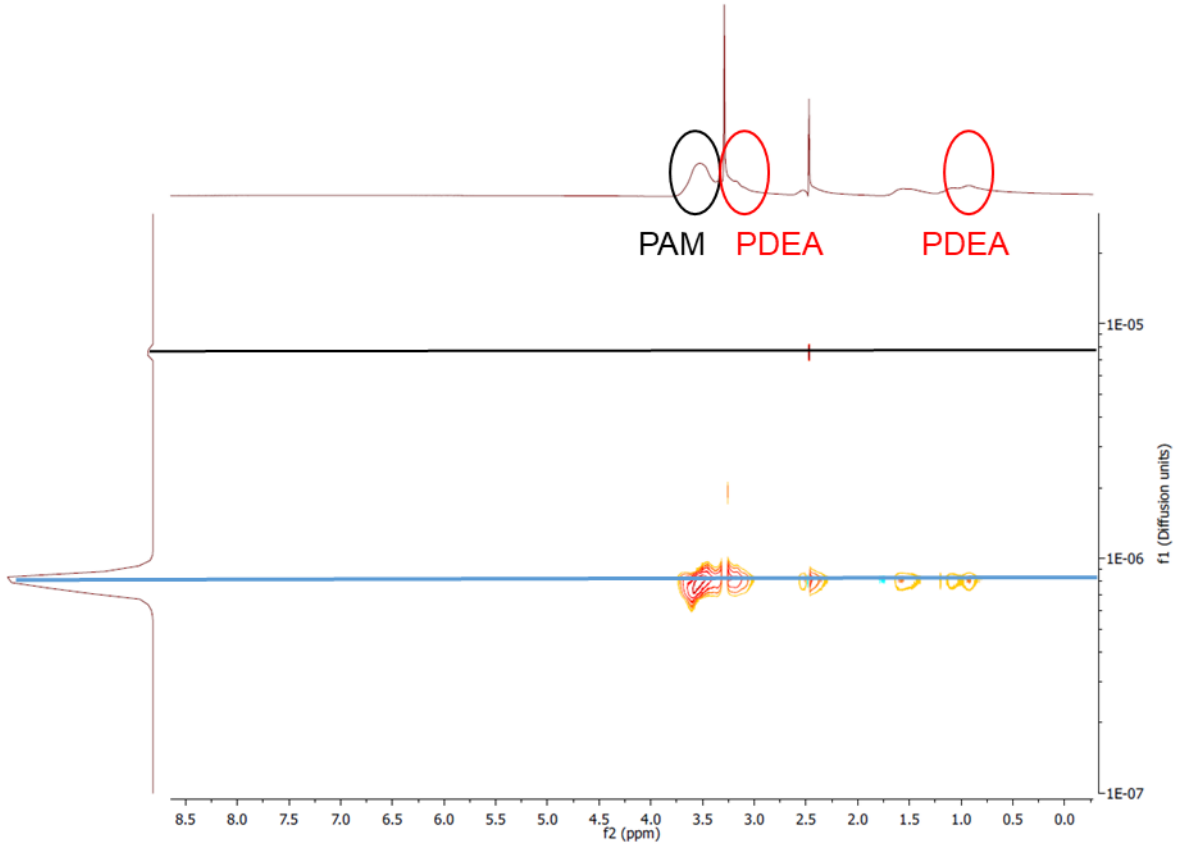

Figure 8.10. DOSY measurement of $PDEA_{1850}$-*b*-PAM_{1380} (measured in DMSO-d_6) with the diffusion coefficient of DMSO-d_6 (black line) and $PDEA_{1850}$-*b*-PAM_{1380} including all ^{1}H-NMR peaks, from all individual blocks (blue line).

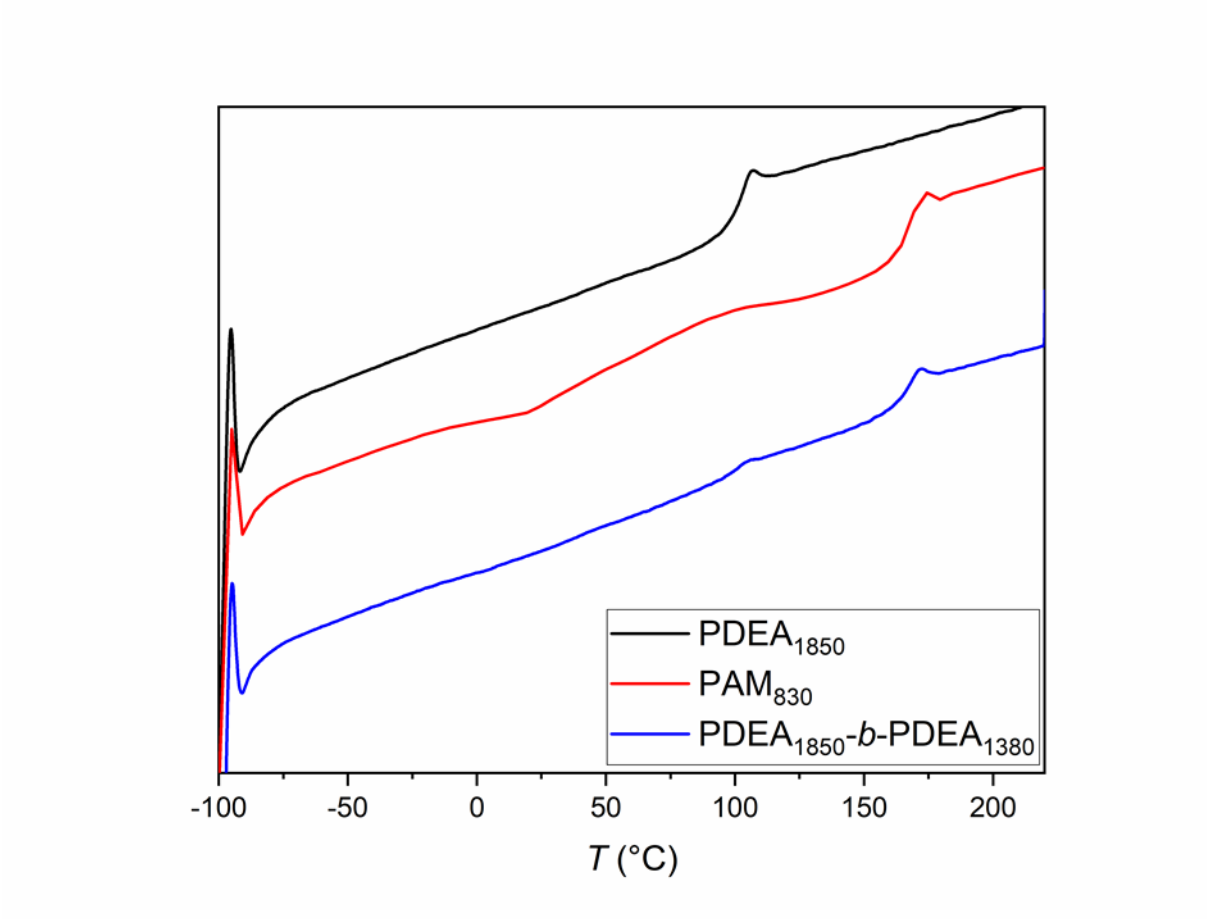

Figure 8.11. DSC thermograms of $PDEA_{1850}$, PAM_{830} and $PDEA_{1850}$-*b*-PAM_{1380}.

Chapter 9

9 Conclusion and perspective

The focus of this thesis was utilising hydrophilic polymers like pol(acrylamides) and pullulan as building blocks for the phase separation and self-assembly of pure water-soluble polymer systems. One the one hand phase separation of a mixture of two or more hydrophilic polymers, on the other hand the self-assembly of double hydrophilic block copolymers (DHBC), in aqueous environment.

The first part of this thesis investigated different combination of poly(acrylamides) and pullulan with different molar mass in aqueous environment. Overall, the results in the phase separation of homopolymers showed a significant influence of the molar mass of hydrophilic polymers for the phase separation and self-assembly. Especially for the phase separation in an ATPS and a w/w emulsion the molar mass was a key factor. Using ultra-high molar mass polymers for the formation of an ATPS and w/w emulsion the critical concentration decreases significantly. It was possible, even at low polymer concentration (below 3 wt% total polymer concentration) to observe phase separation and w/w emulsions could be formed with various types of stabilisers e.g., LDH nanoparticles or PDMAEMA-*b*-POEGMA and external triggers. Overall, the partitioning of the polymers during the w/w-emulsions depends significantly on the ratio of the polymer in emulsion.

The second part of this thesis investigated the self-assembly of different block copolymers based on poly(acrylamides) and pullulan in aqueous and organic environment. The block copolymers show mesoscale phase separation at high concentrations of 20 wt% in aqueous environment, which is reversible upon dilution. The mesoscale phase separation in form of giant droplets could not be stabilised via crosslinking. However, at lower concentration (< 6 wt%) the block copolymers featured smaller aggregates in aqueous and organic (THF or NMP) environment. The aggregate size depended on temperature and concentration.

The results show molar mass has a significant influence of the phase separation and the self-assembly of hydrophilic polymers in aqueous and organic environment. Additionally, cross-linking influences the self-assembly of DHBCs. One challenging aspect on higher molar

mass, especially for block copolymers is the high viscosity at higher concentration. Due to the high viscosity a definitive characterisation is challenging.

Nevertheless, the results for the ATPS and w/w emulsions are promising but more work will be required in the future to overcome the current challenges and to broaden ATPS-based applications to a much wider range of practical applications. The rapidly evolving understanding of ATPSs holds enormous promise for mimicking liquid-liquid phase separation (LLPS) processes, which have important implications for example developing insulin release systems which respond to a high glucose level in the body.

Additionally, for the results of the DHBC self-assembly more tests and a deeper look into polymer architecture and block copolymer composition e.g., ratio of the utilised polymers in the block copolymer, other polymer combinations or the introduction of a third block in the block copolymer is needed. For possible future applications, in for example drug delivery, the emulsions and the block copolymers should be tested for permeability and the possibility to load different biomolecules for example DNA or peptides. Overall, the results bringing us one step closer to a better understanding of the phase separation and self-assembly of pure water-based polymer systems.

Chapter 10

10 References

1. Haag, R.; Kratz, F. Polymer therapeutics: concepts and applications. *Angew. Chem., Int. Ed.* **2006,** 45 (8), 1198-1215.
2. Roy, I.; Gupta, M. N. Smart polymeric materials: emerging biochemical applications. *Chem. Biol.* **2003,** 10 (12), 1161-1171.
3. Stevens, M. P., *Polymer chemistry*. Oxford university press New York: 1990; Vol. 2.
4. Carraher Jr, C. E., *Introduction to polymer chemistry*. CRC press: 2017.
5. Thompson, R. C.; Swan, S. H.; Moore, C. J.; Vom Saal, F. S., Our plastic age. The Royal Society Publishing: 2009; Vol. 364, pp 1973-1976.
6. Mai, Y.; Eisenberg, A. Self-assembly of block copolymers. *Chem. Soc. Rev.* **2012,** 41 (18), 5969-5985.
7. Bates, C. M.; Bates, F. S. 50th Anniversary Perspective: Block Polymers Pure Potential. *Macromolecules* **2017,** 50 (1), 3-22.
8. Jones, M.-C.; Leroux, J.-C. Polymeric micelles–a new generation of colloidal drug carriers. *Eur. J. Pharm. Biopharm.* **1999,** 48 (2), 101-111.
9. Discher, D. E.; Eisenberg, A. Polymer vesicles. *Science* **2002,** 297 (5583), 967-973.
10. Tanner, P.; Baumann, P.; Enea, R.; Onaca, O.; Palivan, C.; Meier, W. Polymeric vesicles: from drug carriers to nanoreactors and artificial organelles. *Acc. Chem. Res* **2011,** 44 (10), 1039-1049.
11. Matyjaszewski, K.; Davis, T. P., *Handbook of radical polymerization*. John Wiley & Sons: 2003.
12. Hawker, C. J.; Bosman, A. W.; Harth, E. New polymer synthesis by nitroxide mediated living radical polymerizations. *Chem. Rev.* **2001,** 101 (12), 3661-3688.
13. Wang, J.-S.; Matyjaszewski, K. Controlled/" living" radical polymerization. atom transfer radical polymerization in the presence of transition-metal complexes. *J. Am. Chem. Soc.* **1995,** 117 (20), 5614-5615.
14. Moad, G.; Chiefari, J.; Chong, Y. K.; Krstina, J.; Mayadunne, R. T. A.; Postma, A.; Rizzardo, E.; Thang, S. H. Living free radical polymerization with reversible addition–fragmentation chain transfer (the life of RAFT). *Polym. Int.* **2000,** 49 (9), 993-1001.
15. Moad, G.; Rizzardo, E.; Thang, S. H. Radical addition–fragmentation chemistry in polymer synthesis. *Polymer* **2008,** 49 (5), 1079-1131.
16. Schmaljohann, D. Thermo-and pH-responsive polymers in drug delivery. *Adv. Drug Delivery Rev.* **2006,** 58 (15), 1655-1670.
17. Ge, Z.; Liu, S. Functional block copolymer assemblies responsive to tumor and intracellular microenvironments for site-specific drug delivery and enhanced imaging performance. *Chem. Soc. Rev.* **2013,** 42 (17), 7289-7325.
18. Shin, H. i.; Min, B. G.; Jeong, W.; Park, C. Amphiphilic block copolymer micelles: new dispersant for single wall carbon nanotubes. *Macromol. Rapid Commun.* **2005,** 26 (18), 1451-1457.
19. Cui, P.-F.; Zhuang, W.-R.; Hu, X.; Xing, L.; Yu, R.-Y.; Qiao, J.-B.; He, Y.-J.; Li, F.; Ling, D.; Jiang, H.-L. A new strategy for hydrophobic drug delivery using a hydrophilic polymer equipped with stacking units. *Chem. Commun.* **2018,** 54 (59), 8218-8221.
20. Zhu, J.; Marchant, R. E. Design properties of hydrogel tissue-engineering scaffolds. *Expert Rev. Med. Devices* **2011,** 8 (5), 607-626.
21. Ge, Z.; Xie, D.; Chen, D.; Jiang, X.; Zhang, Y.; Liu, H.; Liu, S. Stimuli-responsive double hydrophilic block copolymer micelles with switchable catalytic activity. *Macromolecules* **2007,** 40 (10), 3538-3546.
22. Kocherginsky, N.; Tan, C. L.; Lu, W. F. Demulsification of water-in-oil emulsions via filtration through a hydrophilic polymer membrane. *J. Membr. Sci.* **2003,** 220 (1-2), 117-128.

23. Matoori, S.; Leroux, J.-C. Twenty-five years of polymersomes: lost in translation? *Mater. Horiz.* **2020,** 7 (5), 1297-1309.
24. Antonietti, M.; Förster, S. Vesicles and liposomes: a self‐assembly principle beyond lipids. *Adv. Mater.* **2003,** 15 (16), 1323-1333.
25. Chao, Y.; Shum, H. C. Emerging aqueous two-phase systems: from fundamentals of interfaces to biomedical applications. *Chem. Soc. Rev.* **2020** 49, 114-142.
26. Staudinger, H. Über Polymerisation. *Berichte der deutschen chemischen Gesellschaft (A and B Series)* **1920,** 53 (6), 1073-1085.
27. Matyjaszewski, K.; Müller, A. H., *Controlled and living polymerizations: from mechanisms to applications*. John Wiley & Sons: 2009.
28. S. Koltzenburg, M. M., O. Nuyken, *Polymere: Synthese, Eigenschaften und Anwendungen*. Springer Spektrum: 2014.
29. Szwarc, M. 'Living'polymers. *Nature* **1956,** 178 (4543), 1168-1169.
30. Szwarc, M.; Levy, M.; Milkovich, R. Polymerization initiated by electron transfer to monomer. A new method of formation of block polymers1. *J. Am. Chem. Soc.* **1956,** 78 (11), 2656-2657.
31. Webster, O. W. Living polymerization methods. *Science* **1991,** 251 (4996), 887-893.
32. Aida, T. Living and immortal polymerizations. *Prog. Polym. Sci.* **1994,** 19 (3), 469-528.
33. Moad, G.; Rizzardo, E.; Solomon, D. H. Selectivity of the reaction of free radicals with styrene. *Macromolecules* **1982,** 15 (3), 909-914.
34. Hawker, C. J. "Living" free radical polymerization: a unique technique for the preparation of controlled macromolecular architectures. *Acc. Chem. Res.* **1997,** 30 (9), 373-382.
35. Jenkins, A. D.; Jones, R. G.; Moad, G. Terminology for reversible-deactivation radical polymerization previously called" controlled" radical or" living" radical polymerization (IUPAC Recommendations 2010). *Pure Appl. Chem.* **2009,** 82 (2), 483-491.
36. Kato, M.; Kamigaito, M.; Sawamoto, M.; Higashimura, T. Polymerization of methyl methacrylate with the carbon tetrachloride/dichlorotris-(triphenylphosphine) ruthenium (II)/methylaluminum bis (2, 6-di-tert-butylphenoxide) initiating system: possibility of living radical polymerization. *Macromolecules* **1995,** 28 (5), 1721-1723.
37. Matyjaszewski, K.; Xia, J. Atom transfer radical polymerization. *Chem. Rev.* **2001,** 101 (9), 2921-2990.
38. Matyjaszewski, K. Atom transfer radical polymerization (ATRP): current status and future perspectives. *Macromolecules* **2012,** 45 (10), 4015-4039.
39. Bremner, I. Manifestations of copper excess. *Am. J. Clin. Nutr.* **1998,** 67 (5), 1069S-1073S.
40. Perrier, S. 50th Anniversary Perspective: RAFT Polymerization A User Guide. *Macromolecules* **2017,** 50 (19), 7433-7447.
41. Rizzardo, E.; Chen, M.; Chong, B.; Moad, G.; Skidmore, M.; Thang, S. H. In *RAFT polymerization: Adding to the picture*, Macromol. Symp., 2007; Wiley Online Library: 2007; pp 104-116.
42. Moad, G.; Rizzardo, E.; Thang, S. H. Living radical polymerization by the RAFT process. *Aust. J. Chem.* **2005,** 58 (6), 379-410.
43. Chiefari, J.; Chong, Y.; Ercole, F.; Krstina, J.; Jeffery, J.; Le, T. P.; Mayadunne, R. T.; Meijs, G. F.; Moad, C. L.; Moad, G. Living free-radical polymerization by reversible addition− fragmentation chain transfer: the RAFT process. *Macromolecules* **1998,** 31 (16), 5559-5562.
44. Carmean, R. N.; Becker, T. E.; Sims, M. B.; Sumerlin, B. S. Ultra-high molecular weights via aqueous reversible-deactivation radical polymerization. *Chem* **2017,** 2 (1), 93-101.
45. Chen, M.; Zhong, M.; Johnson, J. A. Light-controlled radical polymerization: mechanisms, methods, and applications. *Chem. Rev.* **2016,** 116 (17), 10167-10211.
46. Wang, H.; Li, Q.; Dai, J.; Du, F.; Zheng, H.; Bai, R. Real-time and in situ investigation of "living"/controlled photopolymerization in the presence of a trithiocarbonate. *Macromolecules* **2013,** 46 (7), 2576-2582.
47. Braunecker, W. A.; Matyjaszewski, K. Controlled/living radical polymerization: Features, developments, and perspectives. *Prog. Polym. Sci.* **2007,** 32 (1), 93-146.
48. Feng, H.; Lu, X.; Wang, W.; Kang, N.-G.; Mays, J. W. Block copolymers: Synthesis, self-assembly, and applications. *Polymers* **2017,** 9 (10), 494.

49. Nicolaÿ, R.; Kwak, Y.; Matyjaszewski, K. Synthesis of poly (vinyl acetate) block copolymers by successive RAFT and ATRP with a bromoxanthate iniferter. *Chem. Commun.* **2008,** (42), 5336-5338.
50. Tong, Y.-Y.; Dong, Y.-Q.; Du, F.-S.; Li, Z.-C. Synthesis of Well-Defined Poly (vinyl acetate)-b-Polystyrene by Combination of ATRP and RAFT Polymerization. *Macromolecules* **2008,** 41 (20), 7339-7346.
51. Huisgen, R.; Szeimies, G.; Möbius, L. 1.3-Dipolare Cycloadditionen, XXXII. Kinetik der Additionen organischer Azide an CC-Mehrfachbindungen. *Chem. Ber.* **1967,** 100 (8), 2494-2507.
52. Kolb, H. C.; Sharpless, K. B. The growing impact of click chemistry on drug discovery. *Drug Discovery Today* **2003,** 8 (24), 1128-1137.
53. Kempe, K.; Krieg, A.; Becer, C. R.; Schubert, U. S. "Clicking" on/with polymers: a rapidly expanding field for the straightforward preparation of novel macromolecular architectures. *Chem. Soc. Rev.* **2012,** 41 (1), 176-191.
54. Lutz, J. F. 1, 3-Dipolar cycloadditions of azides and alkynes: a universal ligation tool in polymer and materials science. *Angew. Chem., Int. Ed.* **2007,** 46 (7), 1018-1025.
55. Blanazs, A.; Warren, N. J.; Lewis, A. L.; Armes, S. P.; Ryan, A. J. Self-assembly of double hydrophilic block copolymers in concentrated aqueous solution. *Soft Matter* **2011,** 7 (14), 6399-6403.
56. Arnal, M.; Balsamso, V.; Coenjarts, C.; Gohy, J.-F.; Hillmyer, M.; Li, M.; Müller, A.; Ober, C., *Block Copolymers II*. Springer Science & Business Media: 2005; Vol. 190.
57. Al Nakeeb, N.; Willersinn, J.; Schmidt, B. V. K. J. Self-assembly behavior and biocompatible cross-linking of double hydrophilic linear-brush block copolymers. *Biomacromolecules* **2017,** 18 (11), 3695-3705.
58. Schmidt, B. V. K. J. Double Hydrophilic Block Copolymer Self-Assembly in Aqueous Solution. *Macromol. Chem. Phys.* **2018,** 219 (7), 1700494.
59. Willersinn, J.; Bogomolova, A.; Cabré, M. B.; Schmidt, B. V. K. J. Vesicles of double hydrophilic pullulan and poly (acrylamide) block copolymers: A combination of synthetic-and bio-derived blocks. *Polym. Chem.* **2017,** 8 (7), 1244-1254.
60. Rhim, J.-W.; Park, H.-M.; Ha, C.-S. Bio-nanocomposites for food packaging applications. *Prog. Polym. Sci.* **2013,** 38 (10-11), 1629-1652.
61. Stuart, M. A. C.; Huck, W. T.; Genzer, J.; Müller, M.; Ober, C.; Stamm, M.; Sukhorukov, G. B.; Szleifer, I.; Tsukruk, V. V.; Urban, M. Emerging applications of stimuli-responsive polymer materials. *Nat. Mater.* **2010,** 9 (2), 101.
62. Qiang, X.; Chakroun, R.; Janoszka, N.; Gröschel, A. H. Self-assembly of Multiblock Copolymers. *Isr. J. Chem.* **2019**.
63. Langer, R. Drug delivery and targeting. *Nature* **1998**, 5-10.
64. Kim, K. T.; Cornelissen, J. J.; Nolte, R. J.; van Hest, J. C. A Polymersome Nanoreactor with Controllable Permeability Induced by Stimuli-Responsive Block Copolymers. *Adv. Mater.* **2009,** 21 (27), 2787-2791.
65. Jagur-Grodzinski, J. Polymers for tissue engineering, medical devices, and regenerative medicine. Concise general review of recent studies. *Polym. Adv. Technol.* **2006,** 17 (6), 395-418.
66. Beijerinck, M. Über eine Eigentümlichkeit der löslichen Stärke. *Zentralblatt for Bakteriologie, Parasiten und Infektionskrankheiten* **1896,** 2, 679-699.
67. Beijerinck, M. Ueber Emulsionsbildung bei der Vermischung wässeriger Lösungen gewisser gelatinierender Kolloide. *Zeitschrift für Chemie und Industrie der Kolloide* **1910,** 7 (1), 16-20.
68. Albertsson, P. Fractionation of particles and macromolecules in aqueous two-phase systems. *Biochem. Pharmacol.* **1961,** 5 (4), 351-358.
69. Hatti-Kaul, R. Aqueous two-phase systems. *Mol. Biotechnol.* **2001,** 19 (3), 269-277.
70. Asenjo, J. A.; Andrews, B. A. Aqueous two-phase systems for protein separation: a perspective. *J. Chromatogr. A* **2011,** 1218 (49), 8826-8835.
71. Hatti-Kaul, R., *Aqueous two-phase systems: methods and protocols*. Springer Science & Business Media: 2000; Vol. 11.
72. Gustafsson, Å.; Wennerström, H.; Tjerneld, F. The nature of phase separation in aqueous two-polymer systems. *Polymer* **1986,** 27 (11), 1768-1770.

73. Saravanan, S.; Rao, J. R.; Nair, B. U.; Ramasami, T. Aqueous two-phase poly (ethylene glycol)–poly (acrylic acid) system for protein partitioning: Influence of molecular weight, pH and temperature. *Process Biochem.* **2008,** 43 (9), 905-911.
74. Forciniti, D.; Hall, C.; Kula, M.-R. Influence of polymer molecular weight and temperature on phase composition in aqueous two-phase systems. *Fluid Phase Equilib.* **1991,** 61 (3), 243-262.
75. Wu, Y.-T.; Lin, D.-Q.; Zhu, Z.-Q. Thermodynamics of aqueous two-phase systems—the effect of polymer molecular weight on liquid–liquid equilibrium phase diagrams by the modified NRTL model. *Fluid Phase Equilib.* **1998,** 147 (1-2), 25-43.
76. Keating, C. D. Aqueous phase separation as a possible route to compartmentalization of biological molecules. *Acc. Chem. Res.* **2012,** 45 (12), 2114-2124.
77. Ryden, J.; Albertsson, P.-a. Interfacial tension of dextran—polyethylene glycol—water two—phase systems. *J. Colloid Interface Sci.* **1971,** 37 (1), 219-222.
78. Watanabe, T.; Motohiro, I.; Ono, T. Microfluidic formation of hydrogel microcapsules with a single aqueous core by spontaneous cross-linking in aqueous two-phase system droplets. *Langmuir* **2019,** 35 (6), 2358-2367.
79. Rigoni, C.; Beaune, G.; Harnist, B.; Sohrabi, F.; Timonen, J. V. Ferrofluidic aqueous two-phase system with ultralow interfacial tension and micro-pattern formation. *Commun. Mater.* **2022,** 3 (1), 1-11.
80. Pavlovic, M.; Antonietti, M.; Schmidt, B. V. K. J.; Zeininger, L. Responsive Janus and Cerberus emulsions via temperature-induced phase separation in aqueous polymer mixtures. *J. Colloid Interface Sci.* **2020**, 575, 88-95.
81. Mace, C. R.; Akbulut, O.; Kumar, A. A.; Shapiro, N. D.; Derda, R.; Patton, M. R.; Whitesides, G. M. Aqueous multiphase systems of polymers and surfactants provide self-assembling step-gradients in density. *J. Am. Chem. Soc.* **2012,** 134 (22), 9094-9097.
82. Akbulut, O.; Mace, C. R.; Martinez, R. V.; Kumar, A. A.; Nie, Z.; Patton, M. R.; Whitesides, G. M. Separation of nanoparticles in aqueous multiphase systems through centrifugation. *Nano Lett.* **2012,** 12 (8), 4060-4064.
83. Esquena, J. Water-in-water (W/W) emulsions. *Curr. Opin. Colloid Interface Sci.* **2016,** 25, 109-119.
84. Kim, J. W.; Lee, D.; Shum, H. C.; Weitz, D. A. Colloid surfactants for emulsion stabilization. *Adv. Mater.* **2008,** 20 (17), 3239-3243.
85. Zhang, J.; Hwang, J.; Antonietti, M.; Schmidt, B. V. K. J. Water-in-water pickering emulsion stabilized by polydopamine particles and cross-linking. *Biomacromolecules* **2018,** 20 (1), 204-211.
86. Peddireddy, K. R.; Nicolai, T.; Benyahia, L.; Capron, I. Stabilization of water-in-water emulsions by nanorods. *ACS Macro Lett.* **2016,** 5 (3), 283-286.
87. Hu, Z.; Chen, G. Novel nanocomposite hydrogels consisting of layered double hydroxide with ultrahigh tensibility and hierarchical porous structure at low inorganic content. *Adv. Mater.* **2014,** 26 (34), 5950-5956.
88. Pavlovic, M.; Rouster, P.; Bourgeat-Lami, E.; Prevot, V.; Szilagyi, I. Design of latex-layered double hydroxide composites by tuning the aggregation in suspensions. *Soft Matter* **2017,** 13 (4), 842-851.
89. Zhang, J.; Frank, B. D.; Kumru, B.; Schmidt, B. V. K. J. Graphitic Carbon Nitride Stabilized Water-in-Water Emulsions. *Macromol. Rapid Commun.* **2021,** 42 (8), 2000433.
90. Aveyard, R.; Binks, B. P.; Clint, J. H. Emulsions stabilised solely by colloidal particles. *Adv. Colloid Interface Sci.* **2003,** 100, 503-546.
91. Binks, B. P. Particles as surfactants—similarities and differences. *Curr. Opin. Colloid Interface Sci.* **2002,** 7 (1-2), 21-41.
92. Pickering, S. U. Cxcvi.—emulsions. *J. Chem. Soc., Trans.* **1907,** 91, 2001-2021.
93. Adams, F.; Kabalnov, A.; Petsev, D.; Obey, T.; Vincent, B.; Kunieda, H.; Pons, R.; Solans, C.; Forster, T.; Von Rybinski, W., *Modern aspects of emulsion science*. Royal Society of Chemistry: 2007.
94. Inam, M.; Jones, J. R.; Pérez-Madrigal, M. M.; Arno, M. C.; Dove, A. P.; O'Reilly, R. K. Controlling the size of two-dimensional polymer platelets for water-in-water emulsifiers. *ACS Cent. Sci.* **2018,** 4 (1), 63-70.

95. de Freitas, R. A.; Nicolai, T.; Chassenieux, C.; Benyahia, L. Stabilization of water-in-water emulsions by polysaccharide-coated protein particles. *Langmuir* **2016,** 32 (5), 1227-1232.
96. Hann, S. D.; Lee, D.; Stebe, K. J. Tuning interfacial complexation in aqueous two phase systems with polyelectrolytes and nanoparticles for compound all water emulsion bodies (AWE-somes). *Phys. Chem. Chem. Phys.* **2017,** 19 (35), 23825-23831.
97. Bates, F. S.; Fredrickson, G. H. Block copolymer thermodynamics: theory and experiment. *Annu. Rev. Phys. Chem.* **1990,** 41 (1), 525-557.
98. Flory, P. J. Thermodynamics of high polymer solutions. *J. Phys. Chem.* **1942,** 10 (1), 51-61.
99. Huggins, M. L. Some properties of solutions of long-chain compounds. *J. Phys. Chem.* **1942,** 46 (1), 151-158.
100. Leibler, L. Theory of microphase separation in block copolymers. *Macromolecules* **1980,** 13 (6), 1602-1617.
101. Bates, F. S.; Fredrickson, G. H. Conformational asymmetry and polymer-polymer thermodynamics. *Macromolecules* **1994,** 27 (4), 1065-1067.
102. Matsen, M. W.; Schick, M. Microphase separation in starblock copolymer melts. *Macromolecules* **1994,** 27 (23), 6761-6767.
103. Swann, J. M.; Topham, P. D. Design and application of nanoscale actuators using block-copolymers. *Polymers* **2010,** 2 (4), 454-469.
104. Bangham, A. Liposomes: the Babraham connection. *Chem. Phys. Lipids* **1993,** 64 (1-3), 275-285.
105. Banerjee, R. Liposomes: applications in medicine. *J. Biomater. Appl.* **2001,** 16 (1), 3-21.
106. Oh, J. K. Polylactide (PLA)-based amphiphilic block copolymers: synthesis, self-assembly, and biomedical applications. *Soft Matter* **2011,** 7 (11), 5096-5108.
107. Chen, Y.; Chen, H.; Feng, M.; Dong, Y. Amphiphilic gradient copolymers: Synthesis, self-assembly, and applications. *Eur. Polym. J.* **2016,** 85, 489-498.
108. Israelachvili, J. N.; Mitchell, D. J.; Ninham, B. W. Theory of self-assembly of hydrocarbon amphiphiles into micelles and bilayers. *J. Chem. Soc., Faraday Trans. 2* **1976,** 72, 1525-1568.
109. Wang, C.; Wang, Z.; Zhang, X. Amphiphilic building blocks for self-assembly: from amphiphiles to supra-amphiphiles. *Acc. Chem. Res.* **2012,** 45 (4), 608-618.
110. Discher, B. M.; Won, Y.-Y.; Ege, D. S.; Lee, J. C.; Bates, F. S.; Discher, D. E.; Hammer, D. A. Polymersomes: tough vesicles made from diblock copolymers. *Science* **1999,** 284 (5417), 1143-1146.
111. Hyde, S. Curvature and the global structure of interfaces in surfactant-water systems. *J. Phys. Colloques* **1990,** 51 (C7), C7-209-C7-228.
112. Israelachvili, J. N., *Intermolecular and surface forces*. Academic press: 2011.
113. Blanazs, A.; Armes, S. P.; Ryan, A. J. Self-assembled block copolymer aggregates: from micelles to vesicles and their biological applications. *Macromol. Rapid Commun.* **2009,** 30 (4-5), 267-277.
114. Li, G.; Song, S.; Guo, L.; Ma, S. Self-assembly of thermo-and pH-responsive poly (acrylic acid)-b-poly (N-isopropylacrylamide) micelles for drug delivery. *J. Polym. Sci., Part A: Polym. Chem.* **2008,** 46 (15), 5028-5035.
115. Heskins, M.; Guillet, J. E. Solution properties of poly (N-isopropylacrylamide). *J. Macromol. Sci. Part A - Chem.* **1968,** 2 (8), 1441-1455.
116. Seuring, J.; Agarwal, S. Polymers with upper critical solution temperature in aqueous solution. *Macromol. Rapid Commun.* **2012,** 33 (22), 1898-1920.
117. Idziak, I.; Avoce, D.; Lessard, D.; Gravel, D.; Zhu, X. Thermosensitivity of aqueous solutions of poly (N, N-diethylacrylamide). *Macromolecules* **1999,** 32 (4), 1260-1263.
118. Liu, Y.; Lipowsky, R.; Dimova, R. Giant Vesicles Encapsulating Aqueous Two-Phase Systems: From Phase Diagrams to Membrane Shape Transformations. *Front. Chem.* **2019,** 7.
119. Dimova, R.; Lipowsky, R. Giant Vesicles Exposed to Aqueous Two-Phase Systems: Membrane Wetting, Budding Processes, and Spontaneous Tubulation. *Adv. Mater. Interfaces* **2017,** 4 (1), 1600451.
120. Brosnan, S. M.; Schlaad, H.; Antonietti, M. Aqueous Self-Assembly of Purely Hydrophilic Block Copolymers into Giant Vesicles. *Angew. Chem., Int. Ed.* **2015,** 54 (33), 9715-9718.

121. Casse, O.; Shkilnyy, A.; Linders, J. r.; Mayer, C.; Häussinger, D.; Völkel, A.; Thünemann, A. F.; Dimova, R.; Cölfen, H.; Meier, W. Solution behavior of double-hydrophilic block copolymers in dilute aqueous solution. *Macromolecules* **2012,** 45 (11), 4772-4777.
122. Taubert, A.; Furrer, E.; Meier, W. Water-in-water mesophases for templating inorganics. *Chem. Commun.* **2004,** (19), 2170-2171.
123. Ke, F.; Mo, X.; Yang, R.; Wang, Y.; Liang, D. Association of block copolymer in nonselective solvent. *Macromolecules* **2009,** 42 (14), 5339-5344.
124. Willersinn, J.; Schmidt, B. V. K. J. Self-assembly of double hydrophilic poly (2-ethyl-2-oxazoline)-b-poly (n-vinylpyrrolidone) block copolymers in aqueous solution. *Polymers* **2017,** 9 (7), 293.
125. Rudolph, T.; Crotty, S.; von der Lühe, M.; Pretzel, D.; Schubert, U.; Schacher, F. Synthesis and solution properties of double hydrophilic poly (ethylene oxide)-block-poly (2-ethyl-2-oxazoline)(PEO-b-PEtOx) star block copolymers. *Polymers* **2013,** 5 (3), 1081-1101.
126. Willersinn, J.; Schmidt, B. V. K. J. Aqueous self-assembly of pullulan-b-poly (2-ethyl-2-oxazoline) double hydrophilic block copolymers. *J. Polym. Sci., Part A: Polym. Chem.* **2017,** 55 (22), 3757-3766.
127. Willersinn, J.; Schmidt, B. V. K. J. Pure hydrophilic block copolymer vesicles with redox-and pH-cleavable crosslinks. *Polym. Chem.* **2018,** 9 (13), 1626-1637.
128. Park, H.; Walta, S.; Rosencrantz, R.; Körner, A.; Schulte, C.; Elling, L.; Richtering, W.; Böker, A. Micelles from self-assembled double-hydrophilic PHEMA-glycopolymer-diblock copolymers as multivalent scaffolds for lectin binding. *Polym. Chem.* **2016,** 7 (4), 878-886.
129. Oh, T.; Nagao, M.; Hoshino, Y.; Miura, Y. Self-assembly of a double hydrophilic block glycopolymer and the investigation of its mechanism. *Langmuir* **2018,** 34 (29), 8591-8598.
130. Quan, J.; Shen, F.-W.; Cai, H.; Zhang, Y.-N.; Wu, H. Galactose-Functionalized Double-Hydrophilic Block Glycopolymers and Their Thermoresponsive Self-Assembly Dynamics. *Langmuir* **2018,** 34 (36), 10721-10731.
131. Adharis, A.; Ketelaar, T.; Komarudin, A. G.; Loos, K. Synthesis and Self-Assembly of Double-Hydrophilic and Amphiphilic Block Glycopolymers. *Biomacromolecules* **2019,** 20 (3), 1325-1333.
132. Baskir, J. N.; Hatton, T. A.; Suter, U. W. Protein partitioning in two-phase aqueous polymer systems. *Biotechnol. Bioeng.* **1989,** 34 (4), 541-558.
133. Nicolai, T.; Murray, B. Particle stabilized water in water emulsions. *Food Hydrocolloids* **2017,** 68, 157-163.
134. Forciniti, D.; Hall, C.; Kula, M. Interfacial tension of polyethyleneglycol-dextran-water systems: influence of temperature and polymer molecular weight. *J. Biotechnol.* **1990,** 16 (3-4), 279-296.
135. Scholten, E.; Visser, J. E.; Sagis, L. M.; van der Linden, E. Ultralow interfacial tensions in an aqueous phase-separated gelatin/dextran and gelatin/gum arabic system: A comparison. *Langmuir* **2004,** 20 (6), 2292-2297.
136. Diamond, A. D.; Hsu, J. T. Fundamental studies of biomolecule partitioning in aqueous two-phase systems. *Biotechnol. Bioeng.* **1989,** 34 (7), 1000-1014.
137. Tubío, G.; Pellegrini, L.; Nerli, B. B.; Picó, G. A. Liquid− liquid equilibria of aqueous two-phase systems containing poly (ethylene glycols) of different molecular weight and sodium citrate. *J. Chem. Eng. Data* **2006,** 51 (1), 209-212.
138. Read, E.; Guinaudeau, A.; Wilson, D. J.; Cadix, A.; Violleau, F.; Destarac, M. Low temperature RAFT/MADIX gel polymerisation: access to controlled ultra-high molar mass polyacrylamides. *Polym. Chem.* **2014,** 5 (7), 2202-2207.
139. Xu, J.; Jung, K.; Atme, A.; Shanmugam, S.; Boyer, C. A robust and versatile photoinduced living polymerization of conjugated and unconjugated monomers and its oxygen tolerance. *J. Am. Chem. Soc.* **2014,** 136 (14), 5508-5519.
140. Carmean, R. N.; Sims, M. B.; Figg, C. A.; Hurst, P. J.; Patterson, J. P.; Sumerlin, B. S. Ultrahigh molecular weight hydrophobic acrylic and styrenic polymers through organic-phase photoiniferter-mediated polymerization. *ACS Macro Letters* **2020,** 9 (4), 613-618.

141. da Rocha Patrício, P.; Mesquita, M. C.; da Silva, L. H. M.; da Silva, M. C. H. Application of aqueous two-phase systems for the development of a new method of cobalt (II), iron (III) and nickel (II) extraction: a green chemistry approach. *J. Hazard. Mater.* **2011,** 193, 311-318.
142. Pavlovic, M.; Huber, R.; Adok-Sipiczki, M.; Nardin, C.; Szilagyi, I. Ion specific effects on the stability of layered double hydroxide colloids. *Soft Matter* **2016,** 12 (17), 4024-4033.
143. Mishra, G.; Dash, B.; Pandey, S. Layered double hydroxides: A brief review from fundamentals to application as evolving biomaterials. *Appl. Clay Sci.* **2018,** 153, 172-186.
144. Xu, Z. P.; Stevenson, G.; Lu, C.-Q.; Lu, G. Q. Dispersion and size control of layered double hydroxide nanoparticles in aqueous solutions. *J. Phys. Chem. B* **2006,** 110 (34), 16923-16929.
145. Hu, Z.; Chen, G. Aqueous dispersions of layered double hydroxide/polyacrylamide nanocomposites: preparation and rheology. *J. Mater. Chem. A* **2014,** 2 (33), 13593-13601.
146. Yang, X.-J.; Zhang, P.; Li, P.; Li, Z.; Xia, W.; Zhang, H.; Di, Z.; Wang, M.; Zhang, H.; Niu, Q. J. Layered double hydroxide/polyacrylamide nanocomposite hydrogels: Green preparation, rheology and application in methyl orange removal from aqueous solution. *J. Mol. Liq.* **2019,** 280, 128-134.
147. Fu, P.; Xu, K.; Song, H.; Chen, G.; Yang, J.; Niu, Y. Preparation, stability and rheology of polyacrylamide/pristine layered double hydroxide nanocomposites. *J. Mater. Chem.* **2010,** 20 (19), 3869-3876.
148. Layrac, G.; Harrisson, S.; Destarac, M.; Gerardin, C.; Tichit, D. Comprehensive study of the formation of stable colloids of CuAl layered double hydroxide assisted by double hydrophilic block copolymers. *Appl. Clay Sci.* **2020,** 193, 105673.
149. Tea, L.; Nicolai, T.; Renou, F. Stabilization of water-in-water emulsions by linear homo-polyelectrolytes. *Langmuir* **2019,** 35 (27), 9029-9036.
150. Pavlovic, M.; Plucinski, A.; Zeininger, L.; Schmidt, B. V. K. J. Temperature sensitive water-in-water emulsions. *Chem. Commun.* **2020,** 56 (50), 6814-6817.
151. de Morais Zanata, D.; Isabel Felisberti, M. Thermo- and pH-responsive POEGMA-b-PDMAEMA-b-POEGMA triblock copolymers. *Eur. Polym. J.* **2022**, 111069.
152. Rösler, A.; Vandermeulen, G. W.; Klok, H.-A. Advanced drug delivery devices via self-assembly of amphiphilic block copolymers. *Adv. Drug Delivery Rev.* **2012,** 64, 270-279.
153. Dimova, R.; Lipowsky, R. Lipid Membranes: Giant Vesicles Exposed to Aqueous Two-Phase Systems: Membrane Wetting, Budding Processes, and Spontaneous Tubulation (Adv. Mater. Interfaces 1/2017). *Adv. Mater. Interfaces* **2017,** 4 (1).
154. Lira, R. B.; Willersinn, J.; Schmidt, B. V. K. J.; Dimova, R. Selective Partitioning of (Biomacro) molecules in the Crowded Environment of Double-Hydrophilic Block Copolymers. *Macromolecules* **2020,** 53 (22), 10179-10188.
155. Bernard, J.; Save, M.; Arathoon, B.; Charleux, B. Preparation of a xanthate-terminated dextran by click chemistry: Application to the synthesis of polysaccharide-coated nanoparticles via surfactant-free ab initio emulsion polymerization of vinyl acetate. *J. Polym. Sci., Part A: Polym. Chem.* **2008,** 46 (8), 2845-2857.
156. Gao, H.; Matyjaszewski, K. Synthesis of molecular brushes by "grafting onto" method: combination of ATRP and click reactions. *J. Am. Chem. Soc.* **2007,** 129 (20), 6633-6639.
157. Gregory, A.; Stenzel, M. H. Complex polymer architectures via RAFT polymerization: From fundamental process to extending the scope using click chemistry and nature's building blocks. *Prog. Polym. Sci.* **2012,** 37 (1), 38-105.
158. Gondi, S. R.; Vogt, A. P.; Sumerlin, B. S. Versatile pathway to functional telechelics via RAFT polymerization and click chemistry. *Macromolecules* **2007,** 40 (3), 474-481.
159. O'Reilly, R. K.; Hawker, C. J.; Wooley, K. L. Cross-linked block copolymer micelles: functional nanostructures of great potential and versatility. *Chem. Soc. Rev.* **2006,** 35 (11), 1068-1083.
160. Al Nakeeb, N.; Kochovski, Z.; Li, T.; Zhang, Y.; Lu, Y.; Schmidt, B. V. K. J. Poly (ethylene glycol) brush-b-poly (N-vinylpyrrolidone)-based double hydrophilic block copolymer particles crosslinked via crystalline α-cyclodextrin domains. *RSC Adv.* **2019,** 9 (9), 4993-5001.
161. Al Nakeeb, N.; Nischang, I.; Schmidt, B. V. K. J. Tannic Acid-Mediated Aggregate Stabilization of Poly (N-vinylpyrrolidone)-b-poly (oligo (ethylene glycol) methyl ether methacrylate) Double Hydrophilic Block Copolymers. *Nanomaterials* **2019,** 9 (5), 662.

162. Grover, G. N.; Lam, J.; Nguyen, T. H.; Segura, T.; Maynard, H. D. Biocompatible hydrogels by oxime click chemistry. *Biomacromolecules* **2012,** 13 (10), 3013-3017.
163. Mukherjee, S.; Bapat, A. P.; Hill, M. R.; Sumerlin, B. S. Oximes as reversible links in polymer chemistry: dynamic macromolecular stars. *Polym. Chem.* **2014,** 5 (24), 6923-6931.
164. Collins, J.; Xiao, Z.; Müllner, M.; Connal, L. A. The emergence of oxime click chemistry and its utility in polymer science. *Polym. Chem.* **2016,** 7 (23), 3812-3826.
165. Sims, M. B.; Patel, K. Y.; Bhatta, M.; Mukherjee, S.; Sumerlin, B. S. Harnessing imine diversity to tune hyperbranched polymer degradation. *Macromolecules* **2018,** 51 (2), 356-363.
166. Schmidt, B. V. K. J.; Barner-Kowollik, C. Supramolecular X-and H-shaped star block copolymers via cyclodextrin-driven supramolecular self-assembly. *Polym. Chem.* **2014,** 5 (7), 2461-2472.
167. Ilić, L.; Jeremić, K.; Jovanović, S. Kinetics of pullulan depolymerization in hydrochloric acid. *Eur. Polym. J.* **1991,** 27 (11), 1227-1229.
168. Schatz, C.; Louguet, S.; Le Meins, J. F.; Lecommandoux, S. Polysaccharide-block-polypeptide Copolymer Vesicles: Towards Synthetic Viral Capsids. *Angew. Chem., Int. Ed.* **2009,** 48 (14), 2572-2575.
169. Crisalli, P.; Kool, E. T. Water-soluble organocatalysts for hydrazone and oxime formation. *J. Org. Chem.* **2013,** 78 (3), 1184-1189.
170. Nagarajan, R.; Ganesh, K. Block copolymer self-assembly in selective solvents: theory of solubilization in spherical micelles. *Macromolecules* **1989,** 22 (11), 4312-4325.
171. Champion, J. A.; Katare, Y. K.; Mitragotri, S. Making polymeric micro- and nanoparticles of complex shapes. *Proc. Natl. Acad. Sci.* **2007,** 104 (29), 11901-11904 DOI: 10.1073/pnas.0705326104.
172. Heskins, M.; Guillet, J. E. Solution properties of poly (N-isopropylacrylamide). *Journal of Macromolecular Science—Chemistry* **1968,** 2 (8), 1441-1455.
173. Kyriakos, K.; Philipp, M.; Lin, C. H.; Dyakonova, M.; Vishnevetskaya, N.; Grillo, I.; Zaccone, A.; Miasnikova, A.; Laschewsky, A.; Müller-Buschbaum, P. Quantifying the interactions in the aggregation of thermoresponsive polymers: the effect of cononsolvency. *Macromol. Rapid Commun.* **2016,** 37 (5), 420-425.
174. Suzuki, M.; Hanabusa, K. Polymer organogelators that make supramolecular organogels through physical cross-linking and self-assembly. *Chem. Soc. Rev.* **2010,** 39 (2), 455-463.
175. Asano, I.; So, S.; Lodge, T. P. Location and influence of added block copolymers on the droplet size in oil-in-oil emulsions. *Langmuir* **2015,** 31 (27), 7488-7495.
176. Asano, I.; So, S.; Lodge, T. P. Oil-in-oil emulsions stabilized by asymmetric polymersomes formed by AC+ BC block polymer co-assembly. *J. Am. Chem. Soc.* **2016,** 138 (14), 4714-4717.
177. Appold, M.; Gallei, M. Bio-Inspired Structural Colors Based on Linear Ultrahigh Molecular Weight Block Copolymers. *ACS Appl. Polym. Mater.* **2019,** 1 (2), 239-250.
178. Lu, C.; Urban, M. W. One-Step Synthesis of Amphiphilic Ultrahigh Molecular Weight Block Copolymers by Surfactant-Free Heterogeneous Radical Polymerization. *ACS Macro Letters* **2015,** 4 (12), 1317-1320.
179. Poutanen, M.; Guidetti, G.; Gröschel, T. I.; Borisov, O. V.; Vignolini, S.; Ikkala, O.; Gröschel, A. H. Block copolymer micelles for photonic fluids and crystals. *ACS nano* **2018,** 12 (4), 3149-3158.
180. Dao, V. H.; Cameron, N. R.; Saito, K. Synthesis of ultra-high molecular weight aba triblock copolymers via aqueous RAFT-mediated gel polymerisation, end group modification and chain coupling. *Polym. Chem.* **2017,** 8 (44), 6834-6843.
181. Li, R.; An, Z. Achieving Ultrahigh Molecular Weights with Diverse Architectures for Unconjugated Monomers through Oxygen - Tolerant Photoenzymatic RAFT Polymerization. *Angewandte Chemie* **2020,** 132 (49), 22442-22448.
182. Skey, J.; O'Reilly, R. K. Facile one pot synthesis of a range of reversible addition–fragmentation chain transfer (RAFT) agents. *Chem. Commun.* **2008,** (35), 4183-4185.
183. Schmidt, B. V. K. J.; Hetzer, M.; Ritter, H.; Barner-Kowollik, C. Cyclodextrin-complexed RAFT agents for the ambient temperature aqueous living/controlled radical polymerization of acrylamido monomers. *Macromolecules* **2011,** 44 (18), 7220-7232.

Chapter 11

11 Appendix

11.1 Additional experimental procedures and characterisation

Synthesis of 2-(((ethylthio)carbonothioyl)thio)-2-methylpropanoic acid (EMP)

Based on the literature,[182, 183] ethanethiol (2.2 mL, 29.74 mmol, 1 eq.) was dissolved in a suspension of K_3PO_4 (7.46 g, 32.71 mmol, 1.1 eq.) in acetone (80 mL) at ambient temperature. After stirring for 20 min, carbon disulfide (5.4 mL, 89.22 mmol, 3.0 eq.) was added and the solution turned yellow. 2-Bromisobutyric acid (5.46 g, 32.69 mmol, 1.1 eq.) was added after 20 min and the mixture stirred at ambient temperature for 24 hours. 1 M hydrochloric acid (200 mL) was added, and the aqueous phase was extracted with DCM (3 x 100 mL). The combined organic extracts were washed with deionized water (100 mL), brine (100 mL) and dried over Na_2SO_4. After the evaporation of the solvent, the orange oil was purified over a column with silica gel and an eluent mixture of n-hexane: ethyl acetate 2:1. The yellow fractions were combined and the evaporation of the solvent turned the product into orange crystals (4.02 g, 17.9 mmol, 62%).

^{1}H-NMR (400 MHz, Chloroform-d): [δ, ppm]: 1.27 (t, J = 7.4 Hz, 3H), 1.66 (s, 6H), 3.23 (q, J = 7.4 Hz, 2H).

11.2 List of publications

(* part of this thesis)

*8. A. Plucinski and B. V. K. J. Schmidt, pH sensitive water-in-water emulsions based on the pullulan and poly(*N*,*N*-dimethylacrylamide) aqueous two-phase system**,** *Polym. Chem.,* **2022,** 13(28), 4170-4177.

*7. A. Plucinski, M. Pavlovic, M. Clarke, D. Bhella, B. V. K. J. Schmidt, *Macromol. Rapid Commun.,* **2022**,43, 2100656.

(*) 6. A. Plucinski, Z. Lyu and B. V. K. J. Schmidt, Polysaccharide nanoparticles: From fabrication to applications *J. Mater. Chem. B,* **2021**,9, 7030-7062.

*5. A. Plucinski, M. Pavlovic and B. V. K. J. Schmidt, All aqueous multi-phase systems and emulsions formed via low concentrated ultra-high molar mass polyacrylamides, *Macromolecules*, **2021**, 54(12), 5366-5375

*4. A. Plucinski, J. Willersinn, R. B. Lira, R. Dimova, B. V. K. J. Schmidt, Aggregation and Crosslinking of Poly (N, N-dimethylacrylamide)-b-pullulan Double Hydrophilic Block Copolymers, *Macromol. Chem. Phys.,* **2020**, 221.13, 2000053.

3. M. Pavlovic, A. Plucinski, L. Zeininger, B. V. K. J. Schmidt, Temperature sensitive water-in-water emulsions, *Chem. Com.* **2020**, 56(50), 6814-6817

2. M. Pavlovic, A. Plucinski, J. Zhang, M. Antonietti, L. Zeininger, B. V. K. J. Schmidt, Cascade kinetics in an enzyme-loaded aqueous two-phase system, *Langmuir* **2020**, 36.6, 1401-1408.

1. C. Wei, A. Plucinski, S. Nuasaen, A. Tripathi, P. Tangboriboonrat, K. Tauer, Swelling-induced deformation of spherical latex particles, *Macromolecules* **2017**, 50, 1, 349–363

Register of illustrations

Figures

Schemes

Acknowledgment

First of all, I would like to thank my first supervisor and mentor Dr. Bernhard V. K. J. Schmidt for the opportunity to join his group, for the interesting topic, all the fruitful discussions and for the amazing support during my time in his group.

Furthermore, I would like to thank Prof. Andrew Jamieson for being my second supervisor and for his encouraging talks.

Additionally, I would like to thank Dr. Marko Pavlovic, Dr. Rafael Lira, Dr. Jochen Willersinn, Mairi Clarke, Prof. David Bella, Dr. Rumiana Dimova for the great collaboration during the last years.

A special thanks to Marlis Gräwert, Sascha Prentzel, June Southall, Heike Runger and Antje Völkel for the help with characterisation of some polymers.

Thank you to all former and current group members: Baris, Noah, Qian, Janrui, JB, Hui, Marko, Marlies, Bradly, Cameron and all the bachelor, master, and summer students: Roberta, Catarina, Will, Zan, MD and Michael for helping in the one or another way to some projects.

Moreover, I would like to thank all former and current colleagues in the Max-Planck-Institute and the University of Glasgow for providing a nice and friendly atmosphere with unforgettable moments: Ivan, Baris, Julya, Ralf, Milena, Konstantin, Paolo, Mina, Demetra, Francesco, Enrico, Lukas, Joao, JB, Sophia, Fatma, Danielle, Selma, Ali, Caroline, Laura, Kopano, Catrine, Ignas, Henry, Valentina, Pernille and many more.

Furthermore, I would thank my amazing friends in Berlin: Nico, Sandra, Dario, Marco, Adrian, Oli, Jäzz, Nils, Jessy, Daniel, Anna, Max, and many more for their support and encouraging words.

Finally, yet importantly, I would like to thank my whole family for their invaluable support throughout my last years away from Germany.

Declaration

The present work was carried out during the period from September 2019 to August 2022 at the University of Glasgow under supervision of Dr. Bernhard Schmidt.

I declare that I have written this work on my own and used no other than the named aids and references.

Alexander Plucinski

Glasgow, August 2022